Coordination Chemistry Reviews 514 (2024) 215757

Contents lists available at ScienceDirect

Coordination Chemistry Reviews

journal homepage: www.elsevier.com/locate/ccr

Review

N-heterocyclic carbenes as bridgehead donors in metal pincer complexes

Fengkai He [a,b,*], Konstantinos P. Zois [c,d], Demeter Tzeli [d], Andreas A. Danopoulos [c,*], Pierre Braunstein [a,*]

[a] Université de Strasbourg, CNRS, Institut de Chimie UMR 7177, Strasbourg 67081 Cedex, France
[b] Department of Chemistry, School of Chemistry, Chemical Engineering and Life Science, Wuhan University of Technology, Wuhan 430070, PR China
[c] Inorganic Chemistry Laboratory, National and Kapodistrian University of Athens, Panepistimiopolis Zografou, GR-15771, Greece
[d] Physical Chemistry Laboratory, National and Kapodistrian Unversity of Athens, Panepistimiopolis Zografou, GR-15771, Greece

ARTICLE INFO

Keywords:
Pincer ligands
N-heterocyclic carbenes
Hybrid ligands
Hemilability
Metal complexes
Catalysis

ABSTRACT

Rigid terdentate 'pincer' ligands containing a bridgehead N-heterocyclic carbene (NHC) donor attract considerable interest as spectators in transition metal complexes with broad scope and potential applications in the fields of catalysis, medicinal chemistry and material science. This review aims at compiling and evaluating the developments occurring in the area of complexes with these ligands. The various donor groups in the side-arms that can be associated with the bridgehead NHC donor provide considerable diversity and tunability of the pincer system. In addition to the distinct structural and reactivity features that are discussed in detail, comparisons with related pincer complexes based on all-classical donor sets or mixed donor sets with NHCs at the side-arm(s) only have been undertaken. The review comprises five major sections: the first attempting to differentiate the NHC bridgehead donor as structural element in the pincer ligand design; the following three describing in detail the synthesis, characterization and reactivity of metal complexes with ligand topologies featuring one, two or three NHC donors, respectively; finally the fifth compiling in a tabular format the catalytic applications of the complexes discussed previously, organized as a function of the catalytic reaction, the metal and the ligand type. The review provides a rationally organized coverage of the literature since 2005 in a diverse and fast expanding field dealing with pincer ligand design.

1. Introduction

Terdentate ligands that bind to a metal in meridional or pseudo-meridional fashion in a controlled and rather rigid manner were introduced by Moulton and Shaw in the late 1970s [1], and are now commonly referred to as 'pincer ligands', a term that was coined by G. van Koten *et al.* in 1989 [2]. The adoption by the pincer complexes of persistent, well-defined and modular structures that can be tuned with

Abbreviations: ν, frequency; Δ, heat; 1D, one-dimensional; 2D, two-dimensional; NOESY, Nuclear Overhauser Effect SpectroscopY; COSY, COrrelation SpectroscopY; HRMS, High resolution mass spectroscopy; Ac, Acetyl; OAc, Acetate; OAcF, Trifluoroacetate; acac, Acetylacetonate; Ar, Aryl; BAr^F, tetrakis[3,5-bis(trifluoromethyl)phenyl]borate; DCM, Dichloromethane; dmpm, Bis(dimethylphosphino)methane; HMDS, Hexamethyldisilazide; IMes, N,N'-bis(2,4,6-trimethylphenyl) imidazol-2-ylidene; IXyl, 1,3-bis(2,6-dimethylphenyl)imidazol-2-ylidene; Np, neopentyl; NpH, Neopentane; Xyl, Xylyl; μ_{eff}, effective magnetic moment; μ_B, bohr magneton; *p*-cymene, 4-isopropyltoluene; PNB, Polynorbornene; bpy, Bipyridine; Bn, Benzyl group in benzyl ethers or benzoates; COD, 1,5-cyclooctadiene; COE, Cyclooctene; Cp, Cyclopentadienyl; Cy, Cyclohexyl; DiPP, 2,6-diisopropylphenyl; DME, Dimethoxyethane; DMF, Dimethylformamide; DMSO, Dimethylsulfoxide; DPI, bis(imino)-pyridine; dppm, bis(diphenylphosphino)methane; SiP_3, tris(dimethylphosphinomethyl)methylsilane; 18-C-6, 18-Crown-6-ether; EPR, Electron spin resonance; eq., equivalent; Et, Ethyl; Et_2O, Diethyl ether; ESI-MS, Electrospray ionization mass spectrometry; h, hour; Hz, Hertz; *i*Pr, *iso*-propyl; IR, Infra-Red; KHMDS, Potassium hexamethyldisilazide; NaHMDS, Sodium hexamethyldisilazide; LDA, Lithium diisopropylamide; LiHMDS, Lithium hexamethyldisilazide; *m*-, meta-; MAO, Methylaluminoxane; Me, Methyl; MeCN, Acetonitrile; DMAD, Dimethyl acetylenedicarboxylate; Mes, Mesityl; min, Minute; MMAO, Modified methylaluminoxane; NBD, Norbornadiene; *n*Bu, n-butyl; NHC, N-heterocyclic carbene; NMR, Nuclear magnetic resonance; *o*-, ortho-; *p*-, para-; Ph, Phenyl; ppm, parts per million; Pip, Piperidine; Py, Pyridine, pyridinyl; RT, Room temperature; RE-NHC, Ring-Expanded NHC; *t*Bu, *tert*-butyl; Tf, OTf, OTs, Triflyl, triflate, tosylate; TFA, Trifluoroacetic acid; THF, Tetrahydrofuran; TMED, N,N,N'N'-tetramethylethylenediamine; TOF, Turnover frequency; TON, Turnover number; Tpy, 2,2′:6′,2′-terpyridine; tol, Tolyl; Ts, OTs, Tosyl, tosylate.

* Corresponding authors.
E-mail addresses: hefengkai1990@sina.cn (F. He), kpzois@chem.uoa.gr (K.P. Zois), tzeli@chem.uoa.gr (D. Tzeli), adanop@chem.uoa.gr (A.A. Danopoulos), braunstein@unistra.fr (P. Braunstein).

https://doi.org/10.1016/j.ccr.2024.215757
Received 12 November 2023; Accepted 21 February 2024

regard to their electronic and steric parameters and rigidity opened the way to the discovery of distinctive coordination, organometallic chemistry and reactivity, which on many occasions differentiate these complexes very significantly from non-pincer analogues. Accordingly, the pincer ligand design concept opened the way to the study of structures and reactivity of complexes in a broad range of experimental conditions, leading to a growing number of applications in catalysis, medicinal chemistry and materials science. A schematic representation of the pincer platform and its tunable molecular variables is given in Chart 1.

In the structures from the early days, the bridgehead donor atom D^1 was frequently part of a (hetero)aromatic or aliphatic backbone, *e.g.* the N-atom of a pyridine ring or the negatively charged C2-atom of a 1,3-disubstituted aryl; it was flanked by two identical (*i.e.* $D^2 = D^3$) or (rarely) different (*i.e.* $D^2 \neq D^3$) classical neutral or anionic donor groups; common donors D^2 and D^3 could be phosphane, amine and imine or alkoxide and carboxylate, connected to the bridgehead by a short spacer. This arrangement on metal coordination usually generated two fused, five-membered metallacycles. The combined electronic (mainly σ-/π-donor/acceptor) and steric effects of the D^1 and D^2/D^3 donors were used empirically in an *ad hoc* manner for the development of ligand design ideas and the rationalization of experimental structural and reactivity findings. The overall effects were the modulation of the electron density at the metal center and its steric accessibility that determined the reactivity at the metal.

In the last two decades, the subtle and sophisticated electronic structures of pincer ligands and complexes have reached a new level of understanding. In part, crucial for these developments were the advancements in the electronic structure elucidation methodologies by experimental and computational techniques. For example, the fine structural and reactivity differences of pyridine-bis(imine), pyridine-bis (phosphane) and pyridine-bis(NHC) (NHC = N-heterocyclic carbene) complexes (*vide infra*) with various metals (in particular 3*d*), led to the establishment of the ideas of redox non-innocence in the pincer chemistry, which are flourishing to the present [3–5]. Furthermore, the pincer structure can participate in chemical (catalytic) reactions and cooperate with the metal by 'lending to' and 'borrowing from' it hydrogen atoms during the reactions [6,7]. Thus, the pincer ligand is not any longer restricted to a spectator role but can engage in cooperative reactivity with the metal center.

The emergence of stable and isolable NHCs after the seminal contributions of Arduengo, Bertrand and coworkers [8–12] had also a knock-on effect in the progress of the pincer chemistry. Thus, the pyridine-bis(NHC) ligand backbone (Chart 2**a**) was first reported by Lin and coworkers, adopting a bridging coordination mode in mercury

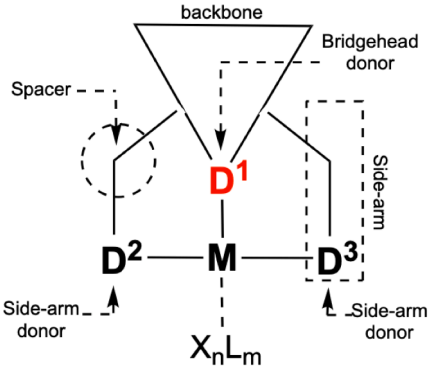

Chart 1. A modular pincer complex platform with its diversity stemming from: (i) the donor groups D^2, D^3 in the two side-arms can be chemically identical or different and the connecting spacers of the same or different nature and length, respectively; (ii) the bridgehead donor D^1 (always a C^{NHC} donor in this review), is part of diverse organic frameworks (e.g. an aromatic or heteroaromatic ring etc.) here is denoted by the triangle; (iii) the metal center M; (iv) the co-ligands X_nL_m

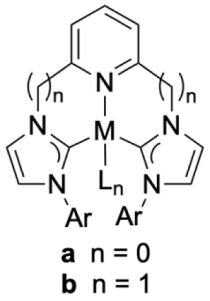

Chart 2. The first pincer backbones with NHC donors that led to structurally characterized and well-defined complexes

complexes of double helical structure [13]. Soon thereafter, the pincer coordination mode of **a** and the corresponding lutidine backbone (**b** in Chart 2), pincer ligands and their bulkier aryl analogues were characterized on palladium and ruthenium complexes by Crabtree and Danopoulos, respectively [14–16]. Furthermore, the NHC-containing pincer motifs expanded with metals from across the Periodic Table, while the search for architectures combining NHCs with other donor functionalities also intensified; these early developments were summarized in a review [17].

Numerous reviews covering various aspects of pincer complexes with at least one NHC donor have recently appeared focusing on specific metals, catalytic reactions or selected topical entries. The ligand design aspects emphasize common underlying ideas *e.g.* stability due to the chelate effect, well defined and persistent donor arrangement, rigidity and hemilability, superior σ-donation by the NHC(s), steric control and practical ligand synthesis aspects; on two occasions the electron/redox non-innocence of the pincer ligands is also briefly mentioned [4,18–25]. A tutorial review with general concepts of pincer ligand design and architecture has also appeared [26].

2. The case for NHC bridgehead donors in pincer ligands

In this review we focus on pincer complexes with one NHC donor occupying the bridgehead position. A systematic classification is presented based on: (i) the ligand architecture, (ii) the nature of the side arms, (iii) the types of donors and (iv) a comparative evaluation of the impact of the ligands on structures and reactivity of their metal complexes. Pincer ligands with NHC bridgehead donors appeared early in the development of the NHC pincer topic; for example, in the earlier review [17], from the dozen of pincer designs covered, almost half included bridgehead NHC donors. However, at that time, when the shallow parallels between NHC, trialkyl phosphane and pyridine donors were a commonplace, the deeper understanding of the pincer complexes was only starting to emerge. At present, with a more thorough and diverse insight into the pincer ligands, based on numerous experimental and computational data, there are good reasons that justify the cross section of the topic attempted here.

2.1. The geometric constraints imposed by the heterocycle housing the C^{NHC} donor

The most common and 'derivatization-friendly' NHC structure is based on the 5-membered imidazole and imidazoline heterocycles (Fig. 1 **A**). As bridgehead functionality, the imidazol(in)-2-ylidene may lead to strained bite angles in a terdentate metal binding arrangement, a fact originating from the natural bite angle(s) [27] imposed by the 5-membered ring. In extreme cases, especially with highly rigid ligand structures, coplanar arrangement of the three donor groups and the metal is disfavored and hemilability [28] or adoption of bidentate coordination modes may be encountered. Conversely, pincer ligands comprising the bridgehead *classical* donor being part of five membered

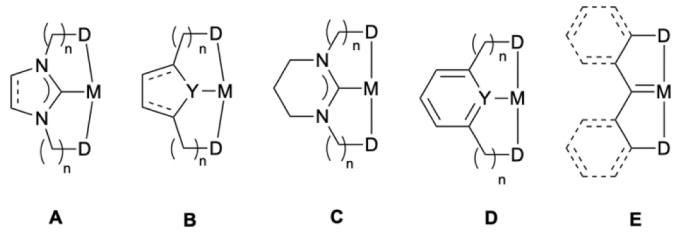

Fig. 1. Generic frameworks of pincer complexes with NHC (**A**, **C**), acyclic carbene (**E**), and classical neutral or anionic donors (**B**, **D**) at the bridgehead position.

ring heterocycle (Fig. 1**B**, Y = N, O, S *etc*.) are surprisingly less abundant.

For example, in the Cambridge Structural Database, *ca.* 450 structurally well-defined complexes of type **B** are found, with pyrrole (as pyrrolide, $Y = N^-$) being the most common representative. Within this group, examples of pyrrolide bridgehead with two phosphane or pyridine side-arm donors are singled out (*ca.* 160 and 40 examples for $D = PR_2$ and D = pyridine, respectively); the remaining comprise other 5-membered saturated or unsaturated heterocycles (with Y = O, S or N). In this analysis, macrocyclic species incorporating *'pincer' subunits* with related topology (*e.g.* subunits of porphyrin complexes) have been excluded. The fact that limited possibilities are available to electronically tune the pyrrole and other N, O, S donor rings is consistent with the relatively narrow scope of pincer ligands with 5-membered ring classical donors at bridgeheads. Analogously, tuning scope in systems with C^{NHC} bridgehead donor as part of a 6-membered ring (**C** in Fig. 1) is also limited, compared to counterparts with classical neutral or anionic bridgehead donors (**D** in Fig. 1, *e.g.* Y = N, pyridine, lutidine; $Y = C^-$, 1,3-phenylene *etc*.). Despite this obstacle, the structural types **C** and **D** constitute platforms to establish meaningful comparisons of the electronic structures and reactivities of complexes with C^{NHC} and classical donor bridgeheads, while maintaining other ligand topological deviations (natural bite angle *etc*.) to the minimum. Lastly, the acyclic carbene functionality as bridgehead donor (Fig. 1**E**) is at the center of some recent ligand design and M=C reactivity developments, but is electronically disparate from the NHC paradigm, exhibiting ambiphilic or radical reactivity [29–31]. Moreover, in Fig. 1**E** the geometrical constraints associated with the natural bite angle discussed above are relaxed and dissociated from the carbene functionality.

2.2. The tuneable HOMO-LUMO gap and the σ-donor-π-acceptor electronic properties of the NHC bridgehead donor (by selecting the NHC type)

Following the introduction of the imidazol-2-ylidenes and, subsequently, the development of a range of NHCs, their σ-donor/π-acceptor/π-donor electronic properties have been recognized and rationalized by manipulating the energies of HOMO and LUMO frontier orbitals as summarized in Fig. 2 [32–37]. Developing this knowledge to a pincer ligand design tool, albeit attractive, has not overtly been made. Tuning the donor characteristics of monodentate NHCs is reasonable through: (i) the choice of heteroatoms α-to the C^{NHC} (*e.g.* N, S, O, C in imidazol-, thiazol-, oxazol- *etc*.), (ii) the choice of the substituents of the N-heteroatom α-to the C^{NHC}, (iii) the choice of the heterocycle ring size, (iv) the choice of the functional groups of the heterocyclic ring at remote positions to the C^{NHC}, (v) the assembling of mesoionic NHC structures or (vi) the targeting of ylide-stabilized carbenes. The emerging diversity renders the electronic character of the carbene donor functionality from σ-donating of variable strength (calculated HOMO energies from −5.6 to 3.1 eV) and negligible π-accepting, to strong σ-donating and π-accepting (*e.g.* in cAAC and related moieties), to σ-donating and π-donating (*e.g.* in the 'cyclic bent allenes' and related). Although the extrapolation of data obtained from monodentate carbene donors to NHC-containing pincer structures may be an oversimplification, the reasoning given here shows the unprecedented versatility and tuneability scope and potential of a C^{NHC} bridgehead, probably not attainable in classical bridgehead donor functionalities.

Furthermore, the spatial anisotropy of the π-symmetry orbital of the C^{NHC}, in conjunction with the ability to modulate torsional angles between the NHC and the metal coordination planes and, consequently, the angle between the interacting π-C^{NHC}- and dπ-M orbitals by ligand tuning (*e.g.* by the choice of bridgehead-side-arm donor spacers), could lead to the tuning of π-type M−C^{NHC} interactions [38]. Thus, not only the inherent σ- and π-donating characteristics of an NHC moiety at the bridgehead position but also its orientation relative to the coordination plane are crucial levers to tailor metal – ligand interactions.

Interestingly, in the following detailed discussion, it will become evident that the mainstream of studies is mainly limited to the (benz)

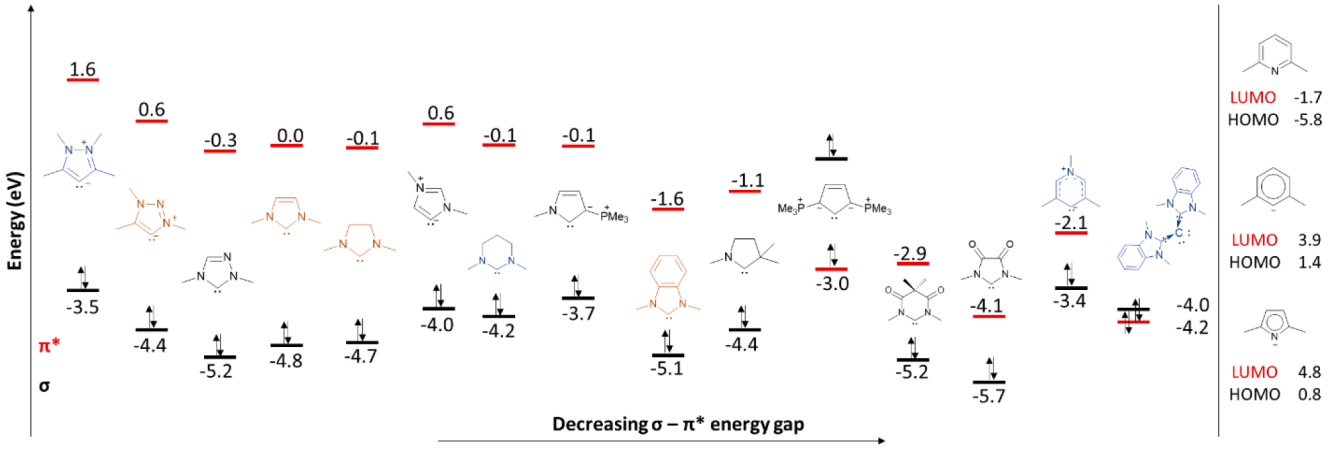

Fig. 2. Energy eigenvalues of molecular orbitals (at the BP86/def2-TZVPP level of theory) for commonly encountered mostly N-heterocyclic carbenes, along with the frontier orbital energies of three classical σ-donors (2,6-lutidine, 1,3-disubstituted-2-xylyl- and 2,5-dimethyl-pyrrolide) for comparison. The energy levels of the carbene lone pair (σ) and the unoccupied orbital (π*) are represented as black and red lines, respectively (for the carbodicarbene in red is the occupied π). It should be noted that the levels given do not necessarily correspond to the HOMO and LUMO; for example, in the imidazol-2-ylidene the π* carbon-centered orbital is the LUMO+1. From this collection of carbene functionalities in orange and blue are those that have been described in pincers as bridgehead as well as side donors and as bridgehead donors only, respectively; carbenes in black have not been encountered in pincer designs yet. The figure has been adapted from refs 32 and 33 and expanded. It is worth noting that for certain structural types shown, more than one resonance forms are plausible and significant, and therefore the electron distribution conveyed as written is not precise and unambiguous.

imidazol(in)-2-ylidene functionalities, with only recent interest intensifying in 6-membered NHCs ring expanded (RE-NHC) and 1,2,3-triazolylidenes (see Fig. 2). Moreover, pincer ligand complexes with carbodicarbene, carbodiphosphorane and cyclic bent allene frameworks have recently been realized [39,40]. Understandably, due to the structural peculiarities of the bridgehead heterocycle, cAAC, abnormal NHC (aNHC) and other inherently non-symmetrical bridgehead structures in pincer ligands may not be amenable to straightforward, rational design or isolation as 'bottleable' entities; in these cases, *in-situ* generation and transmetalation complexations may become more widespread. Some of these possibilities as applied to pincer structures will be illustrated below.

2.3. The NHC-donor at the bridgehead exerts distinctive effects on other coligands

These effects can be expressed as observable structural features or variations in reactivity. Importantly, such a behavior may discern pincer ligands with NHCs at the bridgehead and the side-arms. Accordingly, in the former type of pincers, the well-known high *trans*-influence and *trans*-effect of the NHC functionality is directly exerted towards a potentially catalytically relevant coordination site, whereas in the latter type of pincers, they may result in weaker binding along the side-arm donors vector or in hemilability. Although the nature of these arguments is easily noticed empirically, their prediction, occurrence and quantification may require computational approaches.

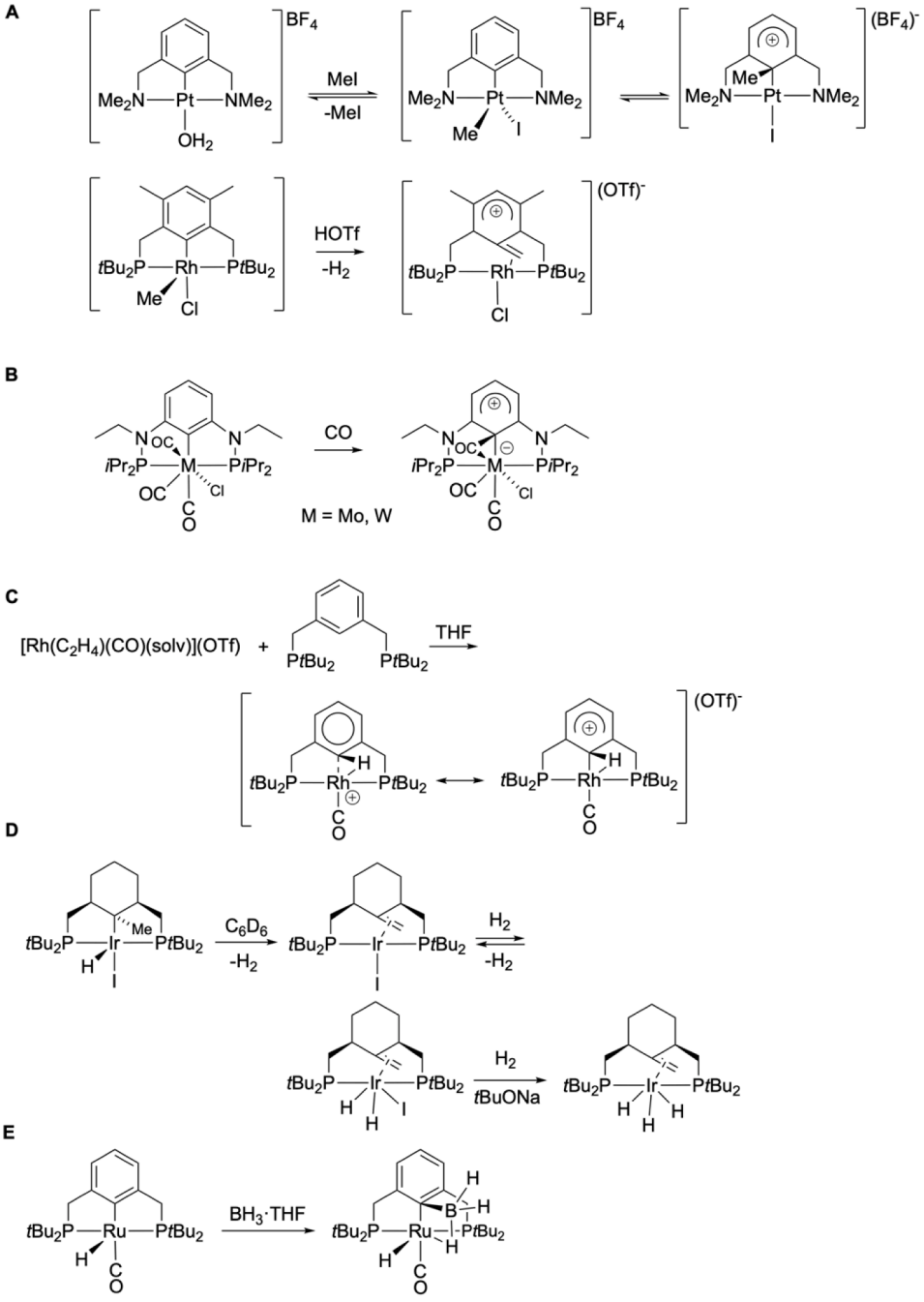

Scheme 1. The reactivity of pincer complexes with non-NHC bridgehead donor: bridgehead-atom participation in reactions leading to substrate activation or catalyst deactivation.

2.4. The positioning of classical donors at the pincer bridgehead may have implications on reactivity, reaction mechanisms and metal–ligand cooperativity

This point may be exemplified firstly, in the non-NHC regime, where it is pertinent to mention: (i) the stoichiometric reactivity of 1,3-phenylene pincer complexes of platinum or ruthenium with electrophiles such as CH_3I or diazomethane leading to arenium complexes (Scheme 1**A**) [41–43]; (ii) the migration of CO in Mo/W carbonyls (Scheme 1**B**) [44]; (iii) the formation of η^2 C−H agostic arene complexes in complexation, hydrogenation and C–H activation reactions (Scheme 1**C**) [45]; (iv) the α-hydrogen and α-alkyl elimination in P,C(sp^3),P Ir pincers (Scheme 1**D**) [46]; and (v) the B-*ipso* donor interaction in borohydride species also found in amine-borane dehydrogenation reaction (Scheme 1**E**) [47,48].

Consequently, in the NHC bridgehead donor regime there are few recent reports, where the C^{NHC} can be the recipient atom in group migration reactions from the metal (the migrating group usually being hydride, alkyl or incipient alkyl) [49–55], formally converting, occasionally reversibly, the NHC into an alkyl functionality (Scheme 2**A** – **C**). Conversely, azolium-to-NHC transformations by low valent metals may proceed *via* anionic alkyls at the bridgehead position (Scheme 2**D** and **E**) [54,56]. Migratory insertion has been rarely observed in pincers with NHC side-arms [57,58] but reductive elimination of alkyl imidazoliums has been more common in this case. A related transformation, which lies at the origin of ligand/metal (Ni) cooperativity and NHC non-innocence is encountered in the N–H activation of NH_3 that occurred by the formal 1,2-addition of the N–H across the M−C^{NHC} moiety, but more likely involving heterolytic activation, where the NHC moiety acts as proton acceptor (Scheme 2**F**, right) [59]. Activation of a variety of E−H bonds (E = H, C, N, O) by addition across the Ni–C^{NHC} has been reported in

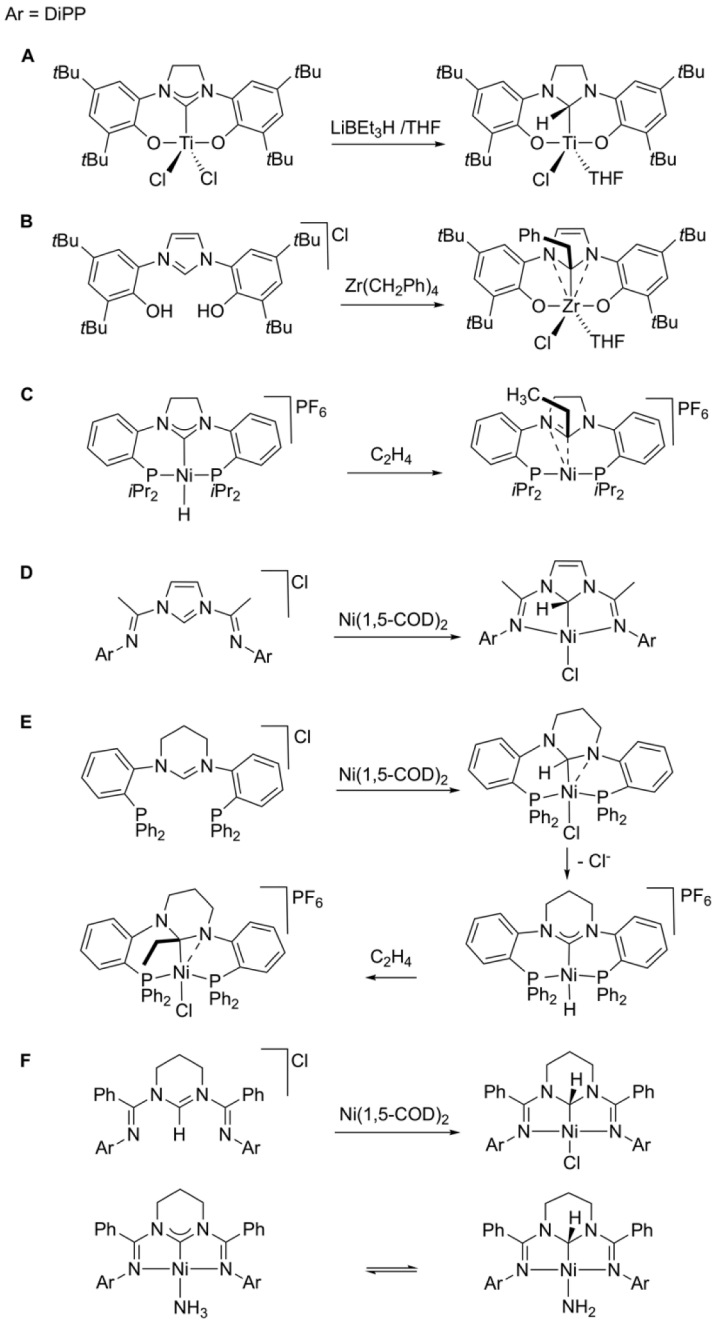

Scheme 2. The reactivity of pincer complexes with NHC bridgehead donor: migration reactions from metal to the C^{NHC}.

pincer alkyl carbenes (*i.e.* not NHC), and therefore the organometallic products resemble in some ways to the NHC-bearing pincers discussed above. Here too, the activation steps could be reversible, which is potentially an attractive feature in catalysis [60]. Furthermore, the high σ-donating character of the central carbon moiety labilizes the ligand in the *trans* position, which could be another attractive feature for the development of catalytic reactions (*vide supra*). Pincer ligands with alkyl carbenes and ambiphilic carbene bridgehead functionality (*i.e.* exhibiting electrophilic, radical or nucleophilic character) have been excluded from this review, however some comparisons between them and the nucleophilic NHC bridgeheads spring up occasionally [30].

2.5. Strength of the overall metal-ligand binding

As mentioned above, the tunable frontier orbitals of the NHC are expected to give metal-donor interactions of variable degree. However, the strength of the overall metal-ligand binding is the outcome of a combination of stereoelectronic factors, which could be linked to the binding space provided by the pincer, the orbital overlap permitted by geometrical ligand constraints and the electronic interaction of the donors between each other and the metal. This may occasionally become apparent as a measurable physical property of the complex (*e.g.* spectroscopic or magnetic behavior), rarely as disparate structural features (*e.g.* significant variation of metrical data) and finally as reactivity changes. Good insights and estimation of the overall metal-ligand binding could also be gained by comparative computational studies of related complexes, where global bonding models could be correlated and rationalized. As a proof of concept, the bonding analysis of the related complexes ((**a**) and (**b**) in Chart 3) was carried out; the observed ground state spin states ($S = 1$ and 2, respectively) have been attributed to tighter binding to the metal of the pincer with one NHC bridgehead donor in (**a**) rather than the one with two NHC side-arm donors in (**b**) [61]. Similar analyses may define precise and sometimes unexpected pincer ligand effects.

In the following, we adhere to a ligand-based organization of the topic, firstly partitioning the ligand family in three broad categories bearing one, two or three NHC donors. Subsequently, within each broad category we rank the ligands with ascending column number of the Periodic Table to which the non-NHC (*i.e.* side-arm) donor atoms belong. For the three most represented families of symmetrical pincer ligands, *i.e.* with oxygen, nitrogen and phosphorus donor side-arms, additional ligand classification based on the backbone motif has also been adopted. Within each group of the Periodic Table, the metals are organized with ascending group number from the left to the right; occasionally and for comparison purposes, different metals belonging to the same group of the Periodic Table are discussed together. Finally, the catalytic applications and the existing computational studies of the complexes are mentioned in the text and summarized at the end in a tabular form to provide the reader with an easier overview.

3. Pincer ligands with one NHC donor

3.1. Type C,C^{NHC},C

Most complexes in this section were obtained by metalation reactions (usually thermally induced) of the side-arms of suitably substituted NHCs. Understandably, complexes with noble metals (Ru, Os, Ir and Pd) that can be involved in facile metalation reactions are exclusively encountered. Some examples featuring polyhapto-carbon ligands have also been reported.

3.1.1. Group 8 metals (Ru, Os)

Two Ru complexes with the dianionic C,C^{NHC},C pincer were obtained by the metalation of the *o*-methyls of the IXyl substituents of the NHC (Scheme 3). Reactions of the monocyclometalated complex **1** with one equivalent of base ($LiCH_2SiMe_3$ or KCH_2Ph) gave the complexes **2** and **3**. The molecular structure of **2** revealed a coordination polymer with a repeat unit featuring two RuCp*(IXyl) subunits bridged *via* one Li^+ cation bound to the two cyclometalated C atoms of one Ru center and the η^5-Cp* ring of the neighboring molecule. The related mononuclear complex anion in **3** also exhibited a doubly-cyclometalated NHC [62,63].

Thermolysis of the Grubbs catalyst analogue **4** with *N,N'*-diphenylbenzimidazol-ylidene (Scheme 4) gave two complexes: **5**, resulting from the insertion of the benzylidene functionality into the *o*-C-H of the NHC phenyl side-arm, and traces of **6** featuring the metalated C,C^{NHC},η^6-C-donor set. Mechanistic studies concluded that the metalation of **5** was affected by the reaction with PCy_3 acting as a base. The η^6-hapticity of the benzyl-substituent was revealed crystallographically (Scheme 4) [64,65].

Complex **8** featuring one doubly cyclometalated dianionic NHC was synthesized by thermally-induced multiple metalation steps from the imidazolium precursor **7** and [Ru(methylallyl)$_2$(COD)] in the presence of KO*t*Bu (Scheme 5) [66]. The structure of **8** also revealed the presence of one η^4-naphthyl bound to Ru. Complex **8** was used as a precatalyst for the highly enantioselective asymmetric hydrogenation of substituted thiophenes [67], benzothiophenes [67], (hetero)arenes [66] and 2-oxazolones [68] (see Section 7).

A rare charge-neutral Os complex **10** was obtained from the hexahydride [$OsH_6(PiPr_3)_2$] and the NHC precursor **9** (Scheme 6) [69]. The κC,κC^{NHC},κC nature of the metalated ligand resulted from *ortho*-CH bond activation of both phenyl substituents of **9**. In solution at room temperature, a symmetrical structure was evidenced by the magnetic equivalence of the two hydrido ligands, the two metalated phenyl groups and the two phosphanes (triplet at δ −5.96, $J_{H\text{-}P} = 19.0$ Hz, triplet at δ 149.8 ppm, $J_{C\text{-}P} = 6.3$ Hz and singlet at δ 10.5 ppm) in the ^{1}H, ^{13}C and ^{31}P{^{1}H} NMR spectra, respectively.

3.1.2. Group 9 metals (Ir)

The iridium complexes **15**, **16**, **21**, **22** and **24** (Schemes 7 and 8) comprise (C,C^{NHC},C) neutral pincer ligands with imidazol-2-ylidene

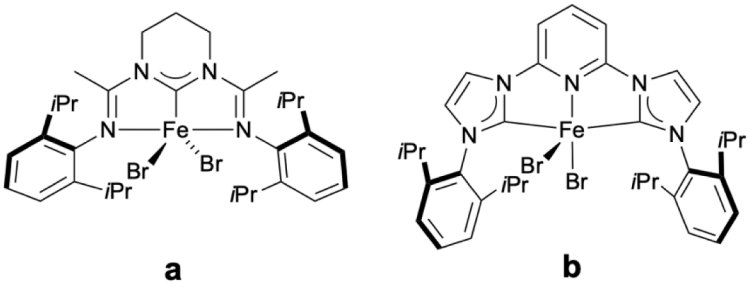

Chart 3. Two iron pincer complexes containing NHC moieties in different positions and 6-membered heterocycles in bridgehead position. The labels c and d refer to the corresponding generic frameworks depicted in Figure 1.

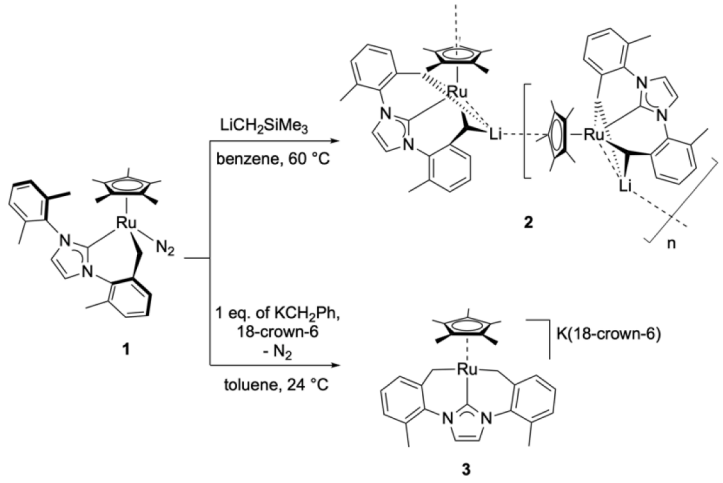

Scheme 3. Synthesis of two Ru complexes by C-H activation.

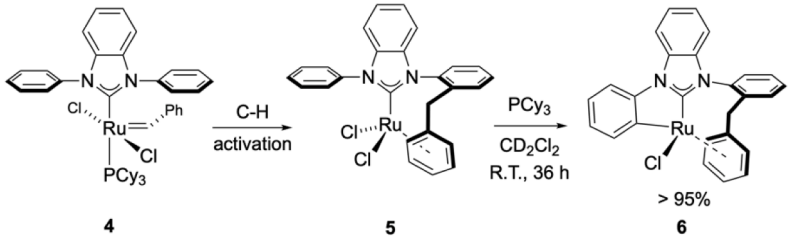

Scheme 4. Synthesis of Ru complexes by C-H activation

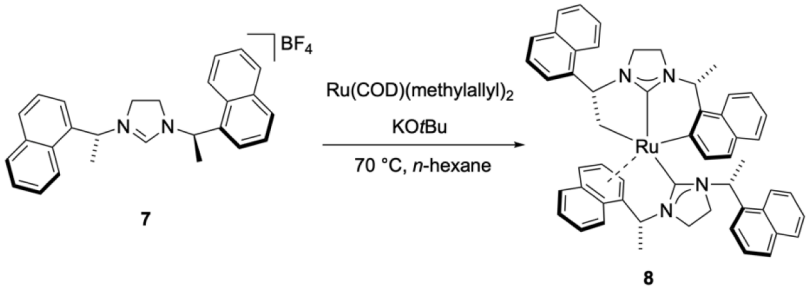

Scheme 5. Synthesis of Ru complex **8** by thermally induced metalation.

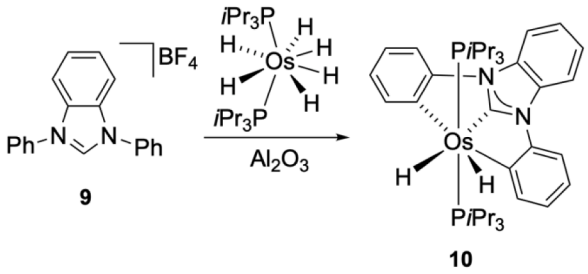

Scheme 6. Synthesis of Os complex 10 resulted from C-H activation.

bridgehead and two η^2-alkene side-arms. Except for **24**, they were prepared in two step reaction sequences (Scheme 7) [70–72]. The NHC donors originated from the precursors **11**, **12** and **17**, **18** and were introduced to the Ir following a coordinated base (*i.e.* Ir-OMe) and silver transmetalation protocols, respectively. NHC binding in **13, 14** and **19**, **20** was accompanied by the adoption of the chelating bidentate (κC^{NHC}, η^2-allyl) coordination mode with one bound and one dangling allyl groups. Following halide abstraction, the ligand rearranged to the

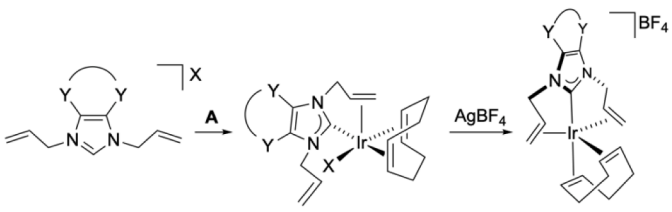

11 X = Br, Y⌒Y = $(CH)_4$
12 X = Br, Y = H
17 X = PF_6, Y = Cl
18 X = Cl, Y = CH_3

13 X = Br, Y⌒Y = $(CH)_4$
14 X = Br, Y = H
19 X = Cl, Y = Cl
20 X = Cl, Y = CH_3

15 Y⌒Y = $(CH)_4$
16 Y = H
21 Y = Cl
22 Y = CH_3

Reagents and conditions:
For **11,12** A: $[Ir(\mu\text{-OMe})(1,5\text{-COD})]_2$;
For **17,18** A: (i) Ag_2O, MeOH; (ii) $[Ir(\mu\text{-Cl})(1,5\text{-COD})]_2$, CH_2Cl_2, 45 °C

Scheme 7. Synthesis of Ir complexes with C,C^{NHC},C backbone

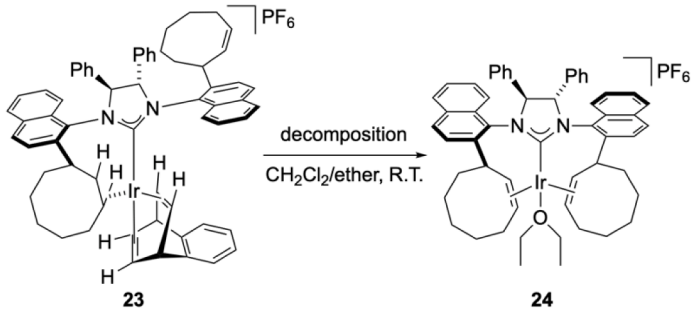

Scheme 8. Synthesis of Ir complex **24** involving a double hydrogenation

formally terdentate (κC^{NHC}, η^2-allyl-, η^2-allyl-) coordination mode. The increased strength of the NHC binding in **15** and **16** compared to **13** was demonstrated by the relevant short Ir–C^{NHC} bond distances determined crystallographically (1.942(2) and 2.015(3) Å, respectively); this may be attributed to chelation and/or reduction of steric interligand interactions around the metal.

The remarkable complex **24** with the C_2 symmetric NHC-bis(alkene) ligand was synthesized by the spontaneous decomposition of **23** in a mixture of CH_2Cl_2 and ether solvents (Scheme 8) [73]. In **24** too, the relatively short Ir–C^{NHC} bond distance (1.944(6) Å) was attributed to the release of steric constraints and the chelate effect (*cf.* complexes **15**, **16**, **21** and **22** above). The transformation of **23** to **24** probably involved a double dehydrogenation sequence of the two pendant cyclooctyl groups, preceded by the liberation of 1,2,3,4-tetrahydro-1,4-ethanonaphthalene.

The iridium complexes **26**–**30** (Scheme 9) and **32** (Scheme 10) bearing the dianionic C,C^{NHC},C-terdentate ligand formally originating by the metalation of two *o*-methyl groups of the IMes, were obtained by C–H activation reactions [74,75]. The complexes **26**–**30** were prepared in good yields by treating the IMes complex **25** with propylene (acting as hydrogen acceptor) in the presence of the reagents shown in Scheme 9 resulting in double metalation of the IMes [74]. The zwitterionic complex **27** and **28** were characterized by X-ray diffraction. Interestingly, although **26**–**29** were accessed by trapping *in situ* formed Ir species associated with the dehydrogenation of **25**, they did not react with dihydrogen or other hydrogen sources in a reverse sense of the cyclometalation process. In contrast, **30** obtained from **28** by substitution of one MeCN donor by P*i*Pr$_3$ reacted with conventional hydrogen sources, implying that these reaction(s) may involve oxidative addition steps to Ir^V intermediates, in which case P*i*Pr$_3$ could render the metal in **30** easier to oxidize or stabilize the relevant intermediate(s).

Complex **33** with the same pincer scaffold as **26**–**30** was prepared from **31** by the reaction with Na(BAr$^F_4$) and Me_3N-BH_3, which resulted in double metalation of the IMes (Scheme 10) [75]. The Ir^{III} species **32** featuring the dianionic C,C^{NHC},C pincer and one neutral IMes tethered to the metal with additional agostic interactions, was obtained by Cl^- abstraction from **31** with Na(BAr$^F_4$) and was characterized crystallographically; complex **32** was also used as precursor to **33** by reaction with Me_3N-BH_3 and was postulated as intermediate for the conversion of **31** to **33**.

Complex **35** (of limited thermal stability) was formed by the C-H metalation of precursor **34** with [Ir(μ-Cl)(COD)]$_2$ in the presence of LiHMDS (Scheme 11) [76]. The characteristic ^{1}H NMR signal of the Ir–*H* was observed at δ_H −10.58 ppm. In the crystal structure of **35**, the Ir-C^{NHC} bond length was 1.967(8) Å, within the normal range of Ir–C^{NHC} bonds [77]. In addition, the Ir–Csp^2 covalent bond length was 2.118(8) and 2.123(9) Å, respectively. Reaction of complex **35** with K_2CO_3 in $CHCl_3$ led to the clean formation of **36**, which on reaction with AgOTf in CH_2Cl_2 gave **37** [76]. Complexes **36**–**37** were characterized by NMR spectroscopy and X-ray diffraction analysis (Scheme 11). Complex **36** was active in homo- and hetero-addition of styrene derivatives and remote olefin isomerization.

Complexes **41**–**44** bearing C,C^{NHC},C-terdentate ligands were also reported (Scheme 12) [78]. A complex mixture containing complex **41** was prepared by treatment of complex **40** with Cs_2CO_3 in acetonitrile under reflux, the latter was obtained from [Ir(μ-Cl)(COD)]$_2$ with the free carbene **39**. Unfortunately, complex **41** could not be isolated and crystallization of the reaction mixture afforded **42** featuring two pincer ligands, as a dark-purple solid. Complex **42** could also be obtained by treatment of **38** with [Ir(μ-Cl)(COD)]$_2$ and an excess of Cs_2CO_3. No C–H bond activation intermediates (complex **41**) was isolated in the transformation of **40** or **38** to complex **42**, suggesting a rapid coordination of a second NHC ligand. In the ^{13}C NMR spectrum, singlets at δ_c 151 ppm

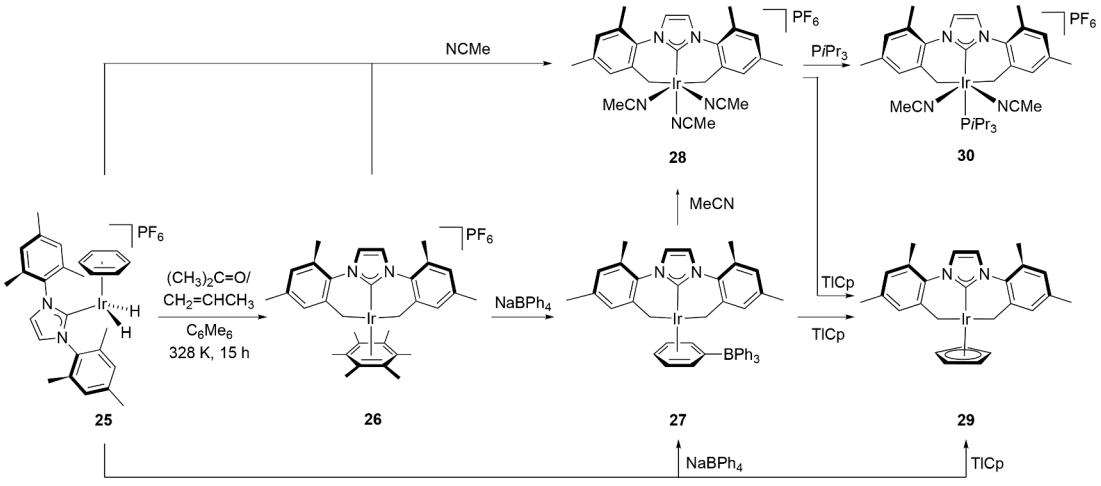

Scheme 9. Synthesis of Ir complexes by C-H activation

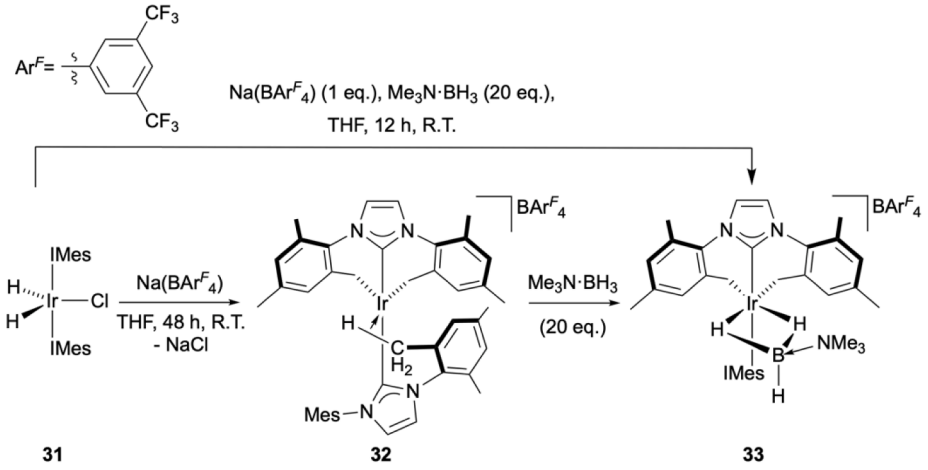

Scheme 10. Synthesis of Ir complexes by C-H activation.

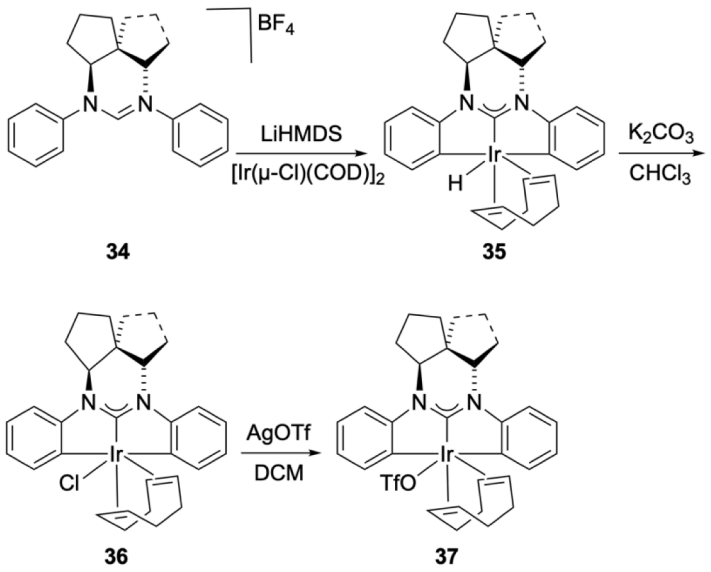

Scheme 11. Synthesis of Ir complexes by C-H metalation

and δ_c 159.78 ppm were assigned to the C^{NHC} and Ir–Csp^2, respectively. The crystal structure of **42** revealed an anionic octahedral bis(κC, κC^{NHC}, κC) iridium complex with S_4 symmetry; a Cs^+ cation bridged two aryl groups. The Ir-C^{NHC} bond length of 1.990(5) Å was shorter than the Ir–Csp^2 (at 2.109(4) and 2.092(3) Å). This feature is consistent with data for octahedral iridium(III) complexes containing all κ-C ligands [79,80]. A XANES experiment was performed to confirm the oxidation state of the Ir center and showed a strong absorption peak assignable to the 2p → 5d electronic transition of intensity similar to that of an Ir^{III} reference compound. Complex **43** was prepared by recrystallizing **42** in the presence of 2,2,2-cryptand. Treatment of complex **42** with Et_3N·HCl resulted in the clean formation of **44**. Its structure showed that an Ir-C bond cleavage reaction had occurred by protonation of an aryl group, resulting in a square-pyramidal coordination geometry at the metal.

An early report on the photo-physics of cationic, homoleptic bis-pincer iridium(III) carbene complexes [Ir(C^{NHC}C C^{NHC})$_2$]$^+$, with a phenylene bridgehead group, showed that they are efficient near-UV emitters [80].

3.1.3. Group 10 metals (Pd)

The reaction of the precursor **45** with [$PdMe_2$(TMED)] in the presence of KO*t*Bu at 50 °C afforded the complex **48** as a result of the activation of the two sp^2 aromatic C-H bonds from the NHC side-arms (Scheme 13) [81]. This pincer framework characterized by the two five membered chelate rings is rare and has only been observed in the Os complex **10** with the related benzimidazole-based ligand discussed above. Mechanistic insight into the transformation of **45** to **48** was obtained by performing the reaction at 0 °C, where **46** was isolated in 83 % yield. When the temperature was raised to 30 °C, **46** was reduced to the Pd^0 complex **47** and ethane was released. Finally, at 50 °C, **47** could be converted to **48**. These experiments suggested that the formation of **48** may proceed initially *via* Pd^{II}/Pd^0 elementary steps although the exact redox changes of palladium in the two subsequent metalations have not been established experimentally. This sequence of events has not been demonstrated with other metal centers.

The unusual Pd complex **49** with tetradentate *ortho*-metalated ylides in a pincer scaffold was obtained in 65 % yield as a 75/25 mixture of two diastereomers by treating the corresponding imidazolium ylides with $PdCl_2$ in the presence of an excess of Cs_2CO_3 in MeCN (Scheme 14) [82]. The evidence for the existence of two diastereomers was provided by ^{31}P NMR spectroscopy, where the two sets of resonances (major: δ_P 28.2 ppm (br s), 29.2 ppm (br s); minor: δ_P 23.3 ppm (s), 31.1 ppm (s)) were assigned to the two diastereomers. The characteristic signal of the *o*-metalated carbon atom was observed at δ_C 183.5 ppm (d,

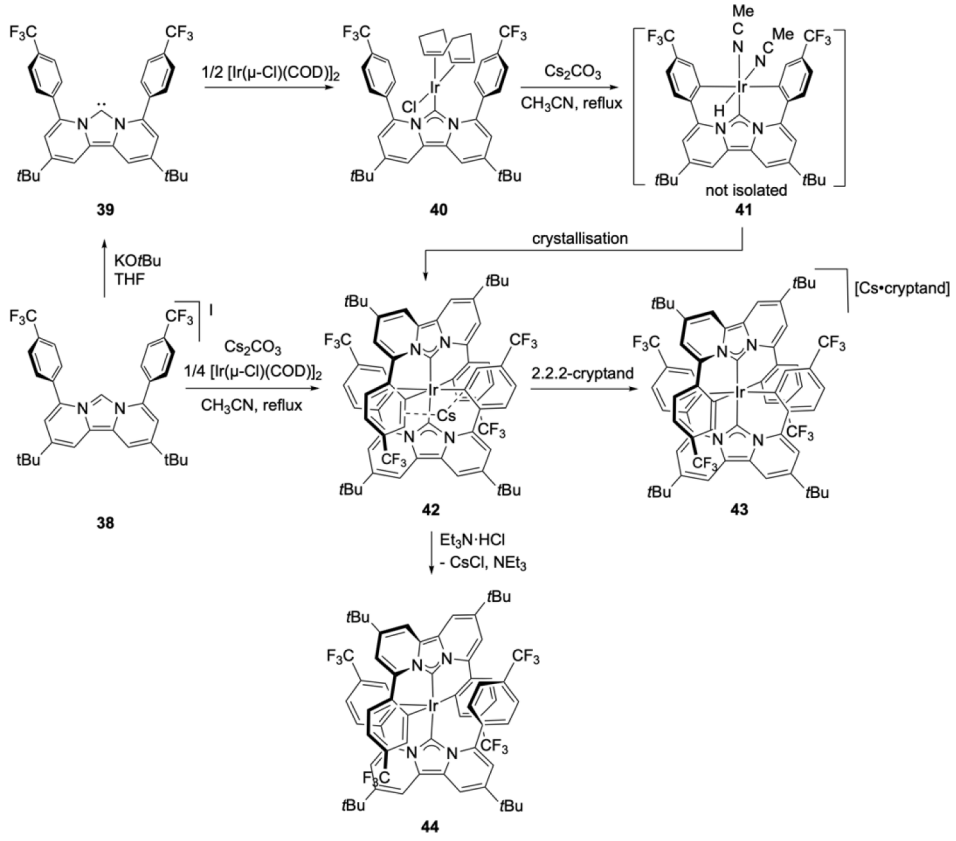

Scheme 12. Synthesis of Ir complexes by C-H activation.

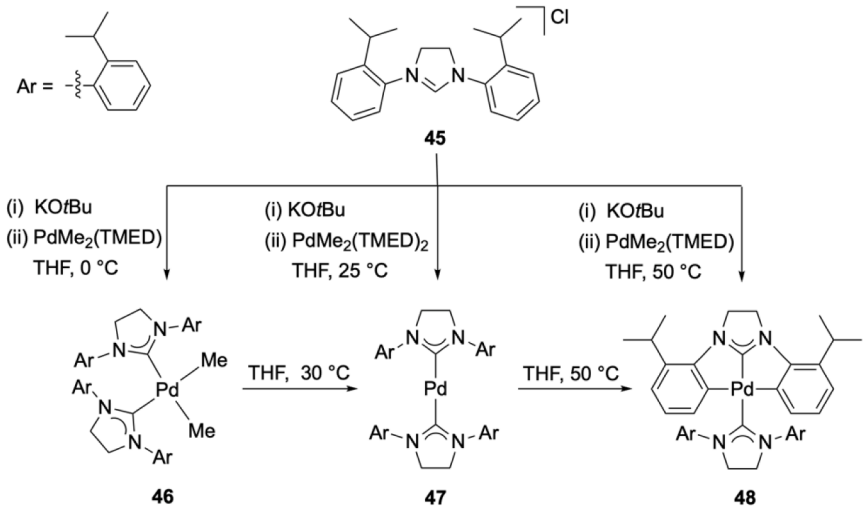

Scheme 13. Synthesis of Pd complexes involving C-H activation.

$^{2}J_{CP} = 36.2$ Hz). Reaction of **49** with one equivalent of HOTf resulted in the formation of the air-stable Pd^{II} pincer complex **50**, isolated again as a 75/25 mixture of two diastereomers, of which *dl*-**50** was characterized by X-ray diffraction [82]. The ^{31}P NMR spectrum of the reaction mixture contained two singlets (minor: δ_P 32.7, major: δ_P 33.8 ppm). Complex **51** was obtained by the reaction of **50** with *t*BuNC. The structure of both diastereomers of **51** could be determined by X-ray diffraction. Similarly, the complex **52** was obtained in 90 % yield after exposure of **50** to a CO atmosphere. The ^{31}P NMR spectrum showed two new singlet resonances (minor: δ_P 33.3 ppm, major: δ_P 35.7 ppm). The ^{13}C NMR spectrum showed two deshielded signals attributable to the CO group (minor: δ_C 181.4 ppm (brs), major: δ_C 183.2 ppm (t, $^{3}J_{CP} = 5.0$ Hz)), suggesting that CO was coordinated to the Pd center [82].

3.2. *Type C,C^{NHC},N*

In all entries of this section the side-arm C-donor originates from (cyclo)metalation reactions of aryl/alkyl substituents in bidentate NHC ligands functionalized with a classical heterocyclic pyridine donor.

3.2.1. *Group 8 metals (Fe, Ru)*

The iron and ruthenium complexes **56** [83] and **57** [84] bearing C,

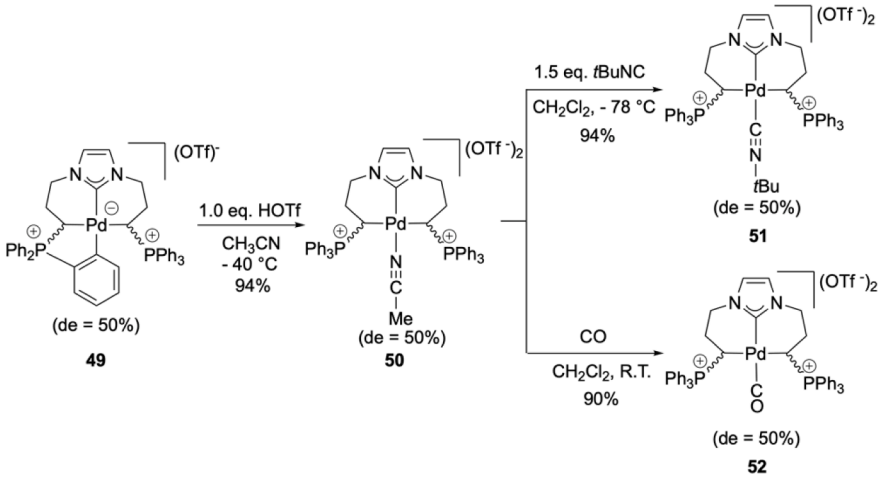

Scheme 14. Synthesis of bis-ylide Pd complexes bearing a C,C^{NHC},C backbone

C^{NHC},N-pincer ligands were prepared in two steps by deprotonation of the imidazolium salt **53** with KO*t*Bu to generate *in situ* the corresponding bidentate NHC, which was then reacted with the precursors [FeClCp*(TMED)] and $[RuClCp^*]_4$ to afford **54** and **55**, respectively, with bidentate (κN, κC^{NHC})-picoline functionalized NHC ligation. Subsequent reaction of **54** and **55** with one equivalent LiHMDS led to **56** and **57**, respectively, both featuring terdentate pincer binding, after base-initiated metalation of an *o*-methyl of the NHC mesityl substituent (Scheme 15). Both **56** and **57** exhibit a diagnostic AB-pattern in the region of δ 4.5–4.0 ppm in the ^{1}H NMR spectra assignable to the diastereotopic methylene protons of the picolinyl functionality. Interestingly, the attack of the base is on the *o*-Me of the mesityl group rather than on the picolinyl methylene. Complex **56** was found to be highly active for the *gem*-specific catalytic dimerization of terminal alkynes [23,83,85].

3.2.2. Group 9 metals (Rh, Ir)

Complex **62** was synthesized in acetonitrile from the Cu complex **58** and $[Rh(\mu\text{-}Cl)(1,5\text{-}COD)]_2$ by transmetalation of the bidentate ligand, in a sequence presumably involving spontaneous rollover C–H bond activation and metalation of the pyridine ring (Scheme 16) [86]. In **62** the Rh–C^{NHC} bond distance is short (1.903(3) Å, *cf.* 2.03(4) Å average for Rh–C^{NHC}). The mechanism of formation of **62** is unclear, in particular in view of the fact that the transmetalation reaction takes a different course in THF (see Section 3.6). However, it has been proposed that **58** first reacted with $[Rh(\mu\text{-}Cl)(1,5\text{-}COD)]_2$ to form the intermediate **59**, with a κN, κC^{NHC}, κN ligand binding at the Rh^I center, which could undergo rollover cyclometalation to generate the final Rh^{III} product by C–H bond oxidative addition. Reductive elimination of HI would convert **60** to **61** which generates the isolated **62** upon oxidation with CuI.

The non-isolable iridium complex **64** was prepared by the reaction of the well-defined Crabtree's hydrogenation catalyst analogue **63** with CD_3CN (Scheme 17). In this solvent, the transient Ir–H species formed by the initially activated C–H bond of the *t*Bu wingtip was reversibly quenched by the C=C double bond of the coordinated 1,5-COD to generate the cyclooctenyl Ir^{III} complex **64**, the structure of which was established by NMR spectroscopic techniques. Reaction of **64** with CO *in situ* resulted in the displacement of CD_3CN and the formation of **65**. Furthermore, diphenylacetylene can be used in CH_2Cl_2 as an external hydride acceptor (*in lieu* of 1,5-COD) to give the crystallographically characterized complex **66** [87].

3.2.3. Group 10 metals (Pd)

Reaction of the salt **67** with $[Pd(OAc)_2]$ in refluxing MeCN yielded the κC, κC^{NHC}, κN-terdentate pincer complex **68** with a square planar Pd coordination geometry, *via* an unusual cyclometalation involving the

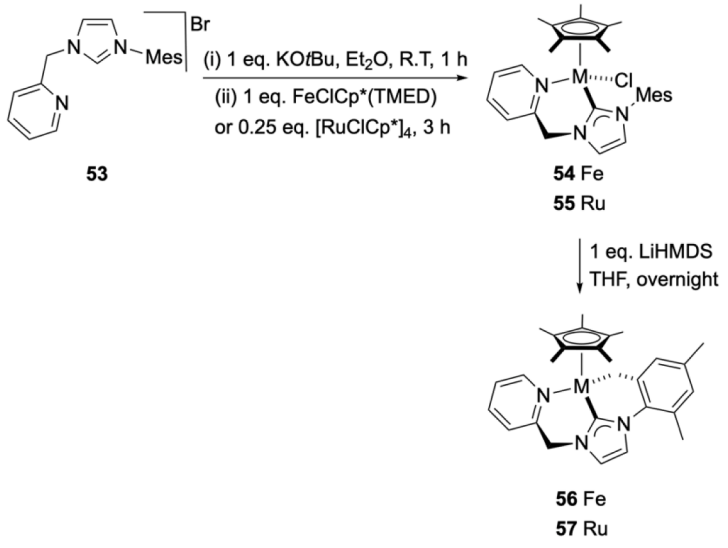

Scheme 15. Synthesis of Fe and Ru complexes by base-initiated metalation

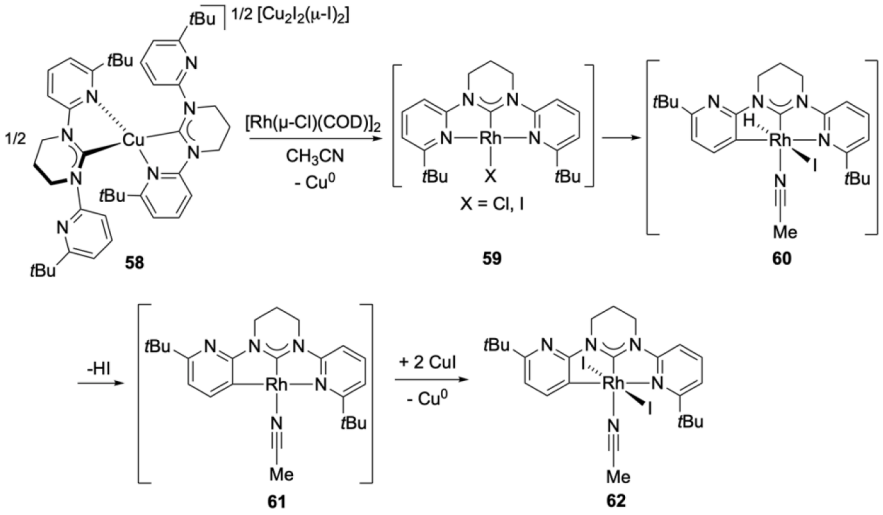

Scheme 16. Synthesis of Rh complexes resulted from Cu complex transmetalation.

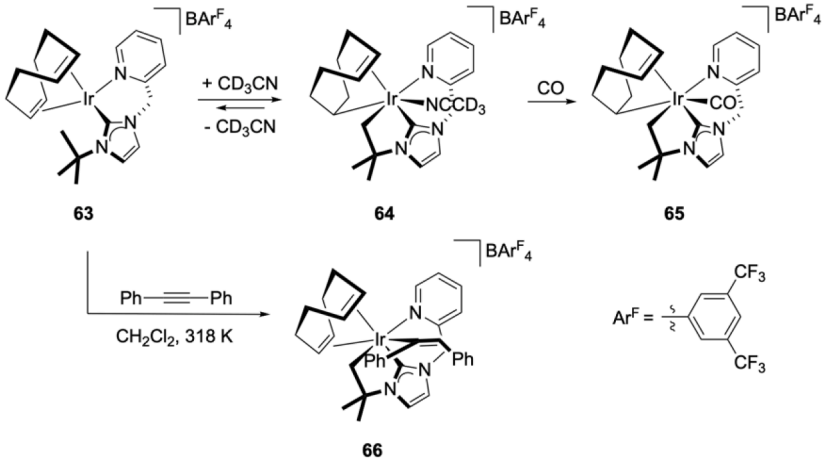

Scheme 17. Synthesis of Ir complexes resulting from C–H bond activation

terminal C–H of the allyl group. In an experiment performed under high dilution conditions, aimed at investigating the mechanism of the palladacycle formation, the δ-alkenyl *endo*-palladacycle **68** was obtained exclusively, pointing to the involvement of an internal acetate base-promoted intramolecular Csp^2–H bond activation (Scheme 18) [88].

3.3. Type C,C^{NHC},P

In common with the examples discussed in the previous sections (3.1 and 3.2), the majority of the entries included in the present section arises from metalation reactions in bidentate ligands with κC^{NHC},κP donors; consequently, noble metals are the only representatives.

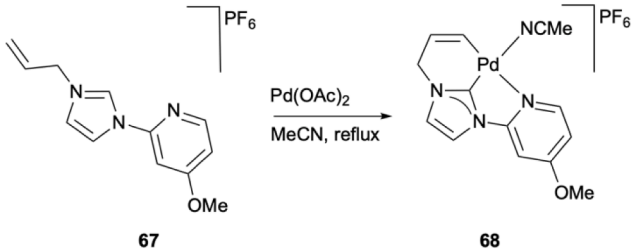

Scheme 18. Synthesis of Pd complex **68** by Csp^2–H bond activation.

3.3.1. Group 8 metals (Ru)

The only Ru^{II} complex **70** with a κC, κC^{NHC}, κP-pincer ligand was obtained by transmetalation to $[Ru(\mu\text{-}Cl)Cl(CO)_3]_2$ from the corresponding silver NHC complex that was generated by *ortho*-metalation of the phosphane-functionalized bisimidazolium salt **69** (Scheme 19) [89]. It was characterized by X-ray diffraction analysis and NMR spectroscopy. The ruthenium center in **70** is in a distorted octahedral environment, with Ru–C^{NHC} and Ru–C^{Ph} bond distances of 2.066(3) and 2.129 Å, respectively, consistent with a Ru–C covalent bond. The Ru–C^{NHC} signal in the ^{13}C NMR spectrum appeared as doublet at δ 154.4 ppm. Complex **70** was active in transfer hydrogenation of ketones at 82 °C in 2-propanol in the presence of KO*t*Bu [89].

3.3.2. Group 9 metals (Rh)

The complexes **74a** and **74b** which contain a C,C^{NHC},P-terdentate ligand were obtained by heating the pincer complexes **72** and **73** in toluene at 60 °C, respectively (Scheme 20A) [90,91]. The ^{31}P NMR spectrum of **74a** showed a pair of doublets of doublets (ABX pattern) at δ 53.7 ppm ($J_{RhP} = 97$ Hz, $^2J_{PP} = 31$ Hz) and 38.3 ppm ($J_{RhP} = 86$ Hz, $^2J_{PP} = 31$ Hz). The solid-state structures of **74a** and **74b** unveiled a rare P–C_{aryl} bond cleavage and insertion of the P*i*Pr_2 fragment into the Rh–H and Rh–CH_3 bonds, respectively; the elementary steps leading to these insertions were proposed to be oxidative addition of the C_{aryl}–P bond followed by H–Rh–P*i*Pr_2 or CH_3–Rh–P*i*Pr_2 bond reductive elimination. It

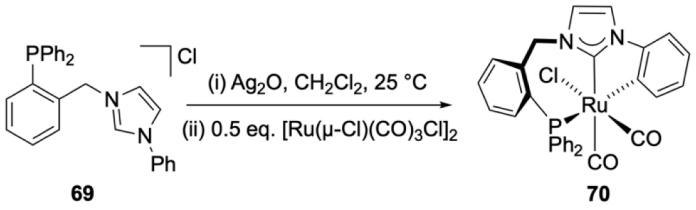

Scheme 19. Synthesis of Ru complex **70** by transmetalation reaction

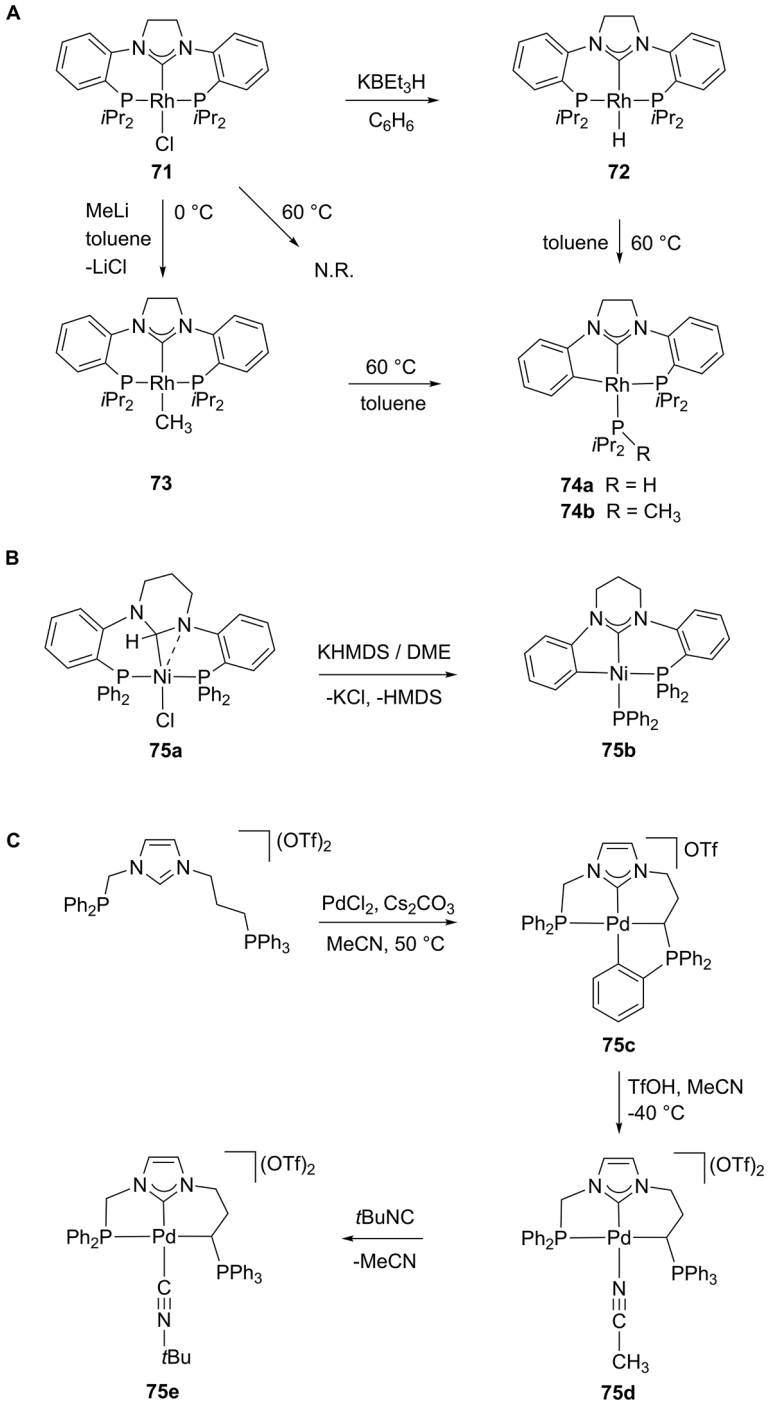

Scheme 20. Synthesis of Rh (**A**), Ni (**B**) complexes involving a rare P–C cleavage reaction and the Pd complexes with $PC^{NHC}C^{ylid}$ ligation (**C**)

is relevant to note that a related C,C^{NHC},P pincer ligand, with a RE-NHC donor group, was recently generated in the Ni(II) complex **75b** as a result of a similar P–C$_{aryl}$ bond activation and a still rare example of terminal phosphanido ligand on Ni was isolated and fully characterized (Scheme 20B) [56].

3.3.3. Group 10 metals (Ni, Pd)

As mentioned in section 3.3.2 above, a Ni^{II} complex with a C,C^{NHC},P pincer ligand containing a RE-NHC donor was recently obtained by P–C^{aryl} bond activation with concomitant generation of a terminal phosphanido ligand (Scheme 20 **B**) [56].

Furthermore, phosphine-NHC-phosphonium ylide pincer ligands have been introduced to Pd centers *via* the methodology depicted in Scheme 20C (*cf.* Schemes 14, 22 and 152 for related transformations). The non-symmetrical phosphine phosphonium precursor was swiftly triply metalated at the imidazolium carbon, the ylidic C and one P–*Ph* by $PdCl_2$ in the presence of Cs_2CO_3 as base following an initial coordination of the PPh_2 arm giving the very stable complex **75c** that was characterized by multinuclear NMR techniques. Selective protonolysis of the Pd–C^{aryl} of the cyclometalated aryl by triflic acid under controlled conditions in MeCN gave the complex **75d** featuring a non-symmetrical pincer ligand with phosphine and ylidic side-arms and coordinated MeCN trans to the C^{NHC}; facile substitution of the latter by *t*BuNC led to complex **75e** (*cf.* complex **51** in Scheme 14). Inspection of the coordinated *t*BuN≡C IR stretching frequency in **75e** provided evidence that the PC^{NHC}C^{ylid} pincer ligand exerts an electronic influence on the metal center similar to that of the pincer ligand C^{ylid}C^{NHC}C^{ylid} in complex **51** (Scheme 14) and identical with OC^{NHC}C^{ylid} pincer in complex **83** (Scheme 22) and the C^{NHC}C^{NHC}C^{ylid} pincer in complex **805** (Scheme 152).[92].

3.4. Type C,C^{NHC},O

3.4.1. Group 5 metals (Ta)

Reaction of **76** with [Ta(CH*t*Bu)(CH$_2$*t*Bu)$_3$] in toluene resulted in the formation of complex **77** of limited thermal stability in 84 % yield (Scheme 21) [93]. The structure of **77** revealed the presence of two types of carbene ligands (alkylidene, NHC) on Ta, the Ta–C^{NHC} bond distance of 2.355(5) Å is unusually long [94–96]. On prolonged standing at room temperature, **77** quantitatively converted to **78** with concomitant release of one equivalent of neopentane. The latter resulted from intramolecular C–H bond activation of a *o*-methyl substituent of the mesityl wingtip. The characteristic ^{1}H NMR resonances attributed to the cyclometalated Ta–CH$_2$–Ar group were observed at δ 2.41 and 1.58 ppm

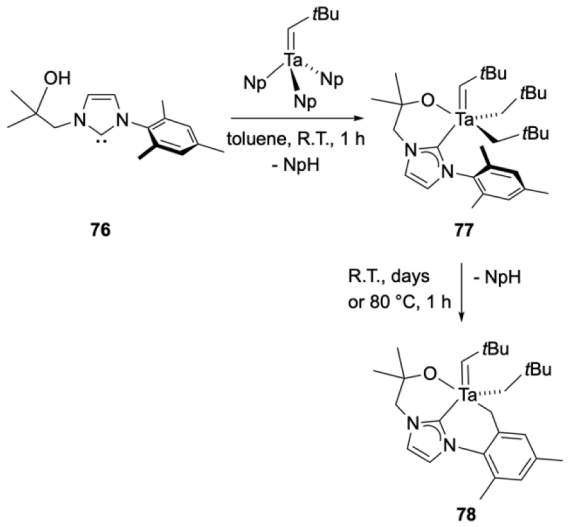

Scheme 21. Synthesis of Ta complexes resulting from C-H activation.

($^2J_{HH}$ = 13.7 Hz). The ^{13}C NMR spectrum revealed two typical signals, at δ 252.3 and δ 205.2 ppm, that were assigned to the alkylidene and the NHC moieties, respectively.

3.4.2. Group 10 metals (Pd)

The air stable, *o*-metalated Pd complex **81** containing a C,C,C^{NHC},O-tetradentate ligand was prepared by the reaction of **79** with Cs_2CO_3 in acetonitrile at 70 °C, it could also be obtained by treating the ligand precursor **80** with $PdCl_2$ and Cs_2CO_3 in refluxing acetonitrile (Scheme 22). Treatment of **81** with one equivalent HOTf in acetonitrile at −40 °C afforded the acetonitrile complex **82** which could be converted to the isocyanide complex **83** by reaction with *t*BuNC. Complex **82** showed high catalytic activity in the allylation of aldehydes [97].

3.5. Type C,C^{NHC},S

3.5.1. Group 10 metals (Pd)

The cyclometalated complex **85** featuring a square planar Pd center and a thioether donor is the only example of κC,κC^{NHC},κS-pincer complex. It was obtained quantitatively by the reaction of the imidazolium salt **84** with $PdCl_2$ in pyridine, in the presence of base (K_2CO_3) (Scheme 23) [98].

3.6. Type N,C^{NHC},N

The pincer complexes described in this section feature either anionic amido or neutral imine (usually in combination with a heterocyclic system) side-arm donors, the former are predominantly encountered with Group 4 and 5 metals. There are some recent examples of non-symmetrical pincer designs with different side-arm N-donors and/or bite angles at the two halves of the ligand. Despite the differentiation of the two coordination half-spaces created, these complexes are discussed as normal κN,κC^{NHC},κN donors following the guidelines given earlier, *i.e.* adhering to the group number of the Periodic Table that the metals belong to. A detailed summary of the ligand designs encountered in the literature is given in Chart 4; the occurrence of the κN,κC^{NHC},κN pincer ligands is given in Table 1. Selected comparative structural and spectroscopic data for all complexes with κN,κC^{NHC},κN pincer ligands are given at the end of the section.*

3.6.1. Group 4 metals (Zr, Hf)

A series of zirconium and hafnium complexes with dianionic amido N,C^{NHC},N-terdentate ligands of type **Ia** was obtained by aminolysis of [M(NMe$_2$)$_4$] (M = Zr, Hf) with the charge neutral free carbene **86** in non-polar solvents leading to the five coordinate complexes **87** (M = Zr) and **91** (M = Hf) (Scheme 24) [99]. The latter two were converted to the chlorides **88** and **92**, respectively, by exchanging the dimethylamido groups using Me_3SiCl. The NMR spectra of the five-coordinate complexes supported symmetric structures in solution. A range of organometallic alkyls **89**, **90** (Zr) and **93**–**96** (Hf) were easily obtained by salt metathetical reactions with Grignard reagents, albeit the Zr species **89** and **90** were thermally unstable at room temperature and presented difficulties in their full characterization.

As expected, the thermal stability of the hafnium dialkyl complexes **93**–**96** was dependent on the nature of the alkyl groups: **93** and **95** were thermally stable, while **96** decomposed at room temperature to **98**, the latter featuring a cyclometalated tetradentate ligand. The decomposition was accompanied by release of ethane. The ^{1}H NMR spectrum of **98** displayed two doublets that were attributed to the diastereotopic –C*H*$_2$ protons of the metalated mesityl and two multiplets assigned to the diastereotopic Hf–C*H*$_2$ of the metal bound Hf–CH$_2$CH$_3$ (at δ 1.00 ppm, δ 2.51 ppm and δ −0.10 ppm, δ 0.10 ppm, respectively). A clearer

* Additional references dealing with ligands of type **Ib**, **IIb** and **IIIb** are given at the end of the document in the Note added in proofs.

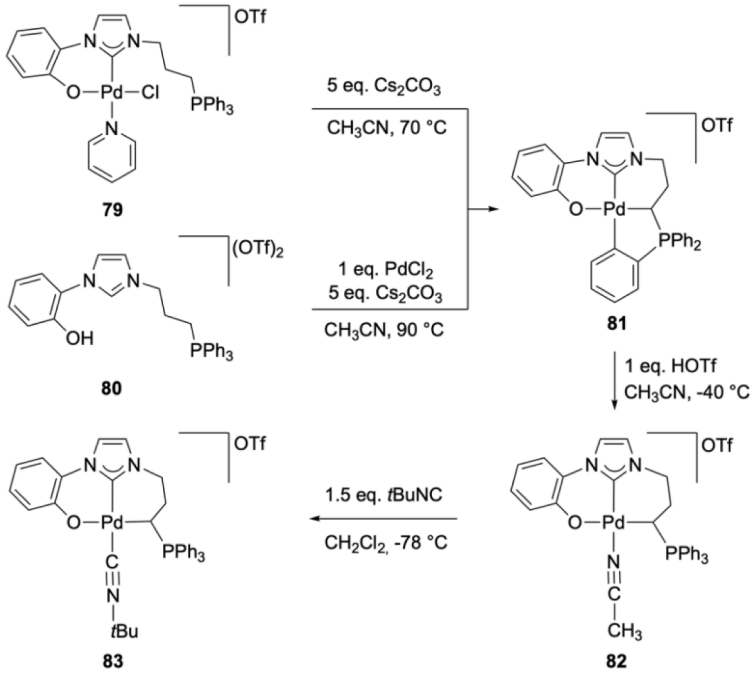

Scheme 22. Synthesis of Pd complexes by metalation

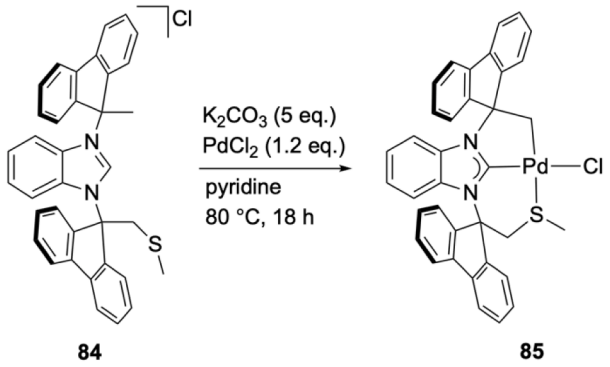

Scheme 23. Synthesis of a Pd complex bearing a C,C^{NHC},S pincer ligand

mechanistic insight of the reactivity was obtained from the study of the decomposition of the d_{10}-**96** diethyl complex, which led to the formation of d_6-ethane, in accord with β-deuterium atom transfer occurring between the two ethyl groups and resulting in the postulated metalacyclic intermediate d_4-**97** that could rearrange to the observed d_4-**98** (Scheme 25) [99].

Insertion of one equivalent xylyl isocyanide (XylNC) in the Hf–CH_3 bond of **93** resulted in the formation of the mono-insertion product **99** exhibiting one imino C atom directly bound to hafnium with a Hf–C bond distance of 2.251(2) Å and characteristic ^{13}C NMR signal for the iminoacyl N=*C* carbon at δ 259 ppm. Further addition of one equivalent of XylNC or isopropyl isocyanide to **99** led to the formation of **100** and **101**, respectively, while the reaction of **93** with two equivalents of isopropyl isocyanide afforded the thermally stable **102** (Scheme 26) [99].

The mono-insertion product **99** was also reacted with CO to give **103**. Its structure unveiled a remarkable amido-enolate metallacycle, arising from a C–C bond formation between the neighboring imino-acyl and acyl functionalities (Scheme 27).[99] Furthermore, the reaction of **93** with CO led to the mixed methyl acyl complex **104**. Mechanistic insight into the carbonylation reaction was gained by performing it with ^{13}CO, demonstrating that one ^{13}CO molecule inserted in the complex. However, **104** has limited stability and rearranges to **106** *via* a hydrogen atom shift from the acyl methyl to a carbene carbon (Scheme 27) [99]. The nature of complex **106** was confirmed by ^{1}H NMR spectroscopy with diagnostic resonances assigned to the –O–CH=CH_2 group appearing at δ 3.47, 3.54 and 5.75 ppm. Further reaction of complex **106** with CO afforded an insoluble white solid, which on the evidence of ESI-MS was the outcome of the insertion of a second CO molecule (molecular ion peak at $m/z = 652$) but further characterization efforts were limited by the insolubility of the product.

Exposure of the bis-isobutyl complex **95** to CO resulted in the formation of **105**, a reaction that was monitored by NMR spectroscopy. The ^{13}C NMR resonance attributed to the Hf-O=C*i*Bu moiety was observed at δ 338.4 ppm, consistent with values found in other early transition metal acyl complexes [100]. Further exposure of complex **105** to CO led to the formation of complex **107**, which was characterized by NMR spectroscopy. Reaction of complex **95** with CO for an extended period of time (3–4 days) resulted in the formation of colorless crystals of **108** in good yield [99]. Their crystal structure revealed a dihafnium bis(enediolate) complex, with C=C bond distances of 1.342(15) Å and Hf–O of 1.928(6) Å; these values compare to those found for similar bonds in other early transition metal enediolate complexes [101].

3.6.2. *Group 5 metals (Ta)*

The tantalum complex **110** (Scheme 28) featuring a κN, κC^{NHC}, κN-pincer ligand (originating from type **Ia** of Chart 4) was prepared by salt metathesis from the lithium complex **109** with [$TaCl_2(NMe_2)_3$] at low temperature. The Ta–C^{NHC} bond distance was 2.365(6) Å. Similar reactions of **109** with [$TaCl_3(NMe_2)_2$(THF)] or [$TaCl_4(NEt_2)(OEt_2)$] resulted in the formation of the complexes **111**–**113** in good yields, respectively, which were characterized by NMR spectroscopy (Scheme 28) [102].

Given the successful metathesis reactions of the lithium salt **109** with the tantalum precursors [$TaCl_2(NMe_2)_3$], [$TaCl_3(NMe_2)_2$(THF)] and [$TaCl_4(NEt_2)(Et_2O)$], the reactions of **109** with alkyl-chlorido tantalum precursors [$TaCl_2R_3$] (R = CH_2tBu, Me, CH_2Ph) were studied. With [$TaCl_2R_3$] (R = CH_2tBu, Me, CH_2Ph), formation of the complexes **114**–**116** occurred in THF at −30 °C (Scheme 29). Interestingly, it was shown crystallographically that one of the six-membered chelate rings in

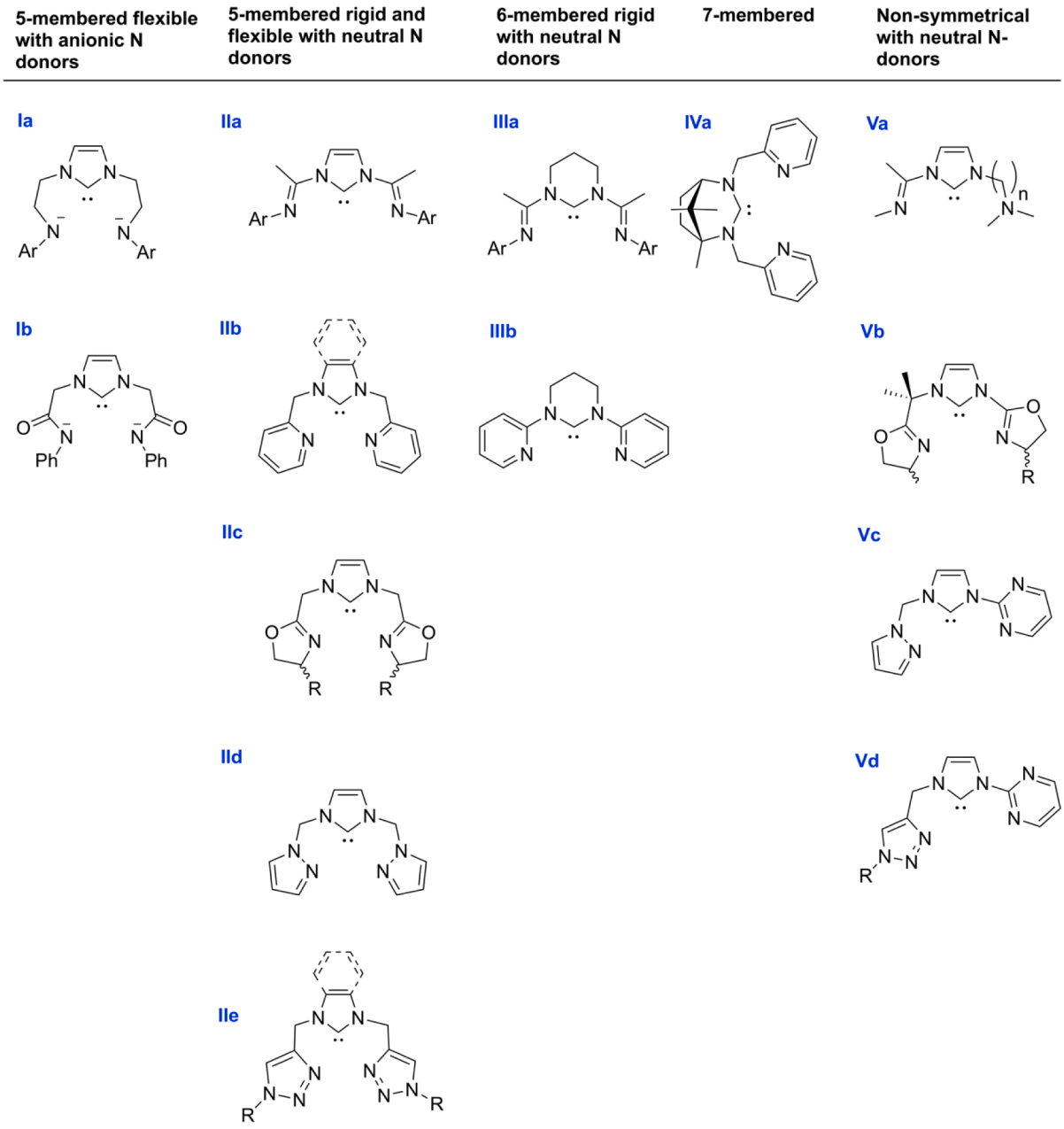

Chart 4. A detailed summary of different pincer type ligands bearing a κN, κC^{NHC}, κN backbone

the complex was metalated α-to the N^{amido}, which was also evidenced by NMR spectroscopy: the imidazole ring hydrogen atoms, the side-arms of the ligand backbone and the two neopentyl groups were inequivalent in support of the lack of any symmetry element in **114**. Reaction of lithium salt **109** with [$TaCl_3$=CH*t*Bu$(THF)_2$] yielded complex **117** in good yield, with a ligand binding mode analogous to that in **114**, with metalation of the carbon atom α- to the N^{amido} and concomitant conversion of the neopentylidene group to neopentyl. DFT calculations on model complexes indicated that the formation of the strained metala-aziridine ring in the unusual complexes **114**–**117** allows the remaining substituents to adopt optimum positions maximizing bonding interactions. The calculations predict that the most favourable pathway to form the metala-aziridine involves a tantalum alkylidene intermediate, which undergoes C-H bond activation α to the amido side-arm [102].

3.6.3. *Group 6 metals (Cr)*

The air stable complex **119** (Scheme 30) with imino donors of the chiral oxazoline functionality as side-arms (type **IIc** of Chart 4) was synthesized by transmetalation from the silver complex **118** to $CrCl_2$. Interestingly, in the course of the reaction the metal was oxidized from Cr^{II} to Cr^{III} by an unclear mechanism (Scheme 30) [104]. Related redox changes, possibly arising from disproportionation reactions of Cr^{II} into Cr^0 and Cr^{III} complexes, have been reported [105]. The structure of **119** revealed a distorted octahedral coordination geometry defined by the chiral terdentate pincer, one bromine and two chlorine donor atoms (Scheme 30).

The chromium complex **121** (bearing a ligand of type **IIIa** of Chart 4) was obtained from the Cu complex **120** by transmetalation with [$CrCl_3(THF)_3$] (Scheme 31) [106]. The solution magnetic susceptibility of **121** (4.1μ_B, Evans' method) points to a $S = 3/2$ state. In the molecular structure of **121**, the Cr–C^{NHC} and Cr–N^{imine} bond distances of 1.989(3)

Table 1
Occurrence of complexes with the ligand architecture **Ia** – **Vd** shown in Chart 4 across the transition metals.

Type	Metal
Ia	Zr, Hf, Ta
Ib	Pd
IIa	Ni, Ge
IIb	Ni, Cu^{I}, Cu^{II}, Ru, Pt
IIc	Ag, Cr
IId	Ni, Ru, Rh, Ir
IIe	Co, Ni, Ru, Pd
IIf	Ru
IIIa	Cr, Fe, Ni, Cu
IIIb	Ni, Ru, Rh
IIIc	Ru
IVa	Ni
Va	Cr, Ni, Ag
Vb	Rh, Pd
Vc	Pd, Pt
Vd	Pd

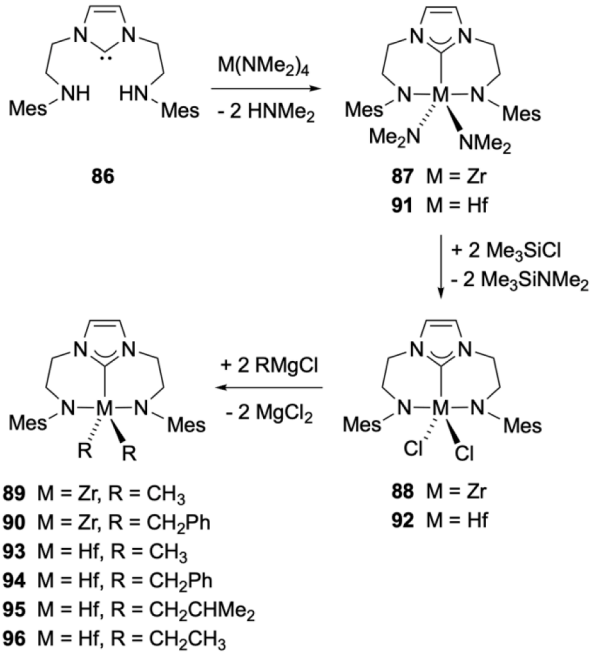

Scheme 24. Synthesis of Zr and Hf complexes bearing type **Ia** backbone

and 2.133(2), 2.142(2) Å, respectively, are shorter than in the majority of $CrCl_3$ complexes [107–109] (*cf.* discussion for the Fe complexes **127** and **128** in Scheme 33, Section 3.6.5).

The two chromium complexes **124** and **125** featuring non-symmetrical $\kappa N^{imine},\kappa C^{NHC},\kappa N^{amine}$ pincers (type **Va** of Chart 4) were synthesized *via* transmetalation accompanied by metal oxidation, with a plausible oxidant being the AgCl side product of the transmetalation as implicated by the appearance of silver mirrors in the reaction vessels (Scheme 32) [105]. Consequently, reactions of **122** and **123** with $[CrCl_3(THF)_3]$ directly afforded the Cr^{III} complexes **124** and **125** in which the length of the amine side-arm can be varied while the imine wing-tip donor remains constant. The complexes **124** and **125** were active precursors in the catalytic ethylene oligomerization [105].

3.6.4. Group 7 metals (Mn, Re)

No example of pincer complexes with these metals has been reported.

3.6.5. Group 8 metals (Fe, Ru)

The Fe^{II} and Fe^{III} complexes **127** [110] and **128** [111] bearing the terdentate $\kappa N^{imine},\kappa C^{NHC},\kappa N^{imine}$ ligand (type **IIIa** of Chart 4) were prepared by the reaction of precursor **126** with $FeCl_2$ in the presence of NaHMDS and oxidation of the product obtained with acetylferricenium tetrafluoroborate in CH_2Cl_2, respectively (Scheme 33). In the solid state structures the iron center is found in a distorted square pyramidal environment and the Fe^{II}–C^{NHC} bond distance (1.812(2) Å) was comparable to the shortest of its kind ever reported [112,113]. Similarly, the Fe–N^{imine} bond distances (2.023(2) and 2.028(2) Å) were even shorter than relevant distances in the higher oxidation state Fe^{III} bis(imino) pyridine complexes (average Fe–N length 2.185 Å) [114]. The magnetic properties of **127** and **128** were evaluated and demonstrated a complex behavior: for **127** the value $\mu_{eff} = 5.0\mu_B$ was obtained at room temperature in THF solution (Evans' method). However, in the solid state at low temperatures (<30 K), **127** displayed low magnetic moments that increased rapidly to a plateau corresponding to χT values typical of the $S = 1$ state (in the range 30 K to 150 K), finally reaching magnetic moments typical of a spin state change to $S = 2$ ground state upon further heating. Data fitting gave a spin transition temperature ($T_c = 563$ K) accounting for the χT values seen at room temperature. Rapidly interconverting $S = 1$ and $S = 2$ spin states at room temperature have also been implicated on evidence of Mössbauer spectroscopy. Similar temperature behavior has been observed for the complex **128**. The magnetic properties and the pincer ligand binding in **127** has been compared and contrasted with those of the iron pyridine diimine (DPI) and pyridine bis-(imidazol-2-ylidene) analogues and rationalized in view of the overall stronger pincer binding in **127** [61]. In addition, complex **129** was obtained from the treatment of complex **127** with sodium 4-methoxyphenolate [115]. The Fe–C^{NHC} and Fe–N^{imine} bond distances of 1.854(2) and 2.064(1)/2.067(1) Å, respectively, were slightly longer than those in **127**. Complex **129** was a highly active catalyst for lactide polymerization [115].

Complex **127** was reduced with excess Na/Hg in the presence of CO to **130** which also features distorted square pyramidal geometry and short Fe–C^{NHC} distance but not as contracted as in **127** (Scheme 34) [116]. The vibration frequency of the $Fe(CO)_2$ substructure in **127** has been compared to DPI and pyridine bis(imidazol-2-ylidene) analogues, testifying for stronger overall σ-donation of the Fe(κN^{imine}, κC^{NHC}, κN^{imine}) system to the π* of the CO coligands; this has been tentatively attributed to the orientation of the carbonyls relative to the NHC maximising π-backdonation. Contrasting to the previous reductive reactivity, the reduction of **127** with a stoichiometric amount of sodium

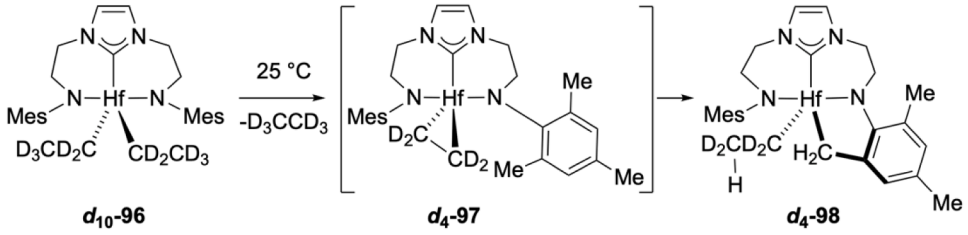

Scheme 25. C-H activation reactivity with the Hf dialkyl complexes bearing backbone of type **Ia**

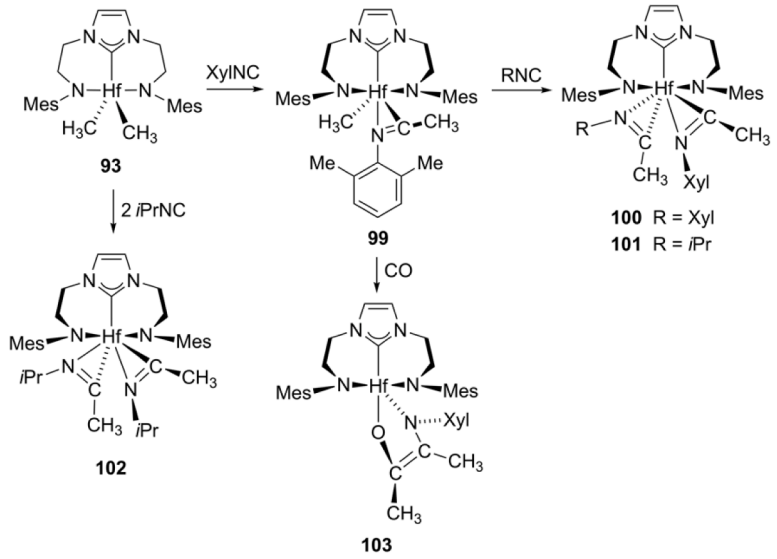

Scheme 26. Isocyanide insertion reactivity of the hafnium dimethyl complexes bearing ligand backbone of type **Ia**.

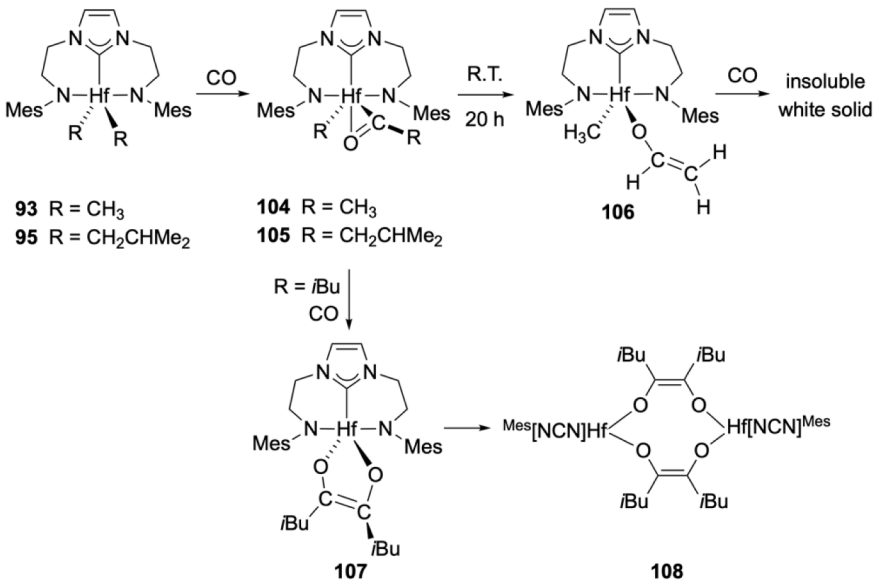

Scheme 27. CO insertion and coupling reactivity of hafnium dialkyl complexes bearing ligand backbone of type **Ia.**

naphthalenide led to the formally Fe^{I} complex **131** with distorted square planar structure. Metrical (*i.e.* short Fe–C^{NHC} and elongated distances between the tetrahydropyrimidine heterocycle and the imine carbons) as well as spectroscopic (ESR, Mössbauer) and broken symmetry DFT data provided insight into the electronic structure of **131**; the data have been interpreted in terms of a redox non-innocent radical anionic pincer ligand accommodating one unpaired electron that participates in an antiferromagnetic interaction with a triplet Fe^{II} center.

A class of *N,N'*-(2-picolinyl)-imidazol-2-ylidene (of type **IIb**, Chart 4) complexes of ruthenium were prepared to gain insight into the catalytic activation of R(H)O–H bonds in relation to hydrogenation or water splitting; the ligand design provided access to Ru complex intermediates with dearomatized pyridine and potential in bifunctional catalysis (Scheme 35) [117,118]. Thus, **134** was obtained by transmetalation to Ru from the Ag complex **133** in acetonitrile. Partial substitution in **134** of two coordinated acetonitrile ligands by *t*Bu-bipy and of the remaining one by bromide gave **135** and **136**, respectively; finally, metathetical exchange of the bromide in **136** by two equivalents of *t*BuOK gave **137**, which featured one *t*-butoxide and one *t*Bu-bipy ligands, while on the pincer backbone one of the methylene spacers of the picoline side-arm was deprotonated and, consequently, the pyridine heterocycle was dearomatized. Dynamic ^{1}H NMR experiments showed that in complex **137** a remarkable intramolecular proton exchange took place between the protonated and deprotonated spacers of the picoline (in concert with reversible dearomatization/aromatization of the pyridine ring), presumably *via* an intermediate involving protonation of the coordinated *t*BuO, which adopted the role of an intramolecular proton shuttle. Substitution of the coordinated bromide in **136** by PPh_3 followed by addition of one more equivalent of base (*t*BuOK) led to the isolation of complex **141**, in which both spacers originating from the picoline side-arms were deprotonated and both pyridine heterocycles were dearomatized. This complex was also obtained from **137** by reaction with PPh_3 and elimination of *t*BuOH. Finally, reaction of **137** with H_2O led to the formation of the corresponding Ru–OH species **140**, in which too the aforementioned H exchange pathways are also operative.

Complex **138** has also been studied as precatalyst for the

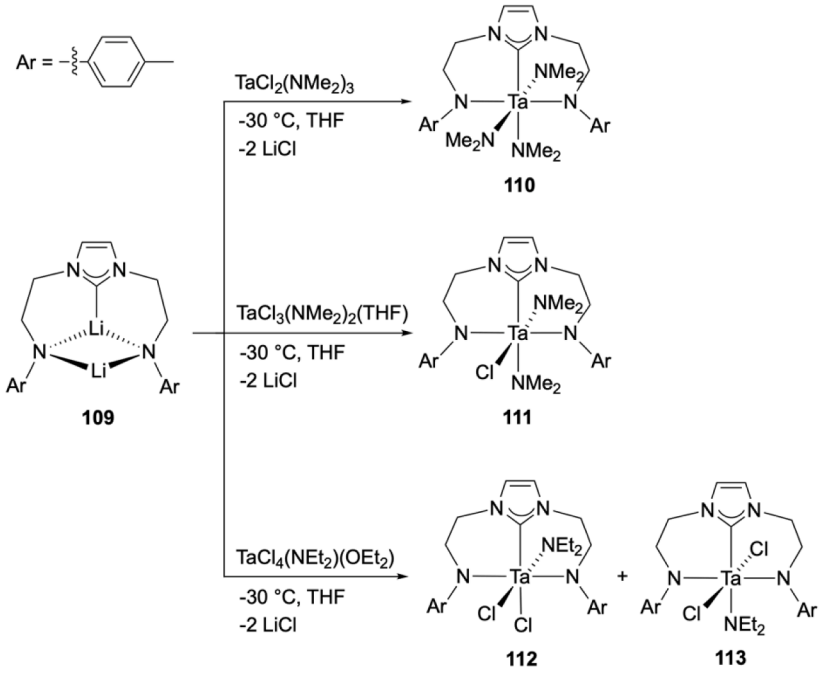

Scheme 28. Tantalum amido complexes bearing ligand backbone of type **Ia**

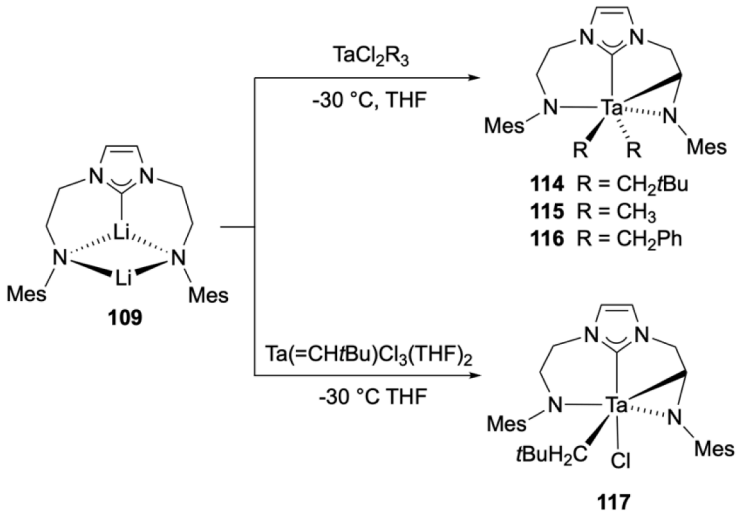

Scheme 29. Tantalum alkyl complexes bearing the ligand backbone of type **Ia**

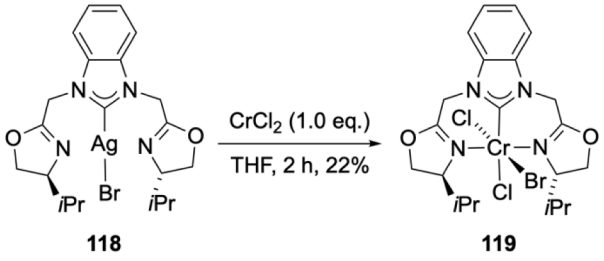

Scheme 30. Chromium complex **119** with backbone of type **IIc** obtained by transmetalation from Ag.

hydrogenation of CO_2 to formate showing moderate activity under mild conditions. In experimental and computational studies aiming to establish the catalytic mechanism, the hemilability of one pyridine side-arm of the pincer was implicated leading to the formation of the alkoxy-hydride species by bifunctional H_2 activation and pyridine re-aromatization effecting the heterolytic splitting of H_2 (Scheme 36) [118]. The octahedral species **138** is catalytically relevant in the hydrogenation reaction. The proposed mechanism is shown in Scheme 36.

The Ru^{II} complex **143** (with the ligand of type **IIb** of Chart 4) was obtained by treatment of the salt **142** with Ag_2O and $[RuCl_2(bpy)(DMSO)_2]$ (Scheme 37) [119]. The structure of **143** revealed an octahedral geometry and the strong *trans* influence of the NHC ligand, as inferred by a long Ru–Cl distance (2.5250(12) Å) compared to the normal range of Ru^{II}–Cl (2.39–2.41 Å) [120,121]. Similarly, treatment of **142** with AgOTf and $NaClO_4$ afforded the Ru^{II} complex **144**, which was oxidized in aqueous solution by one equivalent of $(NH_4)_2[Ce^{IV}(NO_3)_6]$ to the paramagnetic complex **145** ($g_{av} = 2.177$, *cf.* $g_{av} \approx 2.2$ for Ru^{III} complexes, $S = 1/2$) [122]. The Ru–O bond distance in **145** at 2.099(4) Å was shorter than that in **144** (2.119(3) Å) in support of a Ru^{III} oxidation state. Further addition of $(NH_4)_2[Ce^{IV}(NO_3)_6]$ to an

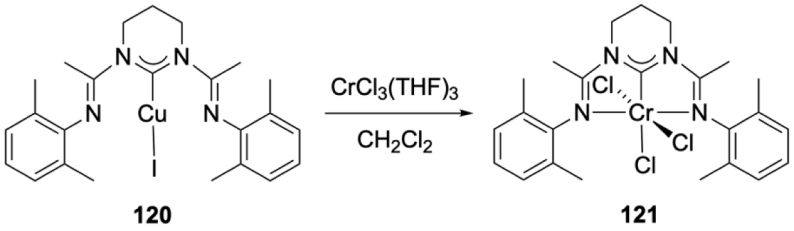

Scheme 31. Chromium complex **121** with ligand backbone of type **IIa** obtained by transmetalation from Cu.

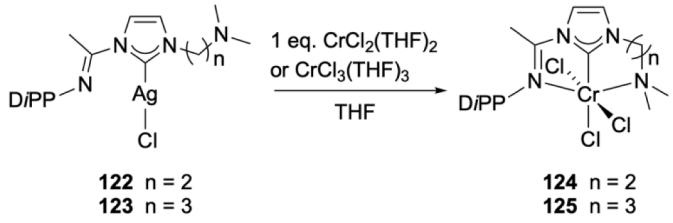

Scheme 32. Chromium complexes with backbone of type **Va** obtained by transmetalation from Ag

aqueous solution of **144** led to the formation of **146**. The resonance-Raman spectrum of the latter displayed a resonance at 732 cm^{-1} associated to the Ru–O bond, which was at lower wavenumbers compared to peaks corresponding to Ru^{IV}=O (ν = 780–833 cm^{-1}) [123–125]. This experimental value is close to that obtained from DFT calculations for a Ru^{III}–O· structure in a triplet state (ν = 767 cm^{-1}). Complex **146** showed high activity in oxidation of benzaldehyde and derivatives to the corresponding benzoic acid through C–H abstraction from the formyl group [119].

The imidazolium salts **147** and **148** (analogous to **132**, and **142,** type **IIb** in Chart 4) served as precursors for the introduction of the corresponding $\kappa N^{pyridine}$, κC^{NHC}, $\kappa N^{pyridine}$ pincer to Ru (originating from the precursor [Ru(μ-Cl)Cl(*p*-cymene)]$_2$ *via* a reductive protocol using Raney nickel in refluxing acetonitrile in the presence of NH_4PF_6 leading to **149** (Scheme 38). The involvement of a tentative nickel-NHC intermediate has been postulated [126]. A structural analysis by X-ray diffraction established the octahedral geometry at Ru^{II} and the terdentate κN, κC^{NHC}, κN pincer; the Ru–C^{NHC} bond distance (1.947 Å) was unusually short [127–138]. Complex **149** is an active catalyst in the transfer hydrogenation of acetophenone, with TOF of 3200 h^{-1} at loadings of 0.01 mol% (Scheme 38) [126].

The yellow complex **150** with picoline-containing side-arms was prepared in moderate yield by the reaction of the benzimidazolium salts **147** or **148** with $RuCl_3$ (Scheme 38) [139]. The ^{1}H NMR spectrum of **150** comprised a diagnostic AB-type pattern for the diastereotopic methylene picoline protons at δ 5.88 and 4.79 ppm and one multiplet at δ 7.91 ppm for the 4-*CH* of the coordinated heterocyclic rings. An X-ray diffraction analysis revealed for **150** an octahedral geometry at Ru with unremarkable Ru–C^{NHC} bonds of 2.020(5) Å and 2.025(5) Å (Scheme 38).

The Ru^{II} complex **152** bearing a $\kappa N^{triazol}$,κC^{NHC},$\kappa N^{triazol}$-terdentate ligand (type **IIe** in Chart 4) was obtained from complex **151** with one dangling triazole by using AgOTf as chloride abstractor (Scheme 39)

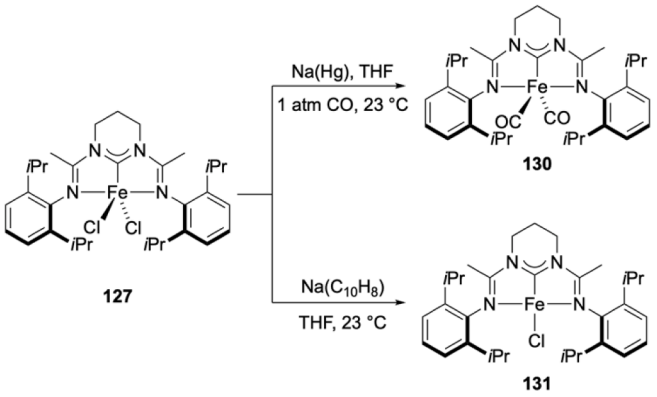

Scheme 34. Fe^0 and Fe^I complexes with ligand backbone of type **IIIa** (Chart 4) where redox non-innocent ligand behavior has been implicated.

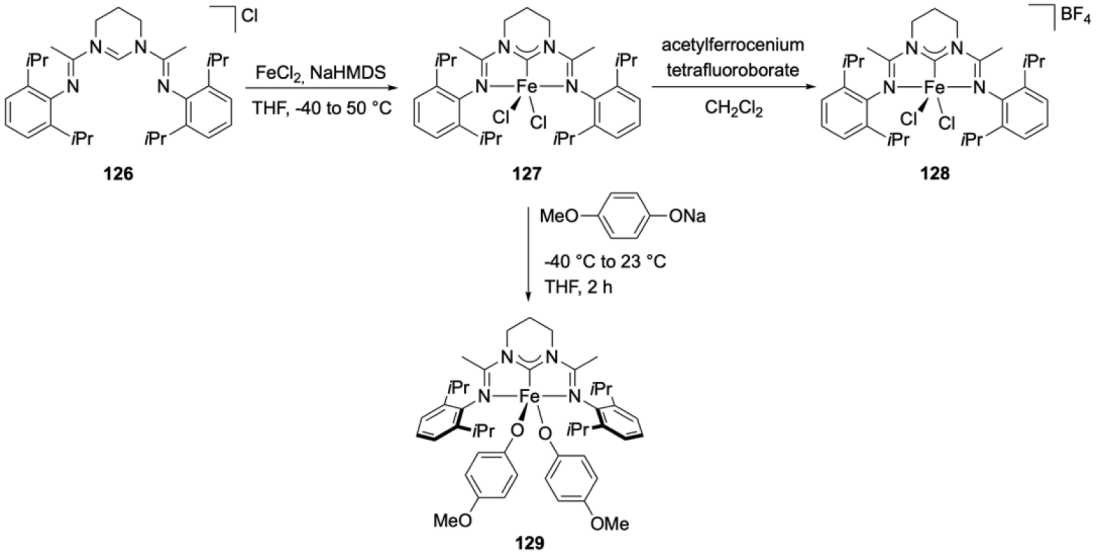

Scheme 33. Fe^{II} and Fe^{III} complexes with ligand backbone of type **IIIa**.

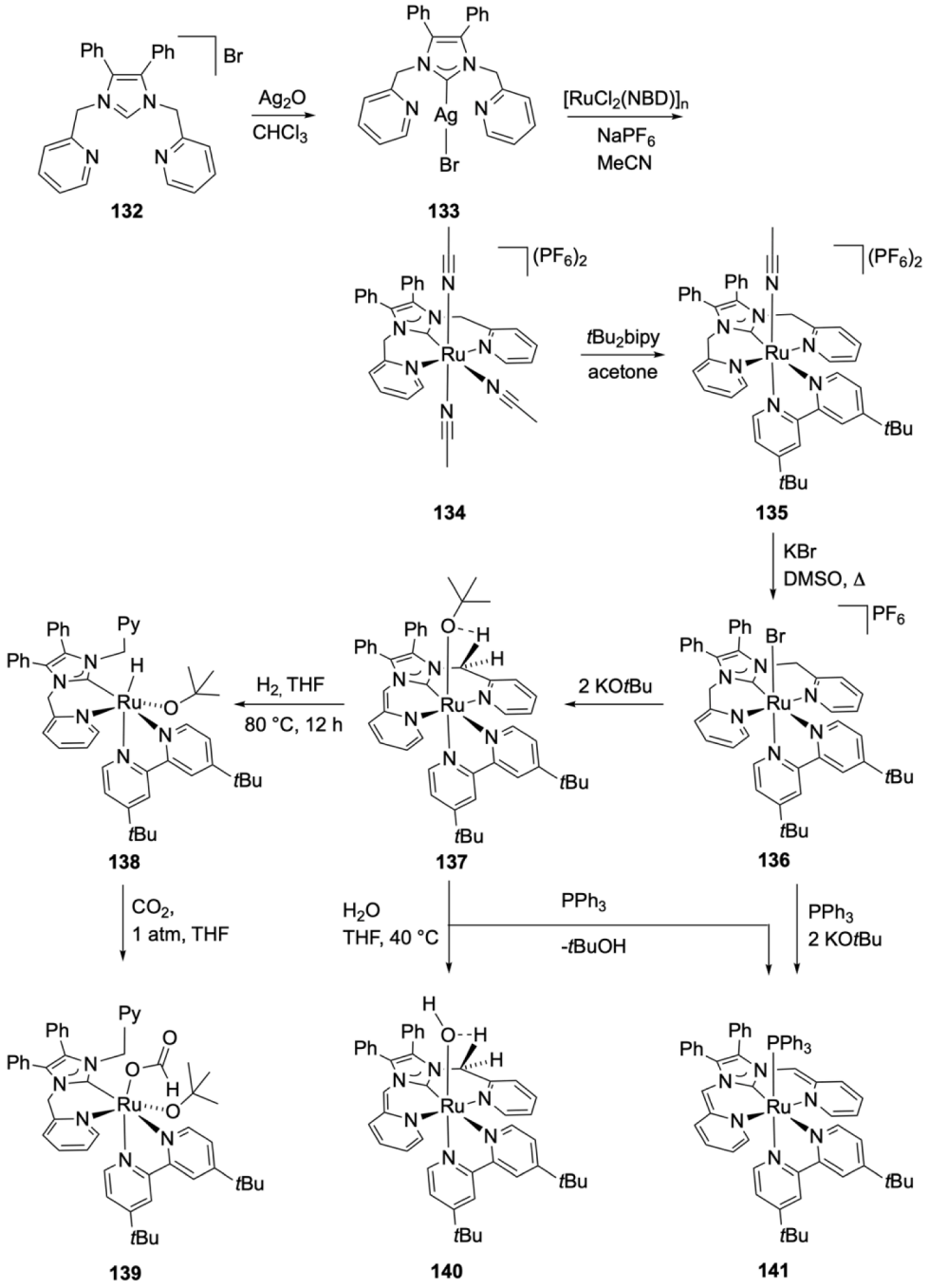

Scheme 35. Ru complexes with ligand backbone of type **IIb** with proton responsiveness and intramolecular proton shuttle behavior

[140]. Complex **152** featured a three-legged piano stool geometry with 'facial' N,C,N pincer ligand and Ru–C^{NHC} and Ru–$N^{triazol}$ bond distances of 2.053(4) and 2.081(4) Å, 2.090(3) Å, respectively. Complex **152** is active in the transfer hydrogenation of acetophenone with TOFs up to 1100 h^{-1} [140].

Complex **154** (with ligand of type **IId** in Chart 4) was obtained by the reaction of the imidazolium salt **153** with $RuCl_3 \cdot xH_2O$ in refluxing ethanol in the presence of NEt_3 (Scheme 40). An X-ray diffraction analysis established the octahedral geometry at Ru^{II} but ligand flexibility accommodated *facial* coordination in the solid state. However, in solution, the presence of two sets of ^1H NMR resonances for **154** was attributed to the coexistence of *fac*- and *mer*-isomers. Complex **154** displayed low catalytic activity in transfer hydrogenation reaction of acetophenone with isopropanol [141].

Two Ru complexes bearing κN, κC^{NHC}, κN-terdentate ligand (type **IId** in Chart 4) were obtained by refluxing in methanol the imidazolium and ruthenium precursors **155** and $[RuCl_2(PPh_3)_3]$, respectively (Scheme 41) [142]. The characteristic triplet at δ_C 182.3 ppm was attributed to the C^{NHC}. In addition, the crystal structure of **156** confirmed the terdentate nature of the ligand (Ru–C^{NHC} bond distance 1.979(6) Å). Exposure of complex **156** in THF to CO in the presence of KHMDS resulted in the formation of a formally Ru^{II} complex **157**. Its structure was established by ^1H NMR and IR spectroscopies and X-ray diffraction analysis. The disappearance of the NH signals in the ^1H NMR spectrum confirmed the formation of the deprotonated bis(pyrazolato)-type complex and the ν(CO) at 1989 cm^{-1} was assigned to the CO ligand. The Ru–C^{NHC} bond distance of 2.064(3) Å in **157** was longer than the corresponding in complex **156**. A similar reaction of **158** (precursor to

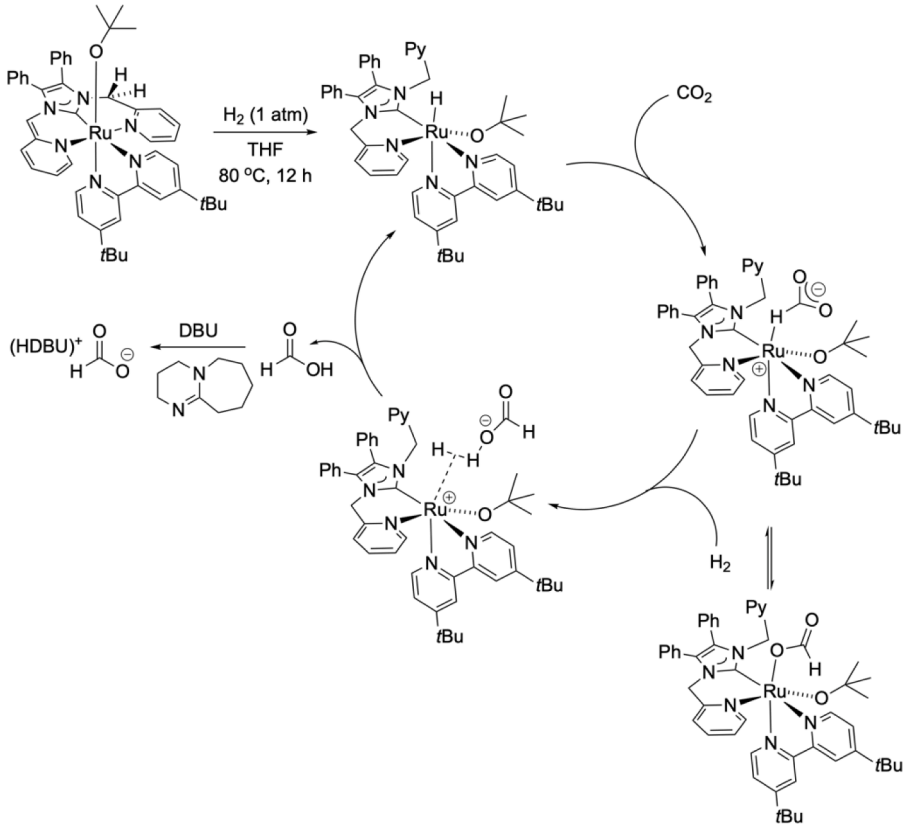

Scheme 36. Formation from **137** of Ru complexes with ligand backbone of type **IIb** as CO_2 reduction catalysts

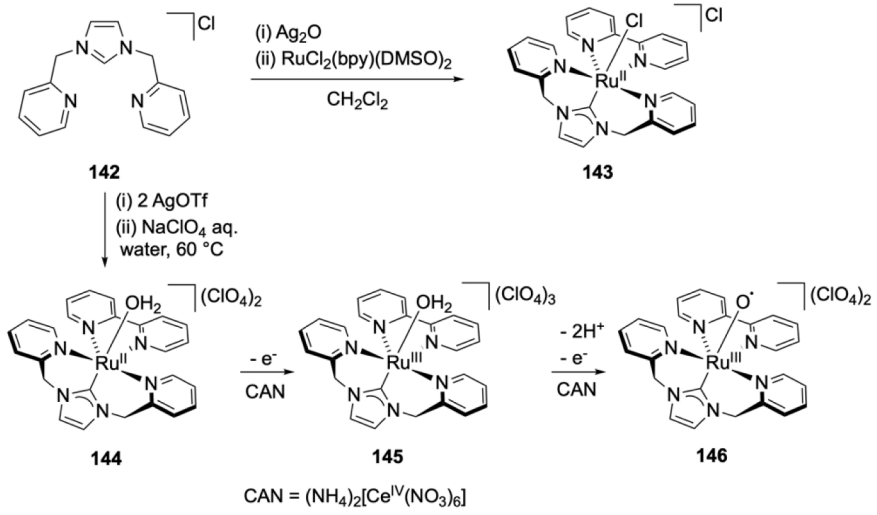

Scheme 37. Ru complexes with ligand backbone of type **IIb**

ligand type **IIIc**) with $[RuCl_2(PPh_3)_2]$ resulted in the formation of the neutral complex **159**, and its crystal structure exhibited a Ru–C^{NHC} bond distance of 2.025(3) Å. The resonance at δ 10.97 ppm attributed to the NH group was observed in the ^{1}H NMR spectrum. The carbene resonance was observed as a doublet at δ 222.4 ppm in the ^{13}C NMR spectrum. All data were consistent with the structure drawn for **159**.

A family of $\kappa N^{pyridine}$, κC^{NHC}, $\kappa N^{pyridine}$ (type **IIIb** in Chart 4) ruthenium complexes, where C^{NHC} is the six membered RE-NHC has been studied (Scheme 42). All these complexes exhibit remarkably short Ru–C^{NHC} bond distances, a fact that has been attributed to the electronic nature of the NHC donor, the framework rigidity and the natural bite angles of the ligand design. Thus, reaction of the *N,N'*-bis(2-pyridyl)-tetrahydropyrimidinium precursor with $RuCl_3$ at elevated temperatures led to the 'homoleptic' complex **161**. Under analogous conditions but using [{4′-(4-methylphenyl)-2,2′:6′,2′′-terpyridine}$RuCl_3$] as Ru precursor, the 'heteroleptic' species **162** was obtained. The structures of both **161** and **162** reveal tight binding of the $\kappa N^{pyridine}$,κC^{NHC},$\kappa N^{pyridine}$ pincer as implied by the short Ru–C^{NHC} and Ru–$N^{pyridine}$ bond distances (Scheme 42). Additionally, electrochemical studies revealed easier oxidizable Ru centers compared to the homoleptic $[Ru(tpy)_2]^{2+}$ (tpy = 2,2′:6′,2′′-terpyridine) analogues, in agreement with the better σ-donor properties of the NHC group. Finally, **161** displayed red solid-

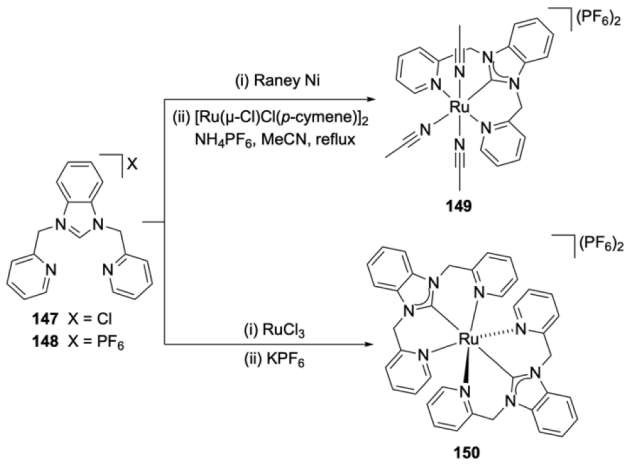

Scheme 38. Ru complexes with ligand backbone of type **IIb**.

state emission ($\lambda_{max} = 753$ nm) considerably red shifted relative to that of $[Ru(tpy)_2]^{2+}$ ($\lambda_{max} = 620$ nm) [143].

Complex **163** was obtained by transmetalation from the complex **58** with $[RuCl_2(p\text{-cymene})]$, halide metathesis with LiI in **163** afforded **164** (Scheme 43) [86]. The X-ray structures of **163** and **164** revealed square-pyramidal geometries with the C^{NHC} in the axial position and remarkably short Ru–C^{NHC} distances of 1.820(6) and 1.815(2) Å, respectively. Accordingly, in the ^{13}C NMR the C^{NHC} signals were found at δ 240.9 and 238.0 ppm, for **163** and **164**, respectively.

3.6.6. Group 9 metals (Co, Rh, Ir)

The Co^{III} complex **166** was prepared by the transmetalation of the pincer ligand from a silver complex, generated *in situ* from the corresponding imidazolium salt **165** (precursors to pincer of type **Vc**, Chart 4)) with Ag_2O, to $[CoCl_2(PPh_3)_2]$, followed by spontaneous oxidation in air of a plausible Co^{II} intermediate preceding the isolation of **166** (Scheme 44) [144]. Although the ligand types are different, it is interesting to note that chelation-assisted metal oxidation was also observed upon deprotonation of the coordinated ketophosphane ligand in the Co^{II} complex $[CoCl_2\{Ph_2PCH_2C(O)Ph\}_2]$ with formation of the *fac*- and *mer*-isomers of the octahedral tris-chelated, phosphinoenolato Co^{III} complexes [145]. The crystallographic characterization of **166** revealed an octahedral geometry comprising one pincer ($\kappa N^{pyrimidine}$,κC^{NHC},$\kappa N^{picoline}$) and one bidentate ($\kappa N^{pyrimidine}$,κC^{NHC}) ligands around the six coordinate Co center with *cis* C^{NHC} donor disposition. The difference in the Co–C^{NHC} bond distances (one *trans* to the chloride at 1.913(4) Å and the other *trans* to the pyrimidine donor at 1.815(4) Å), was ascribed to steric and electronic (*i.e. trans* influence) effects. Complex **166** was found to be an active catalyst precursor for Kumada-Corriu cross-coupling reactions of aryl halides and Grignard reagents at room temperature [144].

The yellow complex **168** was obtained by ligand transmetalation from the Ni^{II} complex **167**, the nature of the metal oxidant was unclear but again metal chelation favored the formation of an octahedral Co^{III} complex from a Co^{II} precursor (Scheme 45) [146].

The complexes **170** and **173** were prepared by the reaction of precursor **153** with $[M(\mu\text{-Cl})(1,5\text{-COD})]_2$ (M = Rh, Ir) in the presence of sodium ethoxide, respectively, and were characterized by NMR spectroscopy and crystallography. An analogous reaction between precursor **169** and $[Rh(\mu\text{-Cl})(1,5\text{-COD})]_2$ and sodium ethoxide led to the formation of **171** (Scheme 46) [147]. Interestingly, the structures of **171** in solution and in the solid state were found to be different: the ^1H NMR spectrum of **171** indicated coordination of the terdentate ligand to the metal (**171A**), while in the solid state the ligand adopted an unsymmetrical bidentate binding mode leading to a square planar geometry at Rh (**171B**). Exposure of a solution of **171** or **173** to 1 atm of CO led to the quantitative formation of the five coordinate **172** and **174**, respectively, the structures of which were supported by ^1H and ^{13}C NMR and FT-IR spectroscopic data (ν_{sym}, ν_{asym} at 2091 and 2034 cm^{-1}, and at 2081 and 2013 cm^{-1}, respectively). Both **172** and **174** were only stable under a CO atmosphere. The complexes **170**, **171** and **173** were proved to be efficient catalysts for the addition of NH and OH bonds to the triple bond of alkynes. Complex **170** also showed activity in hydrosilylation of 1-phenylpropyne with triethylsilane (Scheme 46) [147].

Complex **176** featuring a non-symmetrical $N^{oxazole}$,C^{NHC},$N^{oxazole}$-pincer (type **Vb** in Chart 4) was obtained by a sequence of reactions involving, firstly, the interaction below −30 °C of the imidazolium salt

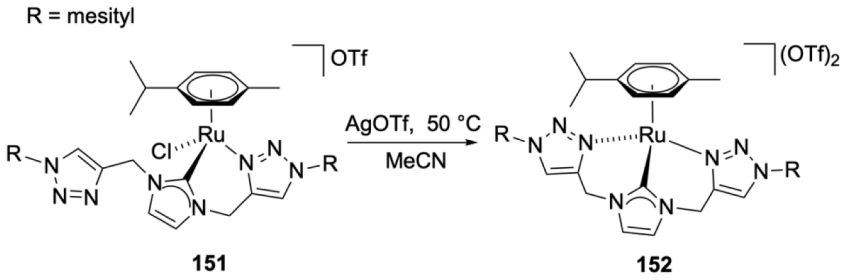

Scheme 39. Ru complexes with ligand backbone of type IIe (Chart 4)

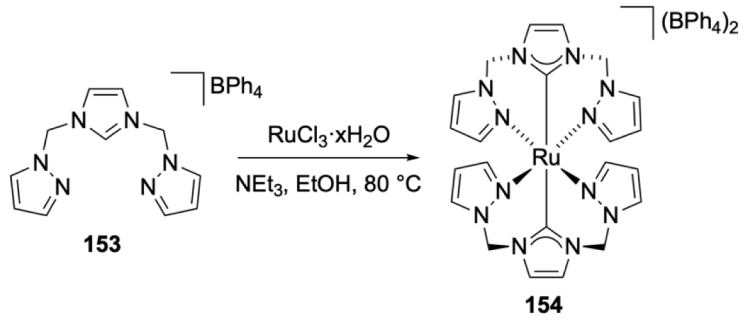

Scheme 40. Ru complexes with ligand backbone of type **IIf**

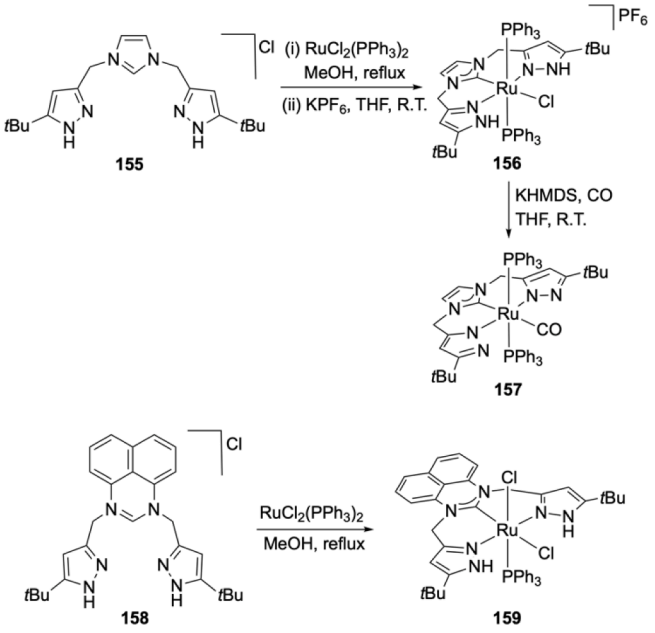

Scheme 41. Ru complexes with ligand backbone of types **IIf** and **IIIc**

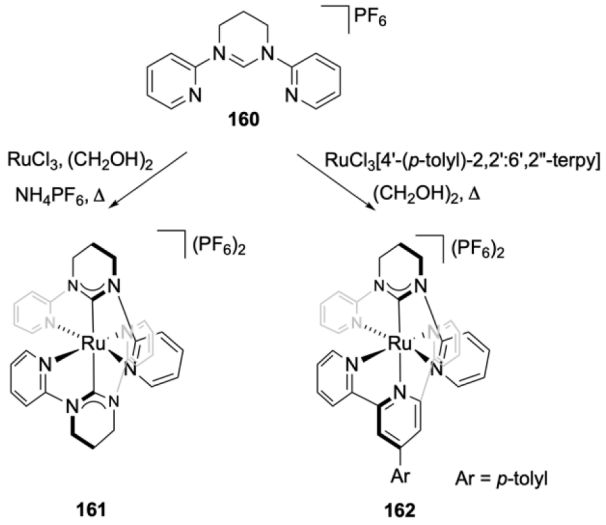

Scheme 42. Homoleptic and heteroleptic octahedral Ru-complexes with ligand backbone of type **IIIb**.

175 with $[Rh(\mu\text{-}OtBu)(NBD)]_2$ to give a Rh^I intermediate, followed by oxidation of the latter *in situ* with one equivalent of bromine (Scheme 47) [148]. The deep red, air stable **176** was purified by column chromatography and characterized spectroscopically (C^{NHC} at $\delta_C = 177.5$ ppm, $\nu(C{=}N) = 1662$ and 1636 cm^{-1}) and crystallographically (distorted octahedral geometry with a Rh–C^{NHC} bond distance of 1.900(4) Å).

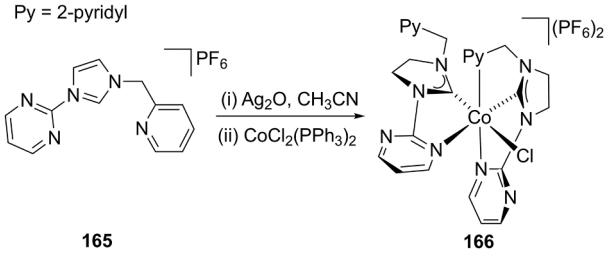

Scheme 44. Co complexes with non-symmetrical pincer ligand.

Complexes **178** (M = Rh) and **179** (M = Ir) were prepared by the reaction of the precursor **177** with $[M(\mu\text{-}OMe)(1,5\text{-}COD)]_2$ (M = Rh, Ir), in MeOH (Scheme 48); the rhodium product was obtained as a mixture of two isomers (*endo,endo)* and (*exo,exo)* originating from the disposition of the CMe_2 bridgehead relative to the 1,5-COD ligand (the initially obtained 50:50 ratio was converted after crystallization from $CHCl_3$ to 90:10 as evidenced by ^1H NMR) [149]. The crystallographically characterized isomers displayed a trigonal bipyramidal geometry, where the terdentate ligand adopted a *fac* coordination mode, with the good σ-donor NHC occupying an axial site (Rh–C^{NHC} = 2.008(7) Å, Ir–C^{NHC} = 2.008(13) Å). The complexes **178** and **179** were active in the transfer hydrogenation of prochiral ketones and hydrogenation with molecular hydrogen of alkenes but with poor enantiomeric induction, presumably due to the inherent ligand flexibility. The analogous **181** and **182** with a chiral C atom at one spacer were obtained similarly [150]; interestingly, the Ir–C^{NHC} bond distance in complex **182** was longer than that in complex **179** (2.058(11) Å). Importantly, in this case the configuration at the C atom of the spacer controlled the stereochemistry of the isolated complexes: exclusively *endo,endo* isomeric complexes were obtained with the *S*-configuration at the C atom, while *R,S*-configuration at C gave a mixture of *(endo,endo)* and *(exo,exo)* complexes [149,150].

Ligand transmetalation from the copper complex **58** to $[Rh(\mu\text{-}Cl)(COD)]_2$ in THF yielded complex **183**, which was characterized by NMR spectroscopy and ESI-HRMS (Scheme 49) [86]. Reaction of the Rh^{III} iodide complex **183** with excess AgCl led to complex **184** [86]. The mechanism for the formation of complex **183** was suggested to involve firstly the formation of the Rh^I species **59** which could then be oxidized by the CuI byproduct to the Rh^{III} iodide complex **183**. The observation of a copper mirror on the walls of the reaction vessel was consistent with this mechanism; for the cyclometalation transformation on **59**, see Scheme 16.

3.6.7. Group 10 metals (Ni, Pd, Pt)

Nickel. The reaction of the rigid imidazolium precursor **185**

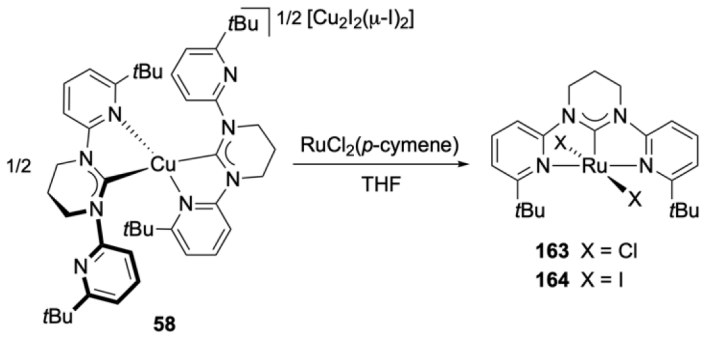

Scheme 43. Ru complexes with ligand backbone of type **IIIb**.

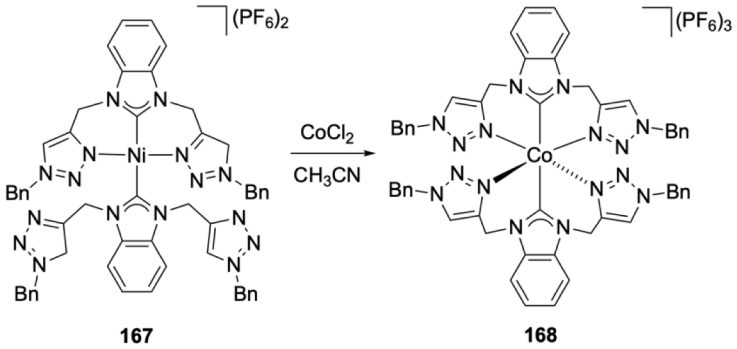

Scheme 45. Homoleptic Co^{III} complexes by transmetalation of the pincer ligand backbone of type **IIe** (Chart 4)

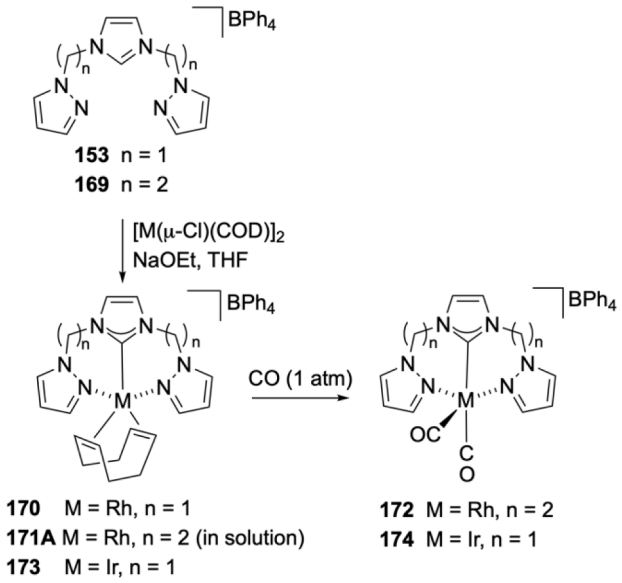

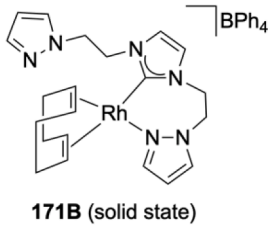

Scheme 46. Homoleptic Co^{III} complexes by transmetalation of the pincer ligand backbone **IIc**

featuring two imine side-arms, at room temperature in pentane, with [Ni(1,5-COD)$_2$] gave the complex **186**, the structure of which was established crystallographically and spectroscopically (Scheme 50). It unveiled the formation of a pincer complex with an anionic imidazolide bridgehead donor and imine side-arms coordinated at a distorted square planar Ni^{II} center; the anticipated NHC hydride obtainable by C–H activation was not observed. In **186** the Ni–$C^{imidazolide}$ bond distance (1.828(3) Å) is rather short, the endocyclic C–N distances correspond to single bonds while the imidazole ring forms an angle of 64.0(1)° with the C–H of the tertiary carbon atom. In the ^{1}H NMR spectrum, the broad singlet at $\delta = 5.73$ (in d^8-toluene) or septet (in CD_3CN, in which it exists as cationic MeCN adduct) for $C^{imidazolide}$–*H*, and the corresponding ^{13}C NMR resonance at δ 87.3 are consistent with such a C(sp^3)–H group (Scheme 50)[54]. The absence of oxidative addition reactivity of the $C^{imidazolium}$–H bond in **185** (*cf.* Scheme 50) can be contrasted to the system described in Scheme 110; the formation of **186** was studied by computational methods and attributed to subtle geometrical constraints of the ligand system. Interestingly, the reaction of **186** with ethylene resulted in the ethyl complex **187** the structure of which displayed again a tertiary Csp^3 bound to the square planar Ni center, the ethylene substrate has formally inserted into the imidazolide C(sp^3)–H bond to give a C–ethyl moiety. Computational studies of the latter transformation suggest that the insertion of ethylene into the C–H bond is direct and does not involve Ni–H intermediates; in contrast, imine side-arm hemilability may promote proximal to the C–H bond coordination of the ethylene at the Ni center followed by insertion into the C–H bond. The reactivity of complex **511** in Scheme 105A with ethylene is also distinct

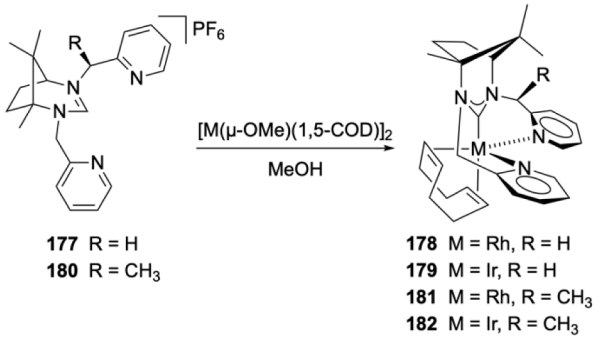

Scheme 48. Rh and Ir complexes with the ligand backbone of type **IVa** (Chart 4).

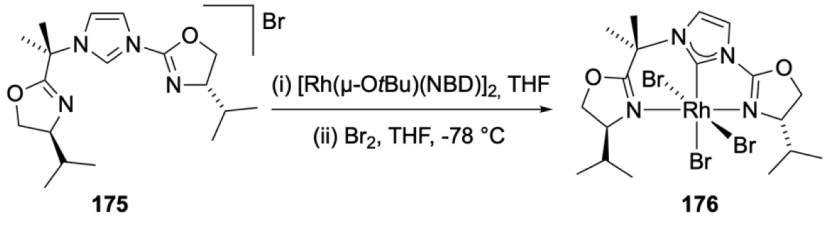

Scheme 47. Rh complexes with the non-symmetric ligand backbone of type **Vb**

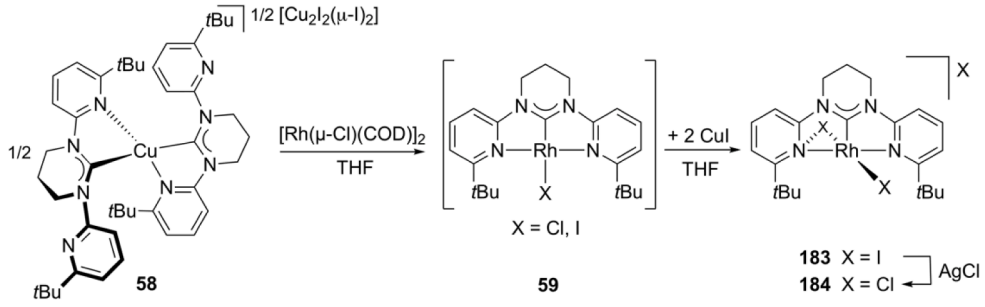

Scheme 49. Rh complexes with ligand backbone of type IIIb (Chart 4) obtained from Cu-transmetalation.

compared to the present system. Although the chemistry described in Scheme 50 does not strictly involve NHC donor pincer, it provides an interesting comparative platform underlining the role of the overall ligand structure in observed reactivity [54].

The square-planar complex **189** was obtained by ligand transmetalation from the Cu^{I} complex **188** with three equivalents $[NiCl_2(PPh_3)_2]$ in acetonitrile (Scheme 51) [151]. The Ni–C^{NHC} and Ni–$N^{pyridine}$ bond distances were 1.836(8) Å, 1.934(6) Å and 1.942(5) Å, respectively, comparable to those found in other nickel-NHC complexes [152–156]. Complex **189** showed good catalytic activity in Kumada-Corriu and Suzuki-Miyaura coupling reactions of aryl halides with organometallic reagents [151].

The complexes **192** and **193** were prepared by a transmetalation sequence from the silver complex **191**, which in turn was prepared by the reaction of precursor **190** with Ag_2O in dichloromethane at room temperature (Scheme 52) [157]. The X-ray structure of **191** revealed a linear [(NHC)–Ag–(NHC)] cationic moiety and a ($AgCl_2$) anion bound to the nitrogen of a pyridine ring. Treatment of **191** with $[NiCl_2(PPh_3)_2]$ in refluxing toluene gave a poorly soluble green complex, which was subjected to anion exchange with KPF_6 or $NaBF_4$ in acetonitrile to give the square planar **192** and **193**, respectively; both were characterized by NMR spectroscopy and X-ray diffraction analysis. They were highly efficient in the Kumada-Tamao-Corriu coupling reactions of 3-bromo-/3-chloropyridine and PhMgBr (Scheme 52) [157].

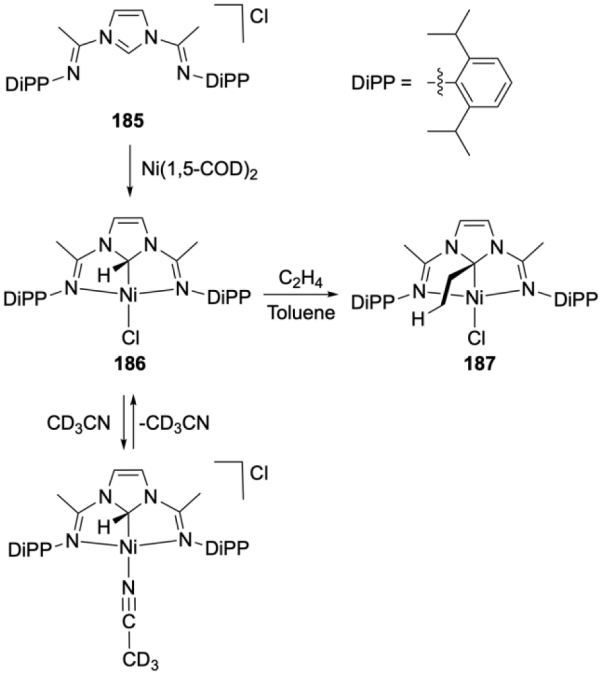

Scheme 50. Ni complexes with rigid ligand backbone of type IIa (Chart 4).

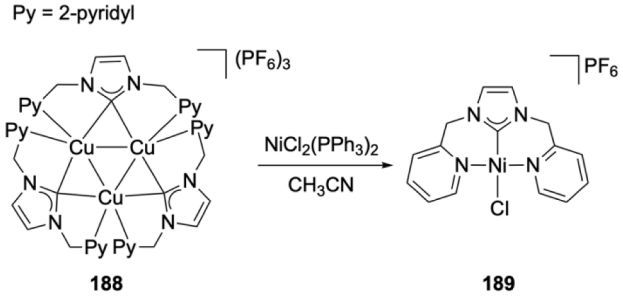

Scheme 51. Ni complex with ligand backbone of type **IIb** obtained by transmetalation from Cu.

The two nickel complexes **197** and **198** featuring square planar nickel centers were prepared by transmetalation from the silver complexes **195** and **196** with two equivalents of $[NiCl_2(PPh_3)_2]$ in THF; both were good catalysts for the Kumada cross coupling reaction (Scheme 53) [158].

Furthermore, reaction of the related imidazolium salt with nickel powder in air resulted in the formation of **167**, which was isolated in 92 % yield (Fig. 3) [146]. The structure of this complex was established by NMR spectroscopy and X-ray diffraction analysis. Interestingly, this methodology is enforcing a 1:2 nickel-to-ligand stoichiometry compared to the milder and more selective Ag transmetalation given above.

Reaction of precursor **199** with $[Ni(1,5\text{-}COD)_2]$ afforded the orange Ni^{II} complex **200** (Scheme 54) [59]. The nature of the Ni–C interaction was probed by NMR spectroscopy, where a characteristic signal at δ 5.82 ppm was assigned to a NC*H*N α-to the metal and therefore **200** can be considered as a β-elimination stabilized Ni-alkyl. The preferential formation of **200** over a plausible isomeric N-heterocyclic carbene hydride was rationalized by invoking an energetically unfavorable NHC structure, missing on mesomeric stabilization by the π-electron donation from the N flanking heteroatoms, the latter being engaged in delocalization over the imines functionalities. The short Ni–C bond distance (1.848(5) Å) could be due to the pincer geometrical constraints. The α-to Ni NC*H*N is quite acidic and treatment of **200** with $KN(SiMe_3)_2$ in toluene resulted in the formation of the NHC complex **201**. This was confirmed by the disappearance of the ^{1}H NMR signal attributed to the NC*H*N. However, the crystal structure of **201** revealed the presence of two anionic 'ate' type LNi^0Cl moieties bridged by the potassium counterions; the Ni–C^{NHC} bond distance (1.795(7) Å) in this dimer was remarkably short, revealing a C–Ni and C–N double bond character in this molecule of which the structure is better represented with the resonance form **201B**. The anionic 'ate' character of Ni in **201** accounts for the reaction of this complex with NH_3 gas in toluene at room temperature, yielding a mixture of two 'tautomeric' species, the ammonia carbene **202** and alkyl amido **203**. In the ^{1}H NMR spectrum, a characteristic resonance corresponding to the coordinated ammonia of complex **202** was observed at δ 0.11 ppm in toluene-d_8 and δ 0.45 ppm in THF-d_8. However, for the complex **203**, the spectrum revealed a signal

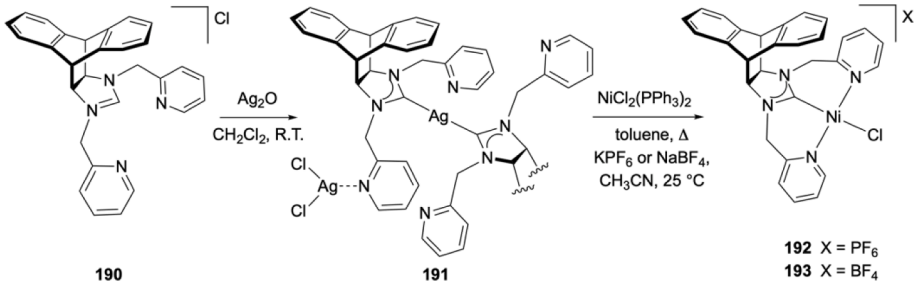

Scheme 52. Ni complexes with flexible ligand backbone related to type **IIb** obtained by transmetalation from Ag.

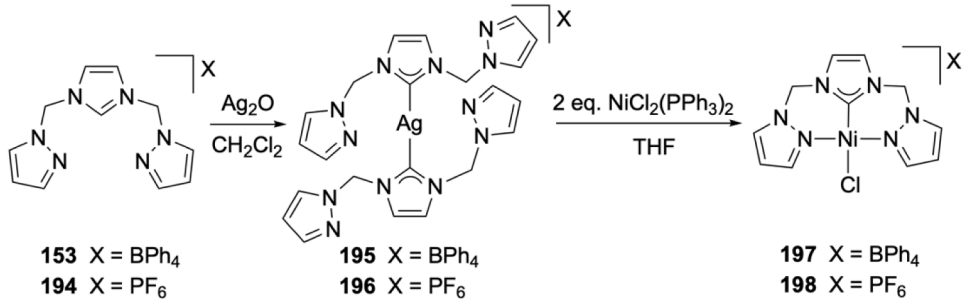

Scheme 53. Ni complexes with ligand backbone of type **IId** obtained by transmetalation from Ag.

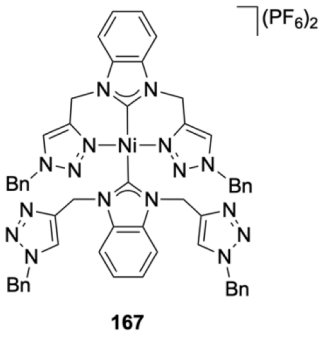

Fig. 3. Ni complex with ligand backbone of type **IIe** (Chart 4).

for the amide protons at δ −2.97 ppm in toluene-d_8 and δ −3.63 ppm in THF-d_8 and a resonance corresponding to the NC*H*N at δ 5.13 ppm in toluene-d_8 (δ 5.22 ppm in THF-d_8). The ratio of **202**/**203** was *ca.* 4:1 in toluene-d_8 (2:3 in THF-d_8). Unfortunately, no crystal suitable for X-ray diffraction analysis could be obtained. The rare N-H activation of NH_3 by **201** has been ascribed to the non-innocent nature of the C^{NHC} in the pincer complex, it constitutes an example of ligand assisted reactivity, where the C^{NHC} acts as proton acceptor.

Treatment of the previously mentioned efficient transmetalating copper complex **58** with [$NiBr_2$(DME)] in THF at room temperature led to the green paramagnetic (3.51μ_B, Evans' method) **204**, displaying a distorted square-pyramidal coordination geometry with two bromide atoms in the axial position (Scheme 55) [86].

The nickel complexes **205**–**206** with a bicyclic NHC bridgehead were obtained from the related imidazolium salts **177** and **180** by the reaction

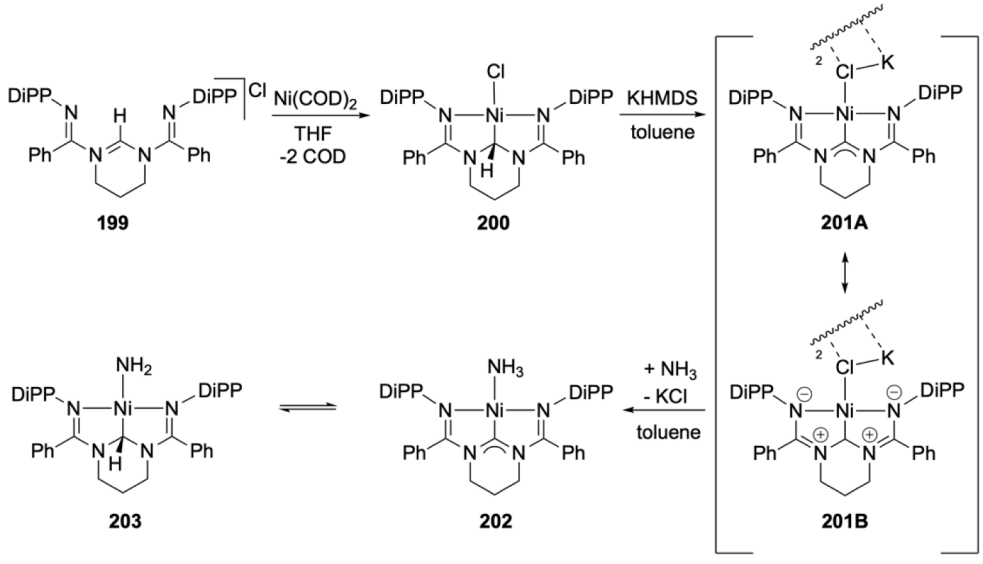

Scheme 54. Ni complexes with rigid backbone of type **IIIa** and the H_2N–H activation.

with [Ni(1,5-COD)$_2$] in THF (Scheme 56). Exposure of the THF solution of complex **205** to oxygen and recrystallization from $CHCl_3$ afforded yellow crystals of **207** [159]. Similarly, exposure of the reaction residue from [Ni(1,5-COD)$_2$] and **180** to air and crystallization from $CHCl_3$ gave **208** as yellow oil which shows characteristic ^{13}C NMR resonance at δ 177.5 ppm for the NHC carbon (Scheme 56) [150].

To explore the influence of the nature of the side-arms and of the spacer length in pincer-type systems, the nickel complexes with unsymmetrical κN^{amine},κC^{NHC},κN^{imine} pincer ligands were prepared (Scheme 57) [105,160]. The structurally characterized **210** was obtained in 67 % yield by the reaction of the imidazolium ammonium salt **209** with [Ni(COD)$_2$] in THF [160]. In contrast, the Ni^{II} complexes **213** and **214** were synthesized by transmetalation reactions of the silver carbene complexes **122**–**123**, generated by reaction of the precursors **211**–**212** with Ag_2O [105]. Their structures were confirmed by X-ray diffraction analysis. Like in the case of the Cr^{III} complexes **124**–**125** discussed above (Scheme 32), the length of the spacer connecting the NHC moiety to the amine group can be varied while the imine wing-tip donor remains constant. The complexes **213**–**214** were found to be active precatalysts for the oligomerization of ethylene [105].

A series of non-symmetrical κN,κC^{NHC},κN pincer Ni^{II} complexes **219**–**225** was synthesized by the reactions of [NiCl$_2$(PPh$_3$)$_2$] with the silver carbene transfer complexes generated from **215** to **218** and Ag_2O and were characterized by single crystal X-ray diffraction and NMR spectroscopy. The rare **224** and **225** featured two Ni pincer containing moieties bridged by an unsupported hydroxide. The ^{1}H NMR resonances at δ −1.58 and −1.20 ppm were assigned to the hydroxyl protons of **224** and **225**, respectively. All complexes were used as catalyst precursors for Suzuki-Miyaura cross-coupling and complex **221** showed a higher catalytic activity in reactions of aryl iodides and aryl bromides (Scheme 58) [161].

Two dinuclear nickel complexes **228** and **229** were synthesized by carbene-transfer reactions to [NiCl$_2$(PPh$_3$)$_2$] from the corresponding silver carbene complexes, the latter were obtained from **226** and **227** and Ag_2O, respectively (Scheme 59). All complexes were characterized by X-ray diffraction analysis and NMR spectroscopy [162]. The ^{1}H NMR spectra of **228** and **229** displayed a distinct feature at δ 1.90 ppm and 1.67 ppm, respectively, attributable to the μ-OH; the C^{NHC} in the ^{13}C NMR spectra were observed at δ 153 ppm. The structures of the binuclear complexes are very similar and featured a bridging arrangement of the tetradentate ligand with hydroxide and pyrazolate bridges, forming a saddle-shaped conformation; the Ni-–Ni distances were 3.255 and 3.216 Å, respectively. Complexes **228** and **229** showed excellent catalytic activities in Suzuki-Miyaura and Kumada-Corriu coupling reactions of various aryl chlorides in excellent yields (Scheme 59) [162].

Palladium and Platinum. A series of palladium and platinum pincer-type complexes **230**/**231**, **233**/**234** and **236**/**237** was prepared by transmetalation reactions (Scheme 60) [146,151,163]. Thus, the pale yellow **230**/**231** and **233**/**234** were formed by the carbene transfer from the triangular trinuclear copper carbene and nickel carbene complexes

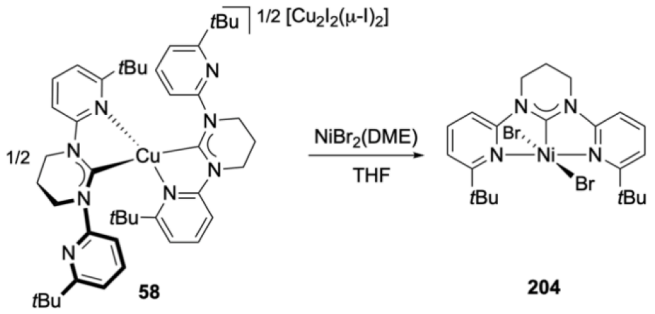

Scheme 55. Ni complex with rigid backbone of type IIIb (Chart 4) obtained by transmetalation from Cu.

188 and **167** to [PdCl$_2$(1,5-COD)] and [PtCl$_2$(1,5-COD)], respectively [146,151]. Complexes **236** and **237** were obtained by the reaction of [PdCl$_2$(NCMe)$_2$] and [PtCl$_2$(1,5-COD)], respectively, with the linear tetranuclear silver complex **235**, which in turn was accessible by the reaction of **218** with Ag_2O [163]. The platinum complex **232** resulted from the reaction of K_2PtCl_4 with the silver carbene complex derived from the reaction of **147** with Ag_2O, followed by the addition of $AgPF_6$ [139]. Its ^{1}H NMR spectrum features an AB-type pattern at 5.93 and 4.85 ppm, which was assigned to the diastereotopic bridging methylene protons. The complexes **230** [151] and **236** [163] were found to be highly active catalysts for Suzuki-Miyaura cross coupling reactions.

Interestingly, a silver transmetalation protocol from the Ag complex obtained by reaction of Ag_2O with **238** to [PtCl$_2$(COD)] led to the binuclear **239**. The lack of N-pyrazol substitution is presumably responsible for the formation of this structure (Scheme 61) [164].

The palladium complex **241** was also obtained by carbene transfer reaction (Scheme 62) [148]. Treatment of the imidazolium salt **175** with Ag_2O afforded the silver carbene complex **240**, which was reacted with [PdCl$_2$(COD)] in CH_2Cl_2 to give complex **241** in good yield [148]. All the NMR data were consistent with the structure shown for complex **241**.

Finally, the complex **243** was obtained by the reaction of precursor **242** with $PdCl_2$ in the presence of K_2CO_3 and pyridine (Scheme 63) [165]. In the ^{13}C NMR spectrum of **243**, a characteristic resonance at 152.7 ppm was assigned to the carbene carbon. This complex was found to be an active catalyst for C-C coupling reactions [165].

3.6.8. Group 11 metals (Cu)

The rare deep blue Cu^{II} complexes **244** and **245** with κN, κC^{NHC}, κN-pincer ligands were obtained by the reaction of the bis(picoline)-functionalized imidazolium salt **142** with $CuSiF_6$ in methanol in air (Scheme 64) [166]. In the structure of **244**, the Cu center has a pseudo-octahedral coordination geometry and the Cu–C^{NHC} bond length of 1.915(3) Å is significantly shorter than those previously reported for Cu^{II}–NHC complexes (average Cu–C^{NHC} bond length of 1.96 Å) [167–170]. Crystals of **245** were obtained by recrystallization of the blue reaction precipitate from DMSO-d_6 over a 2–3 months period in an NMR tube. The crystal structure of **245** revealed that two square-pyramidal Cu^{II}–NHC moieties cocrystallized with one [Cu{SO(CD$_3$)$_2$}$_6$]$^{2+}$ in a 2:1 ratio, respectively. The Cu–C^{NHC} bond length of 1.9319(19) Å is longer than that in complex **244** (Scheme 64) [166].

The analogous rare, air stable and water soluble Cu^{II} complexes **245A** and **245B** with the ligand motif **IIb** were obtained by reacting the precursors **142** and **148** with Cu(OAc)$_2$ • H_2O (Scheme 64). They were characterized by diverse spectroscopic techniques and crystallography. The paramagnetic species adopted distorted octahedral geometries with *mer* disposition of the pincer and κO,κO'chelating acetate ligands and short Cu–C^{NHC} bond distances (1.920–1.935 Å). They displayed isotropic EPR spectra with virtually absent hyperfine interactions and irreversible redox behavior in cyclic voltammetry in MeCN. The complexes have been studied as catalysts for the hydrogenation of 2-acetylpyridine in water using $PhSiH_3$, generally affording the product in moderate yields (up to *ca.* 50 %); the substrate scope of the catalysis was also explored in ethanol. Lastly, attempts to employ the complexes in the presence of DNA as hybrid enantioselective catalysis resulted in poor ee's which was attributed to unfavorable binding of the complexes to DNA. Complex **245A** was also studied as catalyst for the conversion of arylboronic acids to phenols [171,172].

Cu^{II}–NHC complexes containing doubly- or triply-bridging hydroxido ligands were also reported (Scheme 65) [173,174]. The complex **246** was formed by the reaction of the corresponding silver carbene complex with copper powder in MeCN at room temperature [173]. It could also be obtained by stirring the imidazolium precursor **226** with Cu powder in MeCN. In the IR spectrum, a characteristic absorption at 3446 cm^{-1} was attributed to the –OH group. The structure of **246** was established by X-ray diffraction and revealed a dinuclear complex with the copper centers in distorted square-planar environments. Similarly, the

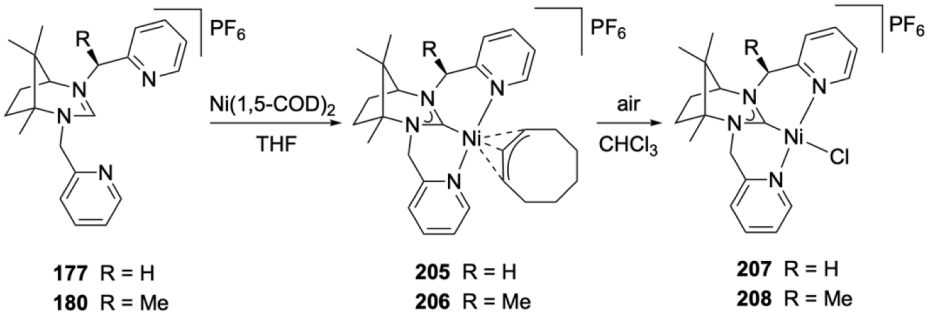

Scheme 56. Ni complexes with pincer backbone of type **IVa** (Chart 4).

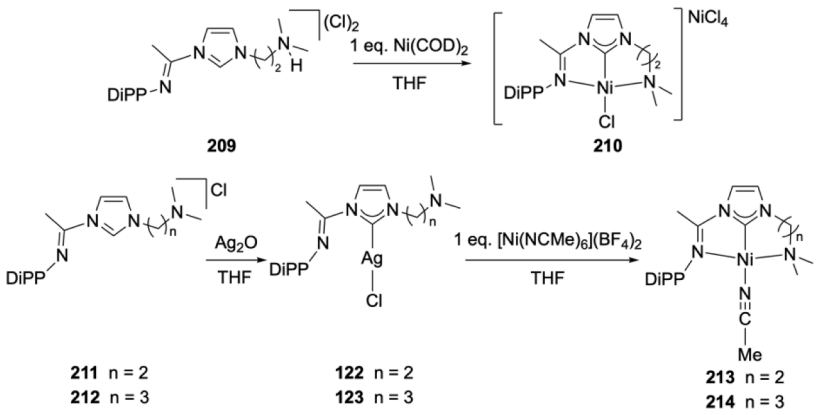

Scheme 57. Ni complexes with non-symmetrical ligand backbone of type **Va** (Chart 4)

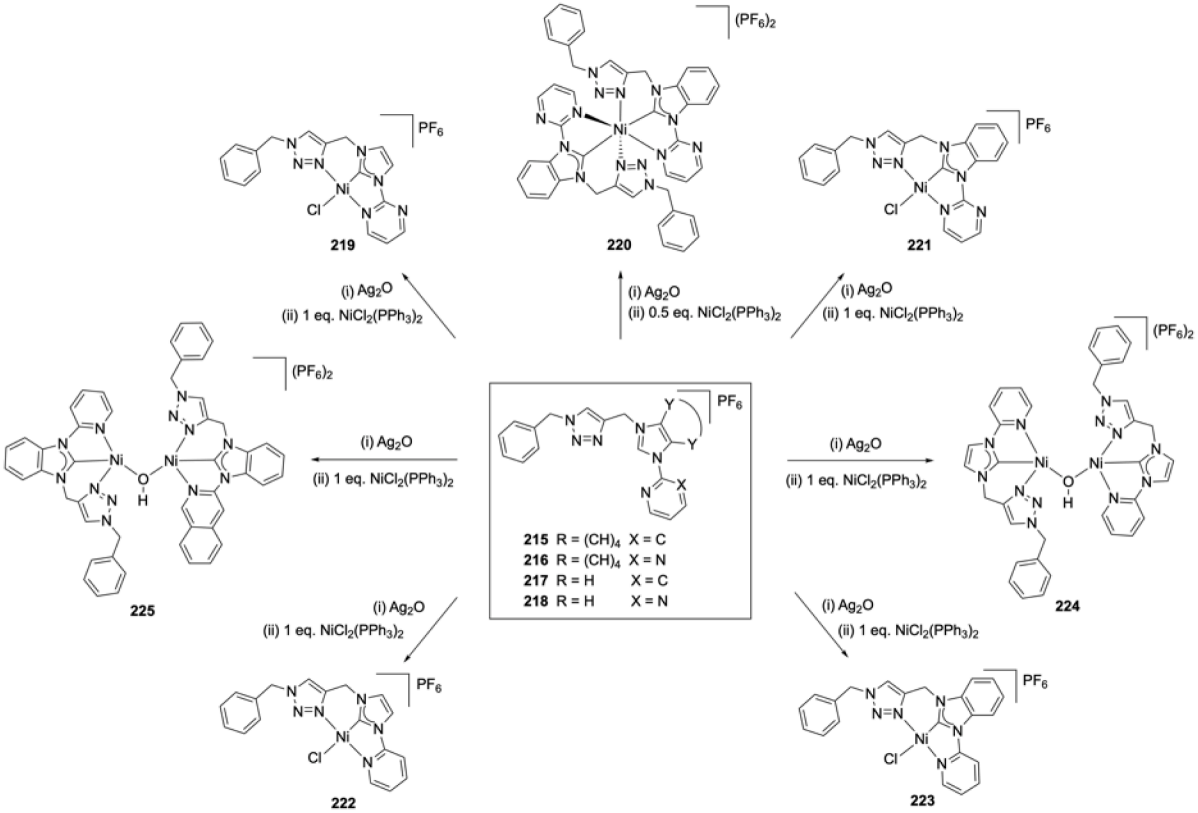

Scheme 58. Ni complexes with pincer backbone related to type **Vb**.

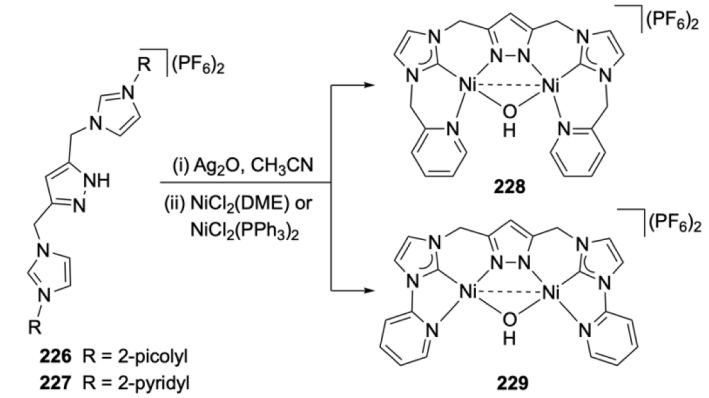

Scheme 59. Binuclear Ni complexes with pincer ligand backbone related to type **Vc**

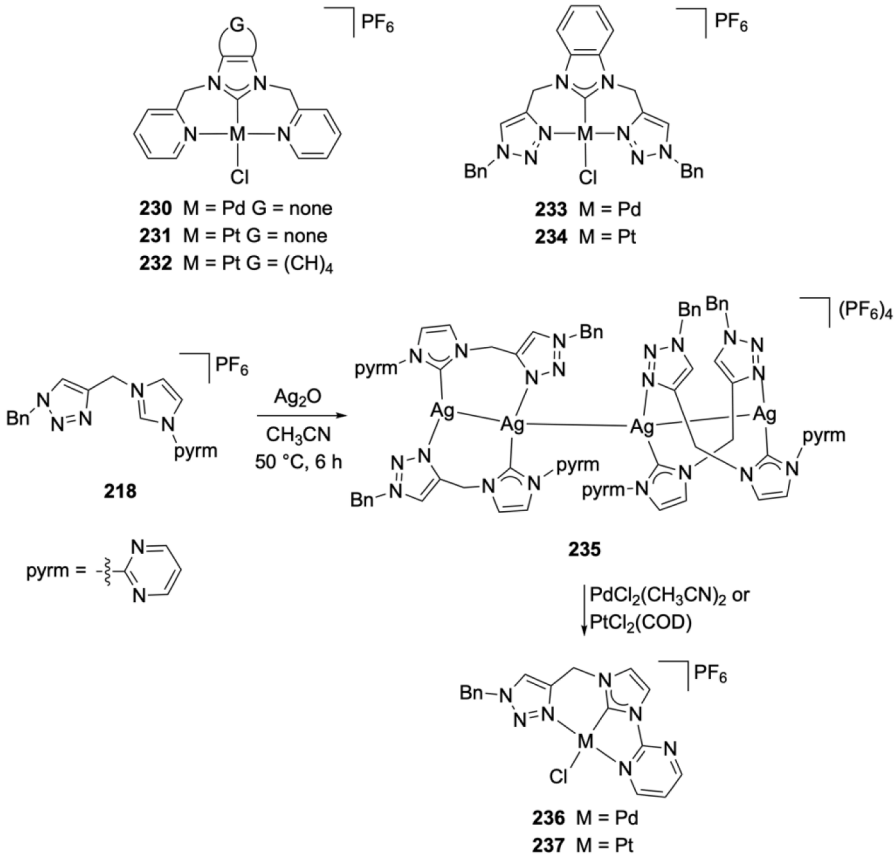

Scheme 60. Pd and Pt complexes bearing backbone ligands of type **IIb**, **IIe** and **Vd**.

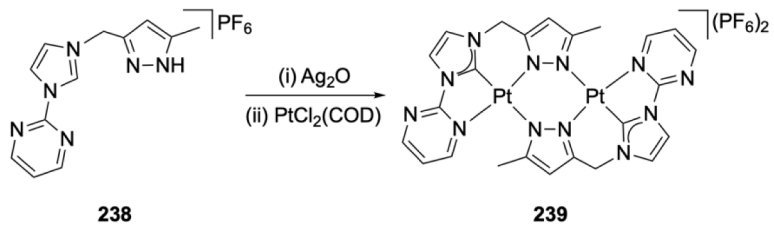

Scheme 61. Binuclear Pt complex with non-symmetrical ligand backbone of type **Vc**

complexes **248** and **249** were synthesized either by the reactions of silver carbene transfer reagents with Cu powder in MeCN or by stirring **227** or **247** with Cu powder. Their structural determination revealed tetranuclear, hydroxido-bridged arrangements. The catalytic activities of **246**, **248** and **249** in N-arylation of imidazoles and aromatic amines were evaluated and **249** was more active than complexes **246** and **248**

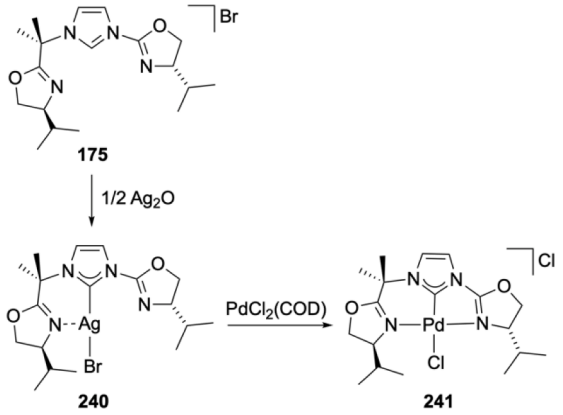

Scheme 62. Pd complex with non-symmetrical ligand of type **Vb**.

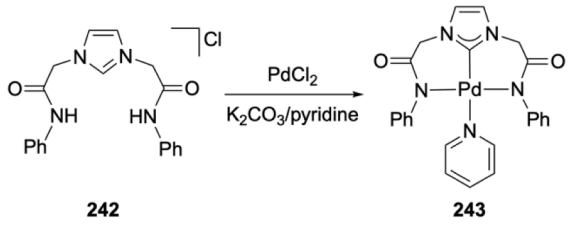

Scheme 63. Pd complex with symmetrical ligand backbone of type **Ib**.

[173].

3.6.9. Group 14 (Ge)

A series of Ge complexes bearing the κN, κC^{NHC}, κN-terdentate ligand (type **IIa**, Chart 4) was reported (Scheme 66) [175]. Complex **252** was obtained by ligand transmetalation from the zinc complex **251** to [$GeCl_2$·diox] in benzene; in turn, **251** was prepared by the reaction of precursor **250** with $ZnCl_2$ in THF in the presence of LiHMDS. Reduction of **252** by KC_8 in benzene resulted in the formation of the dark red **253** that was characterized by NMR spectroscopy with peaks due to the imidazol backbone protons at 6.84 ppm (significantly upfield-shifted compared to the complex **252**). The X-ray structure of **253** revealed the Ge–C^{NHC} bond distance of 1.881(1) Å. Reaction of **253** with CH_3I led to the stable at −25 °C (unstable at RT) **254** the NMR spectrum of which exhibits characteristic methyl group resonances (δ_H 1.16 ppm, δ_C 6.2 ppm) assignable to Ge–*CH_3* species. Warming the solution of **254** to room temperature afforded pure complex **255** in which the germanium bound methyl migrated to the C^{NHC} rendering the NHC ligand an imidazolide; the migration was evidenced by NMR spectroscopies (δ_C 87.8 ppm assigned to the N*C*(CH$_3$)N by ^{1}H–^{13}C HMBC). Treatment of **253** with anhydrous HCl in benzene resulted in the formation of complex **256**, which precipitated from the reaction medium. Its NMR spectra exhibited characteristic bands at δ_H 6.21 and δ_C 88.0 ppm for the NC*H*N unit and its structure revealed a pyramidal geometry around the germylene center (Ge–C^{NHC} at 2.029(4) Å). Furthermore, reaction of **253** with PhI led to the formation of the complex **258**, in which the Ph group has migrated to the C^{NHC} of the NHC ligand. The N*C*N resonated at *δ* 90.4 ppm in the ^{13}C NMR spectrum. Treatment of **253** with excess of $GeCl_2$ or one equivalent of $GeCl_4$ in benzene afforded complex **259** as dark yellow solid, that was also characterized by NMR spectroscopy and X-ray diffraction analysis. The Ge–C^{NHC} bond distance of 2.011(5) Å in **259** was comparable to that in the related imino-NHC-supported Ge complexes. Reaction of **253** with pentafluoropyridine in benzene at 50 °C afforded complex **260**. The structure of complex **260** was established by NMR spectroscopy and X-ray diffraction analysis, with the Ge–C^{NHC} distance of 2.100(3) Å. The combinations of strong σ-donor (NHC) and π-acceptor (imine) sites renders **IIa** ideal for the stabilization of lower oxidation state Ge^0/Ge^{II} centers.

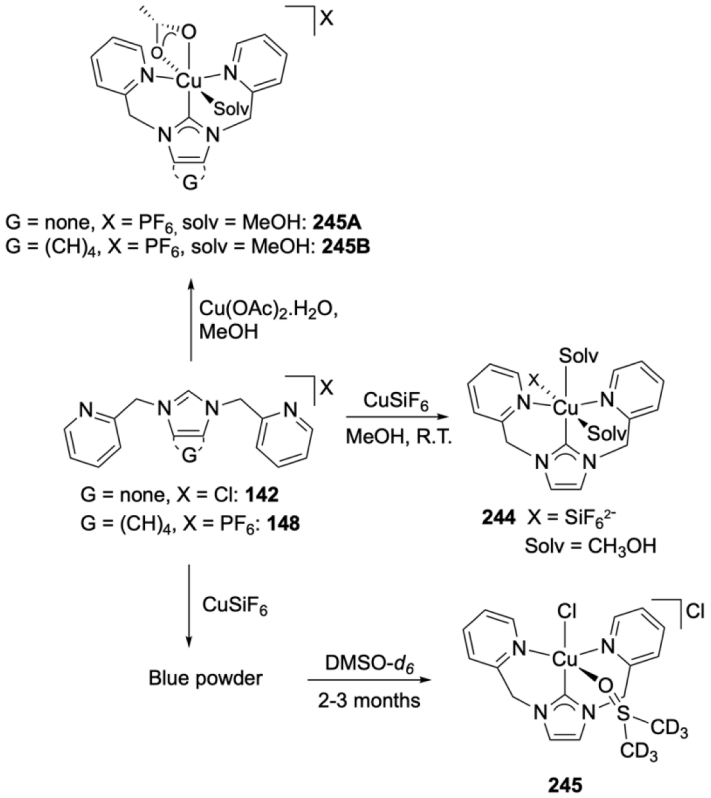

Scheme 64. Synthesis of Cu^{II} complexes with κN, κC^{NHC}, κN-pincer ligands

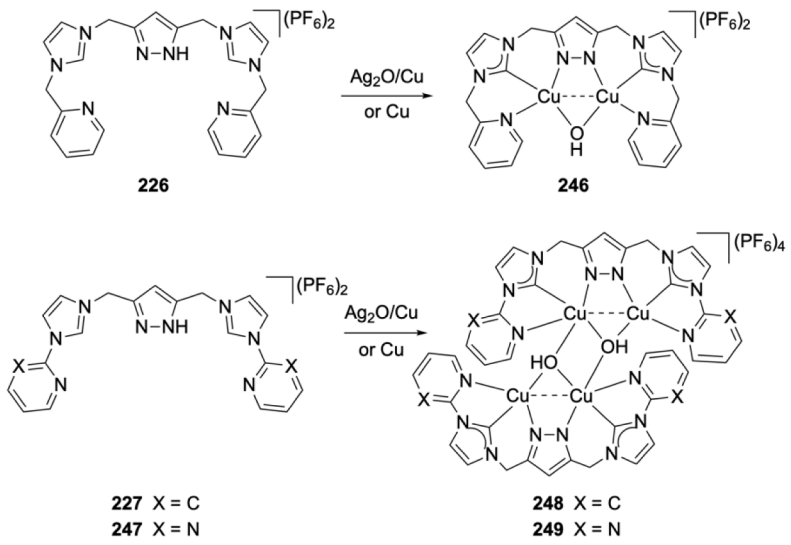

226 **246**

227 X = C
247 X = N

248 X = C
249 X = N

Scheme 65. Bi- and tetra-nuclear Cu complexes with backbone of type **Vc**

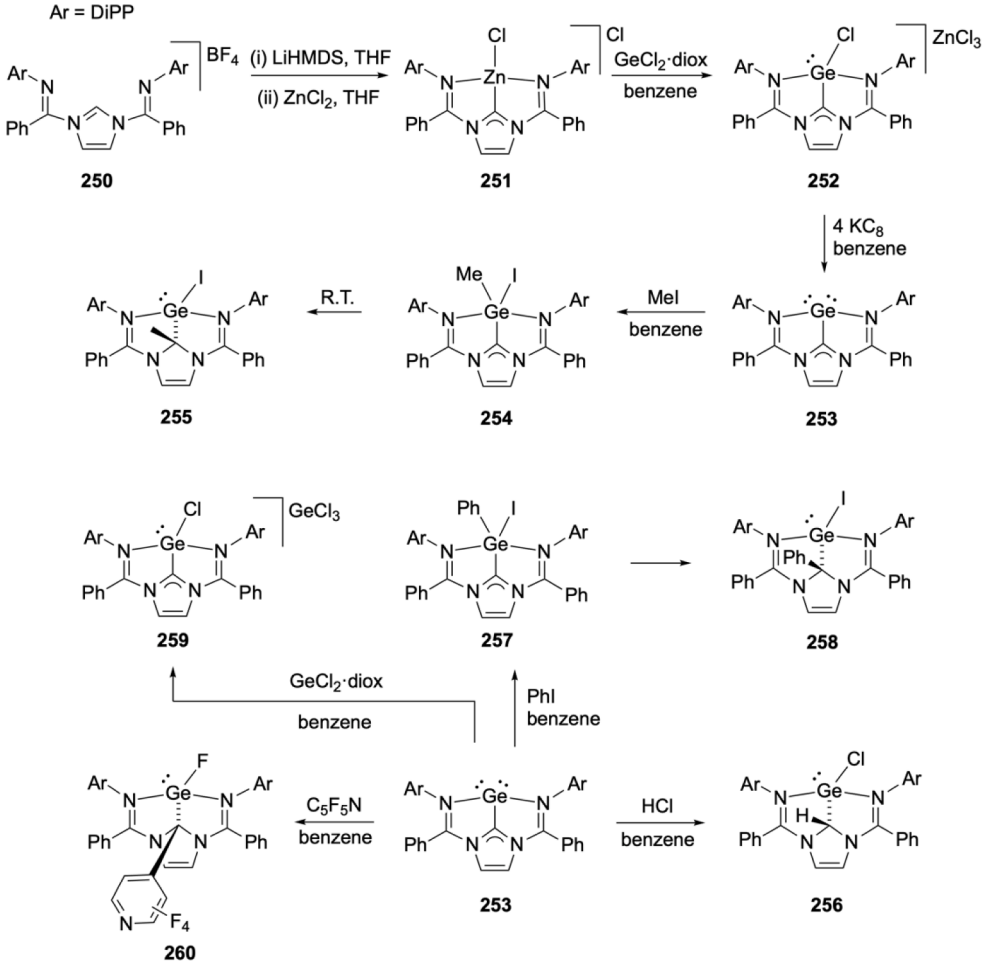

250 **251** **252** **253** **254** **255** **256** **257** **258** **259** **260**

Scheme 66. Ge complexes with pincer ligand of type **IIa**.

3.7. Type N,C^{NHC},P

3.7.1. Group 7 metals (Mn)

The only two manganese complexes bearing a N,C^{NHC},P ligand, **265** and **266**, were prepared in two steps (Scheme 67) [176]. Treatment of the precursors **261** and **262** with the strong base KHMDS, followed by addition of $[MnBr(CO)_5]$, afforded the intermediates **263** and **264**, respectively. These reacted with AgOTf to give complexes **265** and **266** that were fully characterized by X-ray diffraction analysis. Complexes **265** and **266** were active in the hydrogenation of ketones, with **266**

exhibiting higher catalytic efficiency due to the 5,6-fused membered architecture, leading to the dissociation of the pyridine arm and releasing a vacant coordination site favoring the catalytic process [176].

3.7.2. Group 9 metals (Rh)

The rhodium complex **269** (Scheme 68) was accessed in two steps: firstly, the reaction of the imidazolium salt **267** with $[Rh(acac)(\mu\text{-}CO)]_2$ in THF led to the imidazolium intermediate **268**, which was characterized by ^{31}P and ^{1}H NMR spectroscopic methods (doublet at δ 43.3 ppm, $^{1}J_{P\text{-}Rh} = 170.4$ Hz and singlets at δ 7.88 and 8.46 ppm) indicating the presence of uncoordinated imidazolium and pyridine functionalities, respectively. In a subsequent step, heating a solution of **268** at 120 °C yielded **269**. In the ^{31}P NMR spectra, the disappearance of the doublet at δ 43.3 ppm and the appearance of two new doublets (δ 28.8, $^{1}J_{Rh\text{-}P} = 166$ Hz, minor, δ 27.1 ppm, $^{1}J_{Rh\text{-}P} = 165$ Hz, major) were attributed to the formation of two isomers. However, **269** could not be structurally characterized due to its instability (Scheme 68) [177].

The series of Rh^{I} and Rh^{III} complexes **272**–**274** with $\kappa N^{pyridine}$, κC^{NHC}, κP-pincer ligands were prepared from the imidazolium **270** with $[Rh(\mu\text{-}Cl)(COD)]_2$ *via* the phosphane adduct **271**, which was deprotonated with one equivalent of KHMDS in THF to the orange **272** (Scheme 69). The latter was characterized by ^{1}H NMR spectroscopy (absence of imidazolium proton resonance, presence of a resonance at δ 9.38 ppm attributable to the 5-C*H*$_{Py}$ proton indicative of the pyridine coordination to Rh). The ^{31}P NMR spectrum of **272** showed a doublet at δ 86.7 ppm. The instability and poor solubility of **272** hampered crystallographic characterization. However, oxidation of **272** with I_2 produced quantitatively the stable complex **273**, which on treatment with excess KI afforded **274**. The ^{31}P NMR spectrum of **274** comprised a doublet at δ 76.9 ppm ($^{1}J_{Rh\text{-}P} = 127.0$ Hz) and the ^{13}C NMR spectrum, a doublet of doublets at δ 181.7 ppm ($^{1}J_{Rh\text{-}C} = 33.0$ Hz, $^{2}J_{C\text{-}P} = 9.7$ Hz) assigned to the C^{NHC}. The structure of complex **274** revealed a distorted octahedral coordination geometry, with a short Rh–C^{NHC} bond distance of 1.894(3) Å indicative of a strong bond while the high *trans*-influence of the NHC moiety was responsible for a longer Rh–I_{trans} bond (2.7450(3) Å) compared to the Rh–I_{cis} bond (2.6729(3) and 2.6755(3) Å) distances, respectively (Scheme 69) [178].

3.7.3. Group 10 metals (Ni, Pt)

The imidazolium salt **267** (*vide supra*) was also employed for the synthesis of the Ni and Pt complexes **277** and **278**, respectively (Scheme 70) [177]. Thus, treatment of **267** with $[Ni(COD)_2]$ led to the formation of **275**, which exhibits a ^{31}P NMR spectrum with a resonance at δ 13.1 ppm, a ^{1}H NMR spectrum with characteristic resonances assignable to the η^3-cyclooctenyl ligand (δ 5.22 ppm, t, $^{3}J_{H\text{–}H} = 8.5$ Hz, δ 4.36 ppm,

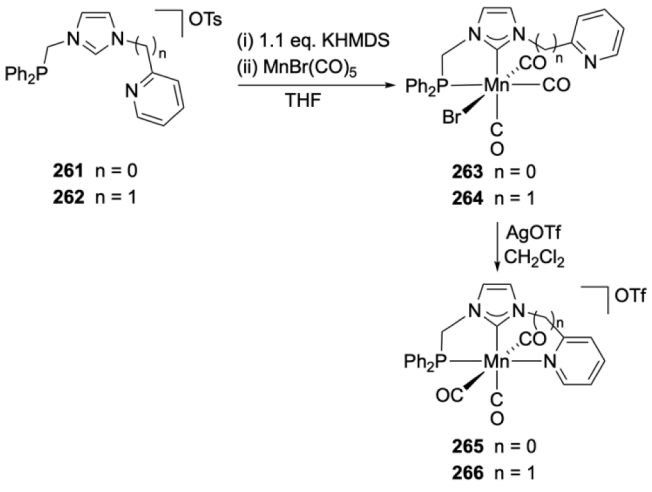

Scheme 67. Mn^{I} complexes with κN, κC^{NHC}, κP ligand backbone

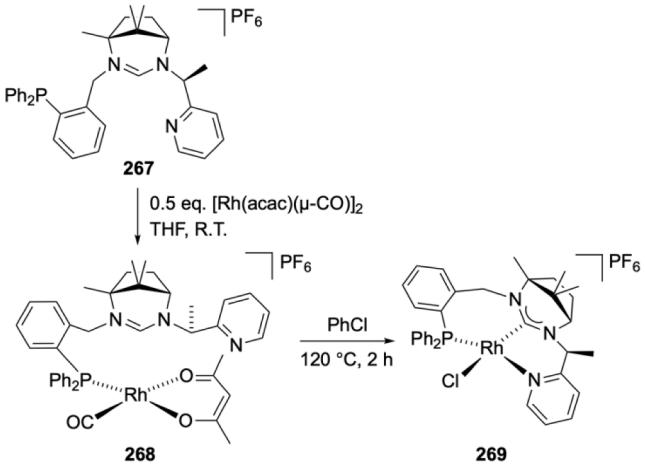

Scheme 68. Rh complex with pincer ligand of type $\kappa N^{pyridine}$, κC^{NHC}, κP

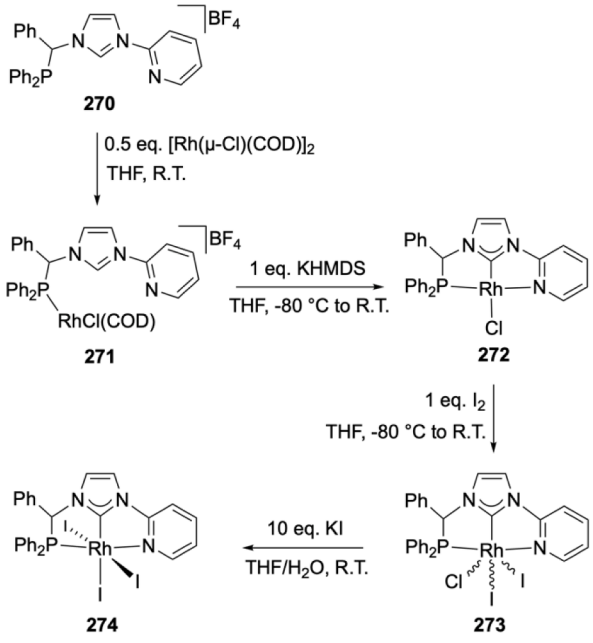

Scheme 69. Rh complexes with $\kappa N^{pyridine}$, κC^{NHC}, κP - pincer ligand.

m and δ 3.91 ppm, m) and a ^{13}C NMR spectrum with a doublet at δ 202.1 ppm, $^{2}J_{P\text{-}C} = 16.5$ Hz for the C^{NHC}. Exposure of a solution of **275** in $CHCl_3$ to air afforded two isomers of complex **277** (two peaks at δ 8.0 and 5.2 ppm in the ^{31}P NMR spectrum) [177]. The structure of **277** showed a square-planar coordination geometry at nickel. The platinum complex **278** with the same ligand was obtained in two steps from the salt **267**: firstly, reaction of **267** with $[K_2PtCl_4]$ in EtOH afforded the *trans* diphosphane complex **276**, then addition of 1.1 equivalent of KHMDS to a THF solution of **276** afforded complex **278** [177]. The structure of **278** was confirmed by X-ray analysis and NMR spectroscopy, with a singlet in the ^{31}P NMR spectrum at δ_P −7.8 ppm with platinum satellites ($^{1}J_{P\text{–}Pt} = 3655$ Hz). The structure of **278** was analogous to that of **277**.

Similarly, the imidazolium salt **270** (*vide supra*) was converted to complex **279** by the reaction with $[NiBr_2(i\text{PrCN})]_n$ in the presence of NEt_3 at 60 °C [178]. In the ^{1}H NMR spectrum of **279**, a broad singlet at δ 8.85 ppm was assigned to the 5-C*H*$_{Py}$ in agreement with coordination of the pyridine moiety; the ^{13}C NMR spectrum featured a doublet at δ 170.5 ppm for the C^{NHC}. The structure of **279** revealed a distorted

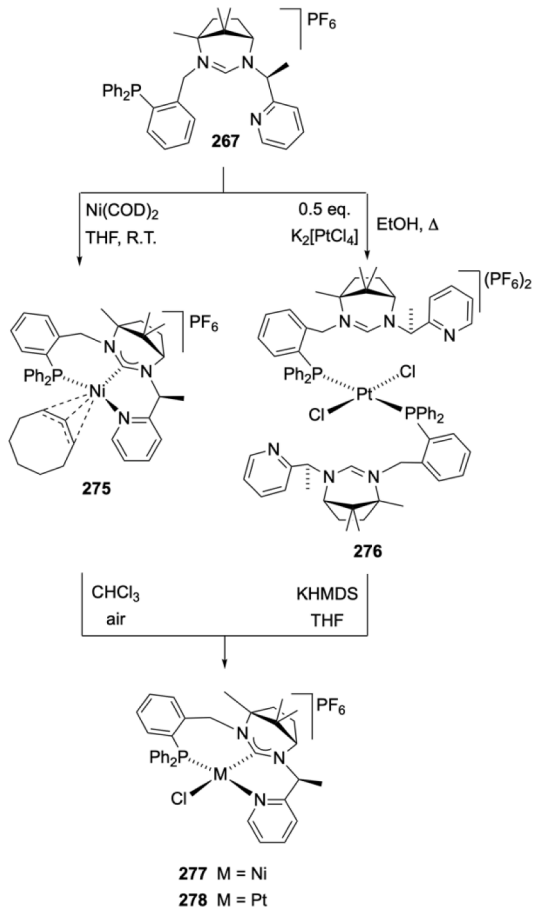

Scheme 70. Ni and Pt complexes with a κN, κC^{NHC}, κP pincer ligand

square-pyramidal coordination geometry and a Ni–C^{NHC} bond distance of 1.797(2) Å, one of the shortest ever reported for this type of bond (Scheme 71) [162,179,180].

3.8. Type N,C^{NHC},O

3.8.1. Group 8 metals (Ru)

A series of ruthenium complexes **281**–**283** bearing $\kappa N^{pyridine}$, κC^{NHC}, $\kappa O^{carboxylate}$ pincer ligands was reported (Scheme 72). Reaction of the zwitterionic imidazolium **280** with Ag_2O, followed by transmetalation with $[Ru(\mu\text{-}Cl)Cl(p\text{-cymene})]_2$ and subsequent addition of 2,2′:6′,2″-terpyridine in DMSO gave **281**. Its ^1H NMR spectrum displayed two singlets at δ 5.72 and 4.60 ppm that were assigned to the methylene protons; the characteristic ^{13}C NMR carbene resonance was observed at δ 192.5 ppm. Similarly, treatment of $[Ru(\mu\text{-}Cl)Cl(p\text{-cymene})]_2$ with the silver carbene complex obtained from Ag_2O and **280**, followed by the addition of 4-picoline in DMSO, generated the complex **282** (C^{NHC} resonance in ^{13}C NMR spectrum at 182.9 ppm). The structure of complex **282** was confirmed by X-ray diffraction analysis. Interestingly, 4-picoline/H_2O exchange reaction with complex **282** under acidic conditions occurs and the nature of complex **283** was confirmed by ESI-MS and ^1H NMR spectroscopy (Scheme 72) [181].

The related complexes **284**–**286** were also synthesized by the reaction of the corresponding precursors with Ag_2O, followed by the addition of $[Ru(\mu\text{-}Cl)Cl(p\text{-cymene})]_2$ and pyridine derivatives in DMSO (Chart 5) [182]. These complexes were characterized by NMR spectroscopy and the structure of complex **286** was also confirmed by X-ray diffraction analysis.

Finally, mixing the precursor **280**, $[Ru(\mu\text{-}Cl)Cl(p\text{-cymene})]_2$ and 2,2′-bipyridine afforded **287** (Scheme 73) [183]. The derivative **288** was formed by refluxing complex **287** in 4-picoline/MeOH. The nature of both complexes **287** and **288** was fully confirmed by NMR spectroscopy [183]. The complexes **282** [181], **284**–**286** [182] and **287**–**288** [183] were highly active catalysts for the water oxidation reaction (Schemes 72,73 and Chart 5).

The imidazolium amide salt **289** was converted with Ag_2O in dichloromethane to the silver complex **290**, which was then reacted with $[RuCl_2(PPh_3)_3]$ in acetonitrile, affording after counter ion exchange with NH_4PF_6 in aqueous solution the pincer complex **291** (Scheme 74) [184]. In the ^{13}C NMR spectrum of this complex, a characteristic resonance at 188.5 ppm was observed for the coordinated C^{NHC}. The structure of **291** revealed a *fac*-pincer arrangement with Ru–O and Ru–C^{NHC} bond distances of 2.143(4) and 1.978(6) Å, respectively. The complex **291** was found to be a highly active precatalyst for the oxidation of alcohols to the corresponding aldehydes or ketones [184].

3.8.2. Group 10 metals (Ni, Pd)

The series of nickel and palladium pincer complexes **295**–**297** [185] and **301**–**304** bearing *o*-aryloxide functionalized NHC ligands were synthesized by the reaction of the corresponding imidazolium precursors **292**–**294** [186] with one equivalent of $[NiCp_2]$ in THF under reflux for 24 h or *via* transmetalation from the *in situ* prepared silver complexes originating from the imidazolium salts **292**, **298**–**300** to $[PdCl_2(COD)]$, respectively, Scheme 75). All complexes were characterized by NMR spectroscopy and X-ray diffraction analysis. The Ni complexes showed high catalytic activities in the homopolymerization of norbornene and the copolymerization of norbornene with 1-octene and the Pd complexes showed excellent catalytic activities in the norbornene polymerization in the presence of MAO or Et_2AlCl as cocatalysts (1.23×10^7 g of PNB (mol of Pd)$^{-1}$h^{-1}) [185,186].

The highly thermally stable complex **306** was prepared by the transmetalation of the corresponding silver carbene complex with $[PdCl_2(NCMe)_2]$ in DMSO at 50 °C (Scheme 76). It showed high catalytic activity in the Heck reaction [187].

The complexes **308**–**311** bearing $O^{alcohol},C^{NHC},N^{amide}$ and $O^{alcoxide}$, C^{NHC},N^{amide} pincer ligands were obtained by the sequence shown in Scheme 77 [188]. Firstly, metalation of the imidazolium precursor **307** with Ag_2O followed by transmetalation to $[PdCl_2(NCMe)_2]$ in acetonitrile at room temperature gave the charge neutral **308** which could be converted to the cationic **309** on reaction with $AgBF_4$ in acetonitrile; the latter complex was found to be highly active in H/D exchange for various substrates in D_2O. In water, **310** was formed by substitution of acetonitrile with H_2O and was subsequently dimerized in the presence of HBF_4 to the binuclear **311**. The latter transformation is reversible (Scheme 77) [188].

The complex **312** was obtained by the reaction of the corresponding imidazolium precursor with $PdCl_2$ in the presence of NaOAc acting as base and was characterized by NMR spectroscopy and X-ray diffraction analysis (Scheme 78). Cleavage of the ester group in **312** with TFA gave complex **313** with a dangling carboxylic acid functionality. In the presence of a base such as NaOH, NaOAc or NEt_3, deprotonation of the dangling carboxylic group occurred, leading to the pincer complex **315**, this step can be reversed by the addition of acid. Alternatively, complex **315** could be accessed directly from precursor **314** with $PdCl_2$ in the presence of NaOAc. Conversely, complex **313** could also be obtained by reaction of **315** with an acid such as HCl or HBr. The preparation of **315** by silver carbene transfer reaction was not possible owing to the acidity of the carboxylic acid. Complex **315** was found to be an efficient precatalyst in cross-coupling reactions (Suzuki-Miyaura and Heck-Mizoroki) (Scheme 78) [189].

Finally, the enolate palladium complexes **316**–**323** were prepared by a microwave-assisted solid-phase approach (Chart 6) [190]. They were characterized by ESI-MS and used as biocompatible catalysts for bioorthogonal prodrug activation due to the presence of free carboxylic acid groups.

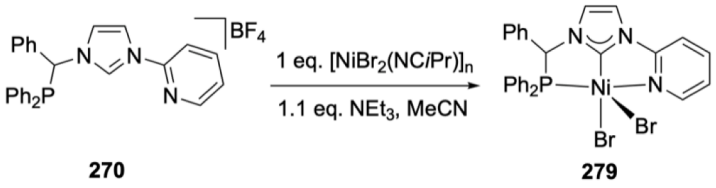

270 279

Scheme 71. Ni complex bearing κN, κC^{NHC}, κP ligand backbone.

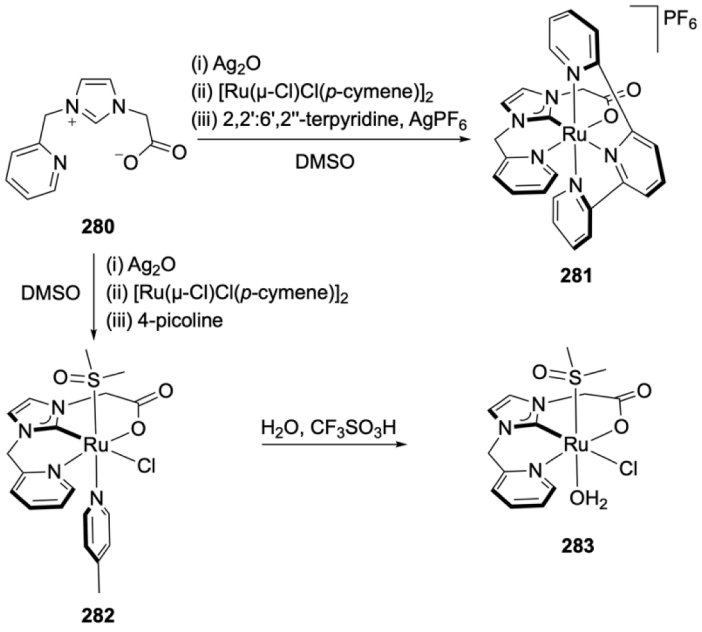

280 281 282 283

Scheme 72. Ru complexes bearing κN^{pyridine}, κC^{NHC}, κO^{carboxylate} pincer ligands.

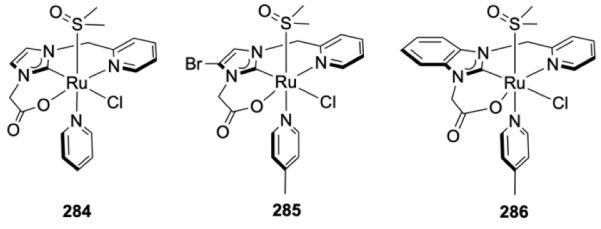

284 285 286

Chart 5. Ru complexes with pincer ligand of type κN^{pyridine}, κC^{NHC}, κO^{carboxylate}

3.9. Type N,C^{NHC},S

3.9.1. Group 10 metals (Ni)

The only two binuclear nickel complexes featuring N^{pyridine},C^{NHC}, S^{thiolate}-terdentate ligands, **326** and **327**, were synthesized by the reactions of precursors **324** and **325** with [Ni(OAc)$_2$] in the presence of tetrabutylammonium bromide under vacuum at 120 °C, respectively (Scheme 79). They were characterized by ^{1}H NMR spectroscopy and X-ray diffraction analysis. Their structures established the pincer binding and the binuclear nature with symmetrical thiolate bridges. The Ni–C^{NHC} bond distances in **326** and **327** were 1.889 and 1.882 Å, respectively. The redox properties and electrocatalytic activities of **326** and **327** were investigated and these complexes possess good catalytic activities in proton reduction. In particular, the complex **327** showed a better catalytic activity with the release of 5×10^{-4} mmol H_2 gas in 10 min in the presence of 6×10^{-3} mmol catalyst [191].

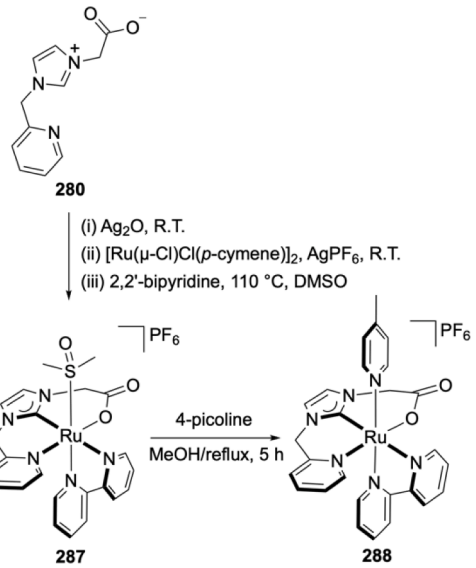

280 287 288

Scheme 73. Ru complexes bearing pincer ligand of type κN^{pyridine}, κC^{NHC}, κO^{carboxylate}.

3.10. Type P,C^{NHC},P

There is a considerable variety of symmetrical κP,κC^{NHC},κP ligands differing in the type of bridgehead NHC, the nature of the phosphane side-arms and the linkers. Despite the electronic analogies between NHC

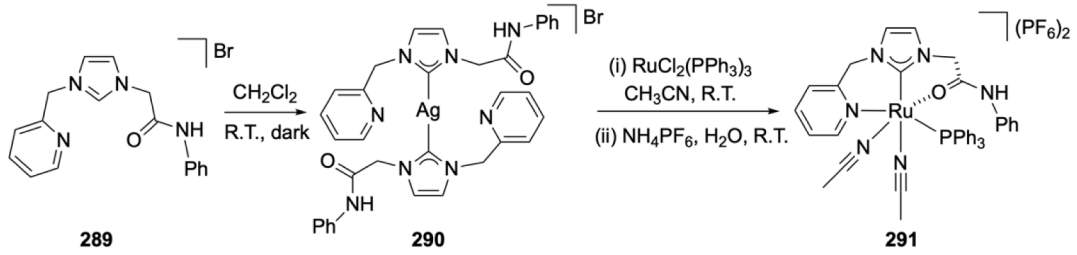

Scheme 74. Ru complex with a $\kappa N^{pyridine}$, κC^{NHC}, $\kappa O^{carboxylate}$ pincer ligand

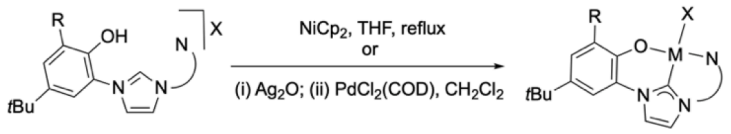

	R	N	X
292	*t*Bu	CH_2Py	Cl
293	*t*Bu	CH_2Py	Br
294	*t*Bu	$CH_2CH_2NMe_2$	Cl
292	*t*Bu	CH_2Py	Cl
298	H	CH_2Py	Cl
299	*t*Bu	$(CH_2)_2NMe_2{\cdot}HCl$	Cl
300	H	$(CH_2)_2NMe_2{\cdot}HCl$	Cl

Py =

	M	R	N	X
295	Ni	*t*Bu	CH_2Py	Cl
296	Ni	*t*Bu	CH_2Py	Br
297	Ni	*t*Bu	$CH_2CH_2NMe_2$	Cl
301	Pd	*t*Bu	CH_2Py	Cl
302	Pd	H	CH_2Py	Cl
303	Pd	*t*Bu	$CH_2CH_2NMe_2$	Cl
304	Pd	H	$CH_2CH_2NMe_2$	Cl

Scheme 75. Pd complexes bearing $\kappa O^{alcohol}$, κC^{NHC}, κN^{amide} pincer ligands

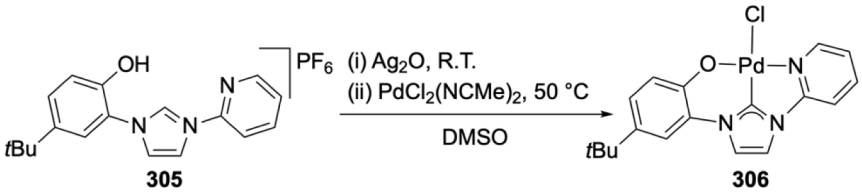

Scheme 76. Pd complex with a pincer ligand of type $\kappa N^{pyridine}$,κC^{NHC},κO.

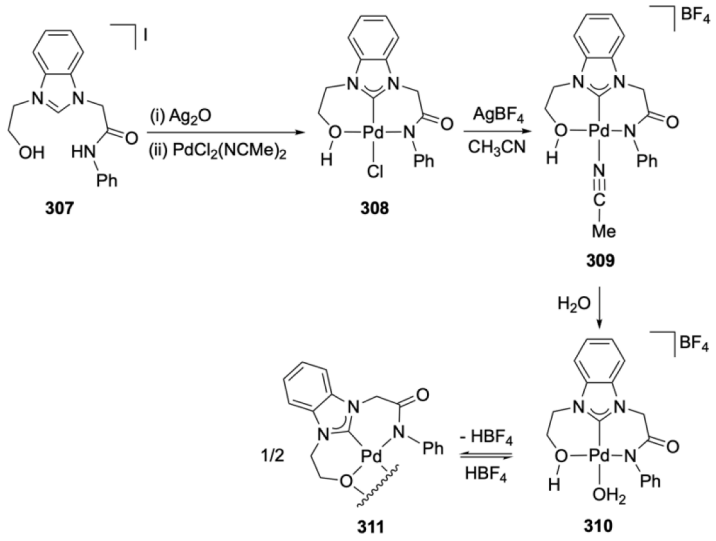

Scheme 77. Pd complexes bearing $\kappa O^{alcohol}$, κC^{NHC}, κN^{amide} and $\kappa O^{alkoxide}$, κC^{NHC}, κN^{amide} pincer ligands

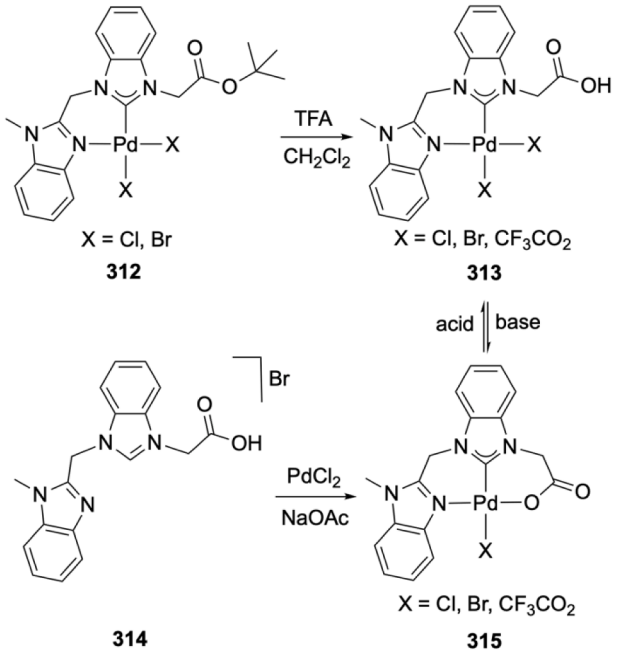

Scheme 78. Pd complexes with pincer ligand of type κN, κC^{NHC}, κO

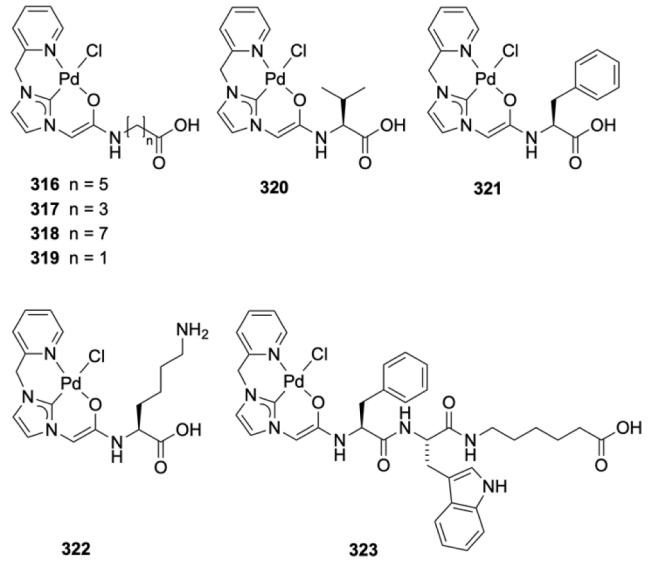

Chart 6. Pd complexes with pincer ligand of type κN, κC^{NHC}, κO

and trialkyl phosphane donors, the underlying design principle that led to P,C^{NHC},P architectures was the desire to replace the pyridine donor in the widespread $P,N^{pyridine},P$ pincers with the stronger σ-donating and easily tunable NHC moiety; as a result, unusual reactivity and catalytic potential were recently uncovered. The earliest P,C^{NHC},P designs employed aryl substituted phosphanes; more recent progress is being witnessed with phosphorus donors substituted with bulky alkyls (*i*Pr, Cy and in particular *t*Bu). Moreover, despite the synthetic difficulties associated with the preparation of rigid designs, they show considerable promise as robust scaffolds in homogeneous catalysis, in particular with the 3d metals, which can adopt a multitude of coordination numbers and geometries. All the known pincer P,C^{NHC},P donor architectures are summarized in Chart 7. The design **VIIc**, despite being macrocyclic is included here in view of it adopting a terdentate coordination, where the metal center is out of the macrocyclic cavity (*cf.* complexes of triazacyclononane). The pincer ligands **Xa**, **Xb** and **Xc** featuring a zero-

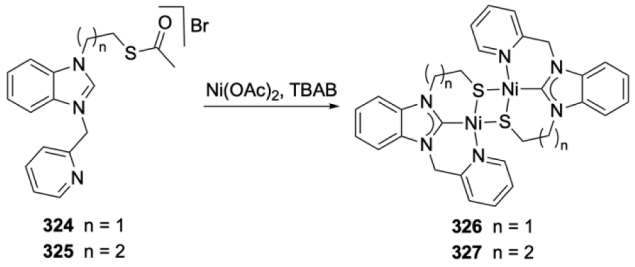

Scheme 79. Binuclear Ni complexes bearing pincer ligand of type $\kappa N^{pyridine}$, κC^{NHC}, $\kappa S^{thiolate}$

valent C atom bridgehead donor fall beyond the scope of this review; they constitute examples of $P,C^{carbodicarbene},P$ pincers and are included in the chart for the sake of comparison and completeness [34,40,192]. Details of the known P,C^{NHC},P ligand designs of Chart 7 and their occurrence within the transition metals are compiled in Table 2; it constitutes a guide for the discussion of this section. Finally, comparative structural and spectroscopic data for all complexes with $\kappa P,\kappa C^{NHC},\kappa P$ pincer ligands are given at the end of the section (Table 3).**

3.10.1. Group 6 metals (Mo)

A series of molybdenum complexes with chelating $\kappa P,\kappa C^{NHC},\kappa P$-pincer ligands **VIc** has been studied (Scheme 80). Reaction of the bis (diphenylphosphino-ethyl)imidazolium salt **328** with KO*t*Bu in THF, followed by the addition of *cis*-$[Mo(CO)_4(pip)_2]$ resulted in the formation of complex **329** [193], the nature of which was confirmed by X-ray analysis and NMR spectroscopy: the metal adopted a distorted octahedral coordination geometry, where the flexible pincer ligand occupies *fac*-sites, the Mo–C^{NHC} bond distance is 2.263(2) Å and the C–O bond distances in the carbonyl ligands that are *trans* to the NHC are longer than those *trans* to the P donors (1.158(3) Å *vs.* 1.149(3) and 1.150(3) Å, respectively). A ^{31}P NMR resonance was observed at δ 27.3 ppm. Computational studies concluded that the *fac* and *mer* isomers were energetically close, but the former was favored to circumvent mutually *trans*-CO ligand placement. Additional findings from the computational studies included the comparable σ-donor strengths of the P and NHC donors and (in contrast to the Mo–P interaction) the lack of any π-bonding in the Mo–NHC interaction, a fact that was attributed to the cancellation of metal-to-NHC π-backdonation from NHC-to-metal π-donation. Similarly, the analogous complex **331** was formed by the reaction of **330** (precursor to **VIb**) with KO*t*Bu in THF, followed by addition of *cis*-$[Mo(CO)_4(pip)_2]$ [194]. Its structure featured *trans*-P–Mo–CO angles of 165.24(11)° and 169.64(10)°, respectively. The Mo–C^{NHC} bond distance of 2.239(3) Å is slightly shorter than that in the corresponding **329** (Scheme 80).

The complexes **334** and **336** with the flexible imidazol-2-ylidenes (type **VIc**) were synthesized by treatment of the Mo^0 precursors **333** and **335** featuring labile PPh_2Me ligands, with the precursor $P,C^{NHC},P{\cdot}HCl$ in the presence of NaO*t*Bu (Scheme 81) [195]. Although **334** was not amenable to structural characterization due to its instability, its nature was supported by IR and Raman spectroscopies, and, in contrast to **329** and **331**, a *mer* coordination mode assigned to the pincer ligand. An absorption band at 1876 cm^{-1} (IR and Raman) was attributed to a coordinated N_2. Interestingly, this value appears to be one of the lowest reported for the N–N stretching vibration for Mo–N_2 complexes, which suggested that N_2 is coordinated *trans* to the NHC functionality. In contrast, the also unstable complex **336**, featuring the chelating dmpm, was characterized by NMR and IR spectroscopy; here the N–N stretching vibration appeared at 1881 cm^{-1} and the ^{31}P NMR spectrum showed an

** Additional references dealing with ligands of type **VIb**, **VIc**, **VIIb** and **VIIIb** are given at the end of the document in the Note added in proofs.

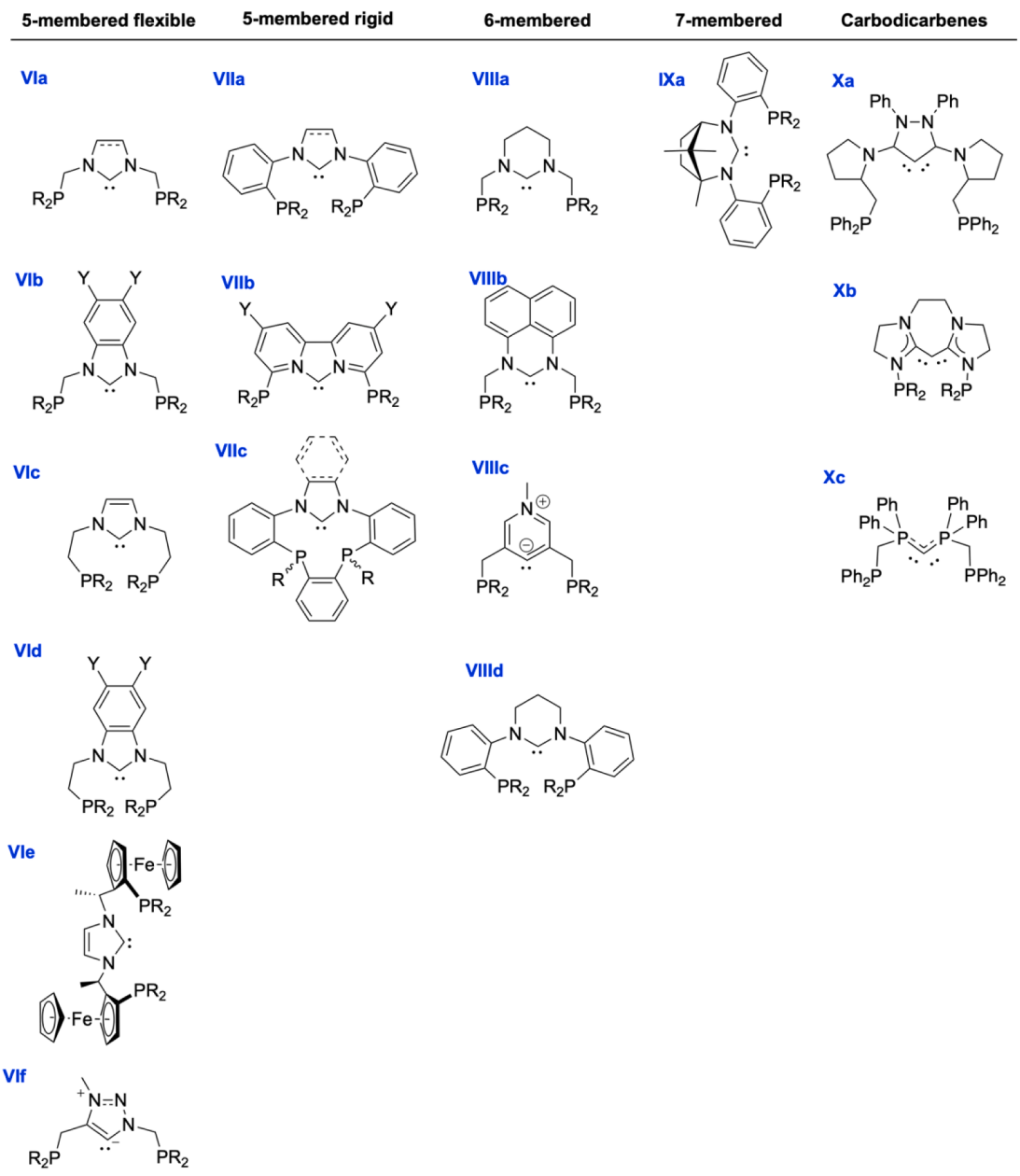

Chart 7. A detailed summary of different pincer type ligand bearing a P, C^{NHC}, P backbone

AA'XX' pattern in agreement with the proposed structure.

An alternative reductive strategy to access Mo^0 dinitrogen complexes has been described. The complexes **337**–**339** were obtained by the reaction of $[MoX_3(THF)_3]$ (X = Cl, Br, I) with the P,C^{NHC},P ligand **332**, and the trichloro Mo^{III} complex **337** was characterized by X-ray crystallography. Na-Hg reduction of **337**–**339** in the presence of two equivalents of $P(OMe)_3$ under N_2 atmosphere resulted in the formation of a mixture of the complexes **340** and **341** (Scheme 81) [195]. Complex **340** was stable and, despite the presence of the less activating π-accepting phosphite coligands, the N≡N stretching vibration in the IR spectrum was still at a low frequency ($\nu = 1932\ cm^{-1}$); this characteristic signal was attributed to the activating effect of the NHC of the pincer, since analogous all phosphane complexes, *e.g.* $[Mo(N_2)(PMe_3)_5]$ or $[Mo(N_2)(SiP_3)(dmpm)]$ (SiP_3 = tris(dimethylphosphinomethyl)methylsilane) exhibited N≡N stretching vibrations at higher wavenumbers ($\nu = 1950$ or $1943\ cm^{-1}$, respectively). The preparation of **340** was always accompanied by the presence of variable amounts of complex **341** which could become the exclusive product if the reduction was carried out in the presence of excess of $P(OMe)_3$. The nature of the rare and unusual phosphorus containing ligand was demonstrated by X-ray crystallography to be a metal-coordinated -P(=O)(OMe) moiety, related to the amido-oxophosphane in $[Cr(CO)_5\{P(=O)(NR_2)\}]$ [196], which, when uncoordinated, forms a trimer. The presence of the coordinated -P(=O)(OMe) was associated with the appearance of a low field multiplet at δ 271.0 ppm in the ^{31}P NMR spectrum, while the C^{NHC} signal in the ^{13}C NMR spectrum appeared at δ 193.8 ppm. The short Mo–P bond distance (2.254(1) Å) was comparable to that in phosphinidene and phosphinidene oxide complexes (*ca.* 2.2–2.3 Å) [197–200] and was attributed to strong Mo–P π-bonding. The mechanism of the formation of the coordinated P(=O)(OMe) was not elucidated, although its formation is associated with the combined demethylation-demethoxylation reaction of a $P(OMe)_3$ which, interestingly, was not observed in related all-phosphane pincer complexes (*i.e.* lacking NHC ligation) [195].

A family of dinitrogen-bridged dimolybdenum complexes bearing

Table 2
Occurrence of complexes with the ligand architectures **VIa** – **Xc** shown in Chart 7 across the transition metals.

Type	R	Y	M
VIa	Cy *t*Bu		Rh^{I} Ni
	Ph		Mn^{I}
VIb	*t*Bu	H or Me	Mo^{0} Mo^{III} Mn^{I} Ru^{II} Ir^{I} Ir^{III} Ni^{II}
	Ph	H	Pd^{II} $Rh^{I, III}$
VIc	*t*Bu	H	Mo^{0} Mo^{III} Ru^{II}
	Ph	H	Mo^{0} Mo^{III} Ru^{II} Rh^{I} Rh^{III} Ir^{I} Ir^{III}
VId	Ph	Me	Mo^{0} Pd^{II} Pt^{II}
VIe	Ph, $C_6(CF_3)_2H_3$		Pd^{II}
VIIa	*i*Pr		Rh^{I} Ni^{II} Pd^{II} Pt^{II}
	Ph		Pd^{II} Pt^{II}
VIIb	*i*Pr	*t*Bu	Fe^{II}
	Ph	*t*Bu	Rh^{I}
VIIc	*o*F-C_6H_4		Mn^{I} Re^{I} Ru^{II}
VIIIa	Ph		Ni^{II} Pd^{II}
VIIIb	*t*Bu		Ru^{II}
	Cy		Ru^{II} Os^{II} Rh^{I} Ir^{I} Ir^{III}
	Ph		Os^{II} Rh^{I} Ir^{I} Ir^{III}
VIIIc	*i*Pr, *t*Bu		Ru^{II}
IXa	Ph		Rh^{I} Pt^{II} Pd^{II} Ag^{I}
Xa			Rh^{I}
Xb			Rh^{I}, Pd^{II}
Xc			Cr^{0} Rh^{I} Ir^{I} Ni^{II} Pd^{II} Pt^{II} Au^{I}

κP, κC^{NHC}, κP ligands of **VIb** and **VIc** architecture (R = *t*Bu) has been prepared and studied as catalysts for the reduction of N_2 to NH_3 (Schemes 82 and 83) [38,201]. The complexes **346**, **349** and **353** were prepared in 33–60 % yields by the reaction of the *in situ* generated pincer ligands (from the corresponding imidazolium salts and $KN(SiMe_3)_2$) with $[MoCl_3(THF)_3]$ and characterized by X-ray diffraction. The respective Mo^{III}–C^{NHC} bond distances of 2.126(7) and 2.4143(12) Å for **349** and **353**, respectively, indicated a weaker pincer binding in the latter. The analogous **347** and **348** were obtained from the corresponding molybdenum halides $[MoX_3(THF)_3]$ (X = Br, I) (Scheme 82) [201].

Reduction of **348** with two equivalents of $[CoCp^*_2]$ under N_2 in toluene at room temperature afforded the Mo^{IV} nitrido complex **350**, presumably arising from symmetrical reductive dinitrogen cleavage in the putative $[\{Mo^{II}(\kappa P,\kappa C^{NHC},\kappa P)\}_2(\mu\text{-}N_2)]$ (Scheme 82). Furthermore, reaction of **348** with Me_3SiN_3 in THF at room temperature afforded in low yields the paramagnetic Mo^{V} complex **351** which was structurally characterized and features short Mo–C^{NHC} and Mo≡N bond distances (2.164(4) and 1.639(4) Å, respectively). Both **348** and **350** in the presence of reducing and proton equivalents ($[CoCp^*_2]$ and 2,4,6-collidinium trifluoromethanesulfonate) act as catalysts for the reduction of N_2 to NH_3 (Scheme 82) [201].

Treatment of the Mo^{III} complexes **346**, **349** and **353** with six equivalents of Na–Hg in THF at room temperature under N_2 (1 atm) resulted in the formation of the corresponding diamagnetic, dinitrogen-bridged dimolybdenum complexes **354**–**356** in moderate yields (37–53 %) (Scheme 83). Their structures revealed significant differences that were rationalized on the basis of structural features of the pincer supporting ligands and correlated with their activity in the catalytic reduction of N_2 to NH_3. Although the binuclear N_2-bridged core with two additional terminal N_2 ligands per Mo center is maintained throughout the series, a conspicuous difference is the conformation adopted by **354** and **355** compared to **357**, originating from the length of the spacers in the pincer arms. As a result, the dihedral angles between the plane of the NHC ring and the Mo–N≡N–Mo vector differ by *ca.* 40° and the adoption of a highly twisted arrangement in **356**. Consequently, variation of the Mo–C^{NHC}, Mo–N_2, Mo–N≡N–Mo and Mo–P metrical data was evident and rationalized based on the strength of the C^{NHC}–Mo π-interaction, which also modulated the Mo–N_2 π-interactions (and N_2 activation). The Mo–C^{NHC} bond lengths in complexes **354**–**356** were 2.064(2), 2.058(2) and 2.153(4) Å, respectively, implying a stronger π-back donation from the Mo^0 to the NHC unit in the former. The ν(N≡N) in the IR spectra the (1978, 1969, 1911 cm^{-1}, respectively) are in agreement with the explanation. Calculations show that the Mo–N and N≡N distances with the N_2(terminal) are 2.032 and 1.137 Å for **354** and 2.016 and 1.142 Å for **356**, respectively, implying that the N_2(terminal) in **356** is more activated than that in **354**. Consequently, the BDE of the Mo–N_2(terminal) in **356** (11.9 kcal/mol) is lower than that of **354** (16.7 kcal/mol). In contrast, the Mo–N distance of the bridging dinitrogen ligand of **354** (2.108 Å) is shorter than that of **356** (2.133 Å) and the corresponding BDE of the Mo–N_2 (bridging) for **354** and **356** are 18.8 and 9.0 kcal/mol, respectively. Experimental results (^{15}N NMR and FTIR spectroscopies) demonstrate that the dinuclear structure in **356** is labile in solution giving easily the mononuclear **357**. This dynamic behavior is thought to be in part responsible for the different N_2 reduction activity of **354** and **356** under reducing conditions ($[CrCp^*_2]$) in the presence of H^+ sources (lutidinium triflate). Throughout the catalytic sequence which is initiated by H^+ attack on a coordinated terminal N_2, it is thought that the Mo–N≡N–Mo unit is maintained and intermetallic electron transfer and synergism between the two Mo centers are essential for successful catalysis. Indeed, **354** under certain conditions can provide up to 100 equivalents of NH_3 per Mo atom compared to 1.6 for **356**. The tight pincer binding and the robustness of the binuclear unit that are features of **354** (but not as pronounced in **356**) are remarkable indications of the tunable advantages offered by certain P,C^{NHC},P architectures [202]. In fact, **354** catalytically outperforms the earlier described pyridine diphosphane complex **358**, the latter having a pyridine rather than NHC bridgehead (Scheme 83) [38]. Detailed experimental, computational and catalytic studies of the related molybdenum complexes **354**/**355** and **358** featuring the ligands of type **VIb** (Chart 7) and 2,6-(α,α'-di-tbutylphoshino-lutidine (P,N,P), with NHC and pyridine bridgehead donors, respectively, attempted to elucidate electronic structure parameters of the pincer design that may be accountable for observed structural, spectroscopic and catalytic properties. The emerging trends summarized below are in line with comparative studies involving other pincer designs with various metals. (i) The electron-donating ability of **VIb** and (P,N,P) is controlled by the carbene and pyridine moieties. The Mo–C^{NHC} bond distance in **354** is significantly shorter than the Mo–$N^{pyridine}$ distance in **358**. Furthermore, the Mayer bond order of the Mo–C^{NHC} bond is calculated to be much larger than that of the Mo–$N^{pyridine}$ bond (0.91 and 0.39, respectively). Consequently, analysis of the calculated orbitals reinforces the idea of a stronger σ-interaction between Mo and C^{NHC} than Mo and $N^{pyridine}$. These findings account for the catalytic longevity of **354** compared to **358** under the conditions for nitrogen reduction. (ii) In **VIb** there is a π-bonding interaction between the Mo atom and C^{NHC} through π-backdonation from a Mo d_π orbital to the vacant, perpendicular to the NHC ring p orbital of C^{NHC}; the NHC acts as a σ-donor and π-acceptor. The backdonation is competing with π-backdonation to

Table 3
Comparative summary of selected metrical and spectroscopic data of the complexes with κP, κC^{NHC}, κP ligands. Abbreviations used in the Table: O.S. oxidation state; C. G.: coordination geometry' oct.: octahedral; sqpl.: square-planar; td.: tetrahedral; ps: pseudo; trbip.: trigonal bibyramidal; sqpy.: square pyramidal.

M	O.S./C.G.	Ligand class	Complex	*r*(M−C^{NHC}) (Å)	⊳ (N-C^{NHC}-N) (°)	δ_C (C^{NHC}) (ppm)	δ_P (ppm)	Ref.
Mo	0/*oct.*	**VIb**	**354**	2.064	103.5	–	105.6	[38]
			355	2.058	104.7	–	105.8	[38]
		VIc	**341**	2.261	102.1	193.8	271.0, 166. 33.8	[195]
			329	2.263	102.5	193.6	27.3	[193]
			356	2.149	101.9	–	27.3	[38]
		VId	**331**	2.239	104.4	205.6	27.3	[194]
	III/*oct.*	**VIb**	**347**	2.110	105.6	–		[201]
			349	2.125	105.0	–		[38]
		VIc	**337**	2.180	102.5	–		[195]
			353	2.170	104.5	–		[201]
	V/*sqpy.*	**VIb**	**351**	2.164	107.2	–		[201]
Mn	I/*oct.*	**VIa**	**360B**	1.973	105.8	195.6		[176]
		VIIb	**361A**	1.934	102.8	–	110.1	[205]
			361B	1.926	102.6	231.8, 227.7	139.6	[205]
			361C	1.954	103.5	–	110.9	[205]
		VIIc	**364**	2.033	107.2	212.4		[206–208]
Re	I/*oct.*	**VIIc**	**365**	2.172	108.6	192.3		[206–208]
			367	2.156	107.0	–		[206–208]
Fe	0/*trbip.*	**VIIb**	**386**	1.828	99.6	–		[215]
			387	1.831	99.6	–		[215]
	II/*trbip.*	**VIIb**	**383**	2.061	102.3	–		[215]
	II/*oct.*	**VIIb**	**384**	1.828	101.6	–		[215]
		VIIIb	**411**	1.877/1.869	112.3/112.4	244.5		[219]
	II/*ps td.*	**VIIc**	**403**	1.895	106.8	143.4		[218]
Ru	II/*oct.*	**VIb**	**370**	2.011	106.5	–	103.2	[209]
		VIc	**374**	1.993/1.992	104.0/102.9	174.5	43.4, 48.5	[211]
			375	2.038	103.9	169.1	10.9	[211]
			378	2.027	103.2	–	9.56	[211]
			379	2.040	104.2	174.4	38.5, 42.4	[211]
			380	2.050	103.9	–	–	[211]
			371	2.087	103.7	–	64.5	[209]
		VIIIb	**413**	1.943	114.6	224.7	34.6	[220]
			421	2.087	116.6	sl	47.3	[221]
			422	2.052	115.7	229.2	45.6	[221]
			420	2.102	116.4	–		[220]
		VIIIc	**427**	2.095	117.2	206.4		[222]
			431	2.107	116.1	206.9		[222]
	II/*ps td.*	**VIIc**	**404**	1.996	107.1	204.3		[218]
			395	2.019	104.5	197.6		[216]
Os	II/*oct.*	**VIIIb**	**414**	2.051	113.9	–	–	[221]
			416	2.002	111.7	211.0	–	[221]
Rh	I/*sqpl.*	**VIa**	**434**	1.991	105.4	188.4		[224]
		VIb	**436**	1.955	106.2	–		[225]
			437	1.933	106.0	198.9	45.8	[225]
			438	1.99	106.9	197.2	55.4	[225]
			440	1.941/1.937	105.6/105.8	–	55.9	[225]
			441	1.89	104.9	–		[227]
		VIIa	**71**	1.929	105.2	201.5	22.4	[90]
		VIIb	**463**	1.905	103.6	–	49.5	[236]
		VIIIb	**466**	1.948	114.3	–	22.9	[237]
			480	1.932/1.928	113.7/113.0	205.8		[240]
	III/*oct.*	**VIc**	**453**	1.987/2.007	103.5/102.8	–	6.4	[228]
			454	2.003	106.1	–	1.7	[228]
		VIIb	**464**	1.904	104.9	–	–	[236]
Ir	I/*sqpl.*	**VIb**	**442**	1.889(5)	105.1	187.2	77.9	[226]
		VIc	**449**	1.959(4)/1.943(5)/1.957(4)	102.5/102.8/102.8	157.9		[226]
	III/*oct.*	**VIb**	**445**	1.921	107.3	179.2	53.0	[226]
			446	1.948	108.1	172.4	27.4	[226]
			447	1.959	106.4	–	89.1	[226]
		VIc	**450**	1.992/1.993	103.8/104.4	–	11.2	[226]
		VIIIb	**468**	2.078	117.6	172.5	–	[237]
			470	1.962	115.9	187.2	–	[238]

(*continued on next page*)

Table 3 (*continued*)

M	O.S./C.G.	Ligand class	Complex	r(M–C^{NHC}) (Å)	⊳ (N-C^{NHC}-N) (°)	δ_C (C^{NHC}) (ppm)	δ_P (ppm)	Ref.
			474	1.943	113.9	189.9	23.7	[238]
Ni	0/*td.*	**VIIId**	**534**	1.9286	113.7	–		[56]
	II/*sqpl.*	**VIa**	**489B**	1.847(2	109.7	196.7	78.5	[49]
			489C	1.859(2)	109.8	–	110.4	[49]
			489D	1.872(3)	109.4	199.3	75.0	[49]
		VIb	**487**	1.828	106.6	–		[86]
		VIIa	**511**	1.863	107.3	189.3		[246]
		VIIIa	**523**	1.899	117.6	186.7		[252]
			524	1.905	117.0	190.0		[252]
		VIIId	**529**	1.899	118.5	150.31		[56]
			533	1.911	118.2	–		[56]
Pd	II/*sqpl.*	**VIb**	**488**	1.9356	108.1	178.8		[225]
		VId	**492**	1.9765	107.5	150.3		[248]
		VIe	**497**	2.040	108.4	146.8		[249]
			499	1.993	106.1	144.5		[249]
		VIf	**506**	1.902	102.7 (⊳CCN)	148.6		[250]
		VIIa	**513**	2.037	109.3	197.3		[246]
		VIIIa	**525**	2.011	118.8	189.9		[252]
			526	1.997	118.3	186.7		[252]
Pt								
	II/*sqpl.*	**VIIa**	**514**	2.008	107.4	196.7		[246]
			521	2.037	107.9	194.0		[251]
			519	2.042	107.7	194.2		[251]

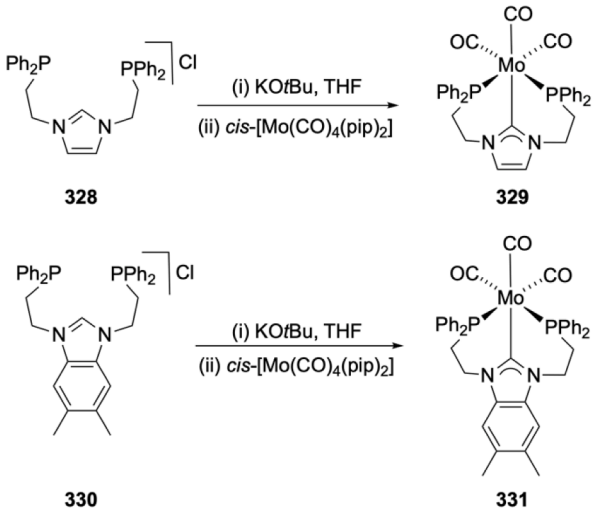

Scheme 80. Mo carbonyl complexes with κP, κCNHC, κP ligands of type **VId** (R = Ph).

other coligands (N_2 in this case) resulting in lower BDEs of the Mo–N_2 bonds and is not pronounced in the (P,N,P) analogue. (iii) Modulation of the latter interaction by altering the orientation of the NHC plane (and the perpendicular *p* orbital on C^{NHC}) through the use of spacers of suitable length resulted in weakening the Mo–C^{NHC}; the NHC acts as a pure σ-donor and, consequently, the Mo–N_2 bonding is strengthened. This tuning handle is not accessible in the P,N,P ligand. Although these features have been extracted on the basis of the Mo^0–(P,C^{NHC},P) and Mo^0-(P,N,P) systems, their scope is expected to be wider (see also section 3.10.4 for a comparative analysis of the electronic structure of Ir–κP, κC^{NHC}, κP and Ir–(P,N,P) complexes).

Chromium complexes with a ligand backbones of type **Xc** have been described. They are mentioned here for comparison, since the bridgehead donors are not classified as N-heterocyclic carbenes [203].

3.10.2. Group 7 metals (Mn, Re)

The Mn^I complex **360B**, with the pincer ligand of architecture **VIa** (R = Ph), was prepared in two steps from the corresponding ligand precursor **359**, [$MnBr(CO)_5$] and $KN(SiMe_3)_2$ (Scheme 84A). In the first step, the generation of the free ligand in the presence of the manganese precursor leads to the formation of the neutral complex **360A** with a bidentate κC^{NHC},κP coordination mode of the ligand and one dangling diphenylphosphino functionality. Subsequently, halide abstraction from **360A** using AgOTf gave the targeted pincer complex **360B** in high yields. The spectroscopic data obtained for **360B** conform to a symmetrical *mer* structure in solution (^{31}P NMR: δ 89.6 (s) ppm; IR (CO region): 2045 (w), 1966 (*vs*), 1942 (s) cm^{-1}), which is also adopted in the solid state as unveiled by X-ray crystallography (Mn–C^{NHC} = 1.9726 (12) Å). The intermediate neutral complex **360A** with bidentate ligand has only been characterized spectroscopically (^{31}P NMR: δ_P 71.0 (s), −17.0 (s) ppm; IR (νCO region): 2015 (s), 1940 (s), 1910 (s) cm^{-1}). The complex **360B** shows moderate activity as hydrogenation catalyst of acetophenone with H_2/KO*t*Bu. Importantly, non-symmetrical κ$N^{lutidine}$,κC^{NHC},κP manganese complexes are superior catalysts for this reaction, a fact implying pyridine ring hemilability in this catalytic system (see also section 3.7.1) [176].

An analogous to **360A** Mn^I complex **360C** based on the ligand motif **VIb** was obtained by deprotonation of the precursor **342A** to form the free pincer ligand *in situ* which was allowed to react with [$MnBr(CO)_5$] (Scheme 84B). In contrast to **360A**, complex **360C** features tridentate coordination of the pincer, a fact that could be ascribed to the forcing conditions employed for its synthesis; the octahedral at Mn coordination geometry with the Br ligand mutually *cis* to the two P donors was established by spectroscopic (multinuclear NMR, IR) and crystallographic methods. Reaction of **360C** with Selectride N resulted in the substitution of the bromide by a hydride donor and isolation of **360D** (Scheme 84B). Both **360C** and **360D** in the presence of base (*t*BuOK) and H_2 (*ca.* 50 bar) catalyze the hydrogenation of terminal alkenes with excellent conversions, low catalyst loadings and a wide substrate scope. The requirement of the use of *t*BuOK in both catalytic systems was accounted for by the postulated mechanism of H_2 activation involving deprotonation of the benzylic linkers by the base, resulting in rare anionic Mn–H complexes that are catalytically relevant [204].

The rigid pincer ligand **382** (of motif **VIIb**), which was obtained by

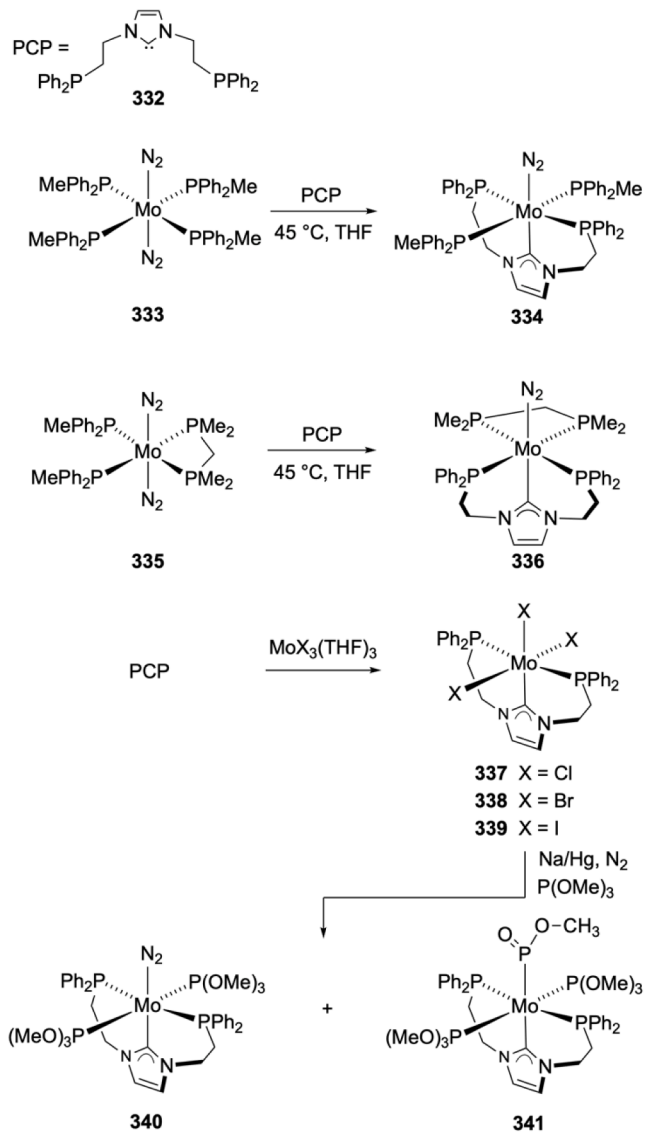

Scheme 81. Mo dinitrogen complexes with κP, κC^{NHC}, κP ligand of type **VIc** (R = Ph)

deprotonation of the precursor **381** with *t*BuOK, was employed to construct a family of Mn^{I} complexes that are efficient catalysts for the α-methylation of carbonyl compounds using methanol as the C_1 source and 'hydrogen borrowing' transformations (Scheme 84C). The catalysis relevant diamagnetic **361B** and the catalytically active **361C** were obtained from **361A** by the reaction with $NaHBEt_3$ in CH_2Cl_2 and $NaPF_6$ in methanol, respectively. The formation of **361C** under catalytic conditions involves the acceptorless double dehydrogenation of methanol to CO in a process that, in contrast to other relevant Mn catalyzed hydrogen borrowing reactions, does not invoke metal-ligand cooperativity [205].

With the aim to access tunable macrocycles with ring-integrated NHC donors, the precursors **362** and **363** served as starting points for the Mn^{I} and Re^{I} template controlled cyclizations of a coordinated rigid diphosphane with a coordinated protic NHC, leading to the Mn^{I} and Re^{I} complexes **364**, **366** and **365, 367**, respectively, all featuring the terdentate architecture **IIc** (Scheme 85) [206–208]. The C–N bond formation-cyclization in **362** and **363** involved a template-directed dehydrofluorination with KO*t*Bu in THF. In the structurally characterized **364** and **365**, the M–C^{NHC} bond distances (M = Mn: 2.033(2) Å; M = Re: 2.172(4) Å) are comparable to those in other Mn and Re-NHC complexes. The complexes **366** and **367** were formed by reaction of complex **364** and **365** with $Me_3NO{\cdot}2H_2O$ in dichloromethane, respectively, and the rhenium complex was also crystallographically characterized (Re–C^{NHC} bond distance: 2.156(4) Å). The ^{31}P NMR spectroscopic data for **364** and **365** (δ 73.4 and 15.8 ppm, respectively) support that the symmetric solid-state structures are maintained in solution; however, the ^{31}P NMR spectra of **366** and **367** comprised three signals (δ 109.1 (m), 106.6 (m) and 83.0 ppm, and δ 30.9 (s) 27.9 (m) and 25.5 (m) ppm), which have been explained by the presence of two isomers in solution (*i.e.* with the halide *cis* and *trans* to the NHC). Interestingly, although this strategy to construct ligands of unusual architectures seems to be attractive, the scope is very limited in terms of using different metals from the periodic table (see also Section 3.10.3 for examples with Ru); furthermore, non-destructive ligand removal from the inert Mn^{I} or Re^{I} templates so far has not been successful (Scheme 85).

3.10.3. Group 8 metals (Fe, Ru, Os)

The Ru complexes **370**, **371** and **372** bearing the ligands of type **VIb** and **VIc** (R = *t*Bu) were obtained by reactions of the free carbenes with Ru precursors (Scheme 86) [209]. Thus, reactions of [RuHCl(CO)$(PPh_3)_3$] with the pincer ligands, generated *in situ* from the imidazolium salts **368** and **369** and 1.4 equivalent of $KN(SiMe_3)_2$ in toluene, yielded upon heating the corresponding complexes **370** and **371**. They were characterized analytically, spectroscopically and crystallographically: in their ^{1}H NMR spectra, signals at δ −16.84 (t) and −17.43 (t) ppm, respectively, were assigned to metal-bound hydrides, which was also confirmed by the IR absorptions at 2109 and 2046 cm^{-1}; additional peaks at 1937 and 1907 cm^{-1} were due to the ν(CO) of the carbonyl ligands. The higher ν(CO) value in **370** was attributed to a stronger π-accepting character of the NHC moiety of the pincers **VIb** and **VIc** due to NHC conformational preferences having an impact on metal-to-NHC back-bonding. For comparison between pincer ligand designs, it is pertinent to note that in the (P,N,P) analogue of **370** (*i.e.* [Ru(H)Cl(CO)(P,N,P)]), the ν(CO) absorption is at 1906 cm^{-1}, which compares with the value recorded for **371**, implying similar degree of Ru-to-CO π-back-bonding in the latter case. The X-ray structures in **370** and **371** revealed distorted octahedral geometries at Ru, with Ru–C^{NHC} bonds lengths of 2.011(6) and 2.087(3) Å, respectively; interestingly, the Ru–C^{NHC} bond distance in **370** is shorter than the corresponding in **371**, a fact rationalized by the involvement of conformation-facilitated π-back donation from the Ru to the NHC unit (*cf.* discussion of Mo complexes above). Reaction of **370** with the base LiN*i*Pr$_2$ in THF-d_8 for 7 h at room temperature afforded the unstable and non-isolable Ru^0 complex **372** after a formal reductive elimination of HCl. The formation of **372** was inferred by NMR and IR spectroscopic methods: the triplet attributed to Ru–H in **370** disappeared in the ^{1}H NMR spectrum, and in the IR spectrum the absorption due to ν(CO) was replaced by a new one at 1845 cm^{-1}. All these data pointed to a square-planar Ru^0 complex coordinated by the PCP pincer and a CO ligand. Complex **370** was tested as catalyst for the direct synthesis of imines from reactions of primary amines with benzyl alcohol in refluxing toluene, and compared against the P,N,P benchmark complex [Ru(H)Cl(CO)(P,N,P)] [210]. Although its activity at the initial stages of the catalytic reaction was inferior to the benchmark, over longer (>24 h) periods of time it outperformed it, presumably due to the higher stability of the catalytically competent structures originating from tighter κP,κC^{NHC},κP pincer binding. In addition, in view of the different behavior of the pincer complexes **370** and [Ru(H)Cl(CO)(P,N,P)] towards the stoichiometric reaction with base [209,210], it has been proposed that the step responsible for the generation of the hydride necessary for the benzyl alcohol dehydrogenation may be mechanistically different: in the case of **370** it may involve the Ru^0 complex **372**, whereas [Ru(H)Cl(CO)(P,N,P)] may call for dearomatization of the (P,N,P) and deprotonation of the CH_2 linkers. Here too, the nature of the pincer ligand and the reluctancy of **Ic** to dearomatize may lead to a mechanistic diversity for the reaction in question (Scheme 86) [209].

The orange salt **374** featuring a binuclear ruthenium complex cation with terdentate ligand of type **VIc** was the first to be targeted as an

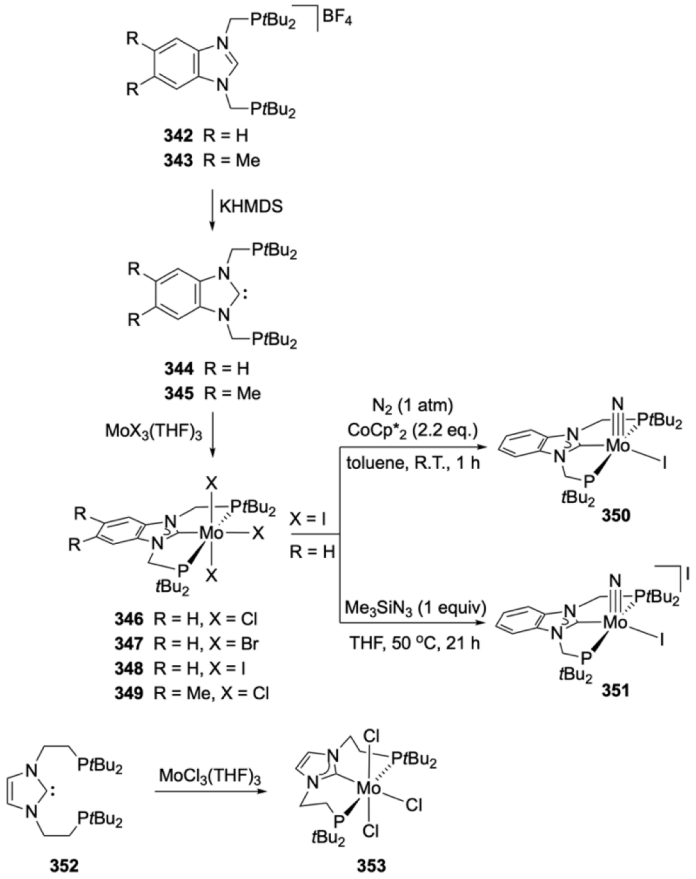

Scheme 82. The synthesis of MoX_3 adducts with pincer ligands of types **VIb** and **VIc** (R = tBu) and stoichiometric reduction of the molybdenum triiodide complex with pincer **VIb** (R = tBu) ligand under N_2.

example of a pincer system with NHC bridgehead (Scheme 87) [211]. It was obtained by ligand transmetalation from the silver complex **373** to the Ru^{II} precursor $[RuCl_2(PPh_3)_2]$ [211]. It could also be prepared directly by heating at 90 °C a mixture of $[RuCl_2(PPh_3)_2]$ and the imidazolium salt **328** in DMF. The cation in **374** adopted a symmetrical binuclear structure with three bridging chlorides and one κP,κC^{NHC},κP pincer at each Ru center in a *fac*-arrangement. The nonbonding Ru-Ru separation was 3.362 Å and the Ru–C^{NHC} distance of 1.99 Å is consistent with that found in related ruthenium complexes [212]. The ^{31}P NMR spectrum comprised two sets of doublets (at δ 43.4 and 48.5 ppm, $^2J_{PP} = 31.3$ Hz) indicating that the two phosphorus nuclei in the tridentate ligand were non-equivalent. In the ^{13}C NMR spectrum, the C^{NHC} resonance at δ 174.5 ppm appeared as a typical triplet with $^2J_{CP} = 21.6$ Hz.

Reaction of **374** with CO in refluxing 1,2-dichloroethane solution yielded the mononuclear **375** [211], displaying only one singlet at δ 10.9 ppm in the ^{31}P NMR spectrum and adopting *mer*-octahedral geometry (Ru–C^{NHC} = 2.038(3) Å *cf.* 1.99 Å in **374**). Treatment of **375** with $NaBH_4$ resulted in the formation of the ruthenium hydride complex **377**; it shows one singlet at δ 9.56 ppm in the ^{31}P NMR spectrum and a characteristic triplet at δ −14.8 ppm ($^2J_{H\text{-}P} = 19.3$ Hz) assignable to the Ru–*H* in the ^1H NMR spectrum. Refluxing a 1,2-dichloroethane solution of **374** with excess phenylacetylene led to the formation of **376**, which was characterized in the ^{31}P NMR and ^1H NMR spectra by a singlet at δ 7.00 ppm and a triplet at δ 3.52 ppm ($^4J_{H\text{-}P} = 3.8$ Hz), respectively, the latter signal being assignable to the protons of a vinylidene ligand. In the ^{13}C NMR spectrum, the metal-bound vinylidene carbon was observed at δ 348.1 ppm ($^2J_{C\text{-}P} = 16.1$ Hz), and the β-carbon at δ 108.3 ppm. In air, **376** was converted into **375** with formation of benzaldehyde (Scheme 87).

The iron NHC hydrido complexes **384** and **387** with the P,C^{NHC},P ligand of type **VIIb** were described and studied as versatile catalysts for (i) the deuteration C–H bonds of aromatic substrates using C_6D_6 as D-atom source, (ii) the *Z*-selective functionalization of terminal alkyne with HB(pin) to *Z*-alkenyl-boronates, (iii) the dimerization of alkynes and (iv) the one- or many-bond isomerization of alkenes (Scheme 88) [213–215]. Treatment of precursor **381** with KO*t*Bu in THF resulted in the isolation of free carbene ligand **382**, which reacted with $FeCl_2$·1.5THF to afford the new paramagnetic species **383** in 88% yield, which was characterized by X-ray crystallography and mass spectrometry. The crystal structure of **383** unveiled a distorted trigonal bipyramidal geometry (Fe–C^{NHC} bond distance at 2.062(6) Å and two long Fe–P bond distances at 2.782(2) Å and 2.765(2) Å) testifying that the phosphane donors were only weakly bound to the Fe center. Reaction of **383** with $NaBHEt_3$ in THF at −110 °C produced the diamagnetic **384** in 70 % yield, which was stable at room temperature for several days (Scheme 88) [213]. The appearance of one triplet at δ −8.79 ppm in the ^1H NMR spectrum of **383** ($^2J_{P\text{-}H} = 43.0$ Hz) suggested a *trans*-dihydride arrangement. A rough crystal structure determination confirmed the proposed 'spectroscopic' structure with a coordinated N_2 *trans* to the C^{NHC}, forcing the two hydrides in a *trans* geometry. It has been conjectured that the coordinated N_2 is important for promoting stability in **384**: by forcing *trans* hydride arrangement, the reductive elimination of H_2 which is a commonly observed decomposition pathway for other *cis* dihydride Fe^{II} complexes was suppressed. Interestingly, **385** was obtained by dissolving **384** in C_6D_6 *via* facile H/D exchange. The disappearance of the typical triplet at δ −8.79 ppm confirmed the formation of **385**. Furthermore, in the ^2H and ^{31}P NMR spectra a triplet (δ −8.68 ppm, $^2J_{P\text{-}D} = 6.6$ Hz) and a quintet (δ 133.27 ppm, $^2J_{D\text{-}P} = 6.2$ Hz) were observed, respectively. Conversely, dissolving **385** in C_6H_6

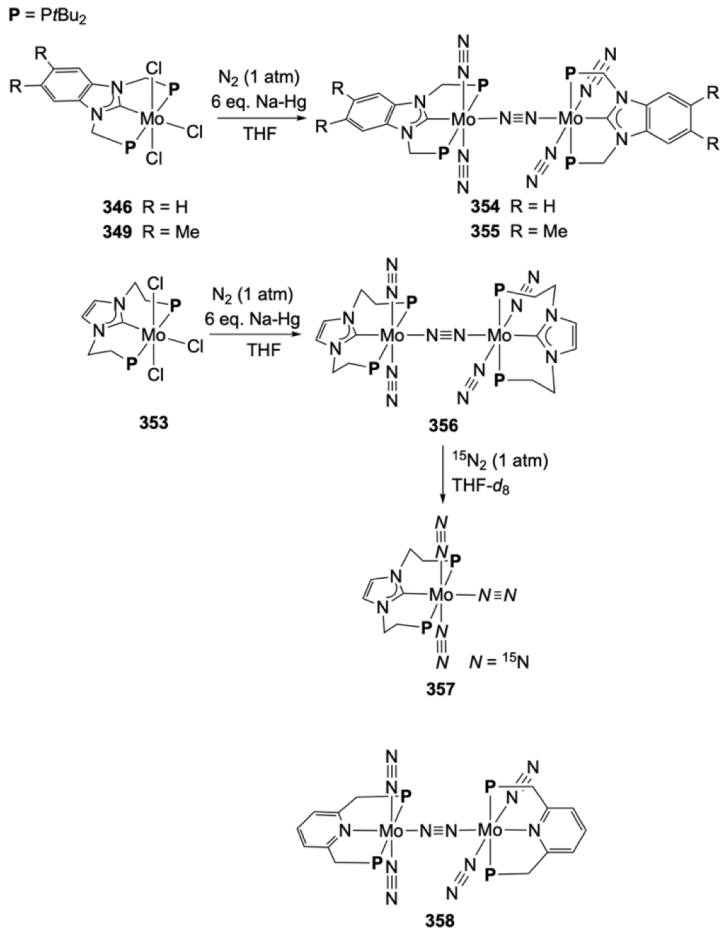

Scheme 83. Mo^0 dinitrogen complexes supported by ligands of types **VIb** and **VIc** (R = tBu).

resulted in the formation of **384** in quantitative yield. The reversible H/D exchange between the solvent and **382** implies a facile reversible C(sp^2)–H activation, initiated by the N_2 dissociation. Thus, **384** has been developed to a deuteration catalyst for organic compounds with good tolerance to a variety of functional groups [213]. In addition, **384** shows remarkable activity as catalyst for the *Z*-selective terminal alkyne functionalization with HB(pin) to *Z*-alkenyl-boronates and the dimerization of alkynes [214].

The anionic complex **387** was obtained from **383** in two steps: reduction with two equivalents of KC_8 in THF under N_2 resulted in the formation of the diamagnetic species **386**, which was characterized by NMR spectroscopic methods and X-ray crystallography (Scheme 88). In a second step, **386** was converted to the anionic Fe^0 NHC hydride complex **387** by the reaction with two equivalents of $NaBEt_3H$. The ^1H NMR spectrum of **387** displays a characteristic triplet at δ −10.85 ppm ($^2J_{P\text{-}H} = 55.1$ Hz); its molecular structure in the solid state features a dimeric dinitrogen bridged iron hydride complex with the metal centers in a trigonal bipyramidal geometry, the hydride and dinitrogen ligands in the equatorial position and two sodium atoms linking the two iron fragments. The Fe–C^{NHC} and Fe–P distances (1.831(2) and 2.174(7) Å, respectively) are rather short. The anionic character of **387** accounts for the coordinated dinitrogen N–N bond distance of 1.155(6) Å, which is indicative of N_2 structural activation. Complex **387** performs as an excellent catalyst for the one-bond isomerization of terminal alkenes. The maximum turn-over number (TON) of **387** for the reaction is *ca.* 160000, a value better than those measured in many precious metal-based catalysts. Computational studies suggest that the isomerization reactions catalyzed by **387** operate by an alkyl-type mechanism, where two-state reactivity ($S = 0$, $S = 1$) is responsible for the exceptional performance (Scheme 88) [215].

The Fe^{II} and Ru^{II} complexes **390**–**391**, **394**–**397**, **403**–**406** bearing the macrocyclic[11]ane-P_2C^{NHC} ligand of architecture **VIIc** (Chart 7) were prepared by the metal template strategy discussed previously (Section 3.10.2). Reaction of **388** and **389** bearing one protic NHC and one rigid diphosphane with two equivalents of KO*t*Bu in CH_2Cl_2 resulted in the formation of complexes **390** and **391** in good yields (Scheme 89) [216–218]. The mechanism of cyclization involved the deprotonation of the NH functions of the protic NHC ligand and attack of the *N*-nucleophiles at the C–F bonds of the *o*-fluorophenyl substituents. The complexes **390** and **391** were characterized by NMR and HRMS spectroscopic methods. The disappearance of resonances for the NH protons in the ^1H NMR spectrum and the singlet in the ^{19}F NMR spectrum indicated the successful formation of the macrocyclic complexes. The resonance for C^{NHC} in the ^{13}C NMR spectrum appeared at δ 222.3 and δ 203.9 ppm, respectively. The molecular structure of **390** and **391** revealed short M−C^{NHC} bond distances (1.895(2) and 1.996(5) Å, respectively). Similarly, deprotonation of the coordinated 2-amino isocyanides in **392** and **393** with excess KO*t*Bu also led to the [11]ane-P_2C^{NHC} macrocyclic complexes **394** and **395**. They were characterized by NMR and MS spectroscopy and the structure of the latter was confirmed crystallographically, revealing a Ru–C^{NHC} bond distance of 2.019(3) Å. Attempts to remove the organometallic coligands of **394** or **395** were successful by heating acetonitrile solutions of the complexes with ammonium chloride under reflux leading to **396** or **397**, which were characterized by NMR spectroscopy [216]. The analogous complexes **403**–**406** also were prepared by similar methods and fully characterized [217,218].

Three more iron NHC hydride complexes, **409**–**411**, related to those

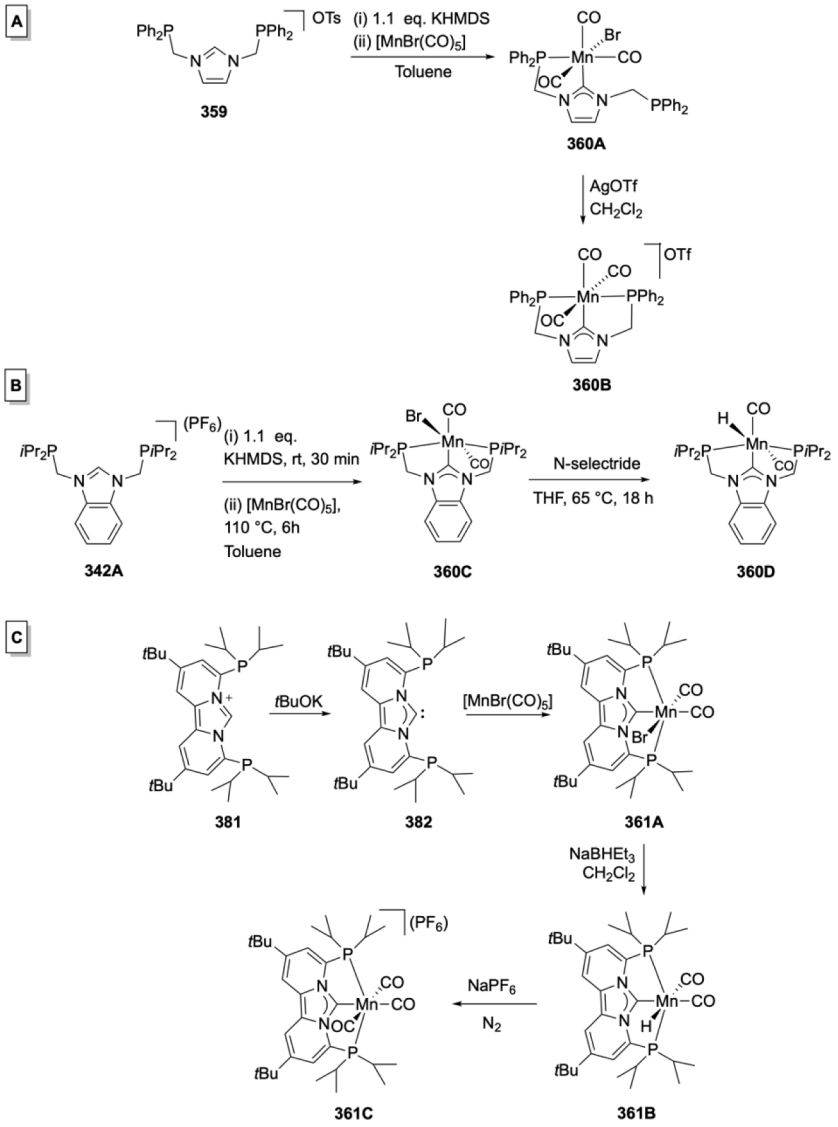

Scheme 84. Mn^{I} complexes supported by ligands of types **VIa** and **VIIb**.

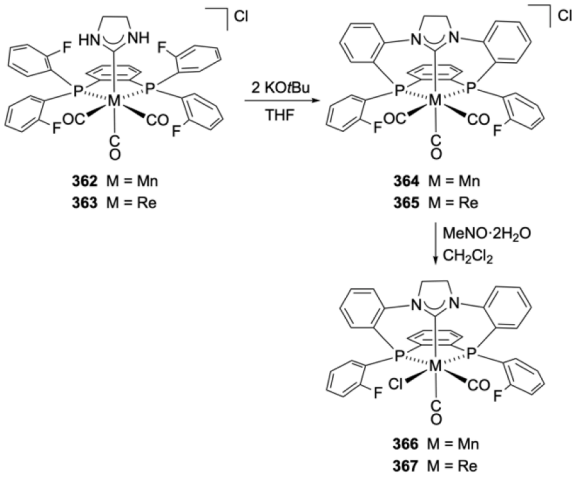

Scheme 85. Mn^{I} and Re^{I} complexes with the type **VIIc** backbone

discussed in the previous section but featuring the pincer ligand architecture **VIIIb** have been described. They were prepared by the remarkable double C–H activation of the perimidine precursor as detailed in Scheme 90 [219]. They constitute the first examples of iron–NHC complexes in which this strategy was successfully applied. The first Fe insertion into the C–H bond occurs *via* a formal oxidative addition and leads to a Fe^{II} (d^6) center that is not electron rich enough to undergo a second oxidative addition (to Fe^{IV}), and therefore the Fe insertion into the second C–H bond would rely on redox neutral hydride transfer steps. Reaction of the neutral methylene phosphane substituted perimidine with the Fe precursor $[FeCl_2(THF)_{1.5}]$ led to the paramagnetic **408** displaying a distorted, trigonal pyramidal geometry. Reduction of **408** with two equivalents of KC_8 under an atmosphere of N_2 furnished a mixture of complexes **409** and **410** as deduced in the ^{31}P- and ^{1}H NMR spectra of the reduction mixture, where two singlets (δ 96.6 and 97.1 ppm) and two triplets (δ −8.1 and −12.4 ppm) both at *ca.* ratio 5:2, **409**:**410**, respectively, were observed. The outcome of the reaction depended on the volume of solvent, and thus the amount of available N_2; the N_2 partial pressure affected the stability of the complexes. Variable-temperature NMR studies displayed reversible change of the appearance of the spectra attributable to reversible $Fe(H_2)$ and $Fe(H)_2$ interconversion. Attempts to crystallize any of the two components by cooling

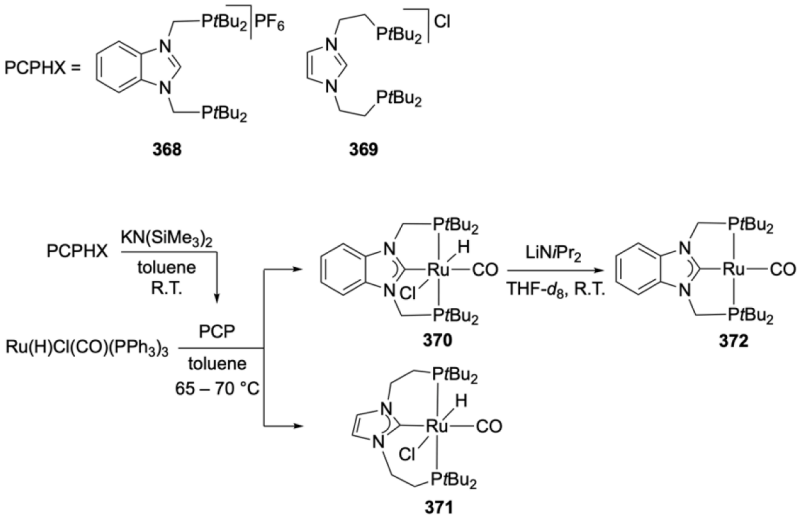

Scheme 86. Ru complexes with pincer ligands of the type **VIb** and **VIc** (R = tBu).

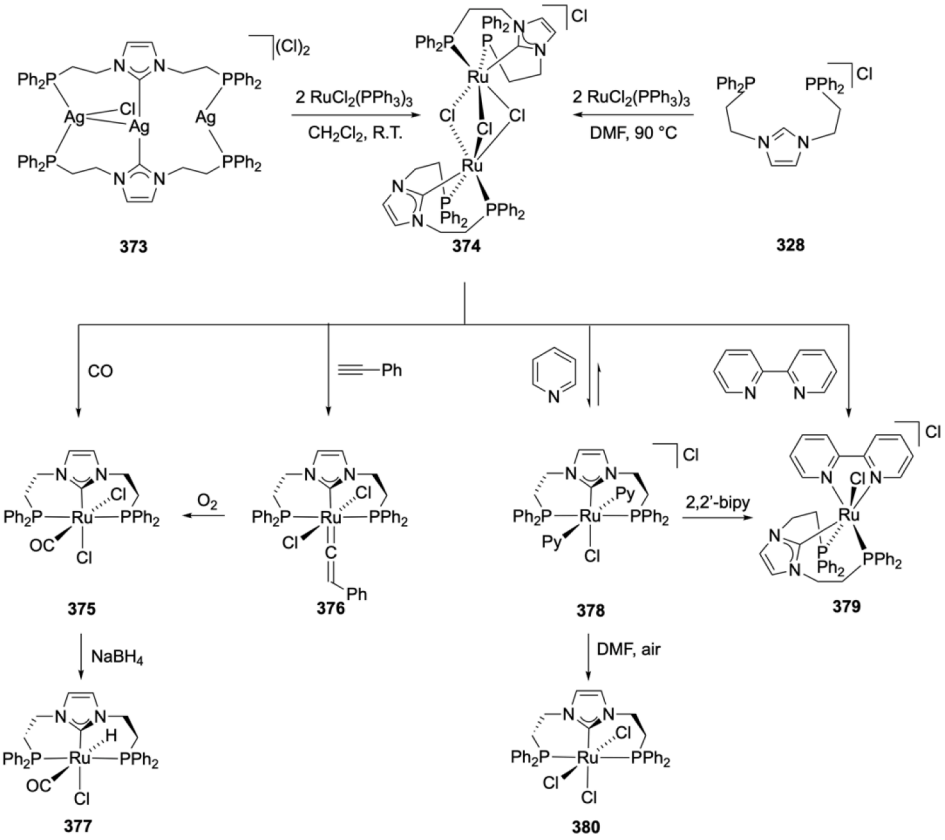

Scheme 87. Ru complexes with type **VIc** backbone (R = Ph).

resulted in the crystallization of the centrosymmetric binuclear **411** after partial N_2 dissociation, where N_2 structural activation was absent (N≡N bond distance 1.125(3) Å) (Scheme 90) [219].

A series of ruthenium complexes with ligands of architecture **VIIIb** was obtained from the precursors **407** (M = Ru, Os) and **412** (M = Os) *via* the double C–H activation methodology of the central C*H*$_2$ group of perimidine also described above for Fe (Scheme 91) [220,221]. Reaction of **407** with [$RuCl_2(PPh_3)_3$] or [$OsCl_2(PPh_3)_3$] in THF resulted in the formation of complex **413** or an isomeric mixture of **414** and **415**, respectively. Analogously, from **412** and [$OsCl_2(PPh_3)_3$], the isomeric mixture of **416** and **417** was isolated. From the mixture of crystallized **414** and **415**, the structure of **414** was successfully determined, while from the mixture of **416** and **417**, complex **416** could be purified by fractional crystallization and its crystal structure determined. The ^{31}P and the ^{1}H NMR spectra of **413** comprised a singlet at δ 34.6 ppm, and a signal at δ 4.24 ppm for the chemically equivalent *PCH*$_2$ groups, respectively. The crystal structure revealed a *mer*-κP, κC^{NHC}, κP ligand, two chlorides and one THF ligand around an octahedral Ru. The Ru–C^{NHC} distance of 1.943(2) Å was in the expected range. Exposure of **413** to a CO atmosphere in dichloromethane resulted in an immediate

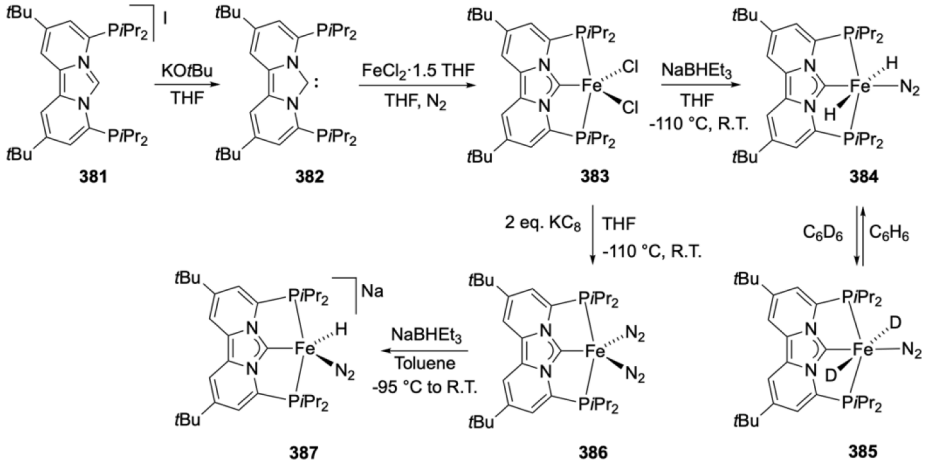

Scheme 88. Fe complexes with type **VIIb** backbone (R = iPr)

color change from orange to yellow; monitoring the reaction by ^{31}P NMR spectroscopy showed the appearance of a resonance at δ 47.3 ppm assignable to the formation of complex **421**, while similarly, treatment of **413** with mesityl isocyanide led to the formation of complex **422**. The C^{NHC} signals in ^{13}C NMR spectra of **421** and **422** appear at δ 223.8 ppm and δ 229.2 ppm, respectively, while the signal at δ 205.5 ppm in the spectrum of **421** was attributed to the *C*O. The crystal structure of **421** revealed a Ru–C^{NHC} bond distance of 2.087(3) Å, longer than the corresponding in **413** (1.943(2) Å), owing to the *trans*-influence of the CO ligand. Reaction of ligand **407** with [Ru(H)Cl(CO)(PPh_3)$_3$] produced the complex **420** and with [RuCl(R')(CO)(PPh_3)$_2$], it afforded complexes **418** and **419**. When a solution of **418** was refluxed in toluene for 4 days, formation of **420** resulted from double C–H activation. This complex was not very soluble in toluene, precipitating out of solution. The ^{1}H NMR spectrum of complex **420** showed a triplet for the hydride resonance at δ −16.45 ppm ($^2J_{P\text{-}H}$ = 19 Hz). The C^{NHC} resonance in the ^{13}C NMR spectrum was observed at δ 225.9 ppm ($^2J_{P\text{-}C}$ = 8 Hz).

Metalation of the 3,5-lutidine-bisphosphane ligands **423** or **424** with [$RuCl_2(COD)_n$] in the presence of base, followed by reaction with CO led to the κP,κ$C^{lutidinyl}$,κP charge-neutral 'classical' pincer complexes **425** and **426**, which displayed characteristic signals for the coordinated P and C donors in the ^{31}P and ^{13}C NMR spectra at δ 74.53 and 181.28 ppm and δ 91.12 and 182.49 ppm, respectively (Scheme 92) [222]. Furthermore, the pincer arrangement was confirmed crystallographically, unveiling a mutually *cis*-CO arrangement and Ru – *ipso* C bond distances at 2.106(2) Å and 2.082(2) Å, respectively. Further reaction of **425** and **426** with MeOTf afforded the complexes **427** and **428** with a pincer complex cation as triflate salts. Whereas the ^{31}P-chemical shifts of **427** and **428** were only slightly affected by the $N^{lutidine}$ quaternization, the *ipso C* were noticeably deshielded to δ 206.41 ppm (**427**) and δ 207.96 ppm (**428**). Importantly, the Ru – *ipso* C bond distance in **427** (2.095(1) Å) is significantly shorter than that in **425**, and the aromaticity of the heterocycle is disturbed as deduced by the unequal C–C bond distances within the ring. The electronic structures of **427** and **428** were studied by DFT methods and the results indicate that the heterocyclic ring displays partial carbenoid character at the *ipso* C, in analogy to the NHCs, with the carbenoid lone pair involved in a 3c-4e bonding with the *cis* Ru–CO bond; the empty *p* orbital at C that is perpendicular to the heterocycle plane accepts electron density from the adjacent double bonds of the heterocyclic ring. Interestingly, there is only minor back-donation from the d_π Ru orbitals in support of relatively long Ru–C_{ipso} bond distances. Rationalization of the variation of the C–C bond distances within the ring can be understood from the Dewar-pyridinium Lewis structure in **427**. Reaction of **427** and **428** with KO*t*Bu or KN($SiMe_3$)$_2$ resulted in abstraction of one proton from one methylene linker and the isolation of the complexes **429** and **430**, respectively, which were characterized spectroscopically and **429** also crystallographically. The lack of any symmetry element in the complexes **429** and **430** was evidenced by the inequivalence of the coordinated P nuclei in the ^{31}P NMR spectra (AB pattern) and, in the ^{1}H NMR spectrum, the appearance of one vinylic and one pair of diastereotopic protons attached to the two disparate pincer arms. Interestingly, the C^{ipso} in the ^{13}C NMR spectrum appeared at δ 180.6 ppm and the ν(CO) vibration in the IR spectra at 2012 and 1943 cm^{-1}. In the structure of **429**, the octahedral coordination geometry at Ru is maintained with the Ru–C_{ipso} distance at 2.106(2) Å.

Calculations (DFT, NBO) aiming at understanding the electronic structure of **429** propose a zwitterionic non-carbenoid ligand structure as the most plausible description of **429** (Scheme 92) [222]. Complexes **428** and **429** react with a range of substrates, *viz.* H_2, PhCN, $PhCH_2OH$ and MeOH to give the products **431**, **432** by a sequence involving metal-ligand cooperation: rupture and addition of the X–H bond (X = H, PhCHCN, $PhCH_2O$ and MeO, respectively) at the deprotonated pincer arm of the zwitterionic ligand, accompanied by substitution of the Cl ligand at Ru, result in regaining of the aromaticity of the heterocyclic ring and formation of complexes with the carbenoid pincer ligand with quaternized lutidine. Decomposition of the alkoxides may follow, leading to hydride complexes (Scheme 93) [222].

Fe complexes with the ligand backbones of type **Xb** have been described. They are mentioned here for comparison purposes only, since the bridgehead donors are not classified as N-heterocyclic carbenes [223].

3.10.4. Group 9 metals (Co, Rh, Ir)

The complex **434** related to type **VIa** ligand architecture was obtained by treatment of the precursor *rac*-**433** with [Rh(acac)(CO)$_2$] at 65 °C in the presence of $NaBF_4$ (Scheme 94). It was fully characterized by IR spectroscopy and X-ray diffraction. The reaction mechanism of the metalation of precursor **433** could involve the coordination of the PCy_2 moieties to the rhodium center followed by deprotonation of the imidazolium C–H by the acetylacetonate ligand acting as an internal base [224].

The complexes **436** and **437** (backbone of type **VIb**) were obtained in 61–76 % yields by treatment of **435** with [Rh(μ-OMe)(COD)]$_2$ in DMSO or MeCN at room temperature (Scheme 95) [225]. The signals in the ^{31}P NMR spectra of **436** and **437** were observed at δ 48.23 and 45.84 ppm as a doublet ($J_{P\text{-}Rh}$ = 151.08 and 152.8 Hz), respectively. The distorted square-planar coordination geometry around the rhodium in **437** was established by X-ray diffraction. In contrast to **436**, **437** was reactive with selected small molecules. Treatment of **437** with CO led to the formation of the yellow complex **438** (δ_P 55.41 ppm (d, $J_{P\text{-}Rh}$ = 138.5 Hz) [225]. The crystal structure of **438** showed a distorted

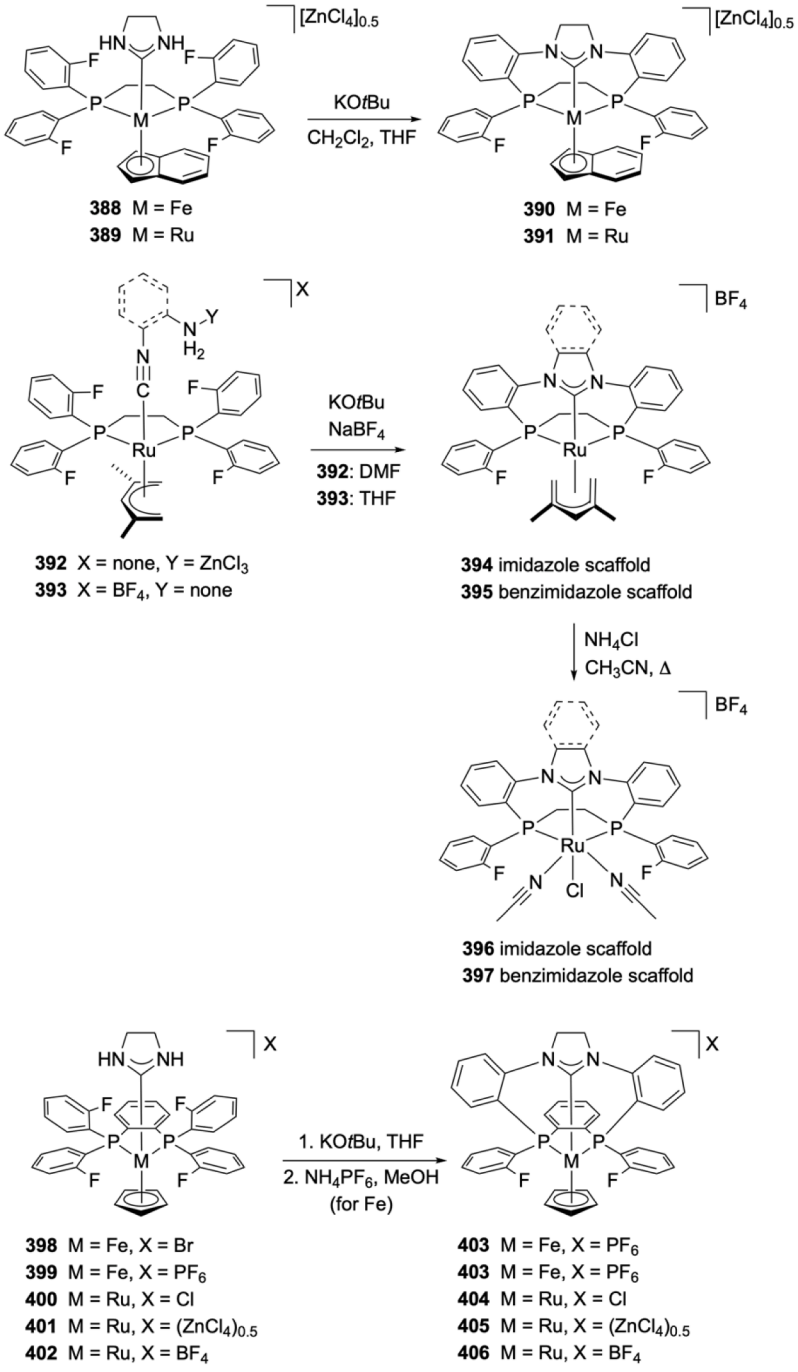

Scheme 89. Fe and Ru complexes with type **VIIc** backbone

square-planar geometry at Rh. In the IR spectrum, the characteristic ν(CO) absorption was observed at 1995 cm^{-1}. Exposure of complex **437** to ethylene gave **439**, as evidenced by ^{31}P NMR spectroscopy (δ_P 61.29 ppm, d, $J_{P\text{-}Rh} = 137.6$ Hz), however, **439** could not be isolated pure due to the reversibility of the reaction leading to its formation. Complex **437** also reacted with 30 equivalents of $KHCO_3$ in THF/H_2O under a H_2 atmosphere to afford quantitatively the unusual hydrido-bridged dinuclear complex **440** the spectroscopic identity of which included a characteristic signal for the μ-hydrido ligand as a multiplet at δ −9.15 ppm, the corresponding methylene groups at δ 4.79 ppm (both in the ^1H NMR spectrum) and a doublet at δ 55.90 ppm (d, $J_{P\text{-}Rh} = 156.5$ Hz) (in the ^{31}P NMR spectrum); these features confirmed that the four phosphorus atoms were equivalent. The Rh–Rh distance of 2.807 Å and a Rh–H–Rh angle of 109.4(13)° provide strong evidence for the occurrence of a metal–metal interaction [225].

A related family of rhodium and, in particular, iridium complexes with the ligand of type **VIb** (R = *t*Bu, Y = H) have been obtained starting either from the corresponding imidazolium precursor based on C–H oxidative addition methodology to $M^{III}(\kappa P,\kappa C^{NHC},\kappa P)$ complexes (M = Rh, Ir **443**, **444**), or from the isolated or *in situ* generated free NHC pincer ligand on substitution of labile ligands (*i.e.* 1,5-COD or COE), leading to the $M^{I}(\kappa P,\kappa C^{NHC},\kappa P)$ species **441**–**442**, respectively (Scheme 96) [226,227]. Deprotonation of the imidazolium salt **368** with KHMDS in toluene afforded the free carbene **344** which was then reacted with [Ir(μ-Cl)$(COE)_2]_2$ in THF to give **442** in 85 % yield; the Rh analogue **441** was similarly obtained starting from [Rh(μ-Cl)(1,5-COD)$]_2$. The crystal structures of complexes **441** and **442** evidenced square-planar geometry, with $M{-}C^{NHC}$ bond distances of 1.892(2) and 1.889(5) Å,

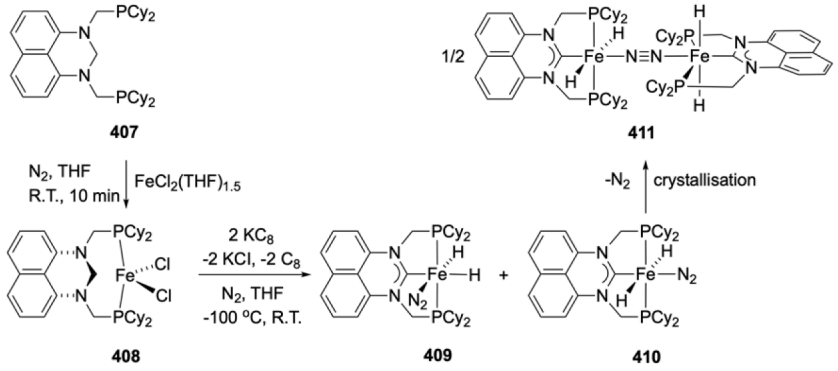

Scheme 90. Fe complexes with type **VIIIb** backbone (R = Cy).

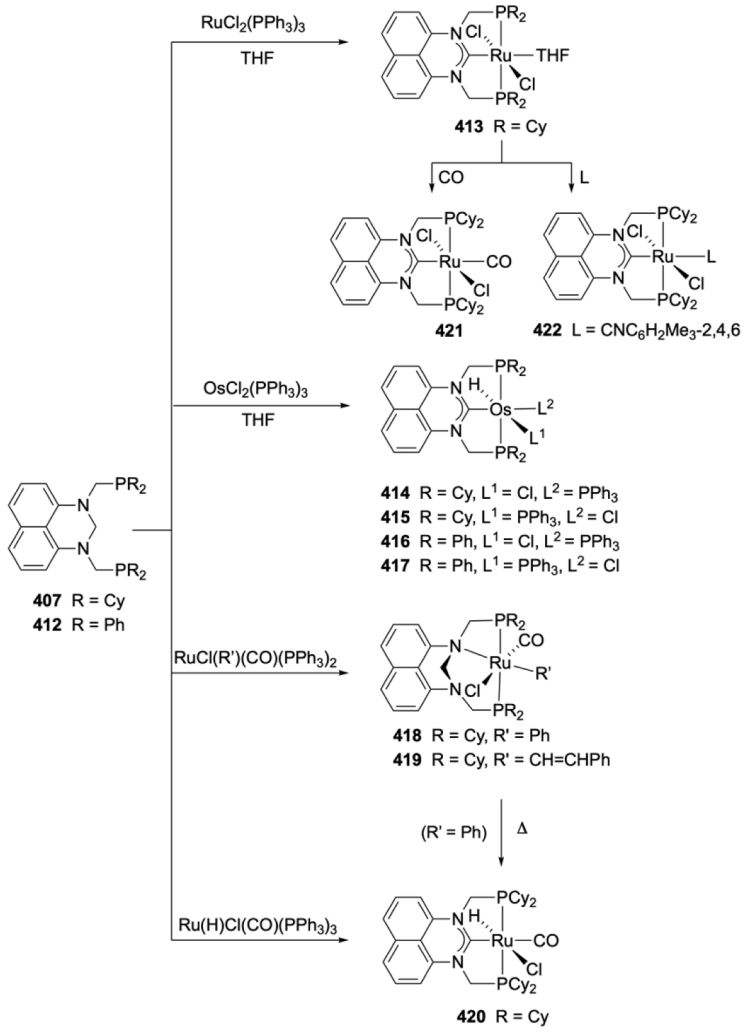

Scheme 91. Ru and Os complexes with type **VIIIb** backbone (R = Cy, Ph).

respectively. Reactions of complex **442** with HCl in THF at room temperature resulted in the formation of complexes **445** [226]. Treatment of complex **442** with hexachloroethane or with $LiHBEt_3$ under 2.5 MPa of dihydrogen resulted in the formation of complexes **446** and **447** in 60% and 43% yields, respectively. However, the cationic chlorido hydrido complex **444** was obtained in one step albeit in low yields by the reaction of the imidazolium salt **368** with $[Ir(\mu\text{-}Cl)(COD)]_2$ and structurally characterized.

Some interesting comparative insight into the electronic structures of complexes **442**, **449** and the corresponding **Ir-(P,N,P)** analogue was gained by DFT calculations. Oxidative addition of H_2 in **442** was found to be endergonic (by 13 kcal/mol) while that to **Ir-(P,N,P)Cl** exergonic (by −17 kcal/mol). This dramatic difference pointed to a stabilization of the low oxidation state by the **VIb** type ligand and could be attributed to the stabilization of occupied Ir d_{yz} and d_{z2} orbitals by back-donation to the vacant p orbital on the C^{NHC}. Although the back-donation was established in the case of **VIc** type ligand, it is less pronounced (due to reduced overlap of the related orbitals originating from the unfavorable

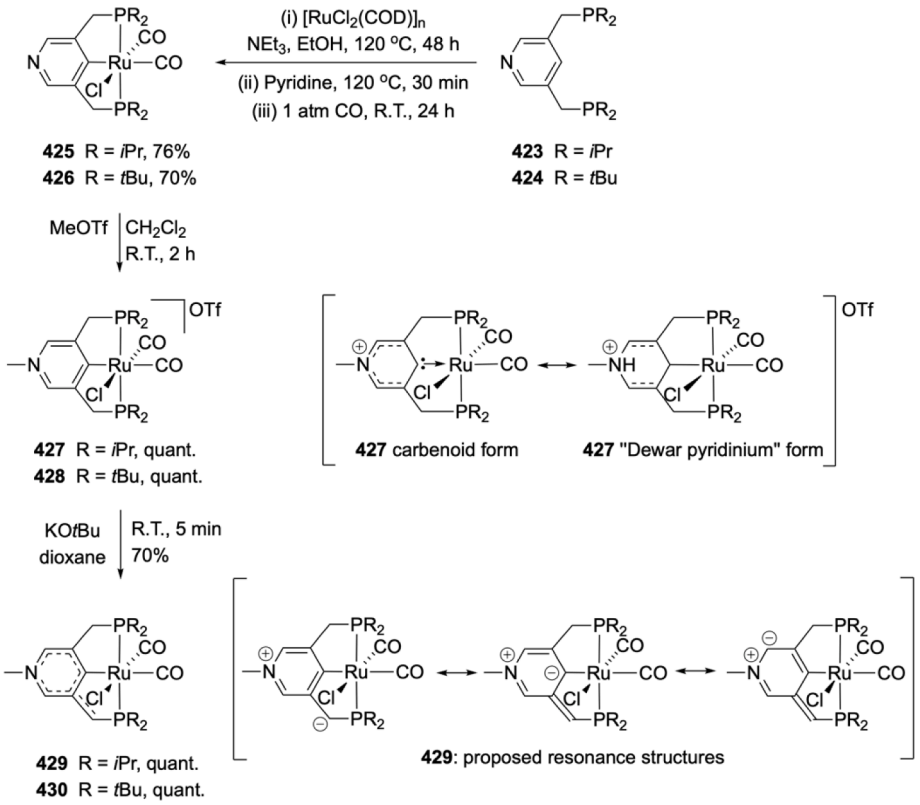

Scheme 92. Synthesis of Ru complexes with type **VIIIc** backbone (R = *i*Pr, *t*Bu).

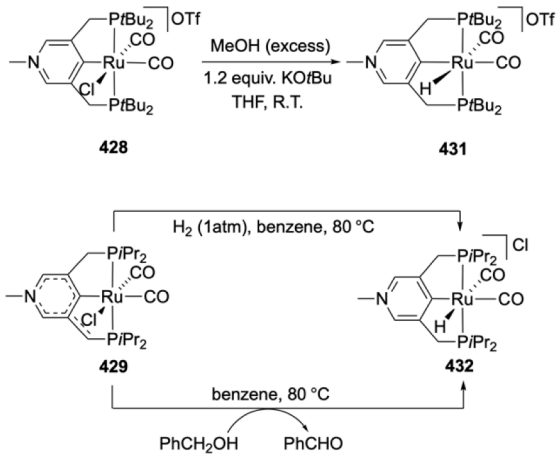

Scheme 93. Reactivity of Ru complexes with type **VIIIc** backbone (R = *i*Pr, *t*Bu).

torsion angle) but still higher than in **Ir-(P,N,P)Cl**. The significantly longer Ir–Cl bond distances in the calculated and experimental structures of **445** and **450** compared to the corresponding **Ir^{III}-(P,N,P)** complex have been attributed to the better electron-donating ability of the bridgehead NHC. Analogous ligand design effects have been concluded in comparing Mo^0-P,C^{NHC},P and (P,N,P) complexes with regard to the N_2 activation and catalyst stability (see section 3.10.1).

The complexes **442**, **445**–**446** and **449** were efficient catalysts for the hydrogenation of carbon dioxide with triethanolamine to ammonium formates. In particular, **442** was shown to exhibit longevity and activity, outperforming the **Ir^{III}-(P,N,P)** analogues that have also been studied for this purpose: under optimal conditions, over 46 h **442** achieved a turnover number (TON) of 230,000 compared to 54,000 by the **Ir^{III}-(P,N,P)** (Scheme 96) [226].

The rhodium complexes **451** and **452** with the P,C^{NHC},P ligand architecture **VIc** were accessed by Ag transmetalation methods (Scheme 97) [228]. Thus, reaction of **373** with [Rh(μ-Cl)(CO)$_2$]$_2$ gave the stable, dark yellow Rh^I complex **452** that was characterized by NMR and IR spectroscopy [228]. The ^{31}P NMR spectrum of the complex displayed a doublet at δ 21.7 ppm, which was assigned to the two equivalent phosphorus donors coupled to Rh. The intense ν(CO) band in the IR spectrum at 1933 cm^{-1} was consistent with values found for most rhodium chlorido-carbonyl complexes containing a terdentate ligand [229]. In contrast, the reaction of **373** with [Rh(μ-Cl)(COD)]$_2$ in CH_2Cl_2 afforded the Rh^{III} complex **453**. Investigations by NMR spectroscopy and X-ray diffraction revealed that **453** resulted from the oxidative-addition

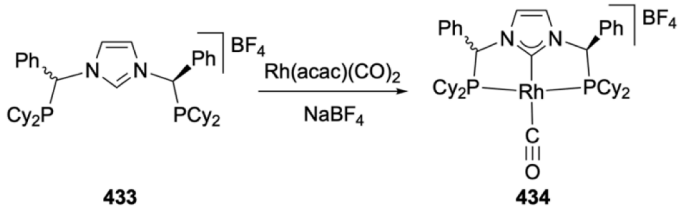

Scheme 94. Synthesis of a Rh complex with chiral **VIa** backbone

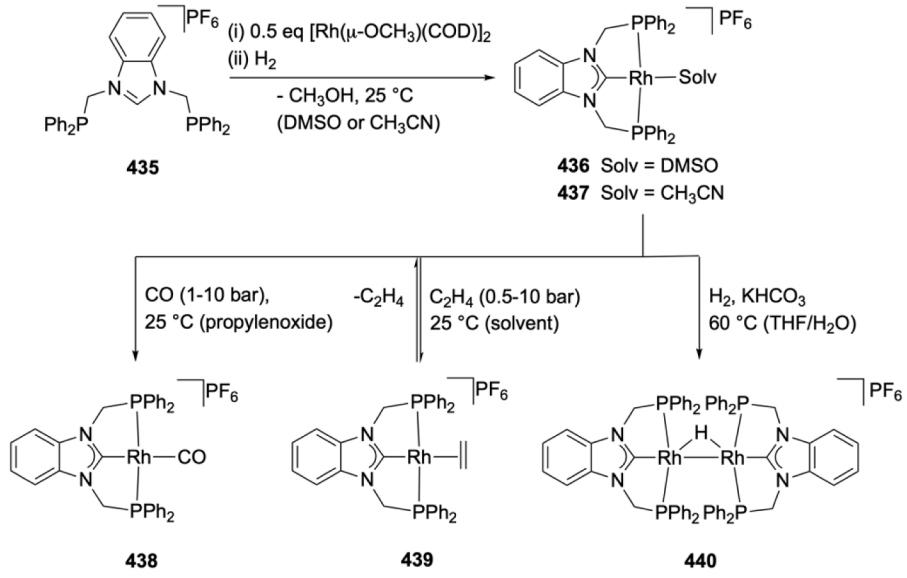

Scheme 95. Synthesis and reactivity of Rh complexes with type **VIb** backbone

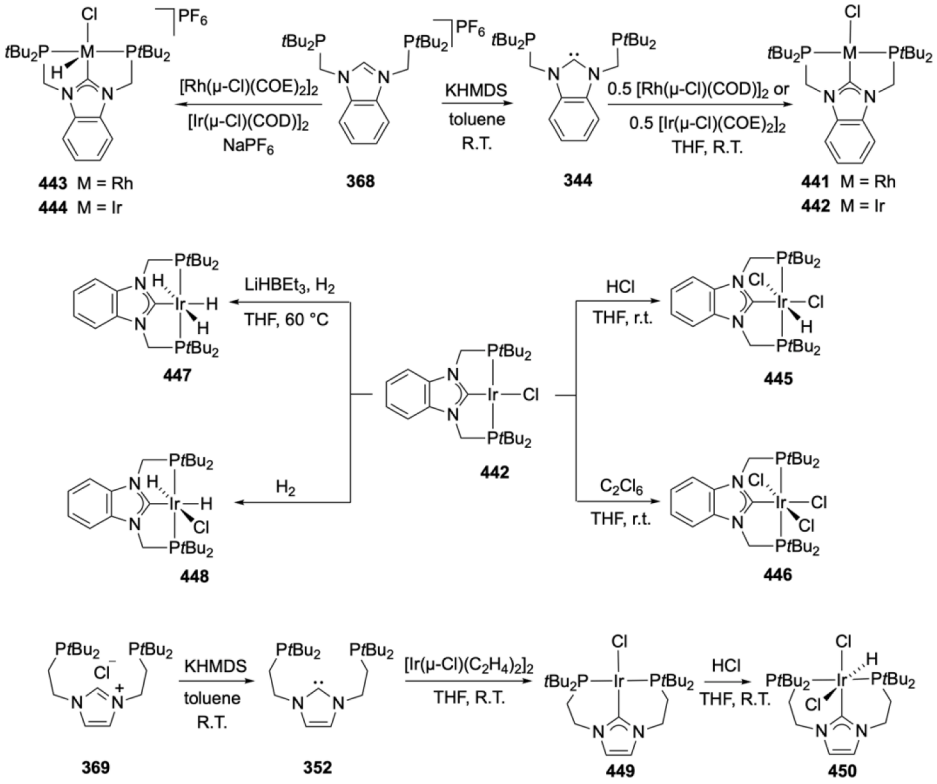

Scheme 96. Synthesis and reactivity of Rh and Ir complexes with types **VIb** and **VIc** backbones

of dichloromethane to the initially formed Rh^{I} intermediate **451**. The ^{31}P NMR spectrum of **453** comprised a doublet at δ 6.4 ppm ($^{1}J_{Rh\text{-}P} = 103.3$ Hz), and the ^{1}H NMR spectrum a triplet of doublets at δ 3.61 ppm ($^{3}J_{H\text{-}P} = 8.1$ Hz and $^{2}J_{Rh\text{-}H} = 2.8$ Hz, respectively), which was attributed to the CH_2Cl group. The X-ray diffraction analysis revealed an octahedral coordination geometry around the rhodium center. The Rh–CH_2Cl distance of 2.086(9) Å was comparable to that of similar rhodium complexes [230–232] and longer than the Rh–C^{NHC} bond length of 2.008(9) Å. Similarly, reaction of complex **373** with [Rh(μ-Cl)(COD)]$_2$ in DMF at 60 °C afforded the complex **454** and precipitation of AgCl (Scheme 97) [228]. Broad signals at δ 2.90 and 4.58 ppm were observed in the ^{1}H NMR spectrum for the NCH_2 and PCH_2 protons, respectively. The ^{31}P NMR spectrum displayed a doublet at δ 1.7 ppm. All data were consistent with the symmetric complex **454**. The crystal structure determination established the coordination of the P,C^{NHC},P and of three chlorido ligands to the Rh center. The reaction mechanism could involve the formation of a highly reactive Rh^{I} complex **451**, which could be oxidized by the byproduct AgCl to afford the Rh^{III} complex **454**. The complexes **452**–**454** were efficient catalyst precursors for the chemoselective hydrosilylation of alkynes [228].

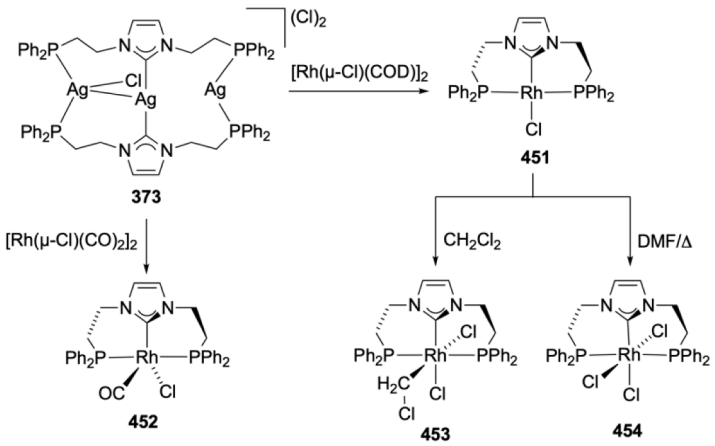

Scheme 97. Rhodium complexes with a P,C^{NHC},P pincer

A range of isotypical Ir^{III} pincer complexes of type **455**–**459**, all adopting octahedral coordination geometry and bearing CO and H ligands *trans* and *cis* to the coordinated E-donor, respectively, were prepared by the E–H activation/oxidative addition to [Ir^{I}Cl(CO)(PPh$_3$)$_2$] or [Ir^{I}Cl(CO)(PPh$_3$)(*p*-toluidine)]. In general, the E–H functionalities ranged from charge cationic to neutral to anionic, leading to the charge cationic, neutral or anionic complexes **455**–**459** (Scheme 98) [233]. The value of the ν(CO) stretching vibration of the resulting complexes [Ir(H)Cl(CO)(κPPh$_2$, κE, κPPh$_2$)]^{q} (q = 1, 0, −1) was used as a spectroscopic handle for classifying the donor properties of E to the Ir^{III} center and was considered of wider applicability than the Tolman Electronic Parameter (TEP), the latter being only limited to neutral ligands and complexes (*i.e.* L, [Ni(CO)$_3$L], respectively). The E–H studied included pyridinium, ammonium, imidazolium, protonated carbodiphosphorane, borane and phenyl groups, leading to the corresponding pyridine, amine, NHC, carbodiphosphorane, boryl and phenylene coordinated pincer bridgeheads. For bridgehead donors of interest in the framework of this review, the ν(CO) trend observed was: pyridine (2040 cm^{-1}) > amine (2030 cm^{-1}) ≅ NHC (2040 cm^{-1}) > carbodiphosphorane (2015 cm^{-1}) ≅ boryl (2015 cm^{-1}) > phenylene (2012 cm^{-1}), the last being anionic; the opposite trend should be valid for the E donor strength. The calculated, predicted ν(CO) values for the complexes with pincers **455**–**459** were 2044, 2042, 2040, 2020–2025 and 1956–1964 cm^{-1}, respectively. Moreover, the chemical shift of the hydrido ligand, which gives rise to specific triplet resonances between δ −14.38 and −17.74 ppm in the ^{1}H NMR spectra has also been correlated with the donor strength of the *cis*-E donor.

The complexes **71**–**73** with the rigid pincer of architecture **VIIa** have been studied (Scheme 99) [90]. The free pincer **461** was obtained by deprotonation of the imidazolinium salt **460**, and then reacted with the precursor [Rh(μ-Cl)(COD)]$_2$ *in situ* to afford the complex which was characterized spectroscopically and crystallographically [90]. The ^{31}P NMR spectrum of **71** showed a doublet at δ 22.4 ppm ($^{1}J_{Rh\text{-}P}$ = 142.5 Hz) and its molecular structure revealed a slightly distorted square planar coordination geometry around the Rh center. The Rh–C^{NHC} bond distance (at 1.929(5) Å) was shorter than the average value of 2.026 Å for this type of bond in other Rh^{I}–C^{NHC} complexes [234], the shortening may be attributed to the weak *trans* influence of the chloride and the constraint of the rigid pincer [235]. Reaction of **71** with potassium triethylborohydride afforded **72**, which shows a characteristic signal in the ^{1}H NMR spectrum at δ −4.1 ppm that was attributed to the Rh–*H*. Treatment of **71** with a slight excess of LiMe at 0 °C produced the complex **73** as a grey solid in 55% isolated yield. In the ^{1}H NMR spectrum of **73** a typical doublet of triplets at 0.55 ppm was observed and was assigned to the Rh–C*H*$_3$; the corresponding methyl carbon resonance in ^{13}C NMR spectrum was found at δ −10.3 ppm (Scheme 99) [90].

The complex **463** with the rigid pincer ligand of type **VIIb** was obtained by the reaction of the imidazolium precursor **462** with LiHMDS followed by addition of [Rh(μ-Cl)(COD)]$_2$ (Scheme 100) [236]. It was characterized spectroscopically and crystallographically: a typical doublet was found in the ^{31}P NMR spectrum at δ 49.5 ppm ($^{1}J_{Rh\text{-}P}$ = 157 Hz), while the crystal structure revealed that the rhodium adopted a distorted square planar geometry with the pincer and an iodido ligand. The Rh^{I}–C^{NHC} is rather short (*ca.* 1.905(6) Å) and the Rh^{I}–P distances of 2.273(2) and 2.293(2) Å were consistent with values

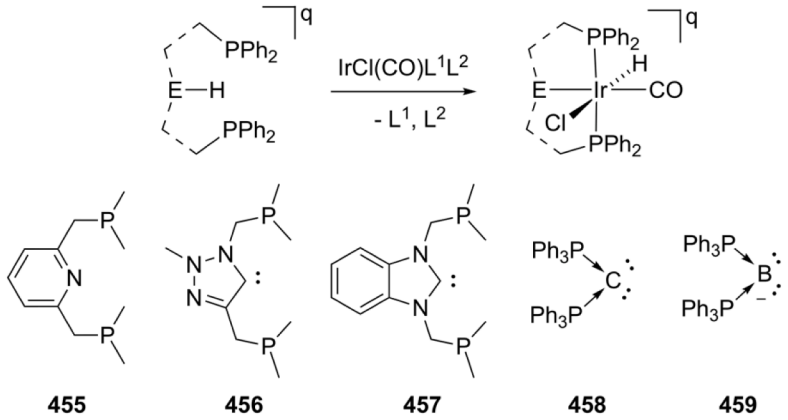

Scheme 98. Comparison of the donor properties of pincer ligands with various bridgehead donors on the Ir(H)Cl(CO) fragment based on experimental (IR, ^{1}H NMR) and computational methods.

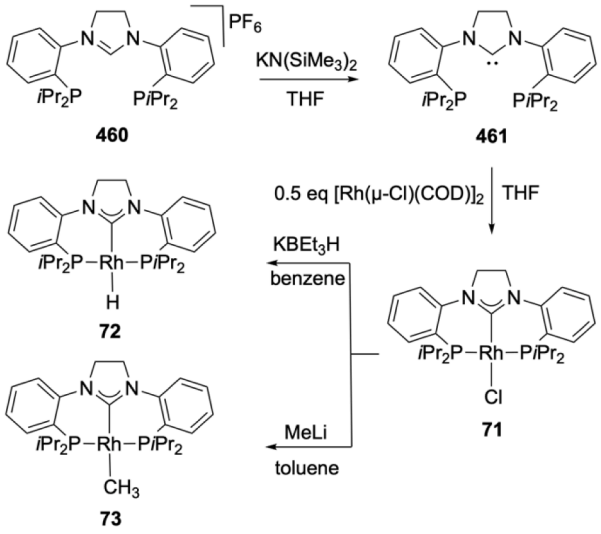

Scheme 99. Synthesis of Ru complexes with type **VIIa** backbone

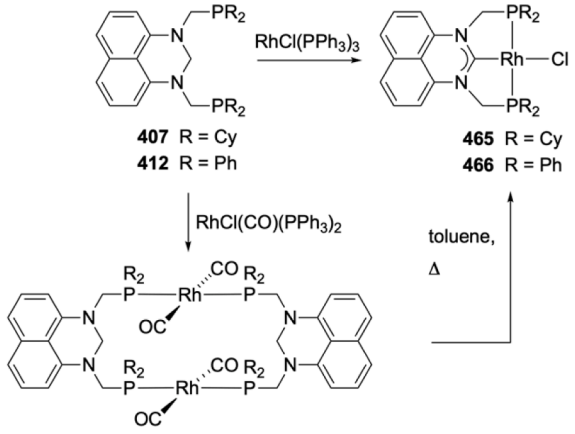

Scheme 101. Synthesis of Rh complexes with type **VIIIb** (perimidine) backbone.

observed in most analogous Rh complexes with flexible terdentate ligands [90,237]. Treatment of the Rh^{I} complex **463** with I_2 resulted in the formation of the air-stable Rh^{III} complex **464** adopting a distorted octahedral coordination environment around the rhodium center, with distances between the phosphorus atoms and Rh^{III} of 2.379(1) and 2.396 (1) Å, while the Rh^{III}–C^{NHC} (at 1.904(4) Å), remained virtually the same as in **463** (Scheme 100).

Reactions of pincer ligand precursors **407** and **412** of type **VIIIb** with $[RhCl(PPh_3)_3]$ resulted in the formation in high yields of complexes **465** and **466** *via* double dehydrogenation (Scheme 101) [221,237,238]. Complex **465** was characterized by NMR spectroscopy, with the C^{NHC} ^{13}C NMR resonance at δ 206.7 ppm. In the similar complex **466**, the structure of which was determined crystallographically, the Rh-C^{NHC} bond distance of 1.948(4) Å was consistent with that in most NHC complexes of Rh^{I}. It was recently found that complexes **465** and **466** could be obtained by thermal activation of dirhodium metallocycles in which the ligands act as diphosphines (Scheme 101) [239].

Iridium complexes with the perimidine backbone of type **VIIIb** have also been described (Scheme 102) [237,238]. Reaction of the precursor **407** with $[IrCl(CO)(PPh_3)_2]$ resulted in the formation of the alkyl complex **467** *via* C–H bond activation [237]. The infrared spectrum of **467** revealed the ν(Ir–H) and ν(CO) absorptions at 2012 and 1940 cm^{-1}, respectively. In the ^1H NMR spectrum, the triplet at δ −17.9 ppm, with a coupling constant of 11 Hz, was attributed to the Ir-H group and the singlet at δ 5.75 ppm to the methine group. Treatment of complex **467** with various silver salts (AgY, Y = PF_6, SbF_6, PO_2F_2) afforded the complexes of type **468** following α-C*H* rather than halide abstraction [237]. The ^{13}C NMR spectrum showed the typical carbene signal at δ 190.1 ppm. The X-ray structure of complex **468** confirmed the formation of a Ir–C^{NHC} bond, with a distance of 2.078(4) Å. Reaction of ligand **407** with the dinuclear complex $[Ir(\mu\text{-}Cl)(COE)_2]_2$ afforded the octahedral dihydrido Ir^{III} complex **469** [238]. Its infrared spectrum showed a characteristic single ν(Ir–H) absorption at 1724 cm^{-1}, indicating a *trans* disposition of the two hydrides. The ^1H NMR spectrum displayed a triplet resonance at δ_H −6.97 ppm ($J_{P\text{-}H}$ = 16 Hz), reflecting the *trans*-IrH_2 stereochemistry; consistently, a singlet was observed in the ^{31}P NMR spectrum at 27.3 ppm. The ^{13}C NMR resonance for the C^{NHC} was observed at 193.3 ppm. Reaction of complex **469** with chloroform afforded the complex **470** in 82 % yield. Its ^1H NMR spectrum comprised a triplet at δ −18.98 ppm for the hydride and the diastereotopic NCH_2P appeared as two distinct resonances, in accord with a *cis*-$IrCl_2$ geometry; finally, the C^{NHC} resonance was observed at 187.2 ppm by ^1H–^{13}C HMBC experiments. The structure of **470** was determined by X-ray diffraction (Ir–C^{NHC} at 1.962(6) Å) [238]. Complex **469** was stable under ambient conditions, however, when a solution was heated to 50 °C for 42 h, it was converted *via* reductive elimination to **471** which is the Rh analogue of **465**. The ^{31}P NMR spectrum of **471** showed a singlet at δ 35 ppm and the C^{NHC} presence was confirmed by ^1H–^{13}C HMBC experiments ($\delta_{C(NHC)}$ at 188 ppm). Exposure of complex **471** to a H_2 atmosphere for 10 min at room temperature yielded the *cis*-H_2 complex **472** by oxidative addition (Scheme 102) [238]. Interestingly, reaction of ligand **412** with $[Ir(\mu\text{-}Cl)(COD)]_2$ afforded complex **473** without C–H bond activation of the NCH_2N group [238]. However, C–H activation and formation of **474** occurred upon heating a solution of complex **473** at 90 °C for 16 h.

Reaction of the rhodium precursor $[RhCl(PPh_3)_3]$ with the ditopic diperimidine pincer precursors **475**–**477** related to **VIIIb** gave the complexes **478**–**480** by a double geminal C−H activation of the central CH_2 and coordination of the ditopic P,C^{NHC},P pincer to the Rh (Scheme 103); complexes **478**–**480** were sparingly soluble in organic solvents and therefore presented difficulties for their conventional characterization. In ^{13}C enriched samples, the chemical shift of the C^{NHC} in the ^{13}C NMR spectra gave evidence for the carbene formation ($\delta_{C(NHC)}$ = 206.1, 205.3 and 205.8 ppm for **478**, **479** and **480**, respectively), and ^{31}P NMR spectroscopy confirmed the pincer-type P donor coordination. The crystal structure of the more soluble and crystallizable **480** unveiled a planar ligand that was coordinated to two square planar rhodium fragments with a Rh−C^{NHC} bond distance of 1.93 Å. Further derivatization

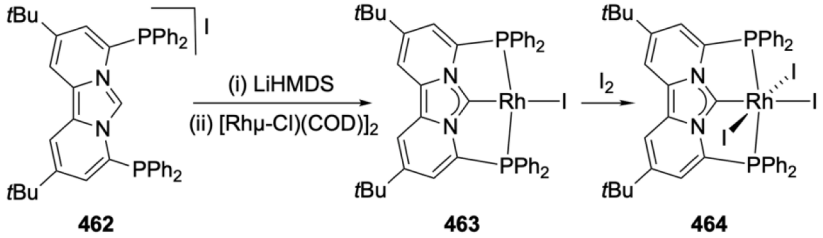

Scheme 100. Synthesis of Rh complexes with type **VIIb** backbone

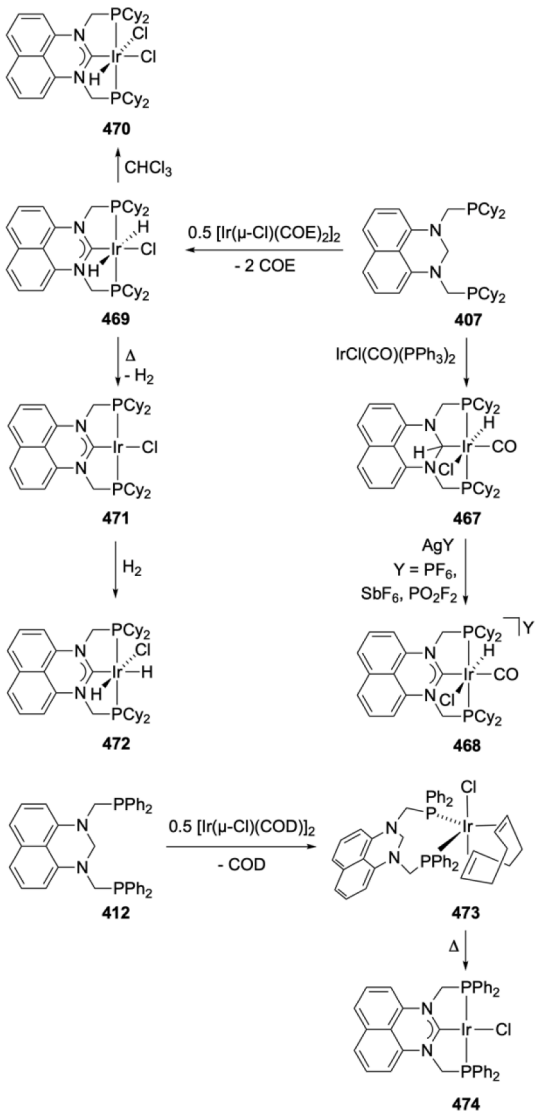

Scheme 102. Synthesis and transformations of Ir complexes with type **VIIIb** (perimidine) backbone.

of the complexes **478**–**480** is achieved by ligand exchange of the chloride, as shown by reaction with lithium phenyl acetylide, or by chloride abstraction with $TlPF_6$ in the presence of PPh_3 or pyridine. The ligand perylene core and its derivatives were also studied by UV – vis and emission spectroscopy exhibiting as a characteristic feature an intense band of the $\pi^* \leftarrow \pi$ transition of the aromatic perylene core origin with partially resolved vibrational progression. Metal substitution had as an effect the bathochromic shift of the absorption maxima by *ca.* 15 nm. (Scheme 103) [240].

The complex **486** featuring a pincer ligand of the type **IXa** (Scheme 104) was prepared by the reaction of the imidazolium salt precursor **485** with $[Rh(acac)(CO)_2]$ in refluxing THF, the acac ligand acting as coordinated base, recrystallized from MeOH and characterized spectroscopically and crystallographically [241]. Its ^{31}P NMR spectrum displayed two overlapping ABX multiplets with $^2J_{P\text{-}P}$ couplings of 268 and 274 Hz and $^1J_{P\text{-}Rh}$ of 134 Hz, in agreement with the *trans* disposition of the phosphane donors. In the IR spectrum the ν(CO) absorption at 2008 cm^{-1} was comparable to values reported in the literature for similar complexes.

Cobalt complexes with the ligand backbone of type **Xb** have been described [223], as well as Rh complexes with the ligand backbones of type **Xa** [39], **Xb** [242–244] and **Xc** [245]. All these are mentioned here for comparison, since the bridgehead donors are not classified as N-heterocyclic carbenes.

3.10.5. Group 10 metals (Ni, Pd, Pt)

Nickel. The nickel complex **511** featuring the ligand with backbone **VIIa** was synthesized by the reaction of precursor **460** with $[Ni(COD)_2]$ in THF in 73 % yield (Scheme 105A) [246]. The complex was characterized spectroscopically and crystallographically: in the ^1H and ^{31}P NMR spectra signals at δ −10.73 ppm (t, $^2J_{P\text{-}H} = 53.5$ Hz) and at δ 47.6 ppm (s) were observed, respectively. The structure of **511** displayed a square-planar geometry at Ni with Ni–C^{NHC} bond distance of 1.863(2) Å, in the range of those found in most Ni^{II}–NHC complexes (1.85–1.89 Å). The reaction of **511** with ethylene unexpectedly led to complex **512**, formally a Ni^0 η^2-iminium diphosphane complex, rather than the formation of a square-planar Ni^{II} ethyl complex $[NiEt(\kappa P,\kappa C^{NHC},\kappa P)]PF_6$ [49]. The ^1H NMR signals of **512** are broad, in particular, the two peaks assigned to the inequivalent imidazoline methylene protons and those due to the inequivalent P*i*Pr$_2$ substituents. In the solid state, the η^2-C–N interaction renders the two phosphane donors inequivalent. However, the $^{31}P\{^1H\}$ NMR spectrum exhibited a singlet, which suggested fast exchange of the η^2-C–N unit between the two N atoms of the heterocycle. To clarify the mechanism of the conversion of **511** to **512**, where two mutually *trans*-disposed groups, the central C^{NHC} and the hydride, are formally involved in the formation of the ethyl by an elementary insertion step, isotopic labelling and computational studies were carried out. It was concluded that the regioselectivity of the reaction was determined by the increased P*i*Pr$_2$ donor sterics, leading to a pyramidalized intermediate with agostic ethyl interaction as precursor to **512**; computationally, PH_2 (in the place of P*i*Pr$_2$) side-arm donors favored the formation of the $[NiEt(\kappa P,\kappa C^{NHC},\kappa P)]^+$ species with a square-planar Ni center (Scheme 105A) [49,246].

Reaction of the diphosphine ligands 1,3bis{(diphenylphosphanyl) methyl}imidazolidine **489A^{Ph}** or 1,3-bis{(di-*tert*-butylphosphaneyl) methyl}imidazolidine **489A^{tBu}** with $[NiCl_2(DME)]$ in the presence of KPF_6 afforded the pincer carbene complexes **489B^{Ph}** and **489B^{tBu}** with **VIa** backbone as a result of activations of the two C – H bond of the methylene linker (Scheme 105B), as previously observed with related six-membered ring hexahydropyrimidine-based ligands (see below Scheme 112). Neither **489B^{Ph}** and **489B^{tBu}** nor the corresponding hydrido derivative **489C^{tBu}** were active catalysts for the hydrosilylation using $PhSiH_3$ of aldehydes, ketones, and nitroarenes to primary, secondary alcohols, and aromatic amines; in contrast, the mono- or bis-(phenylthiolato) derivatives **489D^{Ph}**, **489D^{tBu}** and **489E^{tBu}** were highly active in all three types of the reaction with good scope (Scheme 105B) [247].

The diamagnetic complex **487** with the pincer of type **VIb** (R = *t*Bu, Y = H) was prepared by the reaction of the *in situ* generated ligand from the precursor **368** and $[NiCl_2(DME)]$. Its structure adopted a square-planar geometry with a Ni–C^{NHC} bond distance of 1.828(4) Å (Scheme 106) [86].

Palladium, Platinum. In addition to complex **488** (Scheme 106), the Pd and Pt complexes **490** and **491** with the related ligand precursor of type **VIc** were obtained *via* ligand transmetalation to $[PdCl_2(COD)]$ and $[PtCl_2(NCPh)_2]$, respectively, from the silver complex **489**, which in turn was generated from **330** and Ag_2O in dichloromethane (Scheme 107). In the spectra of **490** the characteristic signals at δ 12.4 ppm and δ 161.8 ppm in the ^{31}P- and ^{13}C NMR spectra were assigned to the coordinated *P*Ph$_2$ and *C*^{NHC}, respectively; similarly, in the ^{31}P, ^{13}C and ^{195}Pt NMR spectra of **491** the corresponding characteristic signals were seen at δ_P 14.1 ppm, δ_C 145.9 ppm (t) and δ_{Pt} −4482 ppm (d, $^1J_{Pt\text{-}P} = 2450$ Hz), respectively. Chloride abstraction from **490** with $AgBF_4$ in pyridine afforded the complex **492** (δ_C 150.5 ppm for the *C*^{NHC}, and δ_P 21.9 ppm for the *P*Ph$_2$). The complex **490** was efficient in Heck-type coupling reactions of several aryl halides with styrene and *n*-butyl acrylate at 110 °C (Scheme 107) [248].

The series of complexes **496**–**498** with the chiral ligand of type **VIe**

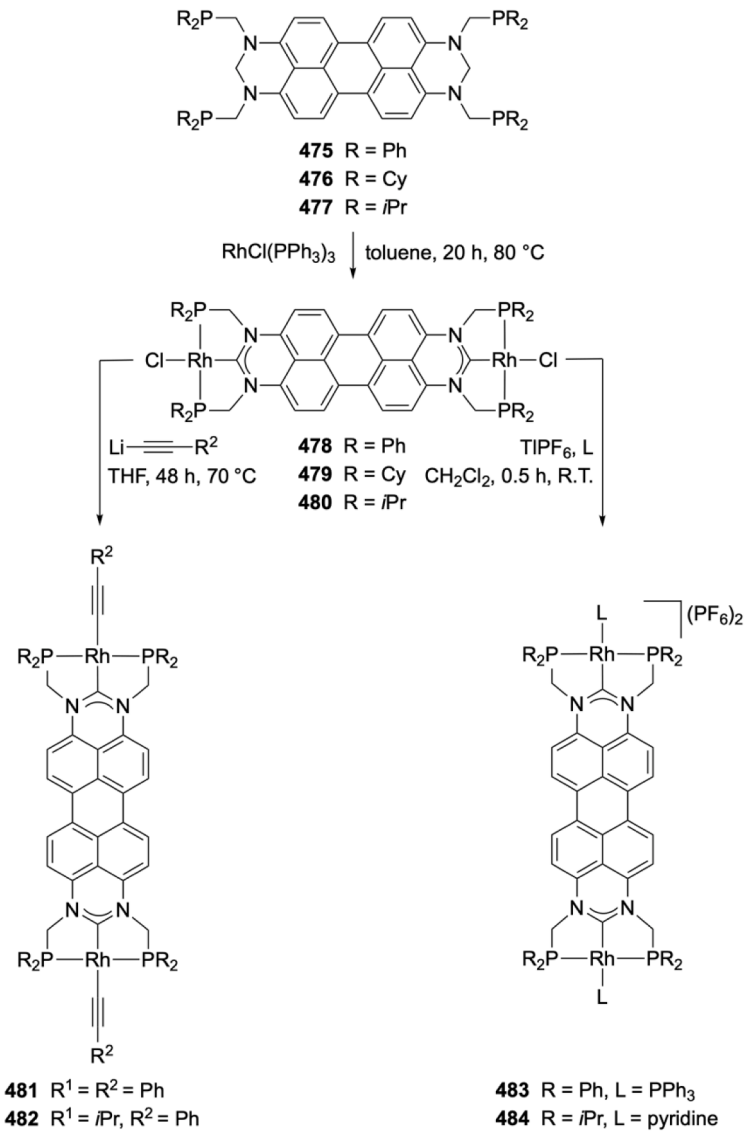

Scheme 103. Synthesis and transformations of binuclear Rh complexes with type **VIIIb** (perimidine/perylene) backbone.

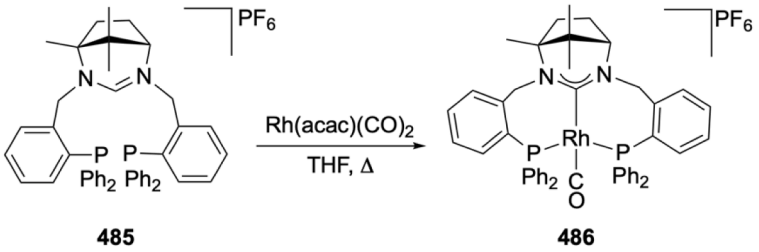

Scheme 104. Synthesis of a Rh complex with type **IXa** backbone.

were obtained by direct palladation of the imidazolium precursors **493**–**495** with $[Pd(OAc)_2]_3$ in THF at 60 °C (Scheme 108); subsequent reactions of **496** and **498** with $(Et_3O)PF_6$ in acetonitrile led to the formation of **499** and **501**, respectively, however, formation of **500** from **497** was not observed under the same conditions. Complex **499** revealed a square-planar geometry at Pd, with a Pd–C^{NHC} bond distance of 1.993 (9) Å. The complexes **499** and **501** were efficient catalysts in the asymmetric addition of thiomorpholine to methacrylonitrile, with *ee* values up to 75 % (Scheme 108) [249].

P,C^{NHC},P pincer complexes with a mesoionic triazolylidene bridgehead (type **VIf**) are very rare and one example **506** has been obtained indirectly by the selective methylation of the triazole ring in the triazolyl complex **504** with CH_3I (Scheme 109). Interestingly, this reaction did not lead to Pd^{IV} methylated species but to ligand methylation. Complex **506** was characterized by multinuclear NMR spectroscopies and crystallographically: the CH_3 of the triazolylidene displayed signals at δ_H 4.14 ppm and δ_C 38.7 ppm, while the C^{NHC} appeared at δ_C 148.6 ppm, slightly upfield shifted compared to the signal of the metalated carbon in

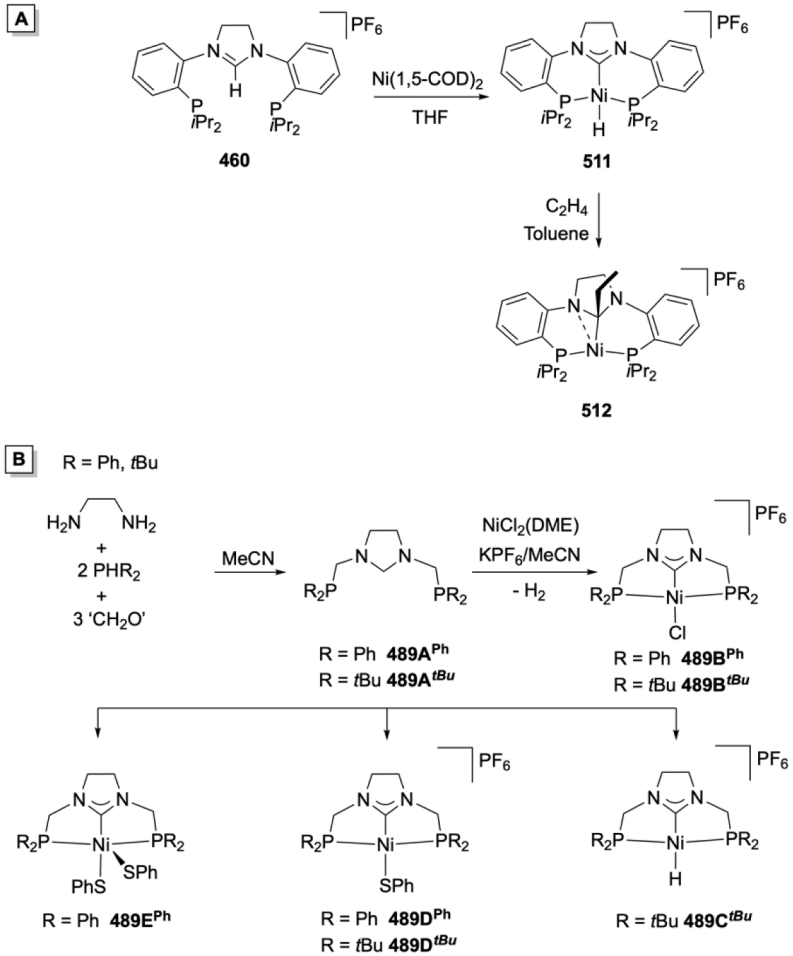

Scheme 105. **A** Reactivity of the Ni complex **511** with type **VIIa** backbone. **B** Ni complexes with type **VIa** backbone

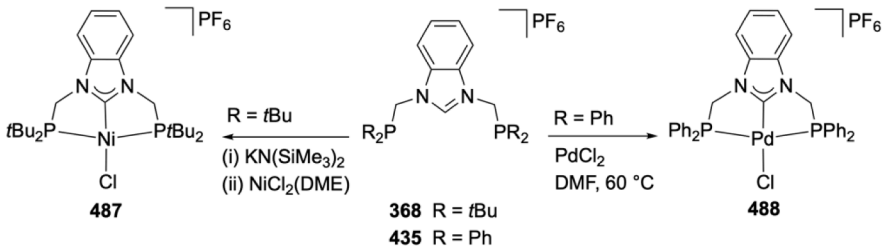

Scheme 106. Ni and Pd complexes with type **VIa** backbone

the triazolyl precursor. The structure of **506** features a square-planar Pd center with a Pd–C bond distance at 1.902(9) Å. By an analogous methodology, *i.e.* by alkylating the metalated Pt complex **505** with the *p*-CF_3-benzyl bromide, the triazolylidene Pt complex **507** was obtained that was characterized only by multinuclear NMR spectroscopy. Complex **507** served as a useful source to other derivatives by substitution of the Cl *trans* to the bridgehead C^{NHC} with the neutral ligands CO or MeCN ligands (Scheme 109) [250].

The reactivity of $[M(PPh_3)_4]$ (M = Pd, Pt) with the precursor **460** was similar to that with Ni summarized above leading to the hydrido complexes **513** and **514** in good yields, respectively, after formal 'insertion' of the metal into the C–H imidazolinium bond (Scheme 110). Characteristic signals corresponding to the M–*H* were observed in the ^{1}H NMR spectra at δ −6.15 ppm (unexpectedly, singlet) and δ −4.43 ppm −4.43 (t with Pt satellites, $J_{P\text{-}H}$ = 14.5 Hz, $J_{Pt\text{-}H}$ = 403.2 Hz), respectively, while the signal due to the heterocycle backbone protons also appeared as singlets, presumably due to dynamic processes in solution. In the ^{31}P NMR spectra the equivalent coordinated P donors appeared at δ 46.1 ppm (Pd) and δ 39.5 ppm (Pt) with ^{195}Pt satellites, $^1J_{P\text{-}Pt}$ = 1241.5 Hz). The molecular structures of **513** and **514** were established crystallographically and comprise distorted square-planar coordination geometries with M–C^{NHC} bond distances of 2.028(4) Å (Pd) and 2.005(4) Å (Pt). A common characteristic of all three structures with this ligand framework is the twisting of the NHC ring making an angle with the metal coordination plane ranging from 31.9° to 41.5° (Scheme 110) [246].

Further insight into the formal 'insertion' of the metal into the C–H imidazolinium bond in the ligand precursors of type **VIIa** was obtained by the reaction of $[M(PPh_3)_4]$ (M = Pd, Pt) with **515** (Scheme 111) [251]. Thus, the reaction of the chloride salt carried out in THF initially afforded the alkyl complexes **516** and **517**, respectively, which were characterized by NMR spectroscopies and X-ray diffraction: diagnostic

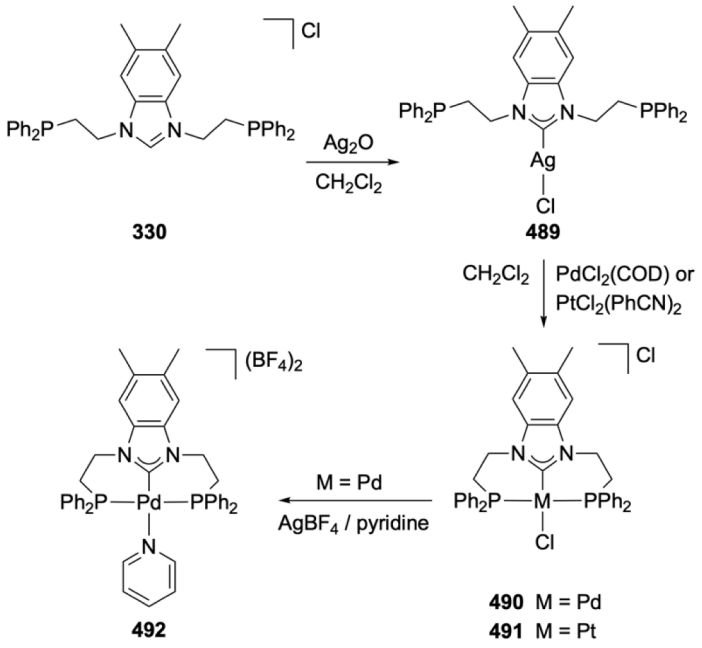

Scheme 107. Pd and Pt complexes with type **VIc** backbone

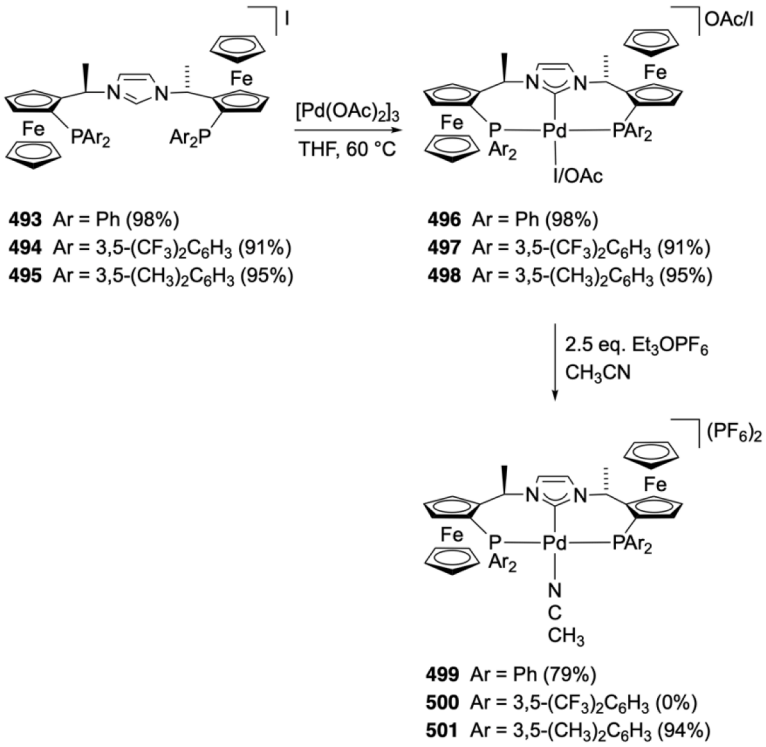

Scheme 108. Pd complexes with type **VIe** backbone

signals at δ 4.78 ppm (t, $^{3}J_{H\text{-}P} = 20.2$ Hz) and δ 4.82 ppm (4.82 dt, $^{3}J_{P-H} = 12.0$ Hz, $^{2}J_{Pt-H} = 52.0$ Hz)) for the M−C^{imidazolinyl}−H were observed in the corresponding ^{1}H NMR spectra; moreover, signals assignable to NC^{imidazolinyl}(H)N in the ^{13}C NMR spectra of **516** and **517** appeared at δ 85.6 ppm and δ 66.3 ppm, in a region associated with metalated α-heteroatom substituted C_{sp3} alkyls, rather than NHCs; finally, the ^{31}P NMR spectra displayed characteristic peaks at δ 9.54 (singlet) and δ 16.3 ppm (d, $^{1}J_{Pt-P} = 2620$ Hz), respectively. There was no evidence for the formation of any M−*H* moieties, a fact that differentiates the reactivity of **515** leading to the present complexes and that of **460** described above. The molecular structures of **516** and **517** attest for the presence of M−Csp^3 alkyl species in view of the non-planar geometry of the metalated carbon and the observed bond distances: Pd–C = 2.0747(12) Å, Pt–C = 2.042(3) Å. Interestingly, in the structure of both complexes the H atoms attached to the metalated C atom were located experimentally and exhibit long M···H distances (Pd···H ≅ 2.57 Å, Pt···H ≅ 2.56 Å) and large M−C−H angle (for Pd/Pt ≅ 110°), both metrical data being outside the range for an agostic

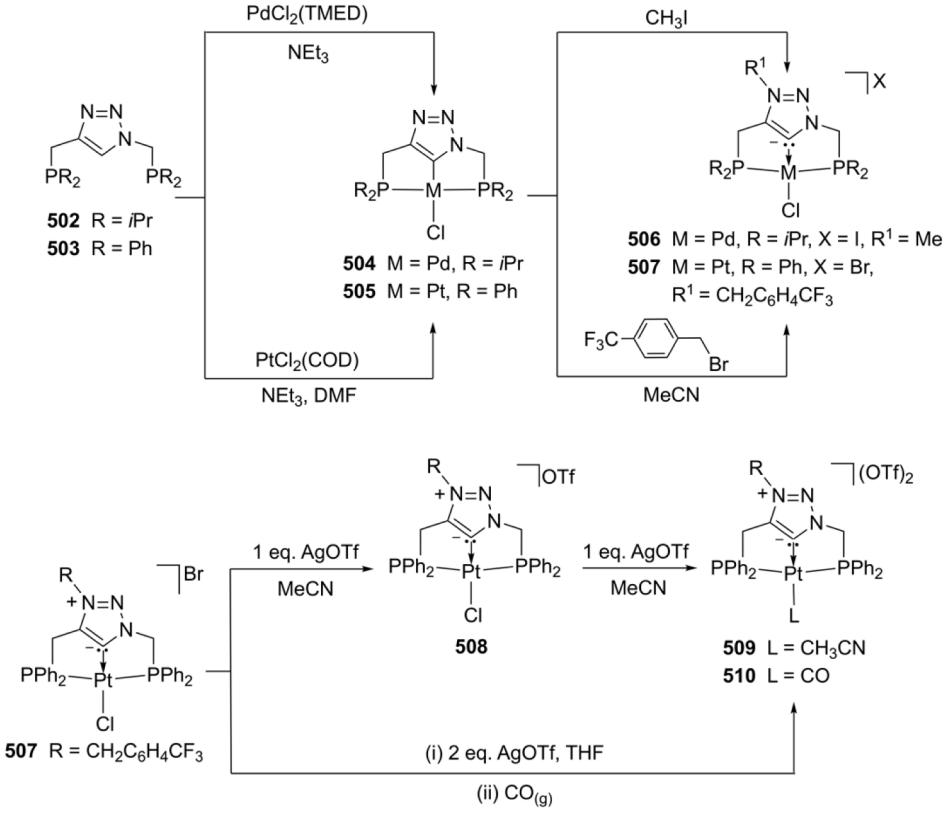

Scheme 109. Pd and Pt pincer complexes with a mesoionic triazolylidene bridgehead of type **VIf**

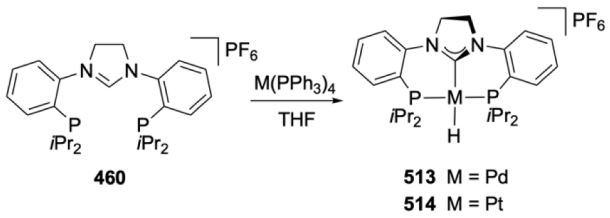

Scheme 110. Pd and Pt complexes with type **VIIa** backbone

C–H–M interaction. The above experimental observations suggest to consider **516** and **517** as 'arrested' intermediates preceding the C–H oxidative-addition resulting from the reaction of [M(PPh$_3$)$_4$] (M = Pd, Pt) with **515** (Scheme 111) [251]. Thus, the reaction of the chloride salt carried out in THF initially afforded the alkyl complexes **516** and **517**, respectively, which were characterized by NMR spectroscopies and X-ray diffraction: diagnostic signals at δ 4.78 ppm (t, $^3J_{H\text{-}P} = 20.2$ Hz) and δ 4.82 ppm (4.82 dt, $^3J_{P-H} = 12.0$ Hz, $^2J_{Pt-H} = 52.0$ Hz)) for the M−C^{imidazolinyl}–*H* were observed in the corresponding ^{1}H NMR spectra; moreover, signals assignable to NC^{imidazolinyl}(H)N in the ^{13}C NMR spectra of **516** and **517** appeared at δ 85.6 ppm and δ 66.3 ppm, in a region associated with metalated α-heteroatom substituted C$_{sp3}$ alkyls, rather than NHCs; finally, the ^{31}P NMR spectra displayed characteristic peaks at δ 9.54 (singlet) and δ 16.3 ppm (d, $^1J_{Pt-P} = 2620$ Hz), respectively. The ^{1}H NMR spectrum of the **518** displays a characteristic triplet for Pd–H at δ −5.73 ppm ($^2J_{P\text{-}H} = 6.0$ Hz); the C^{NHC} resonance in the ^{13}C NMR spectrum occurred at 198.5 ppm. Analogous reactivity was recorded for the Pt complexes: in contrast to the thermally stable Pd complex **516**, complex **517** was easily converted to **521** after refluxing in a polar solvent. The Pt hydrido complex **519** was accessible by the methodology developed for the Pd complexes, *i.e.* by Cl abstraction with TlPF$_6$ from **517**, or directly from **520** and [Pt(PPh$_3$)$_4$]. Spectroscopic and

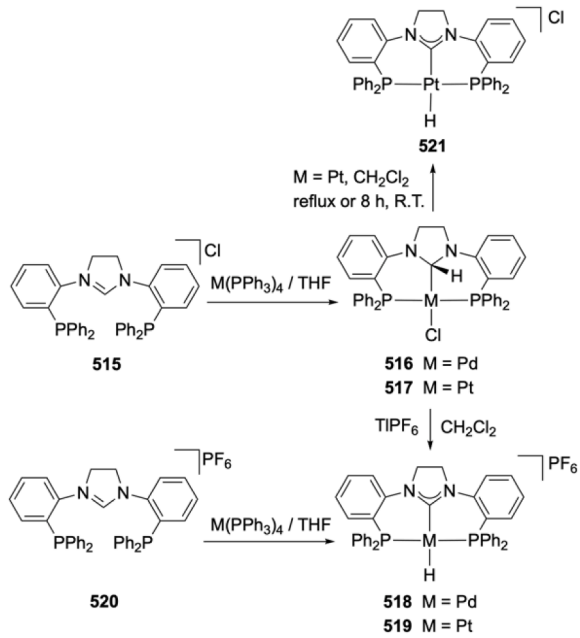

Scheme 111. Further Pd and Pt complexes with type **VIIa** backbone

crystallographic data for **521** are in accord with the proposed structures: Pt–*H* (δ −3.88 ppm, t with Pt satellites $^1J_{Pt-H} = 851.5$ Hz, $^2J_{P-H} = 24.0$ Hz) and Pt–*C*^{NHC} δ 194.0 ppm with both Pt satellites and coupling to ^{31}P ($^1J_{Pt-C} = 684.6$ Hz, $^2J_{P-C} = 11.1$ Hz) (Scheme 111) [251]. Although the bonding situation in the cations of **518** and **521** was established by DFT methods, the observed reactivity trends may call for some empirical understanding: it may be argued that the reactivity

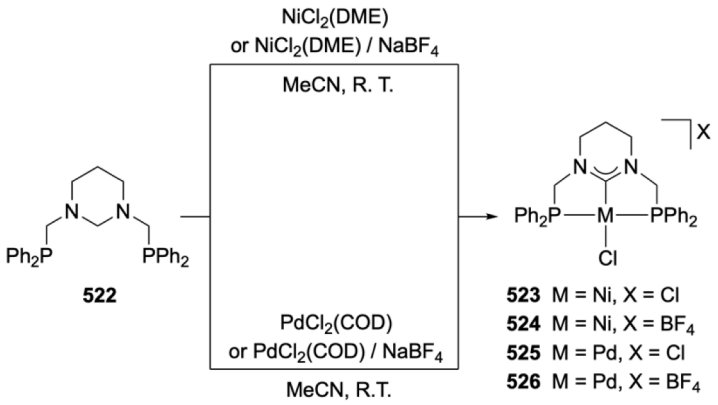

Scheme 112. Ni and Pd complexes with type **VIIIa** backbone

difference between the -PPh_2 and -*i*Pr_2 substituted imidazolinium salts **515** and **460** has steric and mainly electronic origins: (i) the latter precursor bears the more electron rich P*i*Pr_2 moieties, rendering the metal center more reactive towards oxidative addition after the initial association; (ii) the absence of any agostic interactions may also imply geometrical constraints hampering the interaction between the C–H orbitals and the metal; (iii) the reduced thermal stability of **517** may be related to the higher thermodynamic and kinetic tendency of Pt^0 for oxidative addition reactions; (iv) and finally, the labilization of the coordinated halide in **516** and **517** may contribute favorably to the thermodynamics of the oxidative-addition by facilitating the M−Cl bond cleavage.

Using **522** as precursor to ligands of type **VIIIa** the Ni and Pd complexes **523**–**524** and **525**–**526**, respectively, were accessed by reactions involving double C–H activation of the N–C*H*$_2$–N moiety of the heterocycle accompanied with release of H_2 (Scheme 112) [252].

Reactions of **522** with [$NiCl_2$(DME)] or [$NiCl_2$(DME)]/$NaBF_4$ in MeCN afforded the complexes **523** and **524**, respectively, while the precursors used to prepare the Pd complexes **525** and **526** were [$PdCl_2$(COD)] or [$PdCl_2$(COD)]/$NaBF_4$. The proposed mechanism for the transformation involves one oxidative-addition step, followed by a redox neutral concerted H_2 elimination from a cationic [M(H)Cl{η^2,1,3-(PPh_2)$_2$-pyrimidinium}] intermediate complex. All diamagnetic complexes were characterized spectroscopically and **523** and **525** crystallographically. The ^{31}P NMR spectra obtained displayed singlets at δ 24.8 ppm and 25.4 ppm (Ni) and δ 26.3 and δ 25.9 ppm (Pd), respectively, and their ^{13}C NMR spectra a broad singlet at $\delta = 186.7$ ppm or a triplet at $\delta = 190.0$ ppm (Ni) and triplets at δ 189.9 and 186.7 ppm (Pd) for the C^{NHC}, respectively. In the square-planar structures adopted in **523**, **524**, **525** and **526**, the M−C^{NHC} bond distances were at 1.900(3) Å, 1.905(6) Å, 2.011(3) Å and 1.997(4) Å, respectively. The Pd^{II} complexes **525**–**526** were found to be highly effective in Buchwald-Hartwig coupling between bromobenzene and morpholine (Scheme 112) [252].

An extended study of the metalation reactivity of flexible at the bridgehead yet rigid at the side-arm pincer platform of type **VIIId** has been undertaken, and was accompanied by further reactivity of the ensuing Ni pincer complexes with small molecules (Scheme 113) [56].

Thus, reaction of the pyrimidinium precursor **527** with [Ni(1,5-COD)$_2$] in THF afforded the neutral complex **528** with an unusual structure as established by spectroscopic and crystallographic methods: the ^{1}H NMR spectrum of **528** displayed a triplet signal at δ 3.30 assignable to the $NiC^{pyrimidine}$–*H* eliminating the possibility of the direct conversion of the pyrimidinium salt to an RE-NHC–Ni–H functionality *via* a concerted oxidative-addition; the molecular structure of **528** determined crystallographically established the presence of a tetrahedral [NiCl(P,C^{sp3}-*H*,P)] bridgehead donor to the Ni^{II} center, the latter adopting a distorted square-planar geometry, with two *trans* phosphane groups and a chloride ligand *trans* to the sp^3-carbon (Ni–C^{sp3} = 1.942(1) Å). The flexibility integrated into the ligand design allowed the α-N atom to get closer to the Ni center (Ni···N = 2.531(1) Å), thus providing some additional electron density. Abstraction of the chloride ligand with $TlPF_6$ resulted in the conversion of **528** to the cationic carbene hydride **529**, which was also characterized spectroscopically and crystallographically: the ^{1}H NMR spectrum contained the resonance due to Ni–*H* at δ −11.79 ppm (t, $^2J_{H\text{-}P} = 50.0$ Hz) and no signal corresponding to a Csp^3–*H* was observed. Thus, the transformation of **527** to **528** can be viewed as a C=N activation within the heterocycle and preceded the conversion to the NHC hydride by C–H activation. Reaction of **529** with excess ethylene afforded **531**, featuring a sp^3-alkyl bridgehead with ethyl substitution at the metalated tertiary alkyl carbon, after insertion of the ethylene into the Ni–H bond. In agreement to this structural picture, the ^{1}H NMR spectrum evidenced the disappearance of the Ni–H resonance and new signals (a triplet and a quadruplet) corresponding to an ethyl group. The C^{sp3}–C^{sp3} and Ni–C^{sp3} bond distances were 1.519(2) Å and 1.8964(13) Å, respectively. Based on computational results, it was proposed that the conversion of **529** to **531** proceeded *via* the non-isolable **530** obtainable *via* insertion of the ethylene into the Ni–H bond. Attempts to deprotonate the α-C–*H* in **528** by means of the strong base $KN(SiMe_3)_2$ led to the formation of the '*-ato*' NHC pincer complex **532**, formally a Ni^0 species, after H^+ abstraction from the coordinated alkyl. The electron-rich Ni center in **532** was responsible for the facile reaction with CH_2Cl_2 leading to the Ni^{II} species **533**. Moreover, the reaction of **532** with PPh_3 in toluene afforded the charge neutral P,C^{NHC},P Ni^0 species **534**. The reactivity of **534** with the acidic reagents HCl, PhOH and H-C≡CPh yielded the complexes **528**, **535** and **536**, respectively. Interestingly, the product **535** of the reaction with PhOH featured a pincer ligand modification after a P–C bond activation from the Ni^0 and P–C^{aryl} scission. Furthermore, reaction of **528** with KHMDS in DME led after P-C^{aryl} activation to a rare example of *terminal* phosphido ligand on Ni^{II} in the C,C^{NHC},P pincer complex **537** [56].

The complexes **540** and **541** with the pincer ligand of architecture **IXa** were accessed by the reaction of **485** with $K_2[PdCl_4]$ and $K_2[PtCl_4]$ in EtOH initially affording the κ^2-P,P complexes **538** and **539**, which display characteristic ^{1}H NMR resonances at δ 9.58 ppm and δ 9.90 ppm assignable to the imidazolium protons (Scheme 114). The X-ray structures of **538** and **539** revealed average Pd–P and Pt–P bond distances of 2.344 Å and 2.332(5) Å, respectively. Then, **538** and **539** were converted to the pincer complexes **540** and **541** by the reaction with KO*t*Bu in THF. The ^{31}P NMR data revealed two sets of AB doublets, in support of the presence of two isomers in solution, which was further corroborated by the appearance of two resonances in the ^{13}C NMR spectra assignable to the C^{NHC} [241].

Finally, Ni, Pd and Pt complexes with the ligand backbones of type **Xb** [223] and **Xc** [35,253] have been described. They are cited here for the sake of comparison, although the bridgehead donors are not classified as N-heterocyclic carbenes.

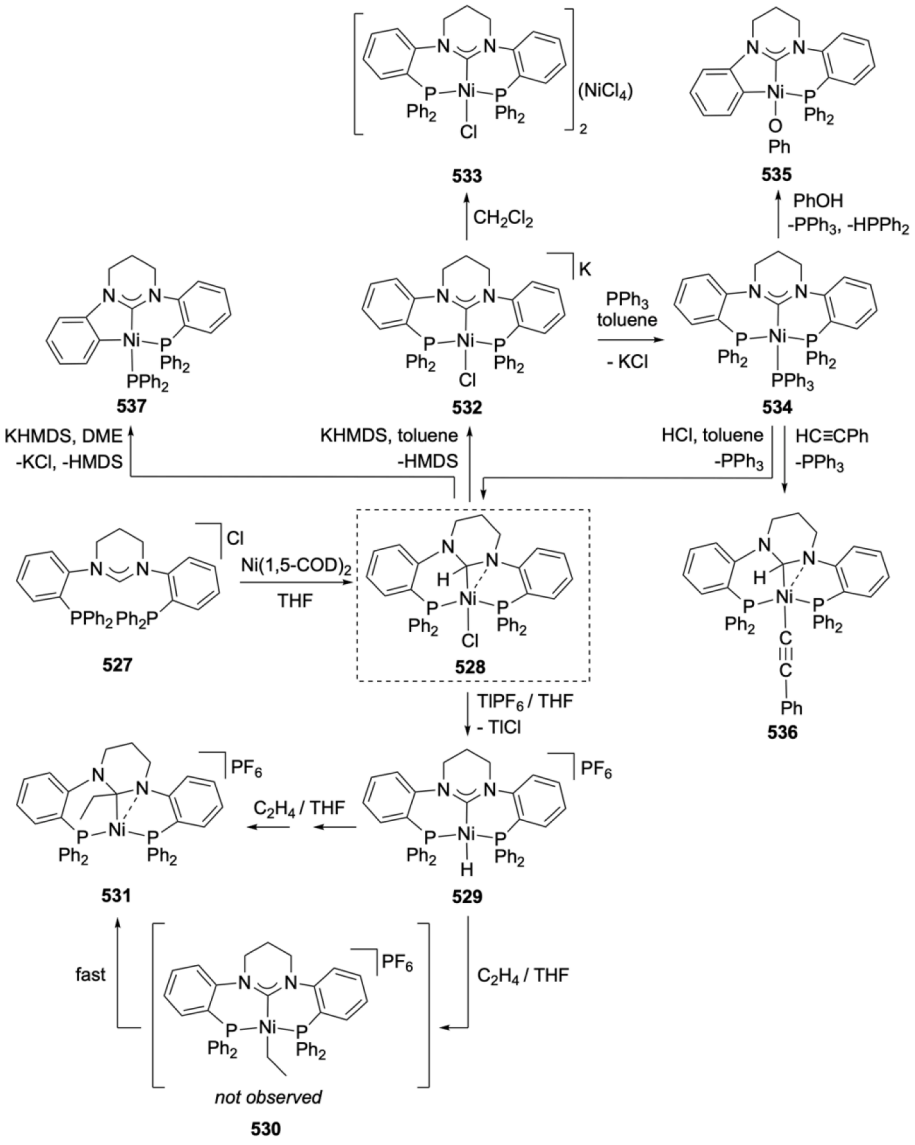

Scheme 113. The rich reactivity of Ni pincer complexes with platform of type **VIIId**

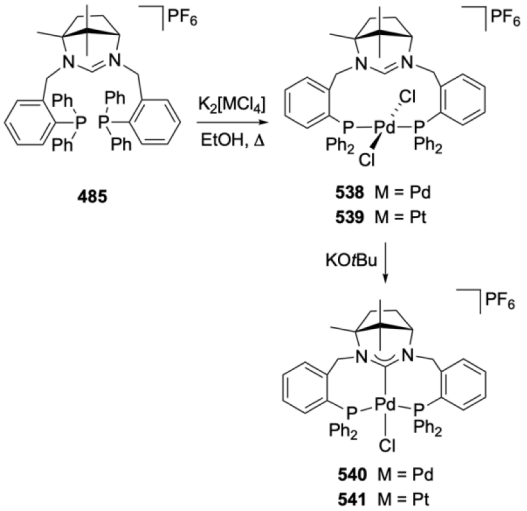

Scheme 114. Pd and Pt complexes with the ligand backbone of type **IXa**.

3.10.6. Group 11 metals (Ag, Au)

The only silver complex bearing a P,C^{NHC},P-pincer ligand is complex **542** that was obtained by the treatment of **485** with AgOTf and KO*t*Bu in THF (Scheme 115). Interestingly, the direct reaction of **485** with Ag_2O did not result in the formation of this carbene complex. The structure of **542** was established by X-ray diffraction analysis and NMR spectroscopy [241].

Moreover, Au^{I} and Au^{III} complexes with the ligand backbone of type **Xc** have been described [254].

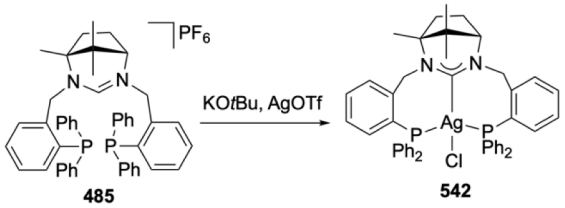

Scheme 115. Ag complex with ligand backbone **IXa**

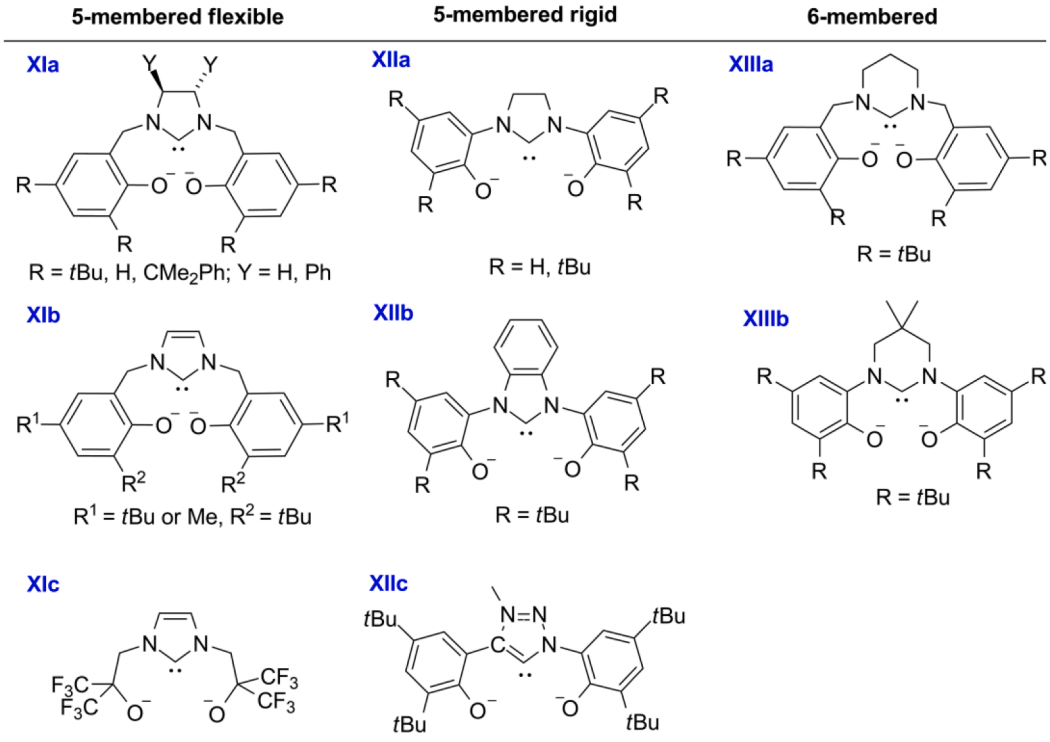

Chart 8. A detailed summary of different type ligand bearing O, C^{NHC}, O backbone

3.11. Type P, C^{NHC}, O

No example with this donor set has been reported to the best of our knowledge.

3.12. Type P, C^{NHC}, S

No example with this donor set has been reported to the best of our knowledge.

3.13. Type O, C^{NHC}, O

The ligand designs of this class are given in Chart 8, with a noticeably reduced ligand diversity compared to the P,C^{NHC},P class, and the dominance of the phenoxide side-arms. Moreover, the occurrence of these ligand designs across the transition metal series is given in Table 4. A comparative summary of selected metrical and spectroscopic data of the complexes with κO,κC^{NHC},κO ligands is given in Table 5 at the end of section 3.13.***

3.13.1. Group 3 and lanthanides (Nd, Y, Sm, La, Er, Yb, Dy)

A family of Ln complexes featuring κO,κC^{NHC},κO-terdentate ligands of types **XIa** (R = *t*Bu, Y = H) and **XIIIa** was obtained by reaction of the precursors **543** and **544** with [Nd{N(SiMe$_3$)$_2$}$_3$(μ-Cl)Li(THF)$_3$] or [Ln{N(SiMe$_3$)$_2$}$_3$] (Ln = Nd, Sm, La, Y) in the presence of KN(SiMe$_3$)$_2$ (Scheme 116A). All complexes were characterized by NMR spectroscopy and/or X-ray diffraction. Interestingly, reactions of [Ln{N(SiMe$_3$)$_2$}$_3$], (Ln = Sm, Y) with **543** and **544** in the absence of external base led to binuclear species with halide and diphenoxide-imidazolinium or -pyrimidinium bridges and no Ln–C^{NHC} bond. The complexes **545**–**551** (backbone **XIIa**) were efficient initiators for the catalytic ring opening polymerization of L-lactide, amongst them **545** being the most active [255,256].

The complexes **549** and **550** containing the six-membered ring NHC ligands (backbone **XIIIa**) were found to be highly active towards the polymerization of *n*-hexyl isocyanate [256]. The polymerization mechanism was investigated, and the reaction was monitored by NMR. The results indicated that the NHC moiety played an important role in the initiation step, in both cases the binuclear diphenoxide-imidazolinium or -pyrimidinium complexes were inactive.

The Dy^{III} complex **553A** with the backbone of type **XIIIb** was obtained by the metalation of the precursor **552A** with [Dy(CH$_2$SiMe$_3$)$_3$(THF)$_2$] under mild conditions (Scheme 116B). Displacement of the coordinated chloride in **553A** was carried out in two steps by the reaction of LiCH$_2$SiMe$_3$ followed by alkanolysis of the coordinated alkyl with (Et$_3$NH)(BPh$_4$) in THF to give the ion pair **553D**. The metal in **553A** and **553D** adopts distorted octahedral geometries with *mer*-pincer coordination and similar Dy–C^{NHC} distances of 2.584(18) and 2.521(9) Å, respectively. Both complexes are rare examples of lanthanide-based single molecule magnets incorporating a NHC-based donor. As a design strategy for new SMMs, the two phenoxides provide axiality and

Table 4
Occurrence of complexes with the ligand architectures **XIa-XIIIb** shown in Chart 8 and described in this section.

Type	R^1/R^2	Y	M
XIa	$R^1 = R^2 =$ *t*Bu, H, CMe_2Ph	H, Ph	Nd, Sm, La, Y, Yb, Er, Ti, Zr
XIb	$R^1 = R^2 =$ *t*Bu, $R^1 =$ *t*Bu, Me; $R^2 =$ *t*Bu		Ti, Zr
XIc			Mo, W, Ni
XIIa			Ti, Zr, Hf, V, Nb, Mn, Fe, Ru, Co, Ir, Ni, Pd, Pt, Al
XIIb			Sc, Zr, V, Mo, Fe, Co, Ni, Pd, Pt
XIIc			Ti, V, Nb, Mo
XIIIa			Nd, Y
XIIIb	*t*Bu		Sc, Dy

*** Additional references dealing with ligands of type **XIIa** and **XIIb** are given at the end of the document in the Note added in proofs.

Table 5
Comparative summary of selected metrical and spectroscopic data of the complexes with κO, κC^{NHC}, κO ligands. Abbreviations used in the Table: O.S. oxidation state; C.G.: coordination geometry' oct.: octahedral; sqpl.: square-planar; td.: tetrahedral; ps: pseudo; trbip.: trigonal-bibyramidal; sqpy.: square-pyramidal.

M	O.S./C.G.	Ligand Class	Complex	*r*(M – C^{NHC}) (Å)	⊳(N-C^{NHC}-N) (°)	δ_C C^{NHC} (ppm)	Ref
La	III/*oct.*	**XIa**	**547**	2.798 and 2.776	107.2 and 106.3	225.27 and 220.26	[256]
Nd	III/*oct.*	**XIa**	**545**	2.724 and 2.707	107.1 and 107.3	–	[255]
			551	2.686	107	–	[255]
Sm	III/*oct.*	**XIb**	**556**	2.610 and 2.606	103.8 and 103.7	–	[259]
			559	2.638 and 2.584	103.2 and 103.6	–	[259]
			560	2.654 and 2.601	103.4 and 103.0	–	[259]
Er	III/*oct.*	**XIb**	**557**	2.504 and 2.525	103.0 and 103.2	–	[259]
Yb	III/*oct.*	**XIb**	**558**	2.492 and 2.515	103.7 and 105.0	–	[259]
Dy	III/*oct.*	**XIIIb**	**553D**	2.584	117.8	–	[257]
			553A	2.521	118.0	–	[257]
Sc	III/*oct.*	**XIIb**	**553C**	2.346	105.5	199.9	[258]
		XIIIb	**553B**	2.415	116.4	214.9	[258]
			553D	2.413	117.1	215.4	[258]
	III/*trbip.*		**554**	2.340	117.6	209.6	[258]
Ti	III/*oct.*	**XIb**	**571**	2.181	100.8	–	[263]
	IV/*trbip.*	**XIb**	**566**	2.187	104.5	188.0	[262]
			567	2.165 and 2.127	105.8 and 106.3	188.1	[263]
			570	2.250	104.0	188.4	[264]
			572	2.177 and 2.194	105.4 and 103.6	185.7	[263]
			573	2.180	103.1	186.0	[263]
			574	2.170	103.2	182.02	[263]
		XIIa	**583**	2.160	109.3	200.0	[266]
			589	2.212	108.5	197.9	[266]
			595	2.212 and 2.222	108.3 and 108.1	199.3	[268]
			596	2.216	106.8	197.9	[55]
			600	2.210 and 2.211	108.4 and 108.7	200.3	[55]
		XIIc	**612**	2.111	103.9	181.8	[269]
	IV/*sqpy.*	**XIb**	**569**	2.207	104.1	185.0	[264]
	IV/*oct.* and *sqpy*	**XIIc**	**610**	2.111 and 2.131	104.9 and 103.8	175.8	[269]
	IV/*oct.*	**XIa**	**580**	2.252	108.5	201.8	[265]
		XIb	**563**	2.200	102.7	164.0	[263]
			568	2.205 and 2.196	104.4 and 104.2	182.4	[264]
		XIIa	**586**	2.185 and 2.179	108.9 and 108.5	197.4	[266]
			587	2.166	108.8	198.6	[266]
			588	2.233 and 2.222	108.7 and 108.5	199.9	[267]
			594	2.231 and 2.210	108.1 and 107.9	199.6	[268]
			593	2.175	110.2	199.6	[268]
			598	2.165 and 2.172	108.7 and 109.2	198.6	[55]
			599	2.149	108.3	197.8	[55]
			602	2.183	108.6	198.4	[55]
Zr	IV/*trbip.*	**XIb**	**629**	2.309	103.8	187.5	[270]
		XIIa	**640**	2.333	108.4	205.8	[273]
		XIIb	**664**	2.336 and 2.334	105.8	199.9	[276]
	IV/*oct.*	**XIa**	**616**	2.417	108.2	209.2	[265]
			618	2.419	108.6	209.3	[265]
			620	2.401	107.9	206.2	[265]
			621	2.411	108.1	214.5	[265]
			619	2.397 and 2.402	109.0 and 108.6	212.9	[265]
		XIb	**627**	2.35	103.6	183.5	[270]
			628	2.382 and 2.380	103.6 and 103.8	185.5	[270]
			633	2.415	102.9	188.3	[272]
			659	2.352 and 2.350	104.6 and 104.4	186.3	[275]
		XIIa	**634**	2.358 and 2.353	108.9 and 108.7	197.0	[50]
			651	2.379 and 2.387	107.9 and 109.0	200.8	[52]
			637	2.398	108.8	204.0	[275]
		XIIb	**665**	2.301	106.6	196.0	[276]
			667	2.324	106.2	199.6	[276]
			660	2.393 and 2.401	105.9 and 106.8	198.0	[275]
			663	2.400	105.3	199.9	[275]

(*continued on next page*)

Table 5 (*continued*)

M	O.S./C.G.	Ligand Class	Complex	r(M – C^{NHC}) (Å)	⊳(N-C^{NHC}-N) (°)	δ_C C^{NHC} (ppm)	Ref
Hf	IV/*trbip*.	**XIIa**	**641**	2.308	108.5	212.6	[273]
	IV/*oct*.	**XIa**	**624**	2.369	108.0	216.9	[265]
		XIIa	**638**	2.333	108.8	204.4	[274]
			635	2.333(6)	108.5	200.5	[273]
			639	2.336(4)	108.1	202.2	[274]
			645	2.356 and 2.350	108.8 and 108.2	206.1	[267]
V	IV/*sqpy*	**XIIb**	**674**	2.153	107.2	–	[280]
		XIIc	**682**	2.070	103.6	–	[281]
	V/*sqpy*	**XIIa**	**672**	2.095	109.0	–	[280]
			676	2.092	109.6	–	[280]
			679	2.128 and 2.132	108.6 and 109.0	–	[280]
		XIIb	**673**	2.132	106.9	–	[280]
		XIIc	**683**	2.067	103.7	–	[281]
			681	2.054	103.8	–	[281]
			689	2.048	103.8	–	[281]
			690	2.049 and 2.064	104.1 and 103.5	–	[281]
			685	2.083	103.7	–	[281]
Nb	V/*oct*.	**XIIc**	**691**	2.196	103.9	–	[269]
Mo	VI/*trbip*.	**XIIb**	**700**	2.193	109.0	191.6	[289]
			704	2.171	106.7	183.1	[289]
	VI/*sqpy*.	**XIIc**	**710**	2.204	103.7	169.9	[269]
		XIIb	**703**	2.267	106.6	199.3	[289]
	VI/*oct*.	**XIIb**	**702**	2.203	107.5	191.1	[289]
			706	2.186	107.6	–	[289]
			705	2.160	106.8	–	[289]
W	VI/*oct*.	**XIIc**	**699**	2.182 and 2.141	104.2 and 104.7	–	[288]
Mn	III/*sqpy*.	**XIIa**	**711**	2.00(1)	109.8(7)	–	[278]
Fe	II/*sqpl*.	**XIIb**	**712**	1.923	106.2	–	[291]
	III/*oct*.	**XIIb**	**713**	1.907 and 1.910	107.0 and 107.6	–	[291]
			714	1.894 and 1.898	107.8 and 107.5	–	[291]
	IV/*oct*.	**XIIb**	**715**	1.936 and 1.950	108.5 and 108.6	–	[291]
			716	1.955 and 1.957	108.5 and 109.2	–	[291]
			717	1.927 and 1.928	107.6 and 107.4	–	[291]
Co	II/*sqpl*.	**XIIa**	**725**	1.811	107.9	–	[293]
			729	1.849	109.7	–	[293]
			722	1.789 and 1.791	108.2 and 108.0	–	[293]
			726	1.830	105.3	–	[293]
		XIIb	**727**	1.81	107.3	–	[293]
	II/*oc.t*	**XIIa**	**730**	1.841	109.2	–	[293]
	III/*sqpy*.	**XIIa**	**732**	1.832	109.6	–	[298]
	III/*oct*.	**XIIa**	**731**	1.843	110.1	–	[298]
Ir	III/*oct*.	**XIIa**	**739**	1.969	109.1	–	[299]
			741	1.944 and 1.944	109.0 and 108.4	–	[299]
Ni	II/*sqpl*.	**XIc**	**743**	1.856 and 1.853	105.1 and 105.2	149.9	[300]
			744	1.880	104.4	148.3	[300]
		XIIa	**747**	1.825	107.0	146.8	[301]
Pt	II/*sqpl*	**XIa**	**755**	1.948	107.2	149.9	[301]
Al	III/*trbip*.	**XIIa**	**757**	2.032	109.0	186.5	[306]
	III/*sqpy*.		**759**	2.037	109.5	–	[306]
	III/trig. monopyram.		**761**	1.970	110.7	–	[306]

slow relaxation while the soft NHC donor may moderate the detrimental influence of the equatorial ligands over the axiality. In a similar manner from **552A** and $[Sc(CH_2SiMe_3)_3(THF)_2]$ the Sc^{III} complex **553B** was obtained, in which the geometrical and structural features at the metal center were similar to those in **553A**. Furthermore, facile displacement of the coordinated THF by pyridine led to **553C.** The binuclear alkyl **554** was obtained from **552A** by a combination of deprotonation and alkanolysis reactions. The benzimidazolium precursor **552B** can serve as a starting point for the synthesis of the octahedral scandium complex **553C**. Interestingly, the longest Sc–C^{NHC} bond to the bridgehead atom is observed with the RE-NHC rather than the 5-membered NHC (2.415(2) and 2.346(2) Å, respectively (Scheme 116B) [257,258].

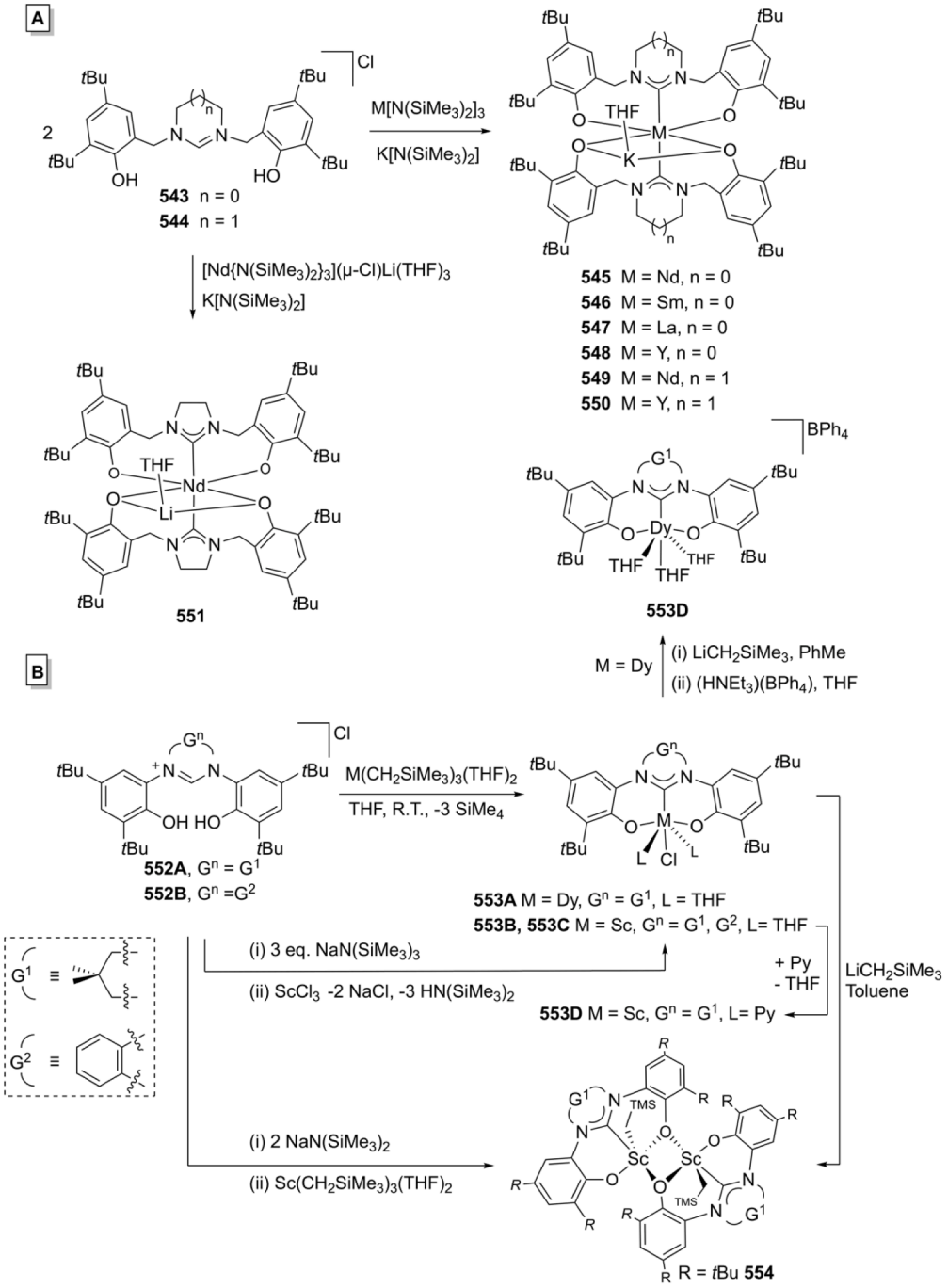

Scheme 116. Syntheses and reactivity of lanthanide complexes with types **XIb** and **XIIIb** backbones.

The anionic lanthanide complexes **556**–**558** with the ligand architecture **XIb** were synthesized by the reaction of precursor **555** with [Li(THF)Ln(N*i*Pr$_2$)$_4$] (Ln = Sm, Er, Yb) and *n*BuLi in THF *via* an aminolysis reaction (Scheme 117) [259]. Crystals of the air sensitive, paramagnetic ion-pairs **556**–**558** were obtained from DME/toluene in *ca.* 60% yields, and the structures were confirmed by X-ray diffraction analysis. The coordination geometries around the lanthanide metals can be described as distorted octahedral, with average Ln–C^{NHC} bond distances of 2.608 (7) (for Sm), 2.515(7) (for Er), and 2.504(8) Å (for Yb). These values were consistent with those reported for other NHC-lanthanide complexes [260,261]. Interestingly, crystallization of Sm-related reaction mixture from THF/toluene afforded the 'ate' complex **559** as light-yellow crystals in moderate yield. A related reaction starting from [Sm{N(SiMe$_3$)$_2$}$_3$] and three equivalents of NaHMDS as base (instead of *n*BuLi) afforded, after crystallization from Et$_2$O the 'ate' complex **560** in low yield. The complexes **559** and **560** were characterized by X-ray diffraction analysis revealing similar structures with Sm and Li/Na ions bridged by phenoxide oxygen atoms; the Sm–O bond distances ranged from 2.201(2) to 2.356(2) Å for **559** and from 2.202(2) to 2.336(2) Å for **560**. The Li–O and Na–O bond distances were equal to 1.932(8), 1.927 (8) and 2.342(2), 2.347(3) Å, respectively [259].

3.13.2. Group 4 metals (Ti, Zr, Hf)

Titanium. The titanium complexes **563** [262,263] and **564** [263] with the ligands of type **XIb** were prepared by the reactions of the titanium precursors (TiCl$_4$ or TiBr$_4$) with the ligand **561**, which was generated by deprotonation of the corresponding imidazolium salt with NaHMDS (Scheme 118). The stable complex **563** was characterized by

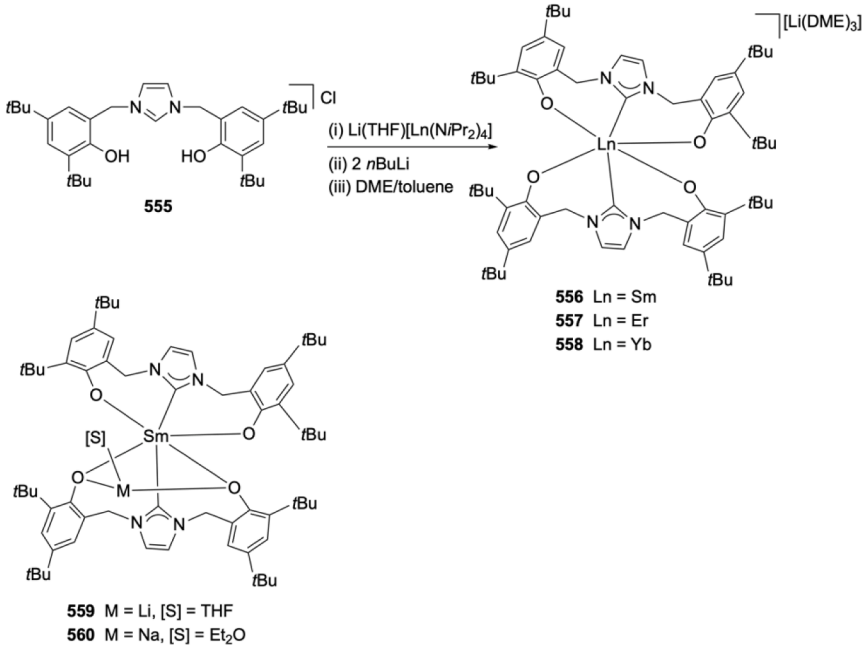

Scheme 117. 'Ato' lanthanide complexes with type **XIb** backbone

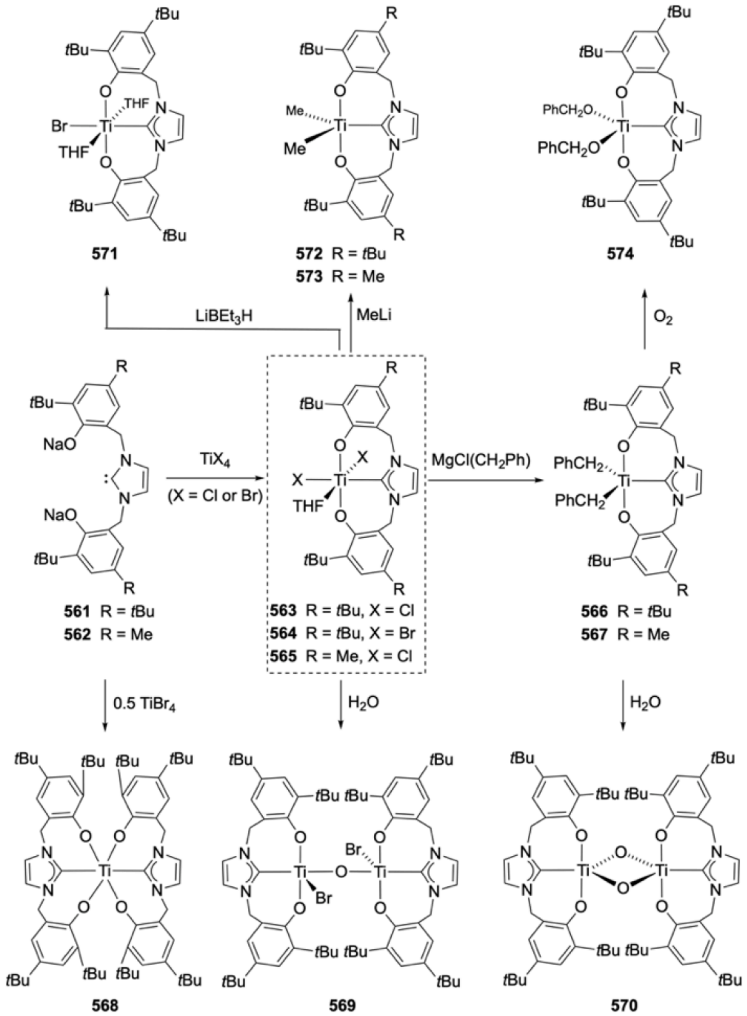

Scheme 118. Synthesis and reactivity of mono- and bi-nuclear Ti complexes with backbone of type **XIb**.

X-ray diffraction analysis and NMR spectroscopy (δ_C C^{NHC} at 164.0 ppm). The X-ray structure confirmed six coordinate geometry with one additional THF ligand to the Ti center. However, NMR experiments revealed a rapid exchange between free and coordinated THF molecules. The analogous complex **564** was characterized by NMR spectroscopy only (δ_C C^{NHC} at 164.8 ppm), but poor crystal quality precluded structural determination. Similarly, **565** was formed by treatment of ligand **562** with $TiCl_4$ in 86 % yield [263].

The complexes **566** and **567** were formed by the substitution reactions of halides in the complexes **563**, **564** and **565** with CH_2Ph using [$MgCl(CH_2Ph)$] (Scheme 118) [263]. They were characterized by NMR spectroscopy (C^{NHC} signal from δ_C 164.0 to δ_C 188.3 ppm) and X-ray diffraction analysis. Interestingly, the Ti–O bond distances in **566** (1.870 (2) and 1.874(2) Å) were longer than in **563** (1.845(6) and 1.850(6) Å), the structure of **567** was similar to that of **566**. The dinuclear complexes **569** and **570** were obtained by controlled hydrolysis of **564** and **566** [262,263]. In **569**, the C^{NHC} appeared in δ_C 185.0 ppm. The structures of **569** and **570** were determined by X-ray diffraction and revealed Ti–C^{NHC} bond distances of 2.208(5) and 2.250(5) Å, respectively. Notably, the Ti–C^{NHC} distance in **570** was longer than that in other titanium complexes owing to the μ-O ligands of the Ti_2O core, binding stronger to the Ti centers.

Reaction of **561** with [$TiBr_4$] in a 2:1 ratio resulted in the formation of the octahedral Ti^{IV} complex **568** of ligand-to-metal stoichiometry 2:1 (Scheme 118) [264]. The complex was characterized by NMR spectroscopy (C^{NHC} signal from δ_C 182.4 ppm) and X-ray diffraction analysis (Ti–C^{NHC} bond distances of 2.2053(9) and 2.196(4) Å). Interestingly, exposure of **566** to O_2 led to the formation of **574** (C^{NHC} signal from δ_C at 182.0 ppm and Ti–C^{NHC} bond distance of 2.170(8) Å) [263]. Treatment of **564** with 1 equivalent of $LiBEt_3H$ afforded the unique paramagnetic Ti^{III} complex **571** [263]. Its structure was determined by X-ray diffraction, revealing a Ti–C^{NHC} bond distance of 2.181(1) Å. Furthermore, the complexes **572** and **573** were formed by the reactions of the complexes **564** and **565** with MeLi, and their nature was confirmed by NMR spectroscopy and X-ray diffraction analysis (Scheme 118) [263]. Complexes **563**–**565** and **569**–**571** showed catalytic activities in ethylene polymerization [262–264]. The complex **563** [263] exhibited the best results with an activity of 290 kg $mol_{Ti}^{-1}\cdot h^{-1}\cdot bar^{-1}$ in the presence of MMAO.

The three titanium NHC complexes **578**–**580** with the pincer ligand of type **XIa** (Y = Ph) and a chair conformation were obtained by the reactions of precursors **575**–**577** with [$Ti(NMe_2)_4$] in THF (Scheme 119) [265]. In the FT-IR spectra of complexes **578**–**580**, the disappearance of the characteristic O–H and C=N stretching vibrations present in **575**–**577** at 3420 and 1640 cm^{-1}, respectively, supported the formation of the complexes. The diamagnetic **578**–**580** were characterized by NMR and IR spectroscopic techniques [265]. The structure of **580** unveiled a distorted octahedral geometry with Ti–C^{NHC} and average Ti–O bond distances of 2.252(2) and 1.993(2) Å, respectively. The latter showed poor to medium catalytic activities for the polymerization of *rac*-lactide in the presence of isopropanol, leading to heterotactic-rich polylactides with conversions ranging from 16 to 70% [265].

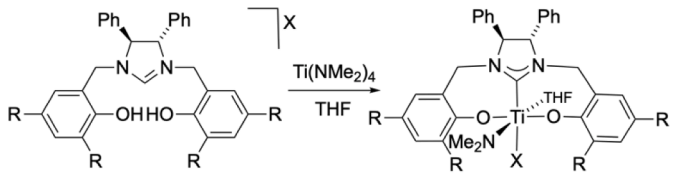

575 X = Br, R = H
576 X = Cl, R = H
577 X = Cl, R = *t*Bu

578 X = Br, R = H
579 X = Cl, R = H
580 X = Cl, R = *t*Bu

Scheme 119. Synthesis by aminolysis of Ti complexes with backbone of type **XIa**

The large family of the Ti^{IV} complexes [Ti^{IV}(κO,κC^{NHC},κO)(X)(X')], featuring the rigid O,C^{NHC},O ligand of motif **XIIa**, and their derivatives arising from a variety of anionic X, X' donors, were described (X, X' = halide, pseudohalide, alkoxide, siloxide, acetate and dimethylamide) [52,55,266–268]. In the majority of the examples, the *mer*-(O,C^{NHC},O) pincer donor adopted a stabilizing, spectator role; however, on attempting to prepare benzyl species (*i.e.* X = Cl or $PhCH_2$, X' = $PhCH_2$) the C^{NHC} of the coordinated NHC acted as recipient of a formally anionic benzyl group, the former being converted to an anionic C_{sp3} bound imidazolide functionality (*vide infra*). The complexes **583**, **585**–**587**, **590** or **591** of 1:1 ligand-to-metal stoichiometry and κO,κC^{NHC},κO coordination, were synthesized following an alcoholysis or aminolysis protocol from the precursor **581** with [$TiCl(OiPr)_3$], [$Ti(OiPr)_4$], [$Ti(NMe_2)_4$] in CH_2Cl_2 and THF, or **582** with [$Ti(OiPr)_4$], thus, the five-coordinate **583** and **585**, or the six-coordinate THF adducts **586**, **587**, **588** and **590**, respectively, were obtained (Scheme 120) [266,267]. It is pertinent to notice that the use of non-coordinating CH_2Cl_2 as reaction medium avoided the formation of six coordinate adducts. Thus, treatment of **581** with 1 equivalent of [$Ti(OiPr)_4$] in CH_2Cl_2 at room temperature led to the quantitative formation of **585**, however, the reaction of **581** with 1 equivalent of [$TiCl(OiPr)_3$] in CH_2Cl_2 afforded a mixture of complexes **583** and **584** in a 1:2 ratio, as evidenced in the ^1H NMR spectrum by the characteristic resonance due to the C*H*-imidazolinium at δ 8.74 ppm; complete conversion to **583** occurred by heating of the reaction mixture in toluene at 90 °C overnight. Finally, employing salt elimination reactions for the introduction of the O,C^{NHC},O pincer starting from **581** and 0.5 or 1 equivalent of [$TiCl_4(THF)_2$] in THF or [$TiCl_4$] in CH_2Cl_2 in the presence of NEt_3, resulted in the formation of the complex **591** of ligand-to-Ti stoichiometry 2:1 and octahedral coordination geometry.

Complex **588** lost coordinated THF under vacuum, converting to the five-coordinate, moderately stable **592** which is structurally analogous to **585**. Interestingly, dissolution of **592** in acetonitrile resulted in the formation of the MeCN adduct **593**, in a process that can be reverted under vacuum, the five-coordinate **592** in solution easily transforms to the dinuclear **594** (see also below) (Scheme 121).

The synthesis of derivatives from [Ti^{IV}(κO, κC^{NHC}, κO)(X)(X')] (X, X' = Cl, O*i*Pr) succeeded by substitution of one or two chlorides from **583**, **587** and **592** or one or two O*i*Pr from **589**, respectively (Scheme 122) [55,266–268]. Reaction of **583** with 2 equivalents of LiOBn in toluene afforded the bis-benzyloxide pincer complex **596**. Introducing the bulkier and electron-withdrawing $OSitBu_3$ ligand was achieved by reaction of the silanol $Si(OH)(OtBu)_3$ with **583** or **589** under elimination of HCl or *i*PrOH, respectively. The complex **597** was quantitatively obtained by treatment of complex **583** with one equivalent of the silanol $Si(OH)(OtBu)_3$ in the presence of NEt_3 in toluene; it was crystallized from THF as the adduct **598**. Similarly, the reaction of complex **589** with $Si(OH)(OtBu)_3$ afforded complex **600**. However, addition of a second $OSi(OtBu)_3$ donor to complex **597** or **600** failed for steric reasons. Displacement of Cl ligand in **587** and **592** by salt metathetical reactions, with LiO*i*Pr and LiOAr' (Ar' = 2,6-tBu_2-4-MeC_6H_2) reagents, afforded the mononuclear derivatives **589** and **595**, respectively. This is to be contrasted to an analogous reaction with the less bulky partners **592** and LiO*i*Pr (1:1 ratio) that afforded the non-symmetrical binuclear **594** featuring two octahedral Ti centers linked by one bridging O*i*Pr and one bridging phenoxide, the latter originating from one of the pincer sidearms.

Finally, complex **599** was formed by the reaction of **583** with 2.1 equivalents of NaOAc in dichloromethane and adopts a rare, seven-coordinate structure with two κ,κ-O,O-acetates and the Ti–C^{NHC} bond distance of 2.148(4) Å (Scheme 122). Elimination of Me_3Si-O*i*Pr in a reaction of **589** with excess of Me_3SiN_3 afforded the mononuclear bis-azide complex **601** characterized spectroscopically ($\nu_{asym}(N_3)$ from 2120 to 2055 cm^{-1} and $\nu_{sym}(N_3)$ 1361 and 1326 cm^{-1}) and crystallographically as THF adduct **602**. Treatment of complex **601** with five equivalents of DMAD in dichloromethane yielded complex **603** after a

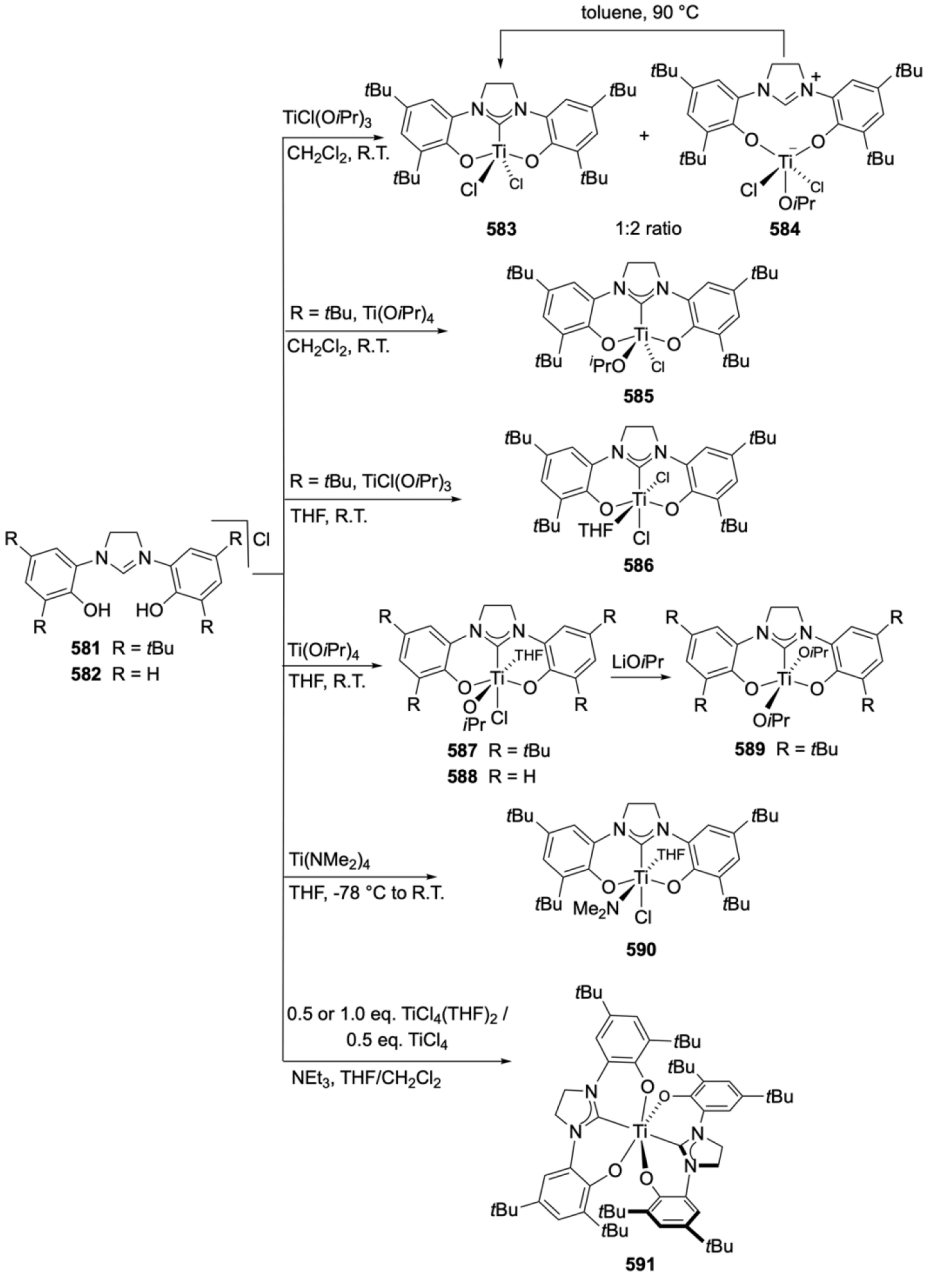

Scheme 120. The synthesis of Ti complexes with pincer ligands of backbone of type **XIIa** by $HNMe_2$, HOiPr elimination or salt metathesis

[3 + 2] cycloaddition with the coordinated azide, along with an impurity (10 %). The ^{1}H NMR spectrum of **603** comprised a resonance at δ 4.12 ppm assignable to the OCH_3 group of a substituted triazolato ligand (the cycloaddition product) and a characteristic singlet at δ 4.73 ppm assignable to the NCH_2 of the imidazolin-ylidene backbone, indicating that **603** may adopt a C_{2v}-symmetric structure in solution. However, single crystals of complex **603** could not be obtained, whereas the aforementioned impurity **604** crystallized and was characterized as the oxo-bridged binuclear complex with two distorted-octahedral titanium centers, each featuring one *mer*-pincer donor. In contrast to the successful isolation of the Ti^{III} complex **571** based on the pincer **XIb** (*vide supra*), attempts to access Ti^{III} complexes with **XIIa** by selective reductions of **583** with a variety of reagents failed.

All Ti^{IV} pincer complexes were evaluated as precatalysts for the copolymerization of cyclohexene oxide with CO_2. Upon addition of [PPN]X cocatalysts (with X = Cl, N_3), all complexes were active at low CO_2 pressure (<0.5 bar) and were highly selective (>99 %) toward the formation of atactic poly(cyclohexene oxide-*alt*-carbonate) [55].

The titanium complexes **605**–**607** [52] were obtained in attempts to prepare Ti alkyls stabilized by the O,C^{NHC},O pincer of type **XIIa** (R = *t*Bu) (Scheme 123), following an alkanolysis methodology. Reaction of the precursor **581** with [Ti(CH_2Ph)$_4$] in toluene resulted in the formation of the dinuclear **605**, which was characterized by 1D and 2D NMR spectroscopy showing the N$\underline{C}$(CH_2Ph)N at δ_C 111.6 ppm and the N$\underline{C}$($\underline{C}H_2$Ph)N at δ_C 29.6 ppm. The observed reaction outcome under these conditions should be contrasted with the results obtained with [M(CH_2Ph)$_4$] (M = Zr, Hf) (*vide infra*). Moreover, the treatment of **581** with [Ti(CH_2Ph)$_4$] in the coordinating solvent THF formed quantitatively complex **606** that was characterized by NMR spectroscopy and X-ray diffraction: in the ^{13}C NMR spectrum, the characteristic resonance for the sp^3 N$\underline{C}$(CH_2Ph)N appeared at δ 110.6 ppm; in the molecular structure the distance of the *sp*^{3} pyramidalized C atom from the Ti center was at 2.026(2) Å. Treatment of complex **586** with 2 equivalents of [MgBr(CH_2Ph)] in THF gave complex **607**, displaying a ^{13}C NMR spectrum

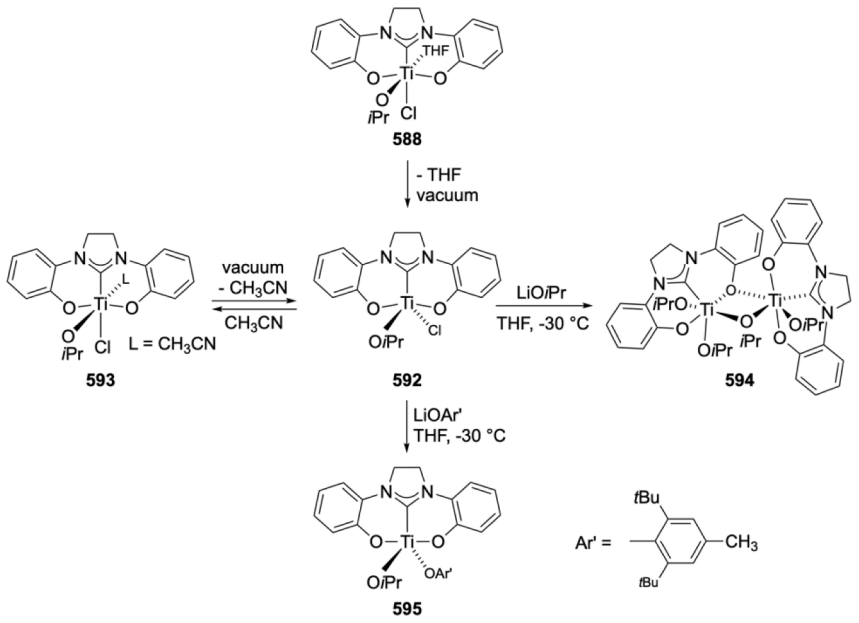

Scheme 121. Substitution reactions of Ti complexes containing a pincer ligand of type **XIIa** (R = H).

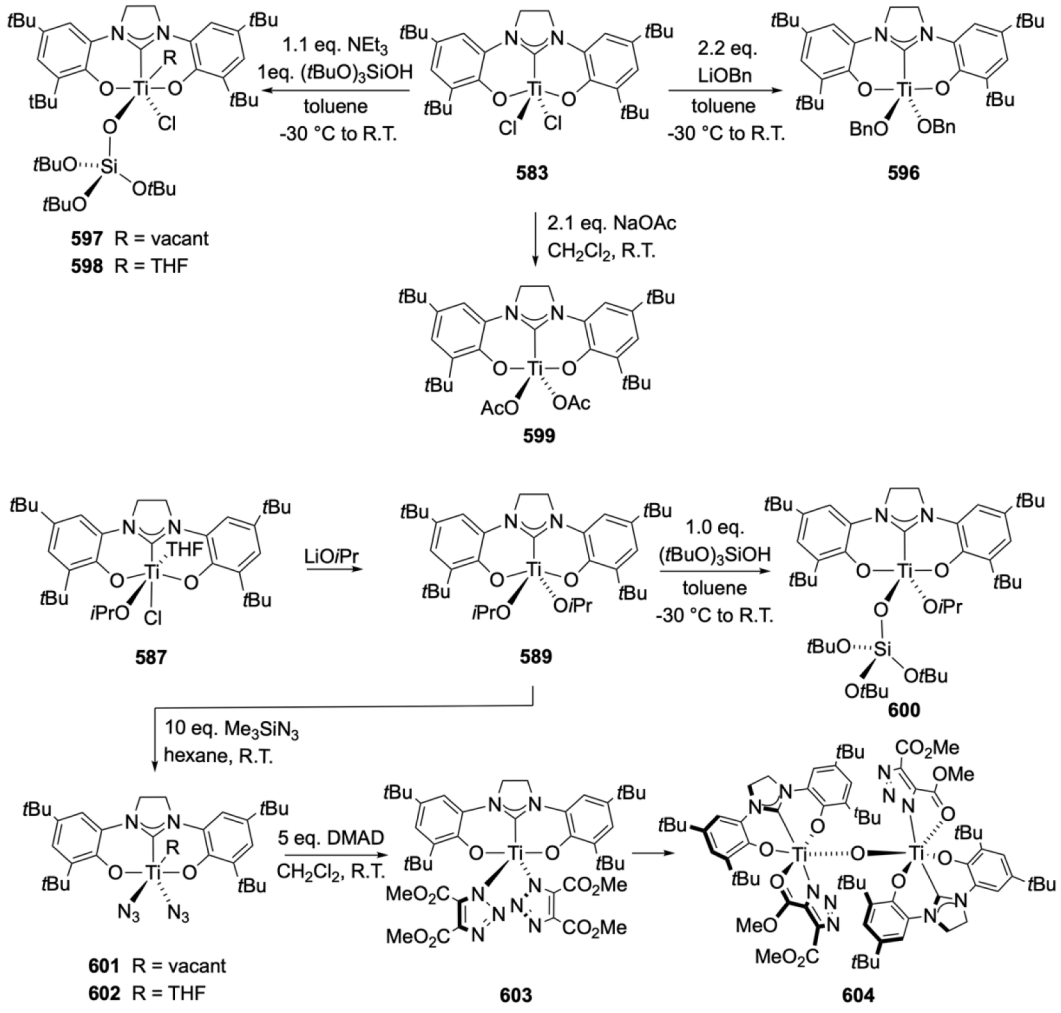

Scheme 122. Diverse reactivity of Ti complexes with pincer ligand of type **XIIa** (R = *t*Bu, H) as spectator ligand.

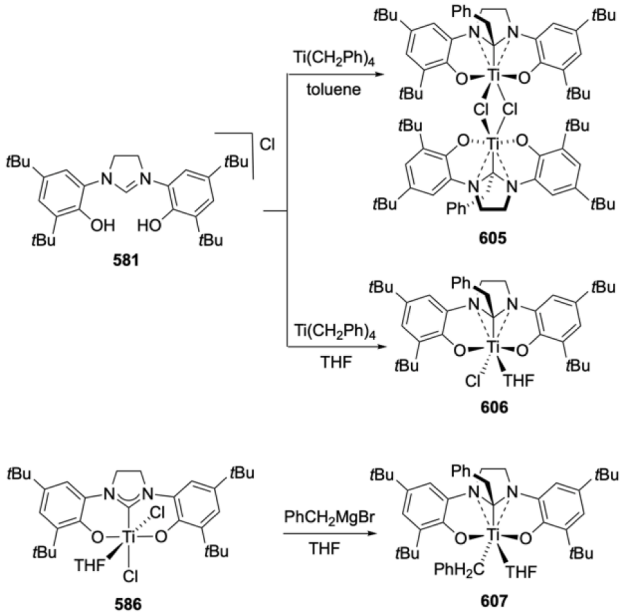

Scheme 123. Benzyl group migration to C^{NHC} in Ti complexes with pincer of type **XIIa** (R = tBu).

with signals due to N*C*(CH$_2$Ph)N and Ti–*C*H$_2$Ph at δ 109.6 ppm and δ 58.8 ppm, respectively, and no evidence of a downfield C^{NHC} signal. By comparison with the analogous Zr and Hf complexes described below and computational studies, it has been proposed that the presence of donor THF critically facilitated the formation of **606** *via* the seven-coordinate species [Ti(κO,κC^{NHC},κO)(CH$_2$Ph)Cl(THF)$_2$], featuring Ti–C^{NHC} coordination and *cis*-arrangement of Ti–benzyl and Ti–C^{NHC} bonds; the latter rearranged to the observed products by intramolecular Ti to C^{NHC} migration of the benzyl group; however, the mechanism of formation of **605** (*viz.* in the absence of THF) may be different.

The triazole-derived mesoionic carbene pincer titanium complexes **609**–**613** of type **XIIc** were prepared by the reaction of precursor **608** with [TiCl(O*i*Pr)$_3$] in dichloromethane (Scheme 124) [269]. Initial efforts along the lines of an alcoholysis protocol afforded complex **609**, which from crystallographic and spectroscopic evidence was assigned a zwitterionic structure featuring a protonated triazolium bridging the two aryloxides. The presence of the triazolium proton was also evidenced by the characteristic ^{1}H NMR low-field signal at δ 9.45 ppm and the ^{13}C NMR spectrum lacking a signal above δ 165 ppm. Upon addition of strong bases such as KHMDS to a solution of **609** in ether, formation of the five-coordinate complex **613** was established by ^{1}H NMR spectroscopy. Treatment of **608** with NEt$_3$, followed by addition of [TiCl$_2$(N*t*Bu)Py$_3$] yielded a mixture of complex **610**, as a minor byproduct, and complex **611**, as major product. **610** could be purified by fractional crystallization of the crude mixture from diethyl ether at room temperature, and it was characterized by X-ray diffraction analysis and NMR spectroscopy, as a binuclear species with a non-symmetrical oxo bridge, one square-pyramidal five- and one octahedral six-coordinate Ti center. Therefore, **610** could be described as an anionic Ti^{IV}=O fragment coordinated to a cationic Ti^{IV}–Cl, both Ti centers being stabilized by the **VIIc** type pincer. The main product **611** could also be prepared independently by the reaction of [TiCl$_4$(THF)$_2$] with **608** at low temperature in the presence of NEt$_3$. All NMR data were consistent with the structure of the distorted octahedral complex **611** of ligand-to-Ti stoichiometry of 2:1, shown in the Scheme 124. Reaction of **608** with [TiCl$_2$(N*t*Bu)Py$_3$] in the presence of LDA cleanly generated the complex **612**, which was isolated as a yellow solid in 54 % yield. Its ^{13}C NMR spectrum contained a typical resonance corresponding to the triazolylidene-5C carbene carbon at δ 181.8 ppm. The X-ray structure revealed the Ti–C^{NHC} bond distance of 2.112(5) Å, which was found to be the shortest Ti–C^{NHC} bond reported so far, which may be due to the good σ-donor aptitude of the mesoionic NHC, reinforced by the weak *trans* influence of the pyridine and the chelate effect of the pincer (Scheme 124) [269].

Zirconium and Hafnium. Many systems with the ligands O,C^{NHC},C discussed in the Ti section find counterparts and similarities with the heavier congeners Zr and Hf, despite expected differences in the stability of individual complexes arising from the different bond strengths of the donors with the heavier 4d and 5d metals.

A family of chiral zirconium and hafnium complexes **615**–**621** and **622**–**624** with the pincer ligand of architecture **XIa** was obtained by the treatment of the chiral imidazolinium **575**–**577** and **614** based on the (*S*, *S*)-diphenyl-1,2-ethanediamine with one equivalent of [M(NR$_2$)$_4$] (M = Zr, Hf) in THF and recrystallization from benzene (Scheme 125) [265]. They were characterized by NMR spectroscopy (supporting a C_2-symmetric structure) or X-ray diffraction adopting distorted octahedral geometries featuring M−C^{NHC} distances of 2.397(4) Å to 2.419(2) Å for Zr, and 2.370(3) Å for Hf all in the typical range for a M−C σ-bond. These complexes acted as precatalysts the polymerization of *rac*-lactide in the presence of isopropanol, leading to the heterotactic-rich polylactides, the activities depended by the size of the metal (both Zr and Hf performing well) and the solvents, best results were obtained in toluene rather than in polar THF (Scheme 125).

A class of Zr and Hf complexes with the pincer ligand of architecture **XIb** have been prepared and studied for their catalytic performance as polymerization or copolymerization catalysts [270–272]. Reaction of the precursor **625** with NaHMDS led to the formation of the sodium adduct **561** (Scheme 126), which was then reacted with [ZrCl$_4$(THF)$_2$] to afford a mixture of mono- and bis-NHC Zr^{IV} complexes **627** and **628** which could be separated based on their different solubilities in organic solvents and isolated in 20 and 38 % yields, respectively [270]. The complex **628** was also formed in good yield (*ca.* 85 %) by treatment of **561** with [ZrCl$_4$(THF)$_2$] in a 2:1 ratio. The structures of both complexes were determined by X-ray diffraction, revealing distorted octahedral geometry at Zr in **627** with the aryloxide units of the pincer occupying mutually axial sites, while in **628** the ligands assume an S-shaped conformation and C_2 symmetrical arrangement. The Zr–C^{NHC} bond distances of 2.35(1) Å for **627** and 2.383(3) and 2.380(3) Å for **628** were shorter than those in previously reported Zr complexes. Temperature-dependent experiments with **627** indicated the existence of isomerization equilibrium between C_1 and C_2 symmetric structures in solution. The equilibrium was monitored by ^{13}C NMR spectroscopy, with a C^{NHC} signal at 183.5 ppm, at room temperature, and two C^{NHC} signals at 182.5 and 183.0 ppm, at 243 K. A characteristic ^{13}C NMR C^{NHC} resonance was observed at 185.5 ppm for **628**. The complexes **629** and **630** were formed by the reaction of the complex **627** with 2 equivalents of [MgCl(CH$_2$Ph)] or [LiCH$_2$SiMe$_3$]. Complex **629** could also be obtained by the reaction of the imidazolium salt **625** with [Zr(CH$_2$Ph)$_4$] in 20% yield. The structure of **629** exhibited a Zr–C^{NHC} bond distance of 2.309(3) Å, which was shorter than that in **627** and **628** (Scheme 126) [270].

The yellow complexes **631** and **632** were prepared by the reactions of the imidazolium salts **625**–**626** with [Zr(NMe$_2$)$_4$] in THF, respectively [271]. They were characterized by ^{13}C NMR spectroscopy (δ_C 186.8 ppm and 186.0 ppm for **631** and **632**, respectively). These complexes acted as stoichiometric intramolecular hydroamination catalysts of 2,2-diphenylpent-4-en-1-amine to 2-methyl-4,4-diphenylpyrrolidine, however, they did not perform catalytically [271].

The macrocylic hexanuclear complex **633** was formed by treatment of the mononuclear zirconium complex **627** with NaOSiMe$_3$ and then Na[N^O] in 37 % yield (Scheme 126) [272]. Its structure was determined by X-ray diffraction analysis and NMR spectroscopy with a characteristic carbene signal at 188.3 ppm. Furthermore, the Zr–C^{NHC} bond distance of 2.415(7) Å was longer than that in **627**. Complexes **627** and **633** showed catalytic activities in ethylene polymerization in the presence of MAO, with TON in the range 2300–6700 [C_2H_4]·mol^{-1} Zr·h^{-1} [272].

Various Zr^{IV} and Hf^{IV} complexes with the rigid pincer ligands of type **XIIa** and **XIIb** have been prepared and aspects of their organometallic

and catalytic chemistry, in particular for oligomerization and polymerization reactions, have been studied. The reaction of **581** with *n*BuLi, followed by addition of $[ZrCl_4(THF)_2]$ generated **634** in low yield (*ca.* 20 %) (Scheme 127) [50]. A better synthetic approach to **634** and its Hf analogue **635** was to first react **581** with $[M(OiPr)_4]$ (M = Zr, Hf) in THF to obtain complexes **636** and **638**, both obtained as crude solids and characterized by ^{1}H NMR spectroscopy [273]. Superior yields of **638** can be obtained by performing the metalation at lower temperatures (*ca.* −30 °C) [274]. Subsequently, both **636** and **638** were conveniently converted to **634** and **635** without isolation by *in situ* reaction with Me_3SiCl in toluene under forcing conditions (typically 110 °C, 3 d) and in good yields. Reaction of **635** with (PPN)Cl led to the anionic complex **639** [273]. Complexes **634**, **635** and **639** were characterized spectroscopically and structurally: their NMR spectra comply with an average C_{2v} symmetric structure (*i.e.* broadened singlet due to the imidazolinium backbone protons) and characteristic C^{NHC} signals (at δ 200.5 ppm (Hf)). Their molecular structures revealed distorted octahedral coordination geometries, with a non-planar (due to geometrical constraints) pincer ligand structure in **634**, **635** and a rather short M−C^{NHC} bond distance (2.358(3) Å, 2.333(6) Å and 2.337(4) respectively) [273,274]. Substitution of the Cl in **636** by O*i*Pr was successfully carried out by the reaction with one equivalent of LiO*i*Pr in THF leading to **637**, which features zirconium center in a distorted octahedral environment with Zr–C^{NHC} bond distance of 2.398(3) Å (longer than that in **610** and **608** at 2.360(3) Å and (2.358(3) Å, respectively) due to the increased π-donation from both *cis*- and *trans*-O*i*Pr groups (Scheme 127) [275].

Treatment of the precursor **581** with one equivalent of $[M(CH_2Ph)_4]$ (M = Zr, Hf) followed by addition of one equivalent of $[MgCl(CH_2Ph)]$ in toluene, yielded the complexes **640** and **641**, which were isolated as yellow or off-white solids in good yield, respectively (Scheme 127) [273]. The ^{1}H NMR spectra comprised singlets at *ca.* δ 1.95 ppm which were assigned to CH_2Ph protons, while the corresponding ^{13}C NMR signals of CH_2Ph were at δ 139.1 ppm and 138.0 ppm ($^1J_{CH}$ = 135 Hz). The crystal structures of the complexes revealed a distorted trigonal bipyramidal geometry at the metal, a planar pincer structure, short M−C^{Bn}_{ipso} distances (for Zr: 2.656(2) Å, 2.866(1) Å; for Hf: 2.279(3), 2.261(3) Å) and angles at the benzylic carbon in the range 86-96°, and M−C^{NHC} distances of 2.333(1) Å (Zr) and 2.308(3) Å (Hf), respectively. These metrical data taken together with the information from the ^{13}C NMR spectra, indicated η^2-coordination of the benzyl ligands. Reaction of **640** or **641** with $[HNMe_2Ph][B(C_6F_5)_4]$ in CH_2Cl_2 led to the quantitative formation of complexes **642** and **643**, which were characterized by NMR spectroscopy (C^{NHC} at δ 203.0 ppm, C_{ipso} at δ 131.8 ppm with $^1J_{C\text{-}H}$ = 140 Hz, in support of a η^2-benzyl) and weak coordination of the

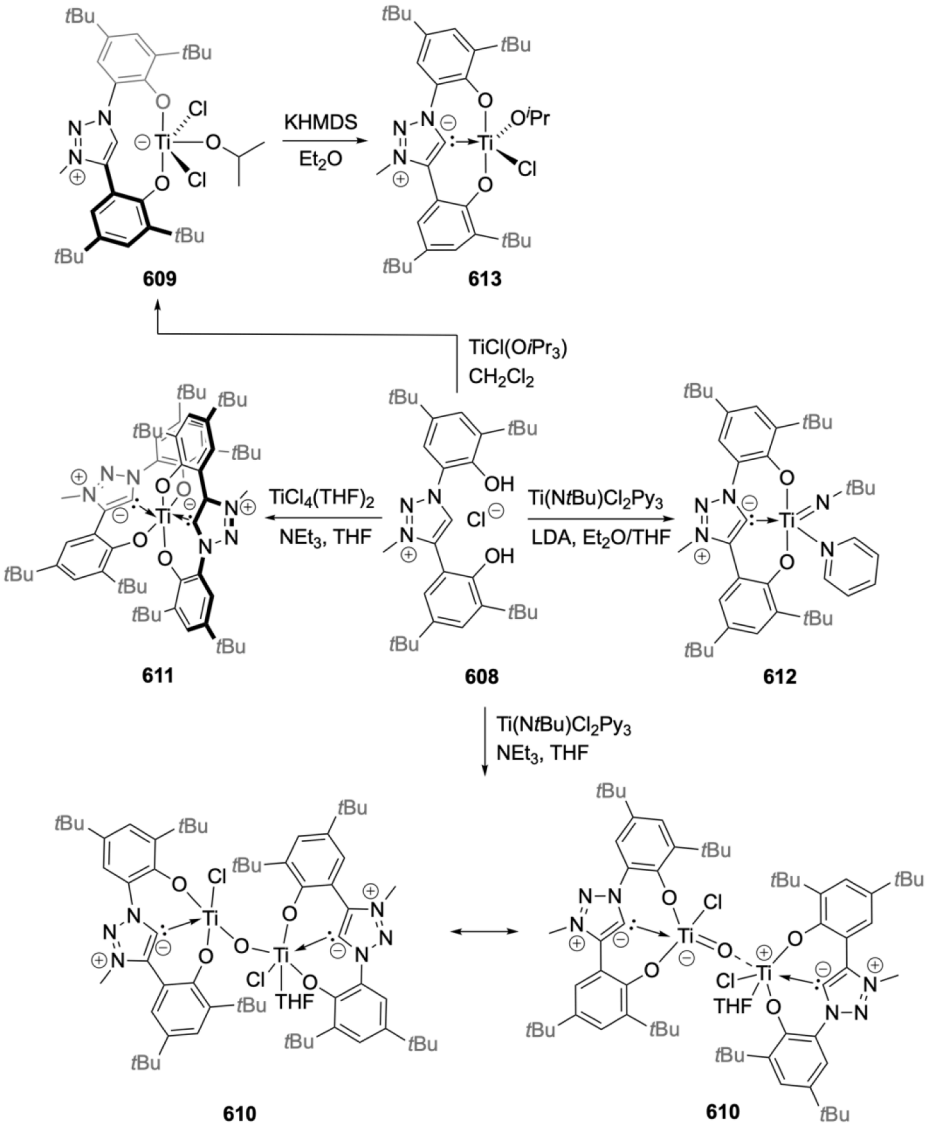

Scheme 124. Titanium complexes with ligand backbone of type **XIIc**.

NMe_2Ph moiety to the metal. Both cations had limited lifetime at room temperature ($t_{1/2}$ *ca.* 30 min) but were stable at −15 °C in CD_2Cl_2 solution.

The complexes **644** and **645** were prepared by the reaction of **581** with 0.5 equivalent of [MCl_4] (M = Zr, Hf) respectively, in the presence of 6 equivalents of NEt_3 (Scheme 127). In the ^{13}C NMR spectra they exhibit characteristic C^{NHC} signals at δ 200.8 ppm and δ 206.1 ppm, respectively. Their molecular structures determined crystallographically unveil distorted octahedral geometries with NHC donors placed mutually *trans*, virtually planar pincer ligands and M−C^{NHC} bond distances at 2.379(2) Å, 2.387(3) (Zr) Å and 2.357(6) Å, 2.351(6) (Hf) Å. Both **644** and **645** can be electrochemically oxidized in up to four one-electron steps (three reversible) and up to three one electron steps (two reversible), respectively, all oxidations are ligand-centered, leading to the formation of radicals. Both **644** and **645** luminesce upon excitation in the LMCT absorption band (at λ = 362 nm) with emissions at 485 and 534 nm (ϕ = 0.08 and 0.12, respectively) (Scheme 127) [267]. Zirconium amido complexes were also reported and the yellow **646** was synthesized in 53 % yield by the reaction of **581** with 1 equivalent of [Zr(NMe_2)$_4$] in THF [273]. In comparison, when the reaction was carried out in a non-coordinating solvent (*e.g.* CH_2Cl_2), complex **647** was the major product [273]. Its ^1H NMR spectrum revealed a signal assignable to the Zr–$HNMe_2$ moiety at δ 1.70 ppm (6H, br, s).

Treatment of **581** with one equivalent of [M(CH_2Ph)$_4$] (M = Zr, Hf) in toluene resulted in the formation of the colorless complexes **648** and **649** in quantitative yield, which were stable in non-coordinating solvents (Scheme 128) [50,52]. In the ^1H and ^{13}C NMR spectra of **648** and **649** characteristic signals were observed at δ 2.89 ppm (Zr), 2.64 ppm (Hf) (PhCH_2) and δ 131.0 ppm (Zr), 131.5 ppm (Hf) (PhCH_2), δ 204.3 ppm (Zr), and 209.1 ppm (Hf) (C^{NHC}), respectively. Upon heating the Zr complex in benzene, it converts to **650**, a dichloride bridged binuclear complex featuring an alkyl (*i.e.* Csp^3-bound) on Zr as outcome of intramolecular migration of the benzyl group to C^{NHC}, the Zr–C bond distance at the two seven-coordinate Zr centers is 2.157(3) Å; surprisingly, the Hf analogue **649** under the same conditions is unreactive. The disparate pathway of the reaction of [Ti(CH_2Ph)$_4$] with **581** has been detailed in the previous section. Upon dissolution in THF, **648** and **649** afforded the complexes **651** and **652**, which can also be synthesized by the reaction of **581** with one equivalent of [M(CH_2Ph)$_4$] in THF. The ^{13}C NMR spectra of **651** and **652** comprised characteristic signals at δ 100.8 ppm and δ 107.5 ppm, respectively, that were assigned to N<u>*C*</u>(CH_2Ph)N. The structure of **651** was confirmed by X-ray diffraction featuring a pyramidalized C atom to Zr and Zr–C bond distance of 2.174 (3) Å. Computational studies showed that the benzyl migration is a strongly synchronous process, where the seven-coordinate THF adduct [Zr(O,C^{NHC},O)(CH_2Ph)Cl(THF)] transformed to the observed **651**.

The related complexes **653** and **654** were formed by addition of THF to **640** and **641** *via* a THF-promoted benzyl migration reaction [52]. The characteristic ^{13}C NMR resonances assigned to the N<u>*C*</u>(CH_2Ph)N were observed at δ 101.9 ppm (Zr) and 109.1 ppm (Hf) and the η^1-CH_2 benzyl as a singlets at δ 49.0 ppm and 53.0 ppm (Scheme 128).

Treatment of **655** with one equivalent of [Zr(O*i*Pr)$_4$·HO*i*Pr] resulted in the formation of a mixture comprising complexes **657** and **659** and **661**, as major and minor components, respectively, that were characterized by NMR spectroscopy (Scheme 129) [275]. In contrast, reaction of **655** with 0.5 equivalent of [Zr(O*i*Pr)$_4$·HO*i*Pr] gave a mixture of the homoleptic **659** and the zwitterionic **661**, as major and minor components, respectively. The inability to observe **657** in the latter case implied its rapid *in situ* consumption due to its reaction with the excess of **655** accompanied by release of HCl and the formation of the homoleptic **659** and the zwitterionic **661** complexes. The Zr–C^{NHC} bond distances in **659** (2.351(5) and 2.350(1) Å) were shorter than that in **644** bearing a saturated *mer*-terdentate NHC ligand [Zr(O*i*Pr)$_4$·HO*i*Pr] in THF only resulted in the formation of a mixture of the homoleptic **660** and the zwitterionic **662** in a 2:1 ratio [275]. Fortunately, single crystals of complexes **660** and **662** suitable for X-ray diffraction were obtained that allowed their structural characterization. In **660**, the zirconium is in a slightly distorted octahedral environment with the Zr–C^{NHC} bond distances of 2.393(3) and 2.401(5) Å, respectively, that are longer than those in other homoleptic complexes. The coordination environment of the Zr center in **662** is distorted trigonal bipyramidal, with the chlorido ligands in apical positions. The formation of complex **663** by the reaction of pure complex **662** with Ag_2O was accompanied by formation of **660**. The disappearance of the C-$H_{benzimidazolium}$ in the ^1H NMR spectrum of **662** was in support of the formation of **663**, moreover, the ^{13}C NMR spectrum of **663** displayed a C^{NHC} signal at δ 199.9 ppm. Both Zr atoms in **663** are in a slightly distorted hexacoordinate environment and are bridged by two hydroxido ligands in the equatorial position. The different metalating aptitude of [Zr(O*i*Pr)$_4$] towards **581**, **655** and **656** has been ascribed to differences in the C–H acidities of the three azolium bridgeheads (Scheme 129) [275].

The catalytic activities of complexes **636**–**637**, **659**–**660** and **662**–**663** in the presence of 1 equivalent of [PPN]Cl, used as an ionic cocatalyst, and **639** were investigated for the copolymerization of cyclohexene oxide and CO_2. The results suggested that complexes **636** and **637** selectively afforded completely alternating polycyclohexene carbonate with TOFs ranging from 26 to 35 h^{-1}. In particular, **639** showed high activity (up to 500 h^{-1}) in the selective alternating copolymerization of epoxides with CO_2 under low pressure. The complexes **659**–**660** and **662**–**663** were found to be inactive for this reaction [274,275].

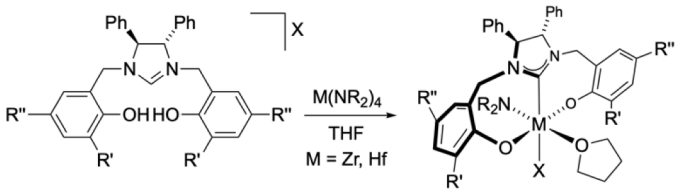

575 X = Br, R' = R'' = H
576 X = Cl, R' = R'' = H
577 X = Cl, R' = R'' = *t*Bu
614 X = Cl, R' = *t*Bu, R'' = H

615 M = Zr, R = Me, X = Br, R' = R'' = H
616 M = Zr, R = Et, X = Br, R' = R'' = H
617 M = Zr, R = Me, X = Cl, R' = R'' = H
618 M = Zr, R = Et; X = Cl, R' = R'' = H
619 M = Zr, R = Me, X = Cl, R' = *t*Bu, R'' = H
620 M = Zr, R = Me, X = Cl, R' = R'' = *t*Bu
621 M = Zr, R = Et, X = C, R' = R'' = *t*Bu
622 M = Hf, R = Me, X = Br, R' = R'' = H
623 M = Hf, R = Me, X = Cl, R' = R'' = H
624 M = Hf, R = Me, X = Cl, R' = R'' = *t*Bu

Scheme 125. Chiral complexes of Zr and Hf with a backbone structure of type **XIa**

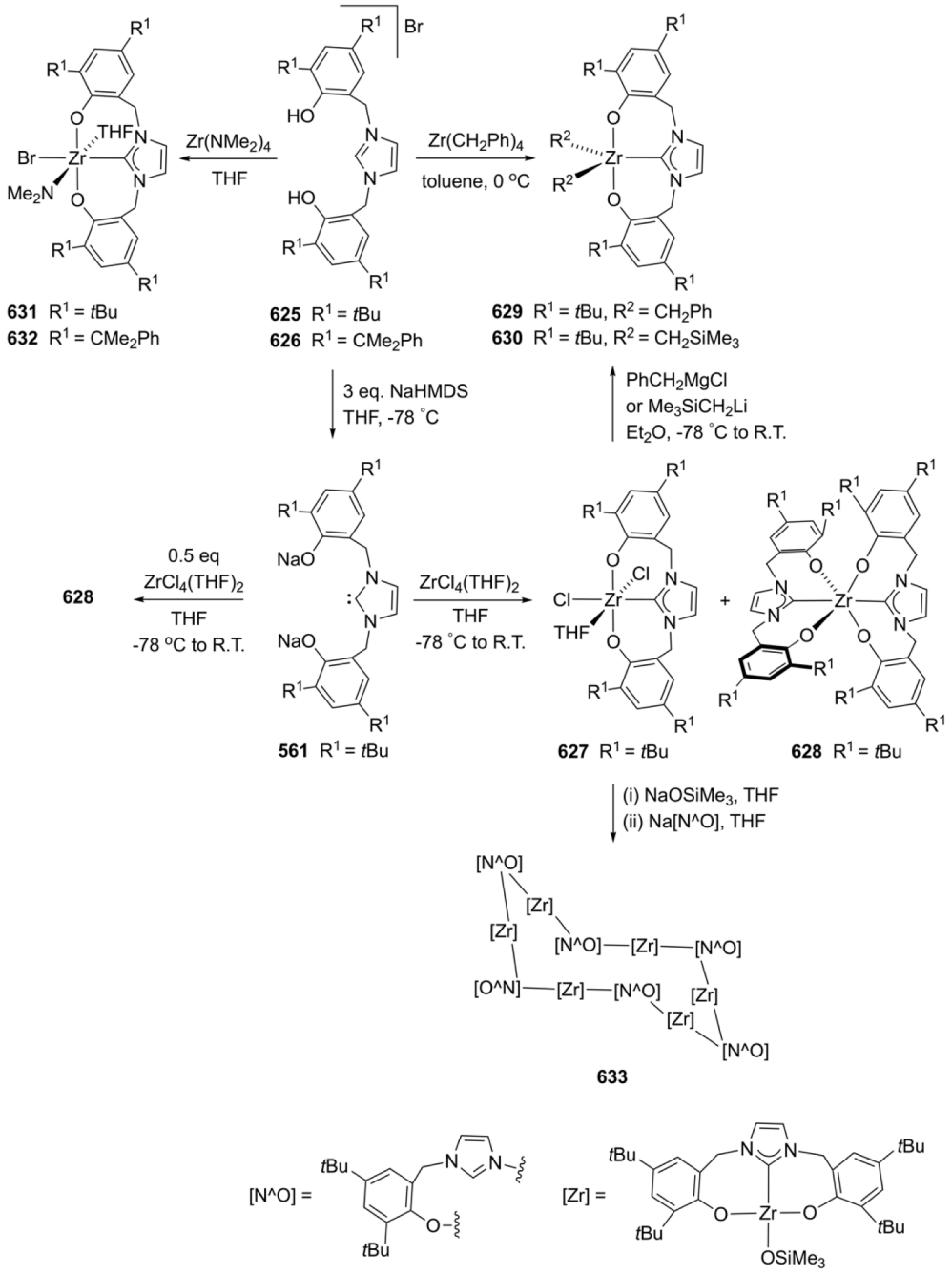

Scheme 126. Zr complexes with ligand backbone of type **XIb**

A family of zirconium complexes bearing O,C^{NHC},O ligands of type **XIIb** has also been described (Scheme 130) [53,276,277]. The complex **664** was prepared by treatment of the pro-ligand **656** with one equivalent of KHMDS, followed by addition of tetrabenzylzirconium at –35 °C, and it was isolated in 88 % yield [276]. The structure of **664** was established by X-ray diffraction analysis and its ^{13}C NMR spectrum showed the Zr–C^{NHC} resonance at δ 199.9 ppm. Reaction of **664** with one equivalent of $[Ph_3C][B(C_6F_5)_4]$ resulted in the formation of **665**, which was characterized by NMR spectroscopy [276]. Crystals of the bis(ether) adduct were obtained by slow diffusion of pentane into a chlorobenzene/ether solution at low temperature and the crystal structure of the adduct **665**·2Et_2O exhibited a distorted octahedral coordination geometry around the zirconium center, with two mutually *cis* ether donors. Reaction of **665** with one and two equivalents of PMe_3 led to **666** and **667**, respectively [276]. Finally, reaction of **664** with one equivalent of $[Ph_3C][B(C_6F_5)_4]$, followed by the addition of one equivalent of 1-hexene afforded the complex **668**, which was characterized by 1D and 2D NMR spectroscopy [277]. The complexes **665** and **666** were active in the polymerization of 1-hexene, but complex **667** was inactive.

Interestingly, the complex **669** was obtained quantitatively by the reaction of **664** with PMe_3 at 50 °C (Scheme 130) [53]. The structure of **663** was determined by NMR and X-ray diffraction. The characteristic ^1H NMR signal of the benzyl methylene protons in NCH(CH_2Ph)N was observed at δ 3.38 ppm. The reaction can be reversed upon treatment of **669** with one equivalent of $[Ni(COD)_2]$ as PMe_3 scavenger to afford **664** and the by-products $[Ni(COD)(PMe_3)_2]$ and $[Ni(PMe_3)_4]$. The complex **670** was obtained upon exposure of complex **664** to an atmosphere of ammonia for 3 h at room temperature and characterized by X-ray diffraction and NMR spectroscopy. However, reaction of **664** with ammonia at −60 °C yielded complex **671**, as confirmed by NMR

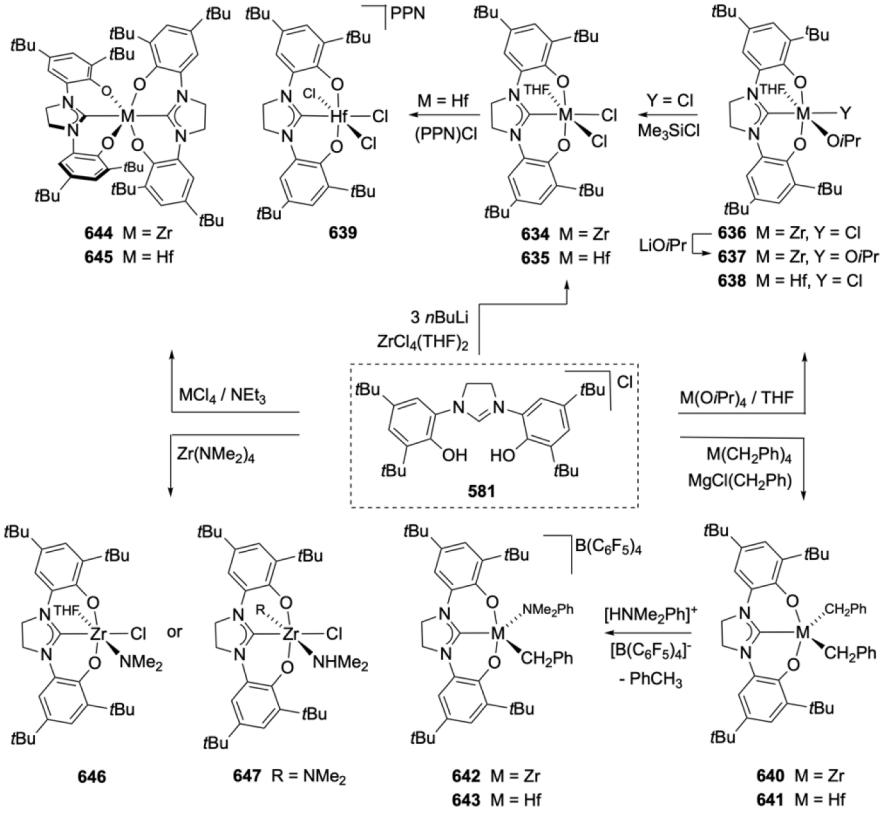

Scheme 127. Synthesis and reactivity of Zr and Hf complexes with ligand backbone of type **XIIa**.

spectroscopy.

3.13.3. Group 5 metals (V, Nb)

A series of vanadium complexes **672**–**680** bearing a κO, κC^{NHC}, κO-terdentate ligand (types **XIIa** and **XIIb**) has been described (Scheme 131) [53,278–281]. Reactions of **581** or **656** with [V(=O)(O*i*Pr)$_3$] in THF afforded the dark orange air-stable **672** and **673** *via* the *i*PrOH elimination. The X-ray structure of the former showed a slightly distorted square-pyramidal geometry at vanadium with V–C^{NHC} bond distance (2.095(3) Å) shorter than that in the other reported V^{V}–NHC

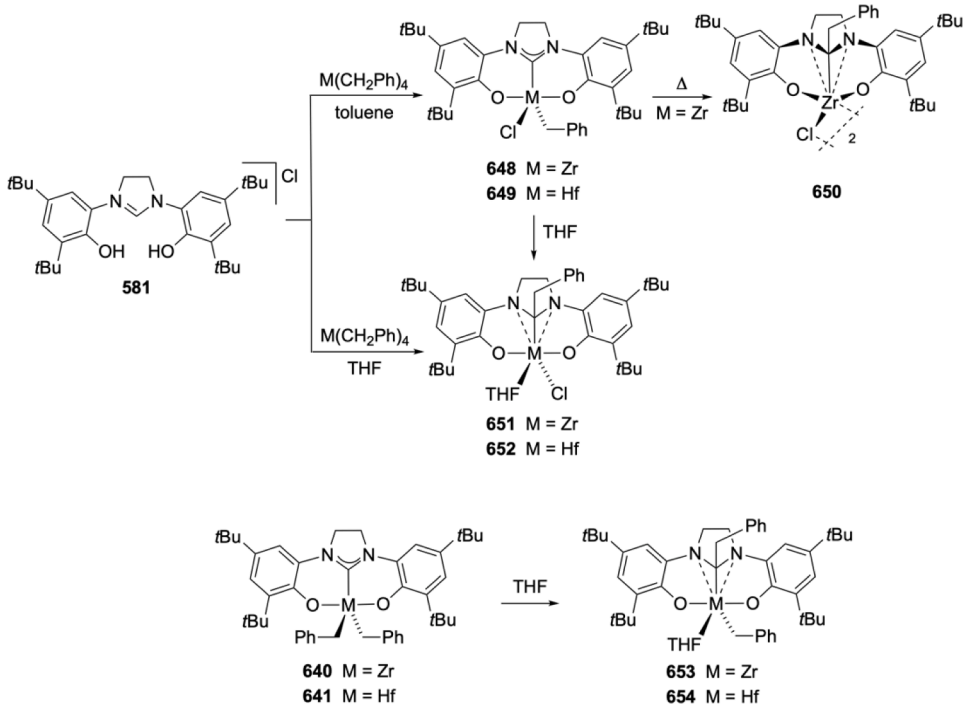

Scheme 128. Migratory reactivity of the benzyl group in Zr and Hf complexes with ligand backbone of type **XIIa**

complexes [282], presumably due to geometrical constraints imposed by the terdentate NHC ligand. The ^{1}H NMR spectrum of the dark green **673** complies with the presence of a C_1 symmetric species in solution, however, in the ^{13}C NMR spectrum signal assignable to C^{NHC} was not observed, presumably due to the quadrupolar nature of the ^{51}V nucleus; in contrast, the ^{51}V-NMR spectrum comprised one signal at δ −503 ppm. The V=O stretching frequencies in the IR, which may be related to the donor ability of the NHC was observed at 1000 cm^{-1}. Furthermore, in the structure of **673** the metal adopts a highly distorted square-pyramidal coordination geometry with the benzannulated heterocycle shifted out of the coordination plane defined by the pincer donors (by *ca.* 16°) and V–C^{NHC} and V=O bond distances of 2.131(3) and 1.585(2) Å, respectively. Complex **673** exhibits a reversible reduction corresponding to the $V^{(V/IV)}$ redox couple at –0.37 V (*vs.* Fc/[Fc]$^{+}$) in CH_2Cl_2. The reduction was successfully carried out chemically using [CoCp*$_2$] as reducing agent, leading to the paramagnetic (1.67 μ_B by Evans' method) **674** which was characterized spectroscopically and crystallographically. The V=O stretching was shifted to 968 cm^{-1}, in agreement with a higher electron density on the metal and increased back-bonding. In addition, **674** exhibits a characteristic eight-line spectrum ($g_{iso} = 1.9666$, $\alpha = 267.7$ MHz), consistent with a single unpaired electron located at the metal (for ^{51}V $I = 7/2$, 99.75 % natural abundance). In the structure of **674** the coordination geometry at the metal is the same as in **673** but the vanadium donor atom distances (*i.e.* V–C^{NHC}, V–O, V=O) increased slightly (by *ca.* 0.1 Å), in view of the larger ionic radius of V^{IV} compared to V^{V}.

The complexes **675**–**677** were obtained by the salt metathesis reaction of complex **672** with the corresponding salts (NaOAc, $NaOAc^{F}$ and LiO*i*Pr) in high yields (Scheme 131). In contrast, **678** could not be prepared by salt metathetical reactions from NaN_3 but by the reaction with Me_3SiN_3 at 80 °C accompanied by Me_3SiCl elimination. The derivative **676** was characterized by X-ray diffraction revealing a V–C^{NHC} bond distance of 2.0922(2) Å. Crystallization of **675**, **677** and **678** afforded **679**, due to adventitious moisture, that was characterized spectroscopically and by X-ray diffraction, adopting an oxo-bridged binuclear structure with distorted square pyramidal geometry around each V center (V–C^{NHC} bond lengths 2.128(2) Å and 2.132(3) Å). Moreover, reaction of the precursor **581** with [V(=NPh)(O*i*Pr)$_3$] resulted in the formation of the mononuclear **680** in quantitative yield, the structure of which was confirmed by NMR spectroscopy. Interestingly, exposure of **680** to CO_2 led to the formation of **672** via a sequence of [2 + 2] cycloaddition and cycloreversion (Scheme 131).

Complexes analogous to **672**–**674** but built on the pincer structure of type **XIIc** provided a suitable platform to compare the impact of the electronic properties of the bridgehead donor on the spectroscopic and structural data (Scheme 132) [281]. The complex **681** was obtained in excellent yields by the reaction of the triazolium salt **608** with [V(=O)(O*i*Pr)$_3$] *via* an alcohol elimination reaction. The characterization data provided overwhelming evidence in support of the better σ-donor properties of the mesoionic triazol-ylidene compared to the benzimidazol-ylidene bridgehead. Of particular notice are the upfield shift of the observed signal in the ^{51}V-NMR spectrum (δ −533 ppm), the V=O stretching frequencies in the IR (986 cm^{-1}) and the cathodic shift by 0.19 V (at −0.56 V (*vs.* Fc/[Fc]$^{+}$) corresponding to the V^{V}/V^{IV} couple as found in the cyclic voltammogram of **681**. The structural data reveal a less distorted square-pyramidal geometry with shorter and almost equal V–C^{NHC} and V=O bond distances (2.055(3) Å and 1.583(3) Å), respectively. Reduction of **681** with [CoCp*$_2$] led to the V^{IV} complex **682**,

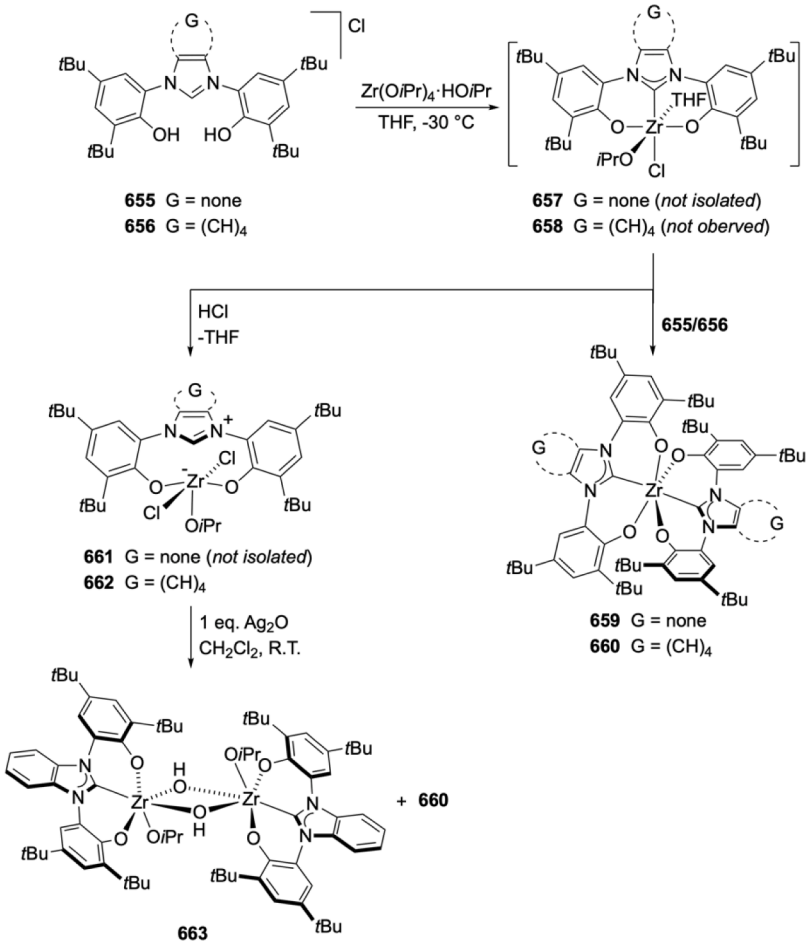

Scheme 129. Zr complexes with backbone structures of type **XIIb**

which is a one electron paramagnet, showing like **674** an eight-line ESR spectrum ($g_{iso} = 1.9715$, $\alpha = 274.1915$ MHz). Attempts to derivatize **681** by substitution of the remaining Cl on the vanadium by salt metathetical protocols were only successful with aryloxide and secondary arylamide nucleophiles, leading to the complexes **683**–**685**, respectively, all of which were characterized spectroscopically and structurally. In contrast, attempts to replace the oxo- by imido-ligand following redox neutral reactions with arylisocyanates (ArN=C=O) were not successful. As an alternative entry to the imido analogues of **681**, the synthesis of the V^{III} complex **686** was successfully undertaken by the reaction of the *in situ* generated NHC pincer from **608** and LiHMDS with $[VCl_3(THF)_3]$, leading to the complex **686** of limited long-term thermal stability, even under inert atmosphere (Scheme 132). The paramagnetic (2.71 μ_B by the Evans' method) and ESR silent species **686** was characterized by a low accuracy structural determination. Computational studies pointed to a triplet ground state with V centered SOMOs. Reaction of **686** with a range of organic azides in benzene at 60 °C led after N_2 evolution to the stable green diamagnetic V^V imido complexes **687**–**690** which were characterized by ^{1}H-and ^{13}C and ^{51}V-NMR spectroscopies and, despite the absence of C^{NHC} signal ascribable to the vicinal quadrupolar V center, they gave strong support for the identity of the complexes. Furthermore, the molecular structure of **688** and **690** determined crystallographically gave a detailed picture of the corresponding complexes. They adopted slightly distorted square pyramidal coordination geometries with $V-N^{imido}$ and $V–C^{NHC}$ bond distances at 1.644(2), 2.048(2) and 1.621(4), 2.048(4) Å, respectively (Scheme 132).

The only niobium complex **691** with O,C^{NHC},O pincer-type ligand was obtained by the reaction of **608** with $[Nb(NtBu)Cl_3Py_2]$ in the presence of LDA (Scheme 133) [269]. Consistently, the ^{1}H NMR signal for triazolium-5H disappeared on formation of **691**. In the structure of **691**, the niobium atom adopted a distorted octahedral coordination geometry and the $Nb–C^{NHC}$ bond distance of 2.196(3) Å was found to be the shortest niobium-carbene distance reported so far [283–286].

3.13.4. Group 6 metals (Mo and W)

Attempts to tune and gain insight into the mechanism of alkyne metathesis catalysts based on Mo and W were focused on the usage of κO, κC^{NHC}, κO pincers of type **XIc**, to stabilize quasi-cationic active species, the fluorinated side-arms of the pincer bear resemblance to the fluoroalkoxides employed in the Schrock metathesis catalysts that are crucial for activity. Complex **696** was prepared by the reaction of **692** with 2.1 equivalents of LiHMDS, followed by addition of **694** in THF; it was isolated in 75 % yield after crystallization from diethyl ether (Scheme 134). The ^{1}H NMR spectrum of **696** revealed two sets of doublets attributed to the protons of the methylene linker of the pincer at δ 4.54 and 4.48 ppm ($^2J_{H\text{-}H} = 14.3$ Hz), and the ^{19}F NMR spectrum showed three resonances at δ −75.5 ppm, −77.0 ppm and −78.6 ppm (s, OCMe$(CF_3)_2$) (Scheme 134). Complex **696** exhibits activity for the homometathesis of 1-phenyl-1-propyne at 35 °C in toluene in the presence of 5 Å molecular sieves. The most active catalyst was **696**, with a terdentate NHC, with TONs of 780 after 3 h [287].

In efforts to stabilize cationic alkylidyne complexes of tungsten that were postulated to be active species in alkyne metathesis reactions, the terdentate pincer of type **XIc** was employed, the additional structural feature of **XIc** with trifluoromethyl groups in α-position to the alkoxide side-arm mimics the electron-withdrawing character of the metathesis

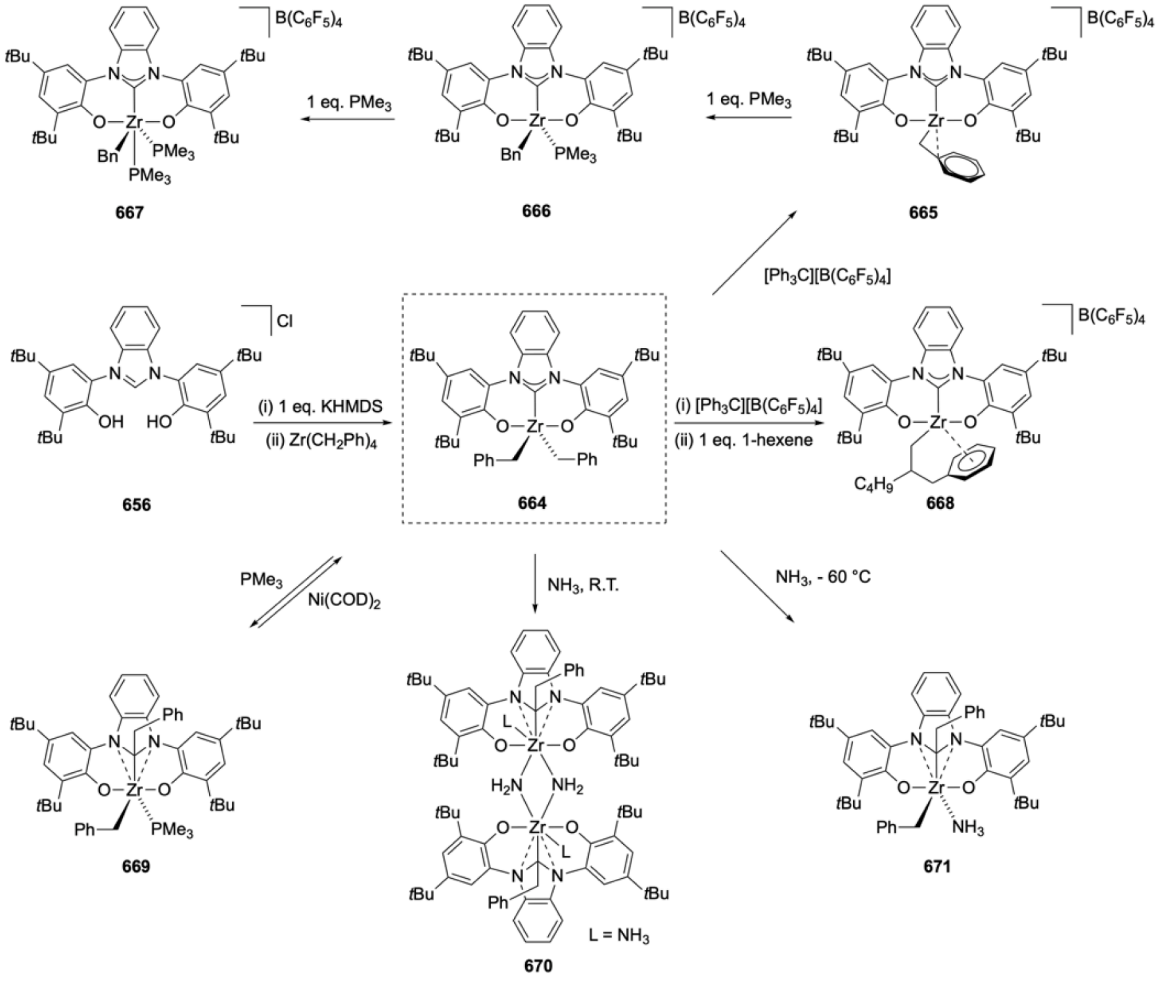

Scheme 130. Migration, insertion and NH_3 activation reactivity of dibenzyl complexes of Zr bearing a pincer backbone of type **XIIb**.

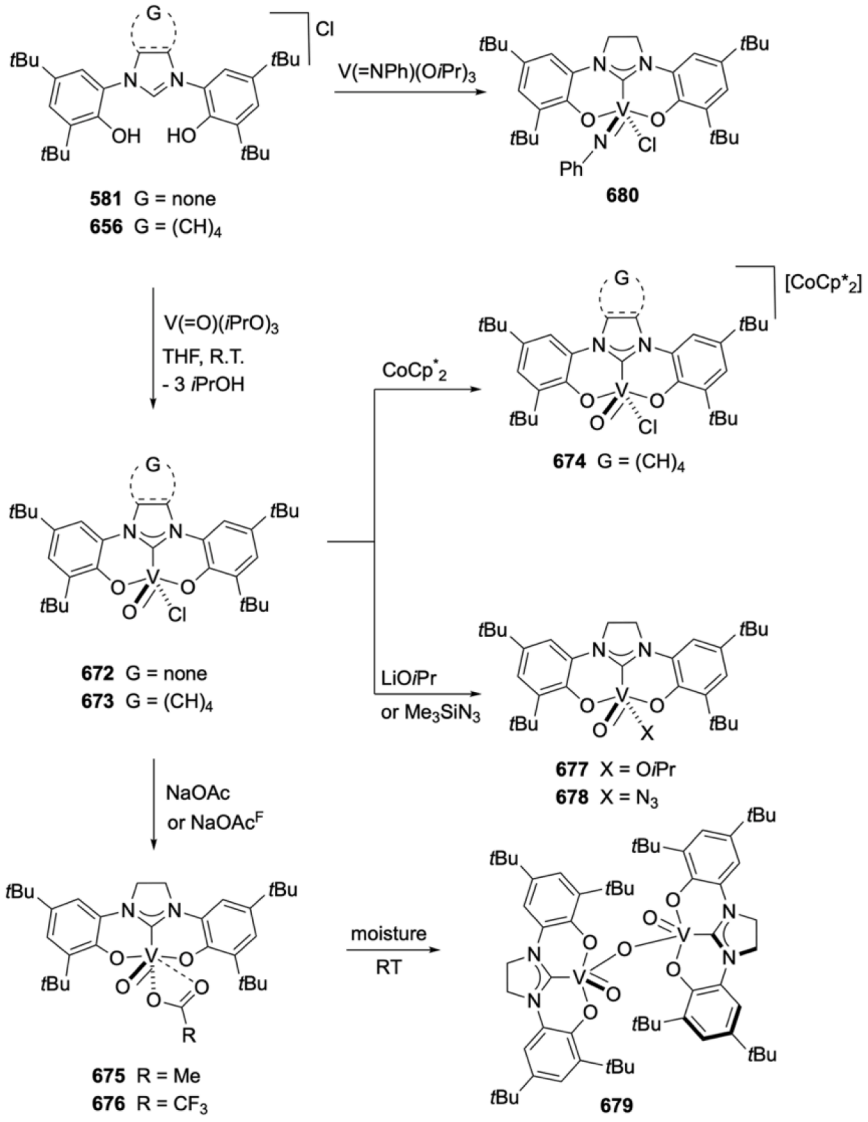

Scheme 131. Synthesis and transformations of vanadium complexes with ligand backbones of types **XIIa** and **XIIb**

catalysts with monodentate fluorinated alkoxides. The reaction of **695** with **693** resulted in the formation of the charge neutral **697**, the W analogue of **696** (Scheme 134). In contrast to the latter, the former does not show any alkyne metathesis activity. For the synthesis of a cationic complex based on the same framework, the remaining alkoxide ligand in **697** was replaced by chloride *via* an alcoholysis reaction with *N,N*-dimethylaniline hydrochloride affording **698**, which in turn was reacted with $AgB(Ar^F)_4{\cdot}3MeCN$ affording the binuclear ditungstatetrahedrane species **699** rather than the targeted cationic alkylidyne complex. Complex **699** features one 'bridging alkyne', one bridging chloride and one acetonitrile bound to one of the tungsten centers, the positive charge is formally distributed between the tungsten centers (Scheme 134). Complex **699** was characterized by NMR spectroscopy and crystallographically. The presence of the nitrile ligand on one W center of the binuclear species results in different bond distances around each of the metals, including the bridging carbons: the W center bearing the coordinated nitrile has significantly longer W–C bond lengths (2.330(4) and 2.282(3) *vs.* (2.035(4) and 2.081(4) Å), other metrical data in **699** include W–W distance of 2.6709 Å, C–C distance in the bridging alkyne of 1.392(5) Å and W–C^{NHC} of 2.141(4) and 2.182(4) Å. NMR spectroscopy indicated that there is no **699** neither in equilibrium with **698** nor any reactivity in homo-metathesis of phenyl-methylacetylene. A plausible scenario for its formation involves bimolecular decomposition of an elusive mononuclear species to **699** (Scheme 134) [288].

A range of Mo^{VI} complexes with the pincer of type **XIIb** were reported in 2019 (Scheme 135) [289]. Treatment of ligand precursors **656** (Scheme 129) with NEt_3 in THF, followed by addition of $[Mo(O)_2Cl_2(DME)]$ resulted in the formation of the air stable complex **700**, which was isolated as a faint yellow solid in 75 % yield. It was characterized spectroscopically and in the solid state by X-ray diffraction studies. The ^{13}C NMR spectrum displayed the C^{NHC} signal at δ 183.1 ppm and the Mo=O stretching modes in the IR spectra appeared at 914 and 939 cm^{-1}. In the solid-state structure, the mononuclear five coordinate *cis*-dioxo (distorted square-pyramidal) and a dinuclear bis-μ-oxo species with six coordinate octahedral metal centers were observed together in the asymmetric unit. In solution only one species (presumably the mononuclear) was detected (by VT NMR). Similarly, reaction of **656** with $[MoCl_2(O)(NtBu)(DME)]$ cleanly afforded **701**. A low-quality structure of **701** determined by X-ray diffraction of crystals grown from THF solutions revealed the formation of the desired pincer-oxo-imido complex, where the metal adopted a distorted six coordinate geometry, the sixth site being occupied by one THF solvent molecule. ^{13}C NMR spectroscopy showed the C^{NHC} signal at δ 191.6 ppm while a ^{1}H-^{15}N-HMBC NMR experiment confirmed the presence of the imido

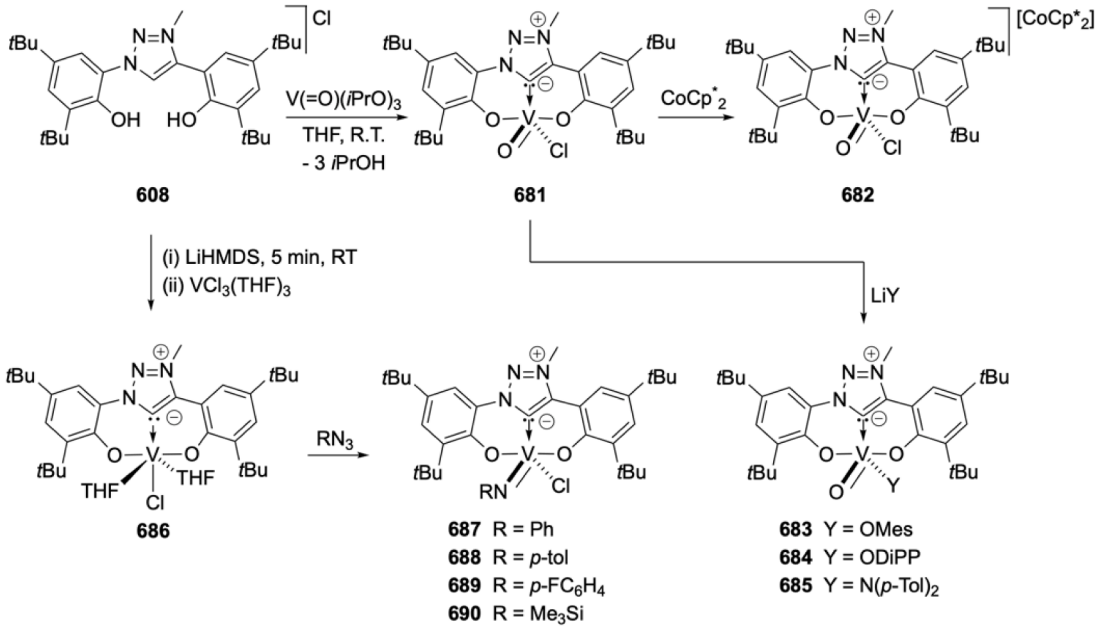

Scheme 132. Vanadium complexes with a pincer ligand structure of type **XIIc**.

group, finally the Mo=O stretching appeared at 910 cm^{-1}. Under similar conditions, treating **656** with [$MoCl_2(NtBu)_2$(DME)] in the presence of NEt_3 afforded **702** in 85 % yield as the single isomer depicted in Scheme 135 (*i.e.* *t*BuNH *trans* to C^{NHC}) [289]. Its ^{13}C NMR spectrum featured C^{NHC} signal at δ 191.1 ppm and its molecular structure a Mo center in a distorted octahedral coordination geometry the sixth site being occupied by a primary *t*BuNH group originating from partial protonation of one *t*BuN ligand, presumably by the weakly acidic $(Et_3NH)Cl$ side product; interestingly, under these conditions neither the C^{NHC} nor the phenoxides are protonated, indicating the high nucleophilicity of the coordinated *t*BuN. In the structure of **702**, the Mo = N*t*Bu and Mo–NH*t*Bu distances were found at 1.711(3) and 1.954(3) Å, respectively. In contrast, treatment of **656** with the stronger base LDA, followed by the addition of [$MoCl_2(NtBu)_2$(DME)], resulted in the formation of **703** in low yield, using KHMDS as base under the same conditions did not lead to **703**. Complex **703** was prepared in higher yield by deprotonation of the N*Ht*Bu group in complex **702** using LDA or KHMDS (Scheme 135). This was evidenced by the disappearance of the ^1H NMR N–H resonance at δ 12.2 ppm and the shift from δ 191.1 ppm to δ 199.3 ppm of the characteristic ^{13}C NMR resonances assignable to C^{NHC} of **702** and **703**, respectively. The X-ray structure of complex **703** revealed a slightly distorted square-pyramidal coordination geometry around the molybdenum. In addition, **701** could also be prepared *via* a ligand exchange reaction between the **700** and the **703** at elevated temperatures. Interestingly, reaction of **656** with the related imido precursor [Mo$(NMes)_2Cl_2$(DME)] in the presence of NEt_3 resulted in the formation of complex **704** rather than a complex analogous to **702**, a difference that was ascribed to the reduced nucleophilicity of the arylimido ligand. Complex **704** was isolated as a dark orange powder in 79 % yield and characterized by ^{13}C NMR spectroscopy (C^{NHC} at δ 193.2 ppm) and crystallographically.

The reactivity of **703** was also investigated: it reacted cleanly with triethylammonium chloride in C_6D_6 to give complex **702** within 1 h, as monitored by NMR spectroscopy. Similarly, treatment of complex **703** with 2,4,6-trimethylphenol in C_6D_6 afforded a mixture of complexes **705** and **706** and other by-products. The complexes **705** and **706** were characterized by X-ray diffraction analysis and NMR spectroscopy. The reaction of **703** with benzimidazole in C_6D_6 was monitored by NMR spectroscopy and gave a mixture of complex **707** and other by-products (Scheme 135) [289].

Complexes **700** and **701** have been studied as catalysts for the deoxygenation of nitroarenes to anilines using pinacol as sacrificial reductant. Mechanistic investigations point to the presence of paramagnetic (2.22–1.96 μ_B (1.11–0.98 μ_B/Mo)) binuclear μ-oxo bridged Mo^V species [(κ,κ,κ-O,C^{NHC},O)Mo(=O)]$_2$(μ-O) (**708**) and κ,κ,κ-O,C^{NHC},O)Mo(=N*t*Bu)]$_2$(μ-O) (**709**) as precatalysts. They have been accessed synthetically by the deoxygenation of **700** and **701** with PPh_3 or PEt_3 in toluene (Scheme 136) [290].

The Mo^{VI} complex **710** with the versatile pincer of type **XIIc** was obtained by the reaction of **608** with [Mo$(NtBu)_2Cl_2$(DME)] in the presence of LDA (Scheme 137) [269]. Its ^{13}C NMR spectrum showed the C^{NHC} signal at δ 169.2 ppm. The molecular structure of **710** revealed a distorted square pyramidal coordination environment around the metal center with one bent and one linear imido groups disposed *cis* to each

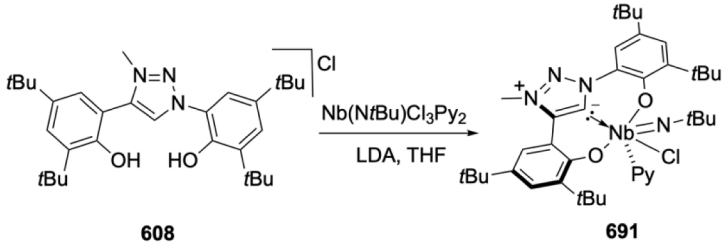

Scheme 133. One niobium complex with pincer ligand structure of type **XIIc**

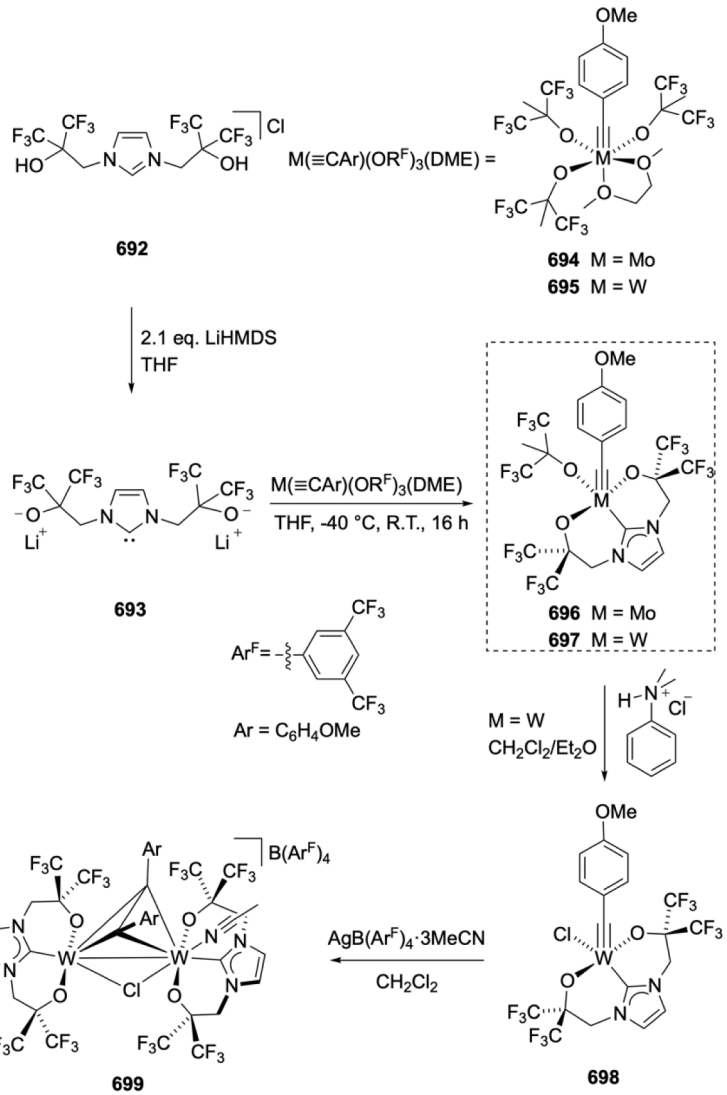

Scheme 134. Mo and W complexes with ligand backbone of type **XIc**.

other. The Mo–C^{NHC} bond distance was 2.204(1) Å and the Mo = N^{imido} bond lengths were 1.741(1) Å and 1.749(1) Å (Scheme 137) [269].

3.13.5. Group 7 metals (Mn)

The rare paramagnetic Mn^{III}-bis-aryloxide-NHC complex **711** was obtained by the reaction of **581** with [Mn(acac)$_3$] in THF as dark purple crystals (Scheme 138). Its structure revealed a distorted square-pyramidal coordination geometry around the metal with Mn–C^{NHC} bond distance (1.999(8) Å) shorter than in previously reported Mn–NHC complexes (aver. 2.20 Å) owing to constraints imposed by the terdentate chelating ligand [278].

3.13.6. Group 8 metals (Fe, Ru)

The complexes of group 8 metals with κO,κC^{NHC},κO ligands are rare and two families of them have recently been described. A series of Fe complexes with the ligand **XIIb** in a range of oxidation states was prepared by the sequence of reactions shown in Scheme 139 [291]. The precursor **656** was deprotonated with three equivalents of KHMDS to the dianionic pincer carbene and reacted *in situ* with $FeCl_2$ in pyridine to give the polymeric -'ato' species **712**. The characterization of the paramagnetic and very sensitive **712** was mainly based on crystallographic studies: the structure of the complex is a linear polymer in the solid state, where the repeat units feature Fe^{II} centers coordinated by two κC^{NHC},κO-bound ligands adopting a rare square-planar geometry; the second side arm of each pincer is twisted away from the Fe center and bridging two potassium atoms, one associated with the repeat unit and one associated with the next one, thus forming a K_2O_2 bridging structure holding the chain of the complex together. The ^{1}H NMR spectrum of **712** in THF-d^8 gave evidence of paramagnetism featuring only three broad signals at δ 15.19 ppm, 0.75 ppm, and −2.72 ppm, the remaining probably buried in the baseline. Although the complex was always obtained in the solid state as a polymer, it was conjectured that a mononuclear species of unknown structure is dominating in polar solvents. Other metrical data of interest included Fe–O bond distances of 1.931(2) Å and short Fe–C^{NHC} distances of 1.923(3) Å, the latter being in agreement with the square-planar coordination geometry. The zero-field ^{57}Fe Mössbauer spectra of **712** at 77 K unveiled parameters ($\delta = 0.45$ and $\Delta E_Q = 1.52$) characteristic of Fe^{II} oxidation state, while SQUID measurements showed a temperature-independent $\mu_{eff} \approx 3\mu_B$ from 60 to 200 K, in support of an overall $S = 1$ configuration as a result of the square-planar geometry, a fact also amplified by the Mössbauer data; at higher temperatures magnetometry showed that a $S = 2$ state was thermally populated [291]. Complex **712** was very sensitive to oxidation. Attempts to prepare derivatives, *e.g.* aiming to complex the K^+ cations with 18-C-6, led to the formation of the red-brown Fe^{III} complex **714**, which was also rationally accessed by a redox neutral sequence,

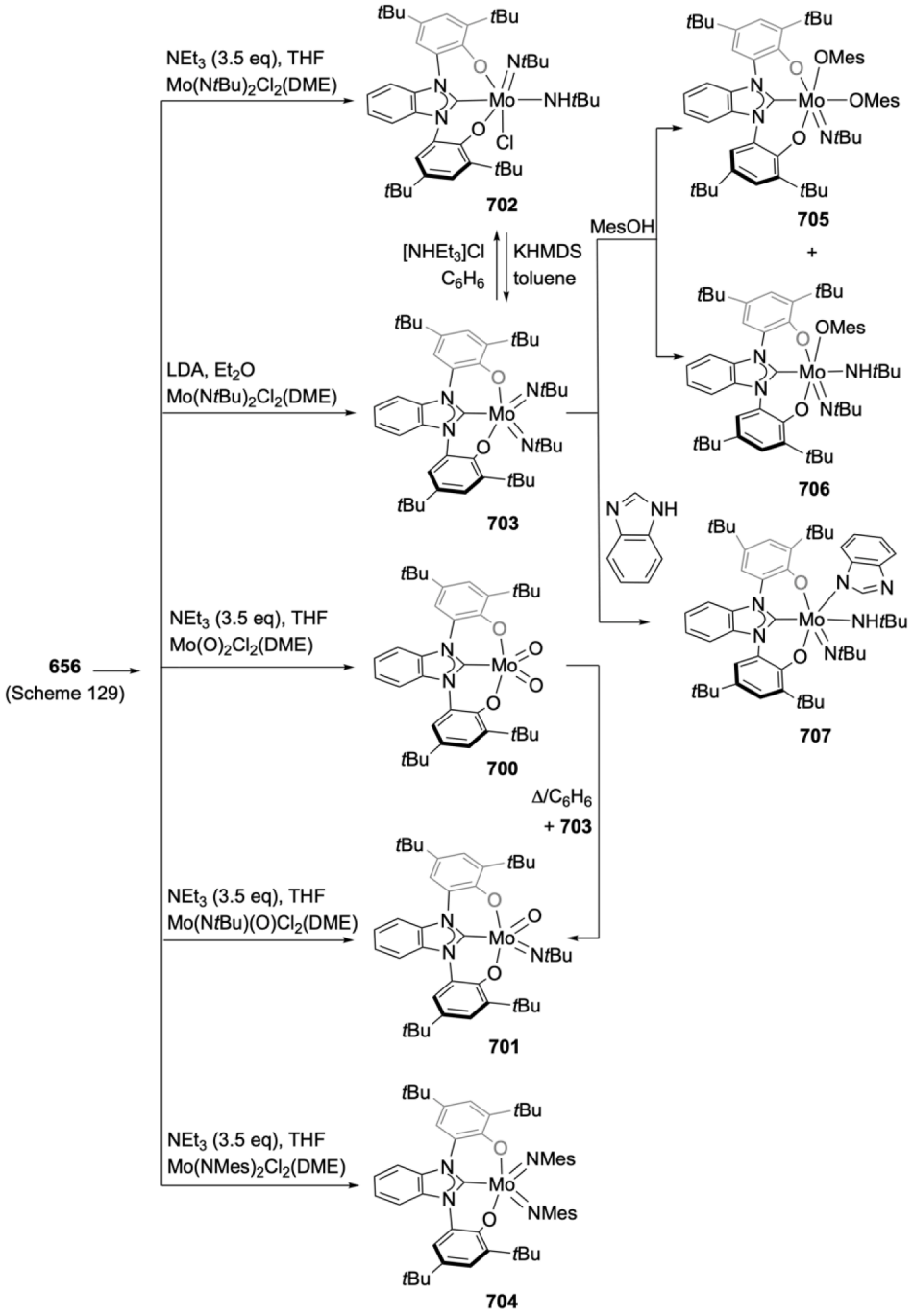

Scheme 135. Mo complexes with ligand backbone of type **XIIIb**

starting from the precursor **656** that was deprotonated with three equivalents of KHMDS to the dianionic pincer carbene as above and further reacted *in situ* with $FeCl_3$ initially affording **713** and by the reaction with 18-C-6 was converted to **714** [291]. The structure determination of **714** revealed a well-separated ion pair with a mononuclear 'ato' anionic species featuring one Fe center in an octahedral geometry ligated by two dianionic *mer*-$OC^{NHC}O$ pincers with a *trans*-disposition of the NHC bridgeheads, accompanied by one $[K(18\text{-C-}6)(THF)_2]$ cation. The Fe–C^{NHC} distances of 1.894(3) and 1.898(3) Å were at the short end of the range and shorter than the corresponding in **712**, other metrical data of interest in **714** were the short Fe–O distances, consistent with a degree of π-bonding, and the $O^{Phenolate} - C^{Ph}$ bond length of 1.321 Å which implies a phenoxide rather than phenoxy radical or quinone ligand redox state. The Mössbauer spectra of **714** with $\delta = 0.18$ and large quadrupole splitting $\Delta E_Q = 5.10$ are indicative of a low-spin electron configuration ($S = 1/2$) and an axially elongated octahedral ligand field. The magnetization data point to a plateau with $\mu_{eff} = 2.07\ \mu_B$ between 2 and 100 K consistent with an $S = 1/2$ ground state (spin only $\mu_{eff} = 1.73\ \mu_B$), which is in accordance with the X-band EPR spectrum that shows an axial signal with anisotropic *g*-values $g_\perp = 2.31$ and $g_\parallel = 1.84$, at higher temperatures some of the iron in the complex is found in the $S = 5/2$ state. The paramagnetic dark-violet, moderately stable **715** was obtained by the one-electron oxidation of **713** with one equivalent of $AgPF_6$ in dichloromethane, purified by crystallization and characterized by crystallographic, spectroscopic and magnetometric techniques. During this reaction, the diamagnetic, non-metal containing **718** was also obtained in variable amounts. The topology of the structure of **715** is broadly similar to the anion in **713** featuring a distorted octahedral Fe

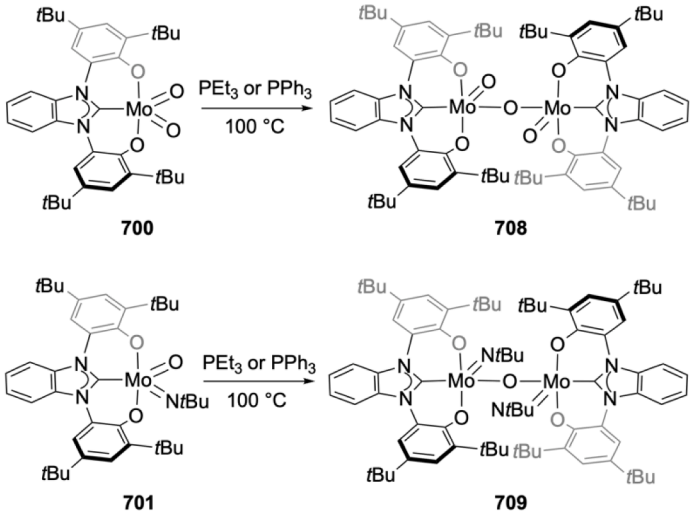

Scheme 136. Mo complexes with ligand backbone of type **XIIb**

center with the κO,κC^{NHC},κO pincers occupying *mer* positions and *trans*-C^{NHC} donors. There are however noticeable differences in the metrical data, *e.g.* the Fe–O bond distances **715** are significantly shorter (av. 1.891 Å) by 0.040 Å than the corresponding in **713**, presumably due to increased O-to-Fe π-donation in the oxidized metal; conversely, the Fe−C^{NHC} (av. 1.943(2) Å) are longer (by 0.047 Å). The O−C^{Ph} distance criterion as a means to judge the ligand oxidation state pointed to coordinated closed-shell phenoxides rather than phenoxy radicals (distances in the range 1.327(2)-1.342(2) Å), and, consequently, a Fe^{IV} (d^4, $S = 1$) center, also supported by the Mössbauer data. Complex **715** is X-band EPR-silent; the assignment of $S = 1$ state is also corroborated by SQUID measurements with room temperature $\mu_{eff} \cong 3.1\mu_B$. The organic compound **718** was characterized by NMR spectroscopic and crystallographic methods as 1,3-bis(3,5-di-*t*Bu-phenyl)benzimidazolone ketal, a 'reductive elimination' product of Fe–C^{NHC} and Fe–O bonds. Two-electron oxidation of **713** with two equivalents of $AgPF_6$ in dichloromethane led to the dark green, paramagnetic **716**. Assignment of the Fe oxidation state in **716** (formally Fe^{V}) based on metrical data was hampered by the poor quality of the crystal structure determination, which confirmed overall the same topology as **715**. Better crystallographic data were collected from the analogue of **716**, **717** obtained by exchange of anion PF_6 with $[Al(OiPr^{CF3})_4]^-$ revealing metrical data comparable to **715**, therefore in this case ligand non-innocence cannot be excluded. Based on other spectroscopic data and computational studies, **715** can be described as Fe^{IV} center antiferromagnetically coupled to a ligand-centered radical (Scheme 139).

The ruthenium complexes **719**–**721** were obtained in good yields by reaction of **581** with Ag_2O in CH_2Cl_2, followed by addition of the corresponding ruthenium precursor and complexes **719**–**721** were characterized by NMR spectroscopy (Scheme 140). The catalytic activities of complexes **719**–**721** towards alcohol amidation with amines were investigated and all pre-catalysts were efficient at low catalyst loading (1 mol%) [292].

3.13.7. Group 9 metals (Co, Ir)

A series of cobalt complexes in different oxidation states, featuring κO,κC^{NHC},κO pincer ligands of types **XIIa**, **XIIb** has been synthesized and their electronic structures studied (Scheme 141) [293]. Reactions of the corresponding ligand precursors **581**, **655** and **656** with three equivalents of NaOMe, followed by addition of one equivalent of $CoCl_2$, afforded the orange to orange-brown **722**–**724** and **725**–**727** after work-up including crystallizations from THF or MeCN, respectively. The complexes **722** and **725**–**727** were characterized by X-ray diffraction analysis. They feature square-planar coordination geometries with small variation of the metrical data and more substantial differences in the pincer conformation (*i.e.* planarity, ring puckering), depending on the nature of the framework incorporating the bridgehead C^{NHC} donor. The Co−O bond distances are constant across the series (av. 1.811 Å), and in line with Co−O^{phenoxide} distances in low-spin square-planar Co^{II} complexes. In contrast, the Co–C^{NHC} bond distances (av. 1.811(2)-1.830(8) Å) although unusually short (typical range for Co^{II}–NHC: 1.9135(19)-2.152(6) Å) tend to elongate for the unsaturated pincer backbones, presumably due to diminished Co–C^{NHC} π-interactions in this case [294–297]. Complexes **722**–**725** are paramagnetic (1.82–1.90μ_B) in support of a d^7, $S = 1/2$ configuration.

Treating a THF solution of **722** with one equivalent of AgOTf afforded the dark green, air-stable **728** which could be converted to **729** by anion metathesis with $NaBPh_4$ (Scheme 141) [293]. The Co center in **729** adopts a five-coordinate, pseudo-square-pyramidal geometry; the observed metrical data aided the oxidation state assignment of the ligand and the metal: shortening and lengthening of the Co−O^{Ar} and Co−C^{NHC} distances by 0.01 Å and 0.06 Å, respectively, and some

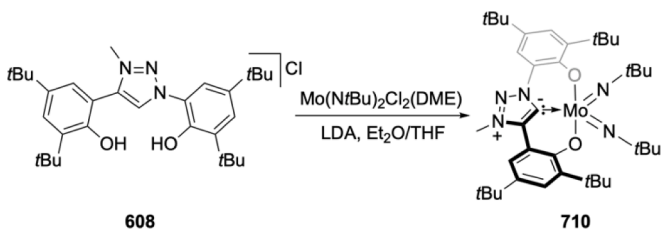

Scheme 137. Mo complex with ligand backbone of type **XIIc**

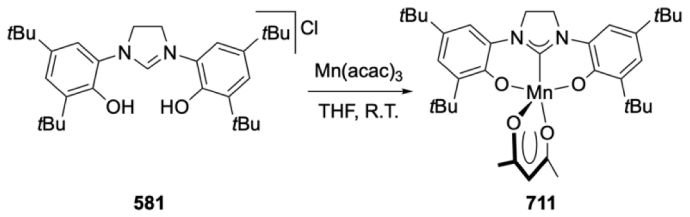

581 711

Scheme 138. Mn^{III} complex with ligand backbone of type **XIIa**.

quinoid-type bond alternations of the phenolic rings, known in phenoxyl radicals, suggested some degree of ligand oxidation. The solution magnetic susceptibility of **728** (2.88μ_B) is consistent with the spin-only value for an $S = 1$ center; this persisted in the solid state at room temperature but diminished down to 0.79μ_B at 2 K. Based on the above and additional ESR data the cation in **728** can be best described as Co^{II} center antiferromagnetically coupled to a ligand radical. Reaction of **722** with 2.1 equivalents of dark blue $[N(p\text{-}C_6H_4Br)_3][PF_6]$ in THF gave the green–brown ion pair **730**, with the dicationic complex featuring one Co center *mer*-coordinated by one pincer and three THF ligands. The limited thermal stability of **730** at room temperature complicated the collection of detailed characterization data, except a crystal structure determination and solution magnetic measurements. In the structure a clear quinoid-type bonding pattern of the wing tips was evident, which was also accompanied by a shortening of C^{Ar}–O and C^{Ar}–N bond distances by 0.044(4) and 0.022(5) Å respectively, reminiscent of quinone-type metrics. Thus, the ligand can be formulated as a charge-neutral doubly oxidized $OC^{NHC}O$ strongly held on the Co by the strong NHC donor. Charge balance implies that the cobalt in **730** is Co^{II}. In support of this formulation, the μ_{eff} in solution of 2.51μ_B has been accounted by the formulation of a low spin state d^7 $S = 1/2$ with substantial orbital contributions.

The cobalt complexes **723**–**730** have to be compared with and contrasted to the iron complexes **712**–**718** described in the previous section: in the Co complexes, extensive non-innocence of the O,C^{NHC},O ligands renders the 'higher oxidation complexes' as Co^{II} or Co^{III} species coordinated to (partially) oxidized forms of the ligands. In contrast, in the Fe complexes the 'innocence' of the O,C^{NHC},O ligand used points to 'true' higher oxidation state at the metal species. The origin of this difference may lie on the relative stability of the oxidation states of the metals in question and/or the differing nature of the complexes (*i.e.* ligand-to-metal stoichiometry 1:1 and 2:1 in Co and Fe families, respectively); these points may deserve further investigations (Scheme 141).

The complex **731** was obtained by the reaction of **725** with $AgCF_3$ in acetonitrile (Scheme 142) [298]. In a reversible transformation, the dark green **731** was converted under vacuum to **732** and redissolving **732** in acetonitrile regenerated **731**. The structures of complexes **731** and **732** were characterized by X-ray diffraction. The Co–CF_3 bond distance of 1.8692(16) Å in **732** was the shortest found for this bond in the CCDC database (*cf.* trifluoromethylcobalamin 1.878(12) Å). Under visible light, arene C–H trifluoromethylation was promoted by activation of the Co–CF_3 bond of complex **732** [298].

The reaction of the imidazolium salt **733** with three equivalents of KHMDS, followed by addition of $[Ir(\mu\text{-}Cl)(COD)]_2$ resulted in the clean formation of iridium complex **734**, which was characterized by X-ray

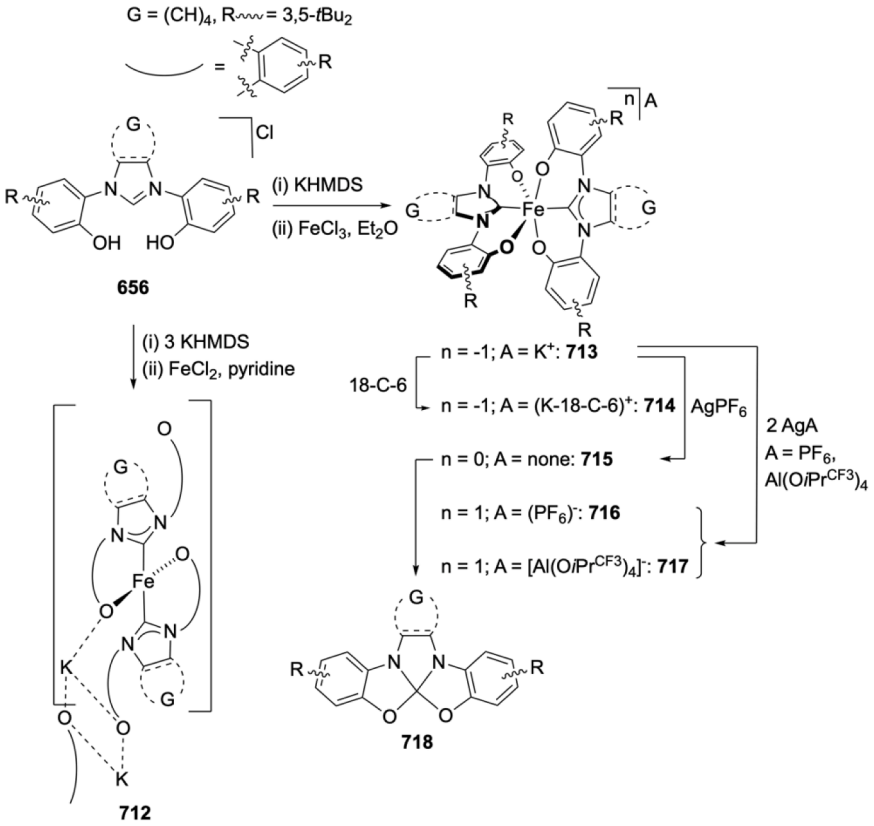

Scheme 139. Fe complexes with ligand backbone of type **XIIb**

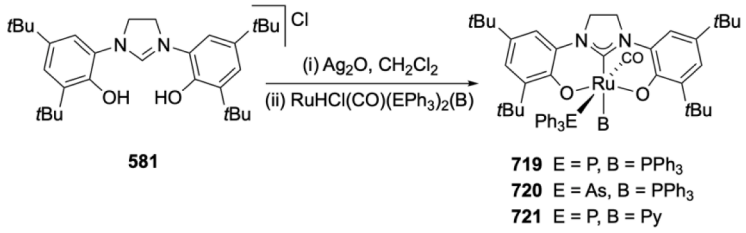

581

719 E = P, B = PPh_3
720 E = As, B = PPh_3
721 E = P, B = Py

Scheme 140. Ru^{II} complexes with ligand backbone of type **XIIa**

diffraction analysis and NMR spectroscopy (Scheme 143) [299]. The molecular structure indicated the presence of one coordinated and one dangling phenoxide groups, the latter associated with a K^+ cation. The ^1H NMR spectrum of **734** clearly pointed to a dynamic equilibrium between **734** and **735** occurring in solution, associated with slow rotation about the phenolate-nitrogen bonds. The Ir^{III} complex **736** was obtained by the oxidation of **734** and **735** with $[FeCp_2]PF_6$ in acetonitrile, all NMR data were consistent with the structure suggested. Heating **736** at 90 °C in acetonitrile afforded the complex **737**, which was identified by mass spectroscopy [299]. Similarly, treatment of complex **736** with an excess of PMe_3 or PCy_3 at 90 °C for 12 h cleanly generated complexes **738** and **739**, respectively [299]. The ^{31}P NMR spectrum of **738** contains the expected doublet and triplet. Consistent with the structure of complex **739**, a ^{31}P NMR singlet was observed for the coordinated PCy_3. Exposure of complex **739** in acetonitrile to CO atmosphere resulted in the formation of a mixture of complexes **739** and **740** in a 2:1 ratio. Conversely, complex **740** could be completely converted to **739** upon degassing or heating. The IR spectrum of complex **740** exhibited a characteristic ν(CO) absorption at 2064 cm^{-1}. The structures of complexes **739** and **740** were characterized by X-ray diffraction analysis since **739** and **740** cocrystallized as a 4:1 mixture. The air-stable complex **741** was obtained by the reaction of **739** with $[NMe_4]Cl$ in acetonitrile and characterized by X-ray diffraction [299].

3.13.8. Group 10 metals (Ni, Pd, Pt)

The complexes **743** and **744** with the κO, κC^{NHC}, κO pincer ligand of type **XIc** (Chart 8) were obtained by dropwise addition of a solution of the anionic fluoroalkoxy carbene **742** to a solution of $[NiCl_2(PPh_3)_2]$ in a 1:1 molar ratio (Scheme 144). The products were easily isolated from the reaction mixture after workup on neutral alumina. The ^{13}C NMR spectrum of **743** showed the characteristic signal for the nickel-bound carbene at δ_C 159.5 ppm, and the ^{31}P NMR spectrum displayed a singlet at δ 6.03 ppm. The ^1H and ^{19}F NMR spectra comprise singlets attributable to the methylene and trifluoromethyl groups at δ 4.05 ppm and −76.88 ppm, respectively. The presence of singlets suggested that the structure of **743** was flexible and symmetric. The X-ray crystal structure of complex **743** revealed a square-planar coordination geometry around the nickel center. The Ni–C^{NHC} and Ni–P bond lengths of 1.853 Å and 2.289 Å, respectively, were consistent with those previously observed in other nickel complexes. The complex **744** exhibited two sets of signals in the ^1H, ^{13}C and ^{19}F NMR spectra, which is consistent with the crystal structure of the complex showing that two alkoxido donors from one carbene ligand were coordinated, whereas two hydroxy groups from the other pincer were hydrogen-bonded to these coordinated alkoxide oxygen atoms. The Ni–C^{NHC} bond of the chelated ligand in **744** (1.903 Å) was longer than in complex **743** (Scheme 144) [300].

A family of complexes **746**–**754** with the pincer ligands of types **VIIa** and **VIIb** and group 10 metals was synthesized in good yields by the reactions of **655**, **656** and **745**, respectively, with 1 equivalent of MCl_2 (M = Ni, Pd, Pt) and an excess of potassium carbonate in pyridine at 100 °C for 12 h (for **746**–**753**) or under the same conditions in cyclohexylamine (for M = Pt, **754**) (Scheme 145) [187,301,302]. In the ^{13}C NMR spectra of the complexes, the C^{NHC} signals were observed at δ 162.4 ppm (**746**) and 146.8 ppm (**747**), 165.3 ppm (**750**) 149.8 ppm (**751**) 153.5 ppm (**752**) and 153.6 ppm (**753**), respectively [187,302]. The X-ray crystal structures confirmed that all these diamagnetic complexes, adopted a square-planar coordination environment. Typically, the Pd–C^{NHC} bond distance in **749** (1.797(5) Å) was shorter than those in related carbene complexes (1.953(5)-2.004(3) Å) [303–305], mostly because of the rigid structure of the terdentate ligand. The structure of **755** is also characterized by a distorted square-planar geometry around the metal center, the Pt–C^{NHC} and Pt–P bond lengths of 1.948(3) Å and 2.3272(7) Å are consistent with values found in related platinum complexes.

In order to explore the electrochemical properties and possible redox non-innocence of the O,C^{NHC},O pincer in **746** and **747**, complex **748** was targeted and obtained quantitatively by chemical oxidation of **747** with 1.2 equivalent of $AgSbF_6$ in dry CH_2Cl_2 at room temperature. The dark green cationic **748** was stable at room temperature for several days. EPR spectroscopy showed a signal at $g_{iso} = 2.056$, a value larger than for free phenoxy radicals (typically 2.005), but smaller than the average g values of reported Ni^{III} complexes. In contrast, the oxidation of **746** required the stronger oxidant, tris(2,4-dibromophenyl)aminium radical ($E_{1/2} = 1.1$ V). However, the reaction was accompanied by a bleaching of the solution and the oxidation product was not stable. An EPR analysis confirmed no paramagnetic species in solution. The X-ray structure determination of **748** revealed a square-planar geometry around the metal center with Ni–O bond distances of 1.774(5) and 1.785(7) Å, significantly shorter than those in **747** (1.835(2) and 1.847(2) Å), respectively, suggesting a substantial 'Ni^{III}' character for the metal in **748**. All these results were consistent with complex **748** being in an intermediate state between a Ni^{II}-radical and Ni^{III} [301].

The complex **749** was stable in the solid-state and in solution, even at high temperature, and highly active for catalytic Heck reactions between iodobenzene and styrene in dimethylacetamide [187].

3.13.9. Group 13 metals (Al)

A family of Al^{III} complexes bearing κO, κC^{NHC}, κO-terdentate ligands has been reported (Scheme 146) [306]. Reaction of **581** with $AlMe_3$ in THF resulted in the formation of the zwitterionic complex **756** *via* methane elimination which was isolated as a colorless solid in good yield. The diagnostic ^1H NMR singlet at δ 8.75 ppm was assigned to the *H*-imidazolinium proton, furthermore the molecular structure was determined by X-ray diffraction. Deprotonation of **756** with bases such as LDA, *n*BuLi, *t*BuLi and KHMDS afforded complex **757**, which could also be obtained by the reaction of **581** with three equivalents of *n*BuLi, followed by addition of $AlCl_2Me$ in THF [306]. In the structure of **757** the Al–C^{NHC} bond length of 2.032(2) Å was comparable to those previously reported for Al–NHC complexes [307–309]. The ^1H NMR spectrum displayed the typical resonance assigned to the Al–Me moiety at δ −6.6 ppm, and the ^{13}C NMR spectrum the C^{NHC} at δ 186.5 ppm. Interestingly, crystallization of complex **757** in a mixture of pentane/CH_2Cl_2 resulted in the formation of complex **761**, presumably arising from the presence of adventitious water (Scheme 146).

Similarly, reaction of **581** with $Al(OiPr)_3$ in toluene at 110 °C resulted in the formation of the zwitterionic complex **758** which was isolated as a colorless solid in 66 % yield [306]. Its structure was established by X-ray diffraction analysis and NMR spectroscopy.

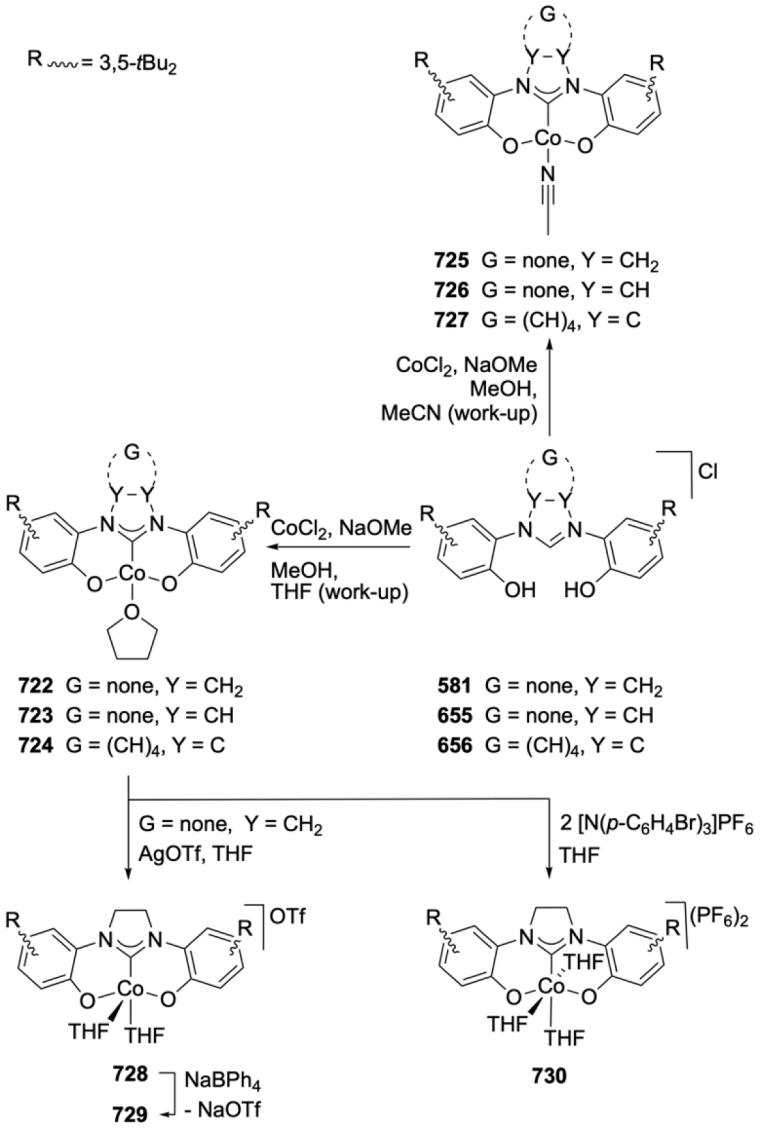

Scheme 141. Co complexes with ligand backbones of types **XIIa** and **XIIb**.

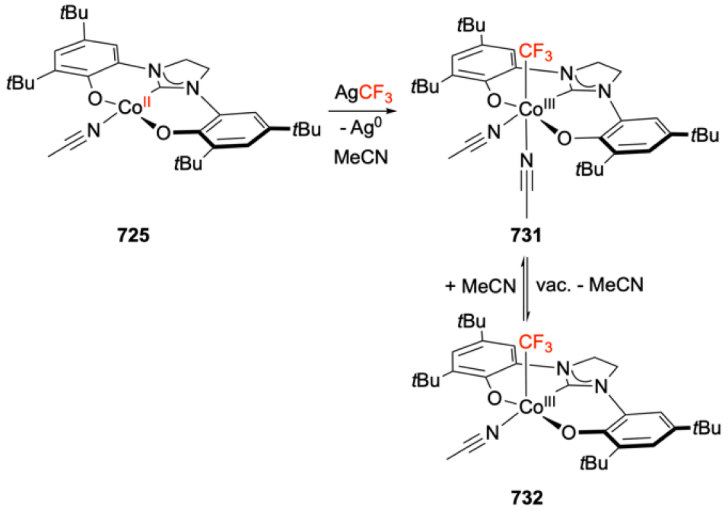

Scheme 142. Co-CF_3 complexes with ligand backbone of type **XIIa**

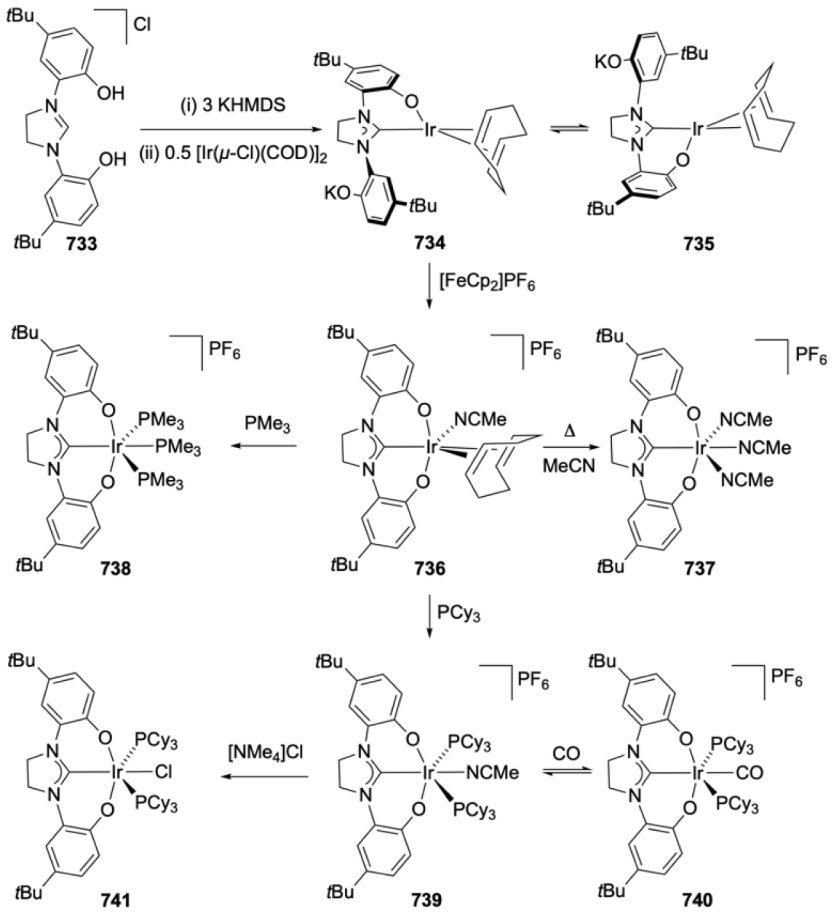

Scheme 143. Ir complexes with the ligand backbone of type **XIIa**.

Subsequent reaction of **758** with one equivalent of LDA in toluene cleanly afforded the Al–NHC alkoxide dimer **759**, as confirmed by X-ray diffraction [306]. The Al–C^{NHC} bond distance of 2.037(2) Å is in the expected range. Interestingly, the complex **759** also could be obtained *via* a methane elimination reaction by the thermal reaction of the Al methyl isopropoxide zwitterion **760**, which was prepared by reaction of the corresponding Al–NHC complex **757** with two equivalents of *i*PrOH in toluene. Complex **760** could also be obtained by reacting the complex **756** with LiO*i*Pr [306] and its structure was proposed based on NMR spectroscopies: for example, ^{1}H NMR spectrum featuring a characteristic imidazolinium-H resonance at δ 8.60 ppm, while the resonance at δ −0.62 ppm was assigned to the Al-Me moiety. The catalytic activity of **759** in the polymerization of *rac*-LA and trimethylene carbonate was examined and complex **759** was found to be highly efficient [306].

3.14. Type O,C^{NHC},S

No example with this donor set has been reported to the best of our knowledge.

3.15. Type S,C^{NHC},S

3.15.1. Group 8 metals (Fe)

A family of Fe complexes with a S,C^{NHC},S pincer ligand was studied as synthetic models of the active site of the FeMoCo nitrogenase (Scheme 147) [310]. Treatment of the precursor **762** with KHMDS in THF resulted in formation of the free, stable under inert conditions, pincer ligand **764** (δ_C C^{NHC} 218 ppm). Addition of **764** to a solution of [Fe$(OTf)_2$] (1 equivalent in THF) gave after work-up complex **765** that was characterized by spectroscopic methods (Mössbauer and paramagnetic NMR spectroscopy) and a low resolution X-ray structural determination, all data supported an octahedral high spin Fe^{II} ion center, with the connectivity shown in Scheme 147. However, in THF solution there was evidence of the presence of a second complex, presumably differing from **765** in the number of coordinated THF ligands. On dissolution in MeCN, it converted to the diamagnetic **766** which featured coordinated acetonitrile ligands to an octahedral low spin center and a *mer*-pincer ligand arrangement, as established by X-ray diffraction and spectroscopic methods (Mössbauer, NMR spectroscopy); on dissolution in THF, **766** reverted to **765**. The bis-thiolate species **767** with one bis(trimethylsilyl)amido coligand was obtained by the reaction of **763** with [Fe$(HMDS)_2]_2$ (1:1 Fe to **763** ratio); structural characterization revealed a dianionic pincer ligand coordinated to the iron center in a distorted tetrahedral geometry and a *fac* pincer ligand arrangement, a fact also supported by Mössbauer spectroscopy. The solution magnetic susceptibility ($\mu_{eff} = 5.1\mu_B$ in C_6D_6) is consistent with a high spin ($S = 2$) configuration at Fe^{II}. Complex **767** did not catalyze the reduction of N_2 to NH_3 in the presence of excess KC_8 and various acids. However, it served as a precursor to complexes **768**–**770** by protonating the silylamide with weaker S–H and N–H acids. The tris(thiolate) complex **768** was obtained by the reaction of **767** with 2,6-Mes_2-C_6H_4SH and exhibits a Fe center in a distorted tetrahedral coordination environment resembling the individual iron sites in the resting state of nitrogenase; the Fe−S and Fe−C^{NHC} bond distances were at ~2.3 and 2.035(2) Å, respectively. Reaction of **767** with phenyl hydrazine and aniline afforded the tetrahedral hydrazido and phenylamido complexes **769** and **770**, respectively, both featuring tetrahedral Fe^{II} centers. In addition to the direct access of **770** from **767**, it can also be obtained from **769** by thermal decomposition in a process that involves N-N cleavage of the coordinated hydrazide (Scheme 147) [310].

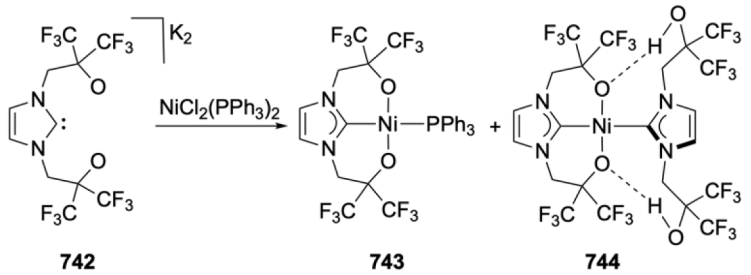

Scheme 144. Group 10 metal complexes with ligand backbones of types **XIIa** and **XIIb**.

3.15.2. Group 9 metals (Rh)

The complex **773** bearing the rigid S,C^{NHC},S-terdentate ligand was obtained by the reaction of the precursor **771** with LiHMDS in THF at room temperature forming the non-isolable carbene ligand which was reacted *in situ* with [Rh(μ-Cl)(COD)]$_2$ in the presence of *n*Bu$_4$NI to afford complex **772** in low yield (Scheme 148) [311]. This complex was characterized by X-ray diffraction unveiling a square planar geometry at the Rh with a Rh–C^{NHC} bond distance at 2.015(11) Å and uncoordinated S-donors. Treatment of **772** with I$_2$ led to the formation of **773** after oxidation of Rh^{I} to Rh^{III}. In this complex, the Rh^{III}–S bond distance was 2.386(3) Å (Scheme 148).

3.15.3. Group 10 metals (Ni, Pd, Pt)

Attempts to crystallize the Ni complex **775** with a tetradentate (NH)$_2$(S)$_2$ ligand in DMF led to the binuclear complex **776** after 'CHO' insertion into the 'NH–Ni–NH' substructure followed by dehydration (Scheme 149). In a more rational and higher yielding approach, the range of complexes **776**, **777** and **778** were obtained in a one-pot

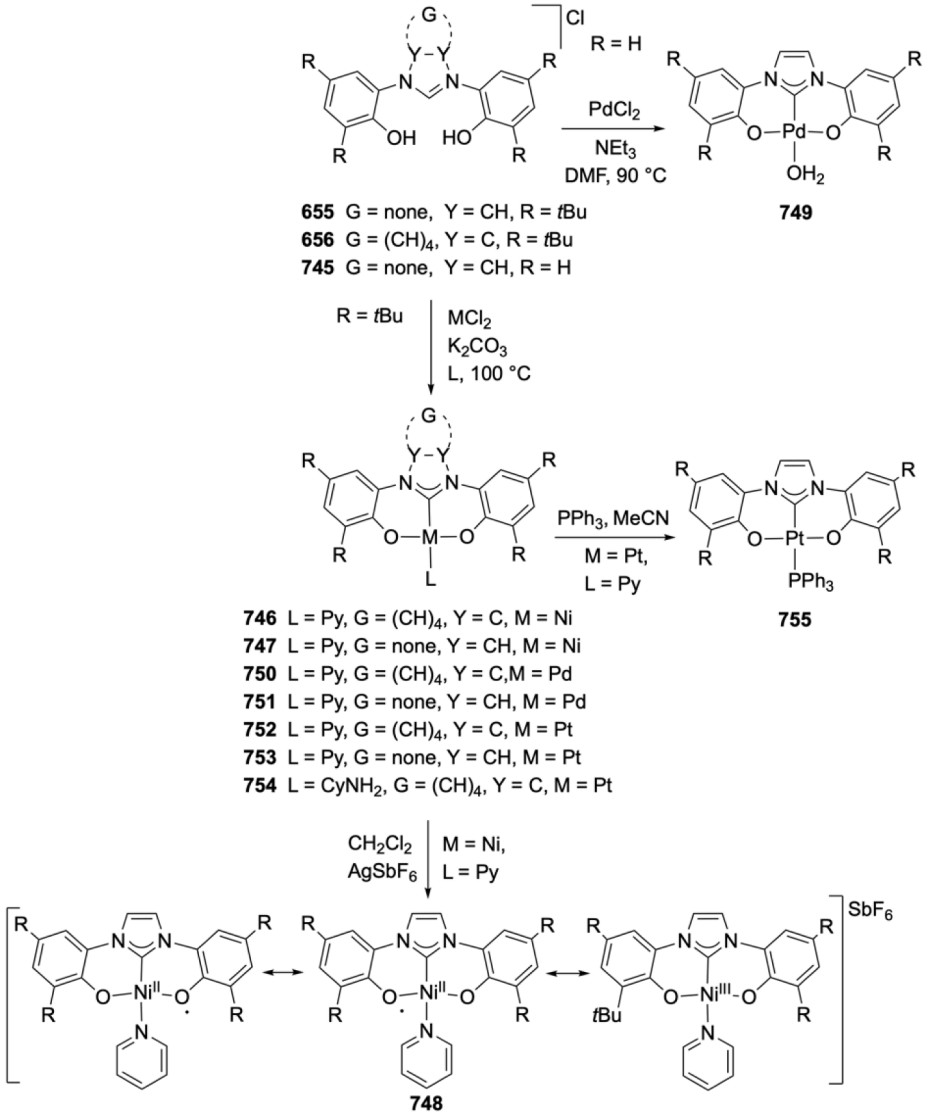

Scheme 145. Group 10 metal complexes with ligand backbones of types **XIIa** and **XIIb**

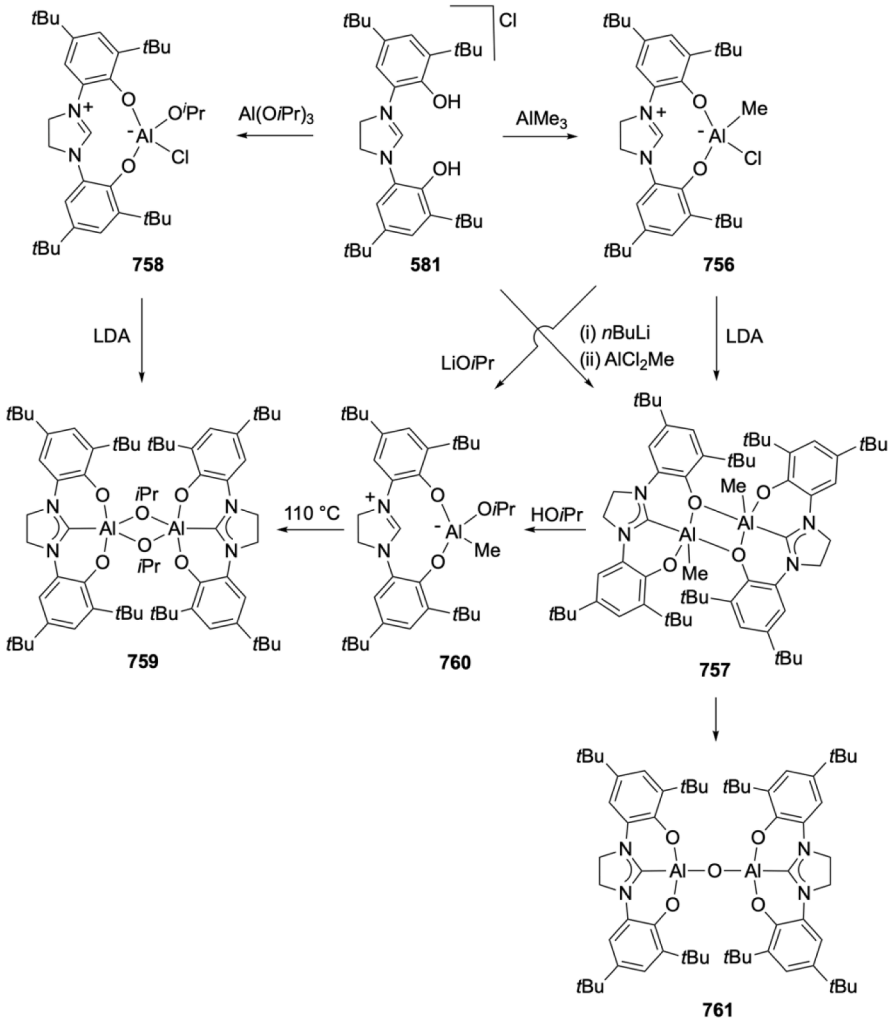

Scheme 146. Aluminum complexes with ligand backbone of type **XIIb**

reaction between the metal precursors $NiCl_2$ and $[MCl_2(COD)]$ (M = Pd, Pt), respectively, and 2 equivalents of $HC(OEt)_3$ at high temperatures (*ca.* 130–150 °C). Reactions of the binuclear complexes with the donor ligands PMe_3, PPh_3, pyridine or CN^- resulted in the symmetrical cleavage of the dimer and the formation of the diamagnetic adducts **779**–**785** that featured square-planar M centers (Scheme 149) [312–314]. The crystal structures of **776**, **779**, **782** and **785** were determined crystallographically unveiling rather short M−C^{NHC} bond distances (1.863(5), 1.903(6), 1.876(5) and 2.020(13) Å), respectively. The M−S distances were found in the normal ranges; all complexes show remarkable thermal stability and are inert to acids. The species **786**–**788** were characterized by NMR spectroscopies (Scheme 149).

The complex **790** was prepared by the reaction of **789** with $PdCl_2$ in DMF or by transmetalation from a non-isolated Ag complex formed *in situ* by treating **789** with Ag_2O, followed by reaction with $[PdCl_2(NCMe)_2]$ (Scheme 150). The crystal structure of **790** revealed a square-planar geometry around the palladium center, the Pd–C^{NHC} bond length in complex **790** was 1.947(5) Å, and the Pd–S bond lengths were 2.3060(12) and 2.3215(11) Å [315].

Finally, the complexes **797**–**799** were obtained in two steps: reaction of the precursors **791**–**793** with excess $[PdCl_2(COD)]$ in dichloromethane at room temperature resulted in the formation of the imidazolium complexes **794**–**796**, displaying in their ^{1}H NMR spectra an imidazolium-H resonance between δ 9.23 and 9.26 ppm. Subsequent reaction with Cs_2CO_3 in the presence of excess KPF_6 in refluxing acetonitrile afforded complexes **797**–**799**, which were characterized by the ^{1}H NMR spectroscopy. In addition, the complex **797** also could be synthesized by transmetalation from the silver NHC complex **800** with $[PdCl_2(COD)]$ and KPF_6 at room temperature (Scheme 151) [316].

4. Pincer ligand with two NHC donors

In this section only ligand designs with discrete terdentate κC^{NHC},κC^{NHC},κL donor set have been included; the donors may be part of a set in a ligand with potential denticity higher than three, provided that only three neighboring donors are bound to the metal, the remaining being dangling.

4.1. *Type C^{NHC},C^{NHC},C*

A group of palladium complexes bearing a pincer of type C^{NHC},C^{NHC}, C with all carbon donor set has been described (Scheme 152) [97]. Treatment of the bis-imidazolium phosphonium ylide precursor **801** with one equivalent of $[PdCl_2(NCMe)_2]$ in the presence of triethylamine resulted in the formation of complex **802** in 75% yield, which was characterized by NMR spectroscopy. In a subsequent step, **803** was formed almost quantitatively by the reaction of complex **802** with three equivalents of Cs_2CO_3 in MeCN at 60 °C. The complex **803** also could be obtained directly from **801** with $PdCl_2$ in the presence of Cs_2CO_3 in MeCN at 60 °C in 69% yield. The *ortho*-metalated complex **803** was characterized by NMR spectroscopy and X-ray diffraction analysis. Its ^{31}P NMR spectrum displayed a singlet at δ 30.4 ppm while the ^{13}C NMR

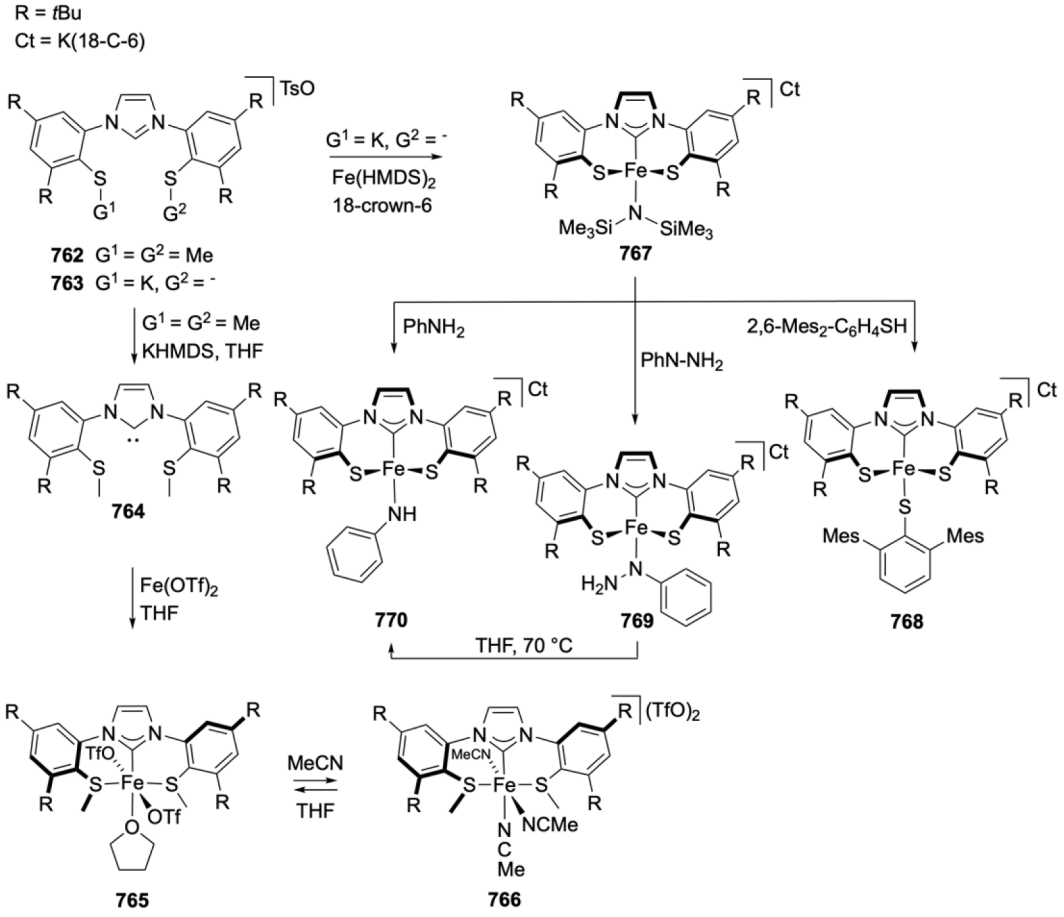

Scheme 147. Fe complexes with S,C^{NHC},S pincer ligands

spectrum revealed the corresponding CH ylide resonance at δ 17.3 ppm, with a coupling constant of 36.2 Hz, and the *ortho*-metalated carbon atom at δ 179.9 ppm. X-ray structure determination of **803** indicated that the Pd atom adopted a slightly distorted square-planar coordination geometry, defined by the two NHC donors, the phosphonium ylide and the *ortho*-phenylated moieties. The NHC–Pd bond distances in **803** of 2.018(2) Å and 2.003(5) Å were comparable to values found in related NHC Pd^{II} complexes. Reaction of complex **803** with one equivalent of TfOH in MeCN at −40 °C yielded complex **804** in 91 % yield. In the ^{31}P and the ^{13}C NMR spectra of complex **804** singlets at δ 33.9 ppm and δ 9.9 ppm were assignable to the ylide moiety, these data were consistent with the structure obtained. The complex **805** was formed by the reaction of complex **804** with *t*BuNC in dichloromethane and its structure was established by NMR and FTIR spectroscopies. Typically, diagnostic signals due to *t*Bu and the ν(C≡N) vibration (at 2206 cm^{-1}) were observed in the NMR and FTIR spectra, respectively. The complex **804**

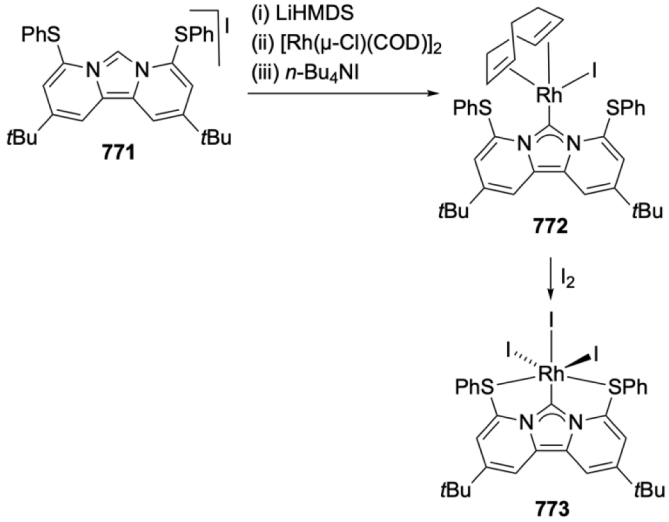

Scheme 148. Rh$^{I/III}$ complexes with the rigid S, C^{NHC}, S backbone

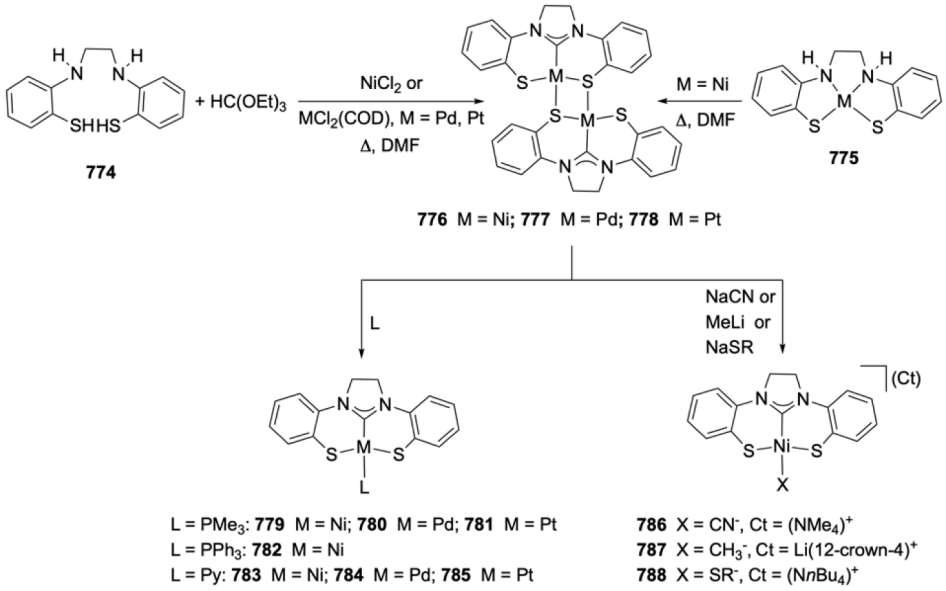

Scheme 149. Pd and Pt complexes with a S, C^{NHC}, S backbone

was efficient in the Pd-catalyzed allylation of aldehydes [97].

4.2. Type C^{NHC},C^{NHC},N

4.2.1. Group 8 metals (Fe)

The reactivity towards isocyanides of the iron complex **806**, bearing the tetradentate, equatorially binding bis(pyridyl-NHC) ligand with the $N^{pyridine}$,C^{NHC},C^{NHC},$N^{pyridine}$ donor set, was studied leading to complexes **807**–**810** with *mer*-pincer type terdentate κ$N^{pyridine}$,κC^{NHC},κC^{NHC} coordination and one dangling pyridine donor (Scheme 153A) [317]. The reactions of **806** were carried out with an excess of CNR (5 equivalents) in MeCN at room temperature. The ^{1}H NMR spectra of the products revealed characteristic resonances for the ortho protons of the pyridyl moieties at around δ 8.75 ppm and 8.30 ppm and the structures of **807**, **809** and **810** were determined by X-ray diffraction unveiling dangling terminal pyridine for all complexes, Fe–C^{NHC} bond distance with the central NHC donor in the range 1.869(4)-1.885(4) Å, and with the NHC donor attached to the dangling pyridine in the range 1.9460(19)-1.952 (4) Å; finally the isocyanides *trans* to the C^{NHC} and *trans* to each other fall within the same range (1.876(2)–1.904(4) Å). The isocyanide ligands had all an effect on the metal centered redox potential as established by CV.

Elongation of the linker in the tetradentate bis(pyridyl)-substituted-bis(imidazol-2-ylidene) ligand results in preferential adoption of *fac*-like coordination leaving two *cis*-sites in the octahedral complex available for catalytic studies. Thus, reaction of the related complexes **806A**-**806C** with NH_3 afforded the *cis*-ammonia complexes **810A**-**810C** which were studied as models of electrocatalysts for the oxidation of coordinated ammonia to nitrogen. The pyridine substitution in **806A**-**806C** altered the potential of the Fe^{II}/Fe^{III} couple within a wide range and resulted in the mono- or di-substituted ammonia complexes **810A**-**810C**. With electron releasing substituents at the pyridine rings, an equilibrium was established in MeCN between the mono- and di-substituted species. Furthermore, the acidity of the coordinated NH_3 in the Fe^{III} complexes was higher in **810A** than **810C** due to the substituent effects of the pyridine donor (Scheme 153B) [318].

The reaction of [Fe(HMDS)$_2$] and K(HMDS) with the ligand precursor **811** led to the complex **812** (Scheme 154) [319]. Crystallographic characterization revealed a six-coordinate Fe^{II} center ligated by two terdentate pincer strands bound in a *mer* fashion, two amide donors in the *cis* position and the remaining amide groups dangling. The Fe–C^{NHC} and Fe–N^{amide} distances were within 1.917–1.929 and 2.032–2.040 Å, respectively. The Mössbauer spectra support an octahedral low-spin ($S = 0$) Fe^{II} center.

4.2.2. Group 9 metals (Co)

The Co^{III} complex **815** bearing a C^{NHC},C^{NHC},N-terdentate ligand was synthesized in low yield *via* complex **814** which in turn was obtained by transmetalation between [$CoCl_2(PPh_3)_2$] and the silver carbene complex generated *in situ* from **813** and Ag_2O (Scheme 155). The structure of **815** was confirmed by X-ray diffraction analysis and NMR spectroscopy. However, **814** was not stable in solution, and easily converted to **815**, as monitored by NMR spectroscopy. The ^{1}H NMR spectrum of complex **815** displayed two doublets assignable to the CH_2 linkers at δ 6.73 and 6.40 ppm, respectively. All data indicated the formation of the complex **815** [144].

4.2.3. Group 10 metals (Pd)

The only palladium complex in this category **817** was prepared in low yield by treatment of the precursor **816** with [$PdCl_2(NCMe)_2$], followed by anion exchange (Scheme 156) [320]. The structure of **817** was established by NMR spectroscopy and X-ray diffraction analysis. The

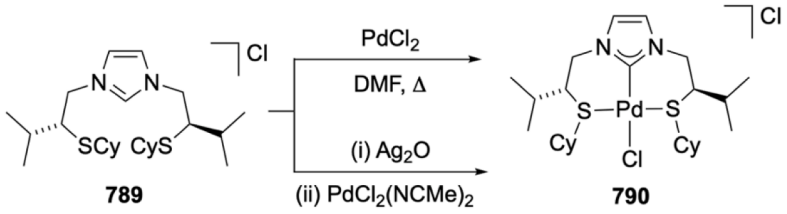

Scheme 150. Pd complex with a flexible S, C^{NHC},S backbone

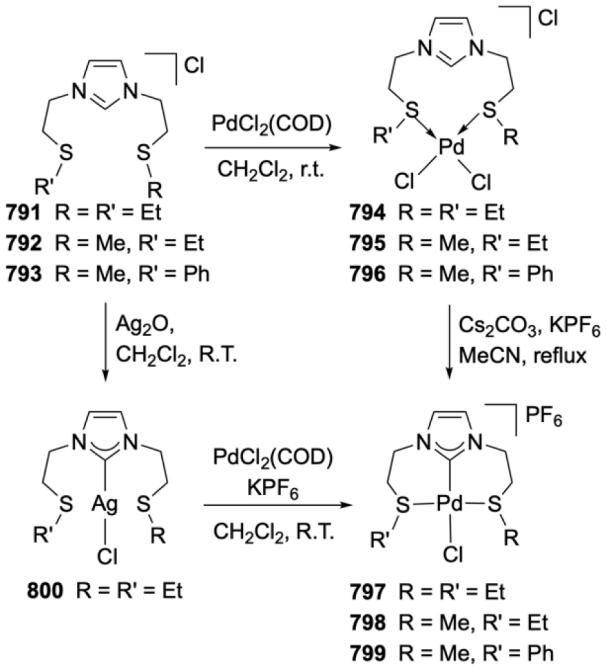

Scheme 151. Pd complexes with a flexible S, C^{NHC}, S ligand

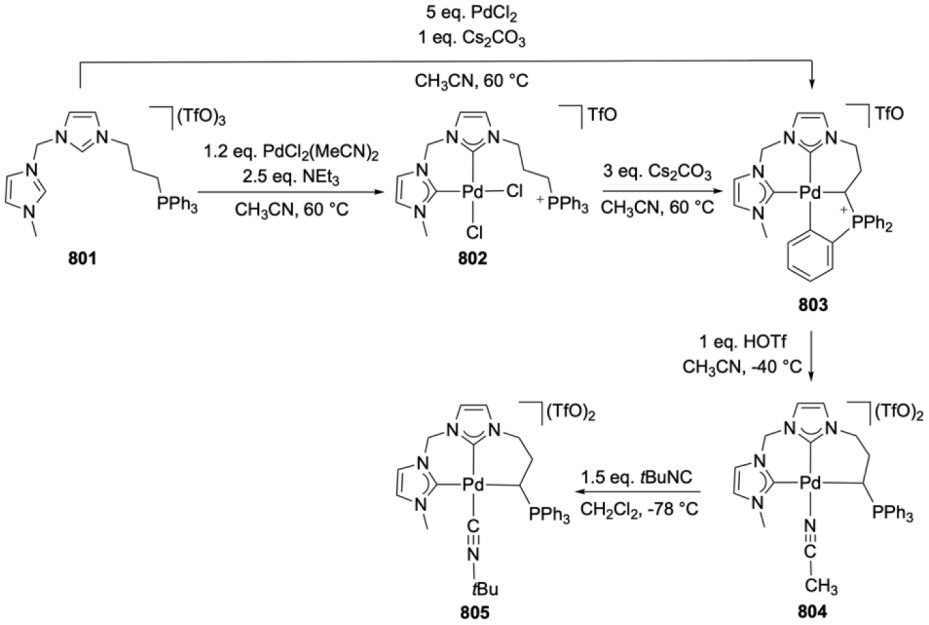

Scheme 152. Pd complexes with a κC^{NHC}, κC^{NHC}, κC backbone.

two stereoisomers (*P*- and *M*-) were obtained owing to the twisted conformation of the $C^{NHC}C^{NHC}N$ pincer ligand and were observed in the ^{1}H NMR spectrum. However, only the *P*-isomer was observed in the solid state: the X-ray structure featured a Pd–N bond distance of 2.109(3) Å. The stable complex **817** was an efficient, high turnover number catalyst for Suzuki-Miyaura cross-coupling reactions in water [320].

4.3. Type C^{NHC},C^{NHC},*P*

There is no example in this category, to the best of our knowledge.

4.4. Type C^{NHC},C^{NHC},*O*

C^{NHC},C^{NHC},O donor ligands on Ru centers were studied in conjunction with the search for analogues of the Grubbs-Hoveyda catalysts based on pincer ligands. Complexes **822** and **823** were prepared by transmetalation reactions from the silver complexes **820** or **821** to ruthenium using $[RuCl_2(PPh_3)_3]$ or $[RuCl_2(=CHPh)(PCy_3)_2]$ as precursors, respectively (Scheme 157) [321–323]. Complexes **822** and **823** were characterized by X-ray diffraction analysis which revealed octahedral coordination geometries around the ruthenium centers. The corresponding Ru–O bond distances for **822** and **823** were 2.295(6) and 2.4852(11) Å, respectively, which are similar to those previously reported for relevant ruthenium complexes and confirm the coordination

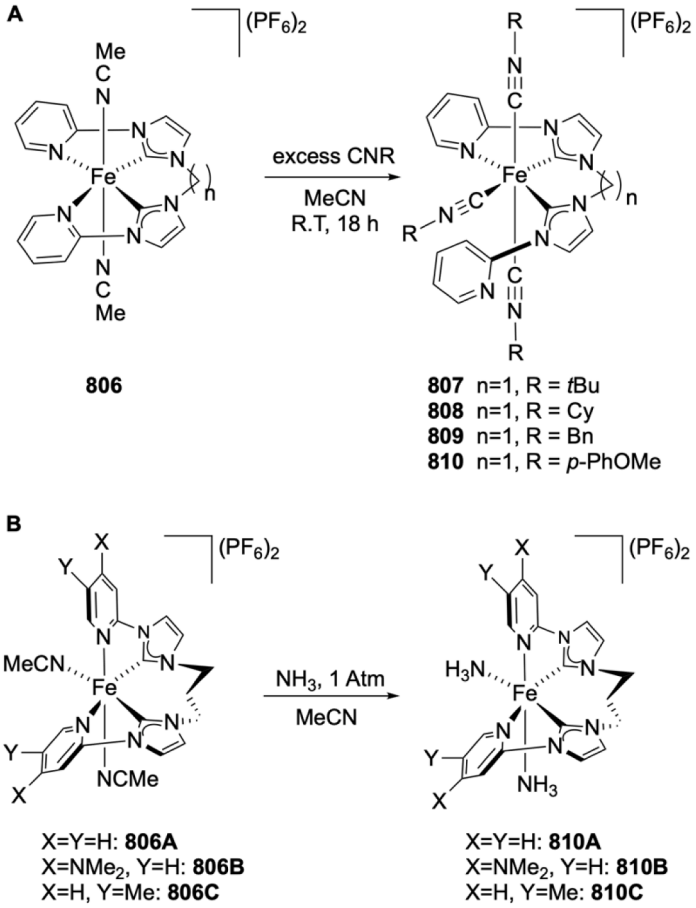

Scheme 153. *mer*-Fe complexes showing hemilability of the tetradentate N, C^{NHC}, C^{NHC}, N backbone (**A**); *fac*-Fe NH_3 complexes studied as potential electrocatalysts for NH_3 oxidation

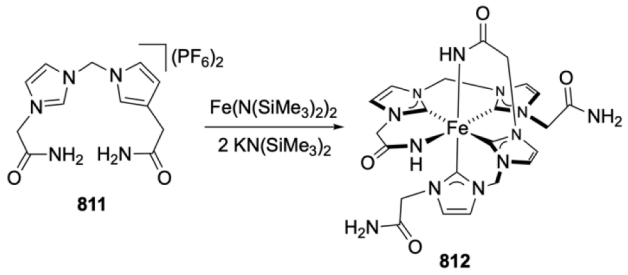

Scheme 154. Fe complex with ligand backbone κN, κC^{NHC}, κC^{NHC}

of the OMe group to the metal. Their catalytic performance in standard metathesis reactions was not satisfactory.

4.5. Type C^{NHC},C^{NHC},S

No example with this donor set has been reported to the best of our knowledge.

5. Pincer ligands with three NHC donors

In this class only ligand designs with discrete terdentate $\kappa C^{NHC},\kappa C^{NHC},\kappa C^{NHC}$ donor set have been included; the donors may be part of a set with denticity potentially higher than three, provided that only three neighboring donors are bound to the metal, the remaining being dangling.

5.1. C^{NHC},C^{NHC},C^{NHC}

5.1.1. Group 8 metals (Fe, Ru)

A series of iron and ruthenium complexes bearing a C^{NHC},C^{NHC},C^{NHC}-terdentate ligand substructure as part of a linear tetradentate ligand design has been described (Scheme 158) [324,325]. Reaction of **824** with $[Fe\{N(SiMe_3)_2\}_2(THF)]$ in acetonitrile afforded a mixture of complexes **825** and **826**, which could not be separated by precipitation or selective extraction [324]. However, in the presence of protic reagents, the complex **825** was converted to **826**, the structure determination of which revealed an iron center in an octahedral coordination geometry with a *mer*-C^{NHC},C^{NHC},C^{NHC} moiety as part of a potentially tetradentate ligand, with one dangling imidazolium moiety. Fe–C^{NHC} bond distances of 1.900(3)–1.989(3) Å were observed, which were comparable to literature values for this bond. The Fe–N_{MeCN} bond distances in **826** were 1.931(3) and 1.986(3) Å.

Stirring a mixture of **824**, Ag_2O and $[Ru(\mu\text{-}Cl)Cl(p\text{-cymene})]_2$ in

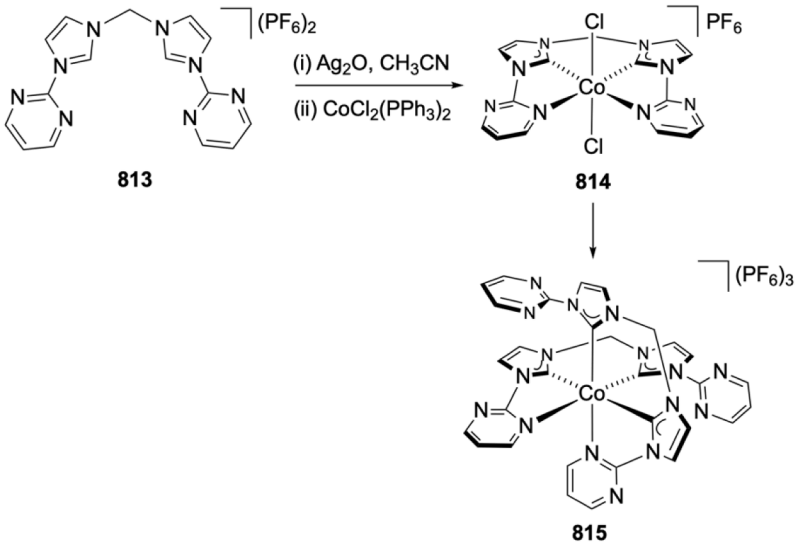

Scheme 155. Co complex **815** with κC^{NHC}, κC^{NHC}, κN terdentate ligand.

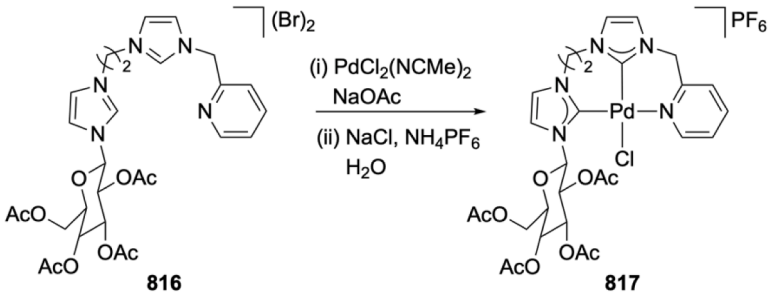

Scheme 156. Pd complex with a κC^{NHC}, κC^{NHC}, κN terdentate ligand

acetonitrile under microwave irradiation resulted in the formation of a mixture of complexes **827** and **828** (Scheme 159) [325]. The complex **827** was purified by column chromatography and isolated in 20 % yield. Interestingly, the presence of the imidazolium moiety in complex **827** was most likely due to the formation of water *in situ*; **827** could be quantitively converted into **828** in the presence of Cs_2CO_3 as a base. A characteristic singlet at δ 8.45 ppm was observed in the ^{1}H NMR spectrum of **827**, which was attributed to the imidazolium moiety. In addition, two different resonances at δ 3.83 and 3.90 ppm for the terminal methyl groups also were observed in ^{1}H NMR spectrum. The X-ray structure analysis unveiled a distorted octahedral coordination geometry of the Ru in **827**, and Ru–C^{NHC} distances in the range 1.998(2)-2.062 (2) Å, consistent with literature values [326,327].

Treatment of the salt **829** with Ag_2O followed by reaction with [Ru(μ-Cl)Cl(*p*-cymene)]$_2$ yielded the air stable complex **830**, which was isolated as a yellow solid in 40 % yield (Scheme 160) [139], the structure of which was confirmed by X-ray diffraction analysis and NMR spectroscopy. The ^{1}H NMR spectrum showed a singlet for the two terminal methyl groups of the triazolylidene at δ 4.20 ppm, and a single resonance for the methylene groups at δ 5.33 ppm. The ^{13}C NMR

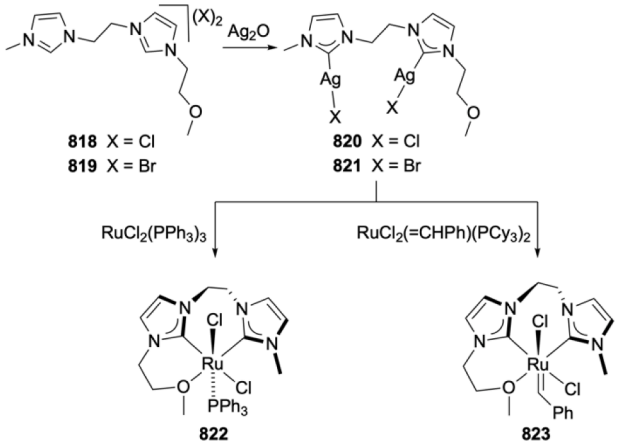

Scheme 157. Ru complexes with κC^{NHC}, κC^{NHC}, κO donor ligands

spectrum revealed two characteristic signals for the carbene carbon atoms at δ 172.6 and 185.3 ppm. The Ru center adopted an octahedral coordination geometry with Ru-$C^{imidazolylidene}$ distance of 2.015(5) Å. Interestingly, the Ru–$C^{triazolylidene}$ distances of 2.091(4) and 2.096(4) Å were longer than in most abnormal triazolylidene ruthenium(II) complexes. The complex **830** displayed a catalytic activity for ketone reduction *via* transfer hydrogenation reaching 98 % conversion [139].

5.1.2. Group 10 metals (Pd)

The pincer complex **832** was obtained as a red, air stable solid by treatment of tris-azolium precursor **831** with palladium acetate in MeCN at 100 °C (Scheme 161). The ^{13}C NMR spectrum of **832** features two C^{NHC} signals in a 2:1 ratio at d 157.3 ppm (triazolylidene) and δ 165.5 ppm (imidazolylidene) consistent with a *mer*-coordination of the pincer ligand. The molecular structure of **832** comprised one slightly distorted square-planar Pd center with one κC,κC,κC pincer and one iodine ligand. Interestingly, the Pd – $C^{imidazolylidene}$ bond distances range from 2.000(6) to 2.010(6) Å while the Pd-$C^{triazolylidene}$ bond distances are slightly longer (2.037(5) – 2.053(5) Å). The elongation of the latter has been attributed to the flexibility of the methylene linker and the mutual *trans* placement of the two triazolylidene ligands. Treatment of **832** with an excess of $AgSbF_6$ furnished **833** which shared similar spectroscopic and metrical data as **832**. Complexes **832** and **833** were active under low catalyst loadings in cross-coupling reactions showing high conversions under mild reaction conditions and in the hydrosilylation of terminal alkynes with good selectivity toward the *E*-isomer [328].

6. Computational studies

Quantum chemical calculations have developed to indispensable tools for gaining insights into the molecular structure of metal complexes (with examples covered in this review [32–37,116], or relevant organometallic and inorganic topics), by providing reliable models of electronic structures and bonding. As a consequence, magnetic, (photo)physical and spectroscopic properties, *e.g.* spin states, absorption or emission electronic, IR, EPR and NMR spectra can be extracted, in good agreement with the experiment. Furthermore, the computed representation of the frontier molecular orbitals can contribute towards the rationalization of stoichiometric or catalytic reactivity and the underlying mechanisms. Despite the widespread availability of 'user-friendly' software packages for *ab initio*, DFT or semi-empirical calculations and the diminishing computing costs, pitfalls and errors can arise from the usage of this methodology by non-experts, mainly due to partial misunderstanding, possible erratic choice of technical settings and/or of details and other aspects of the calculations [329]. In this section, after a brief exposition of the relevant computational methodologies, and judicious strategies for their application, we highlight and group together their successful usage to elucidate, understand and compare aspects of the chemical, structural and physical properties of pincer complexes with a bridgehead NHC donor described in the previous sections.

By far, the most extensively employed methodology in the topics

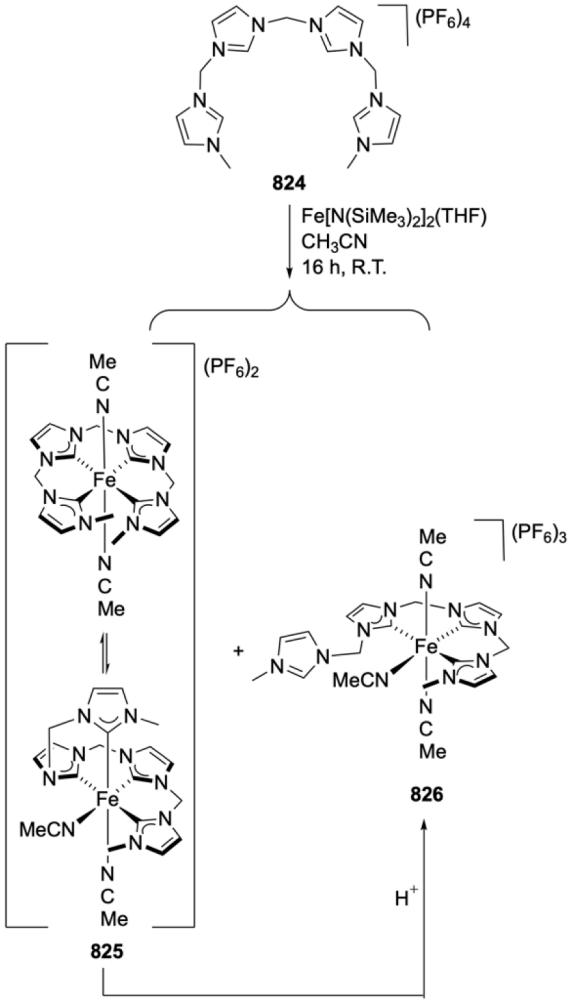

Scheme 158. Fe complexes with a κC^{NHC}, κC^{NHC}, κC^{NHC} terdentate ligand

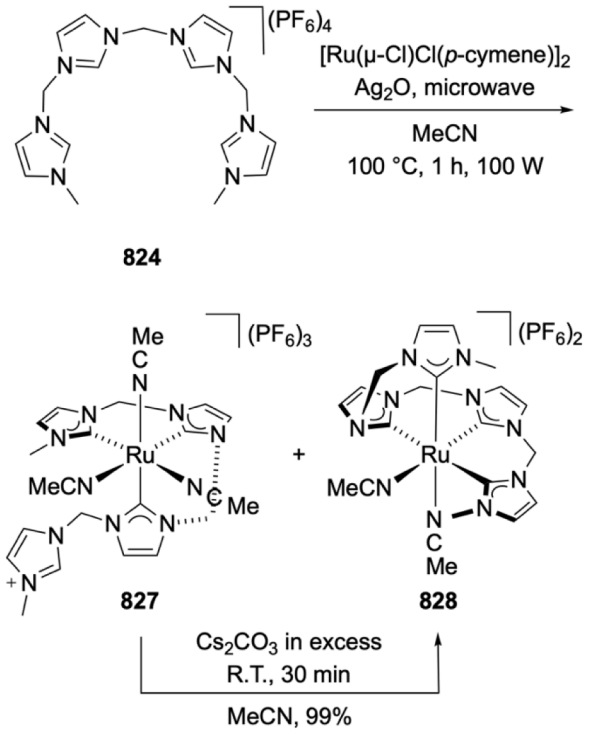

Scheme 159. Ru complexes with a κC^{NHC},κC^{NHC},κC^{NHC} terdentate ligand.

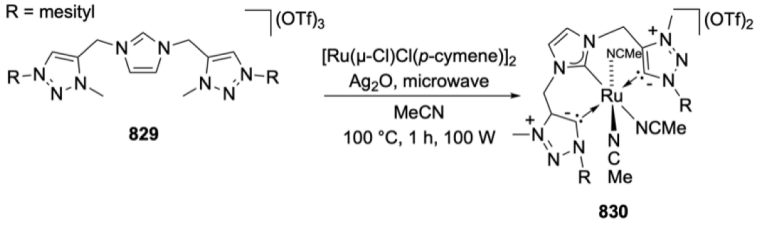

Scheme 160. Ru complex with ligand backbone κC^{NHC}, κC^{NHC}, κC^{NHC}

described above is the 'researcher-friendly' DFT, in view of its speed and the generally accurate results it provides, if used cautiously. The thoughtful choice of functionals and basis sets are crucial; functional-dependent results can occasionally be obtained, where spin-state changes, very thick group of excited states and dominant van der Waals interactions are encountered. The recommended way out of this state of affairs involves preliminary investigation(s) with different combinations of functionals and basis sets aiming at obtaining data on the (ground state) geometry, which subsequently should be compared with the one obtained with accurate multireference techniques (*vide*

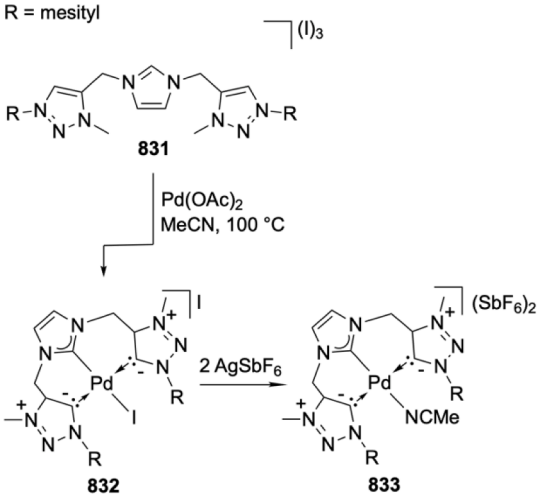

Scheme 161. Pd complexes with ligand backbone κC^{NHC}, κC^{NHC}, κC^{NHC}

Table 6
Publications on pincer complexes with NHC bridgehead donors that include computational studies.

Complex	Ligand type/Metal/ Scheme	Summary of Computational Methodology	Type of study[a]	Reference
1	C,C^{NHC},C/Ru/3	DFT(B3LYP)/6-31G(d,p)	M	[63]
5	C,C^{NHC},C/Ru/4	DFT(B3LYP)/6-31G(d,p) LANL2DZ	M	[65]
35	C,C^{NHC},C/Ir/11	DFT(B3LYP)/SDD_{Ir}6-311 + G(d,p)/$LANL2DZ_{Ir}$6-31G(d)	M	[76]
43, 44	C,C^{NHC},C/Ir/12	DFT(ω-B97XD)/6-31G(d) LANL2DZ	M	[78]
68	C,C^{NHC},N/Pd/18	DFT(M06)/6-31G(d) LANL2DZ	M	[88]
74a 74b	C,C^{NHC},P/Rh/20A	DFT(ωB97XD)/DGDZVP	M	[91]
75b	C,C^{NHC},P/Ni/20B	DFT(ωB97XD)/6–31 + G(d,p) SDD	M	[56]
81, 82, 83	C,C^{NHC},O/Pd/22	DFT(PBE-D3)/6-31G(d,p)/$LANL2DZ_{Pd}$	E	[97]
85	C,C^{NHC},S/Pd/23	DFT(PBE)/ZORA-TZ	E	[98]
114–117	N,C^{NHC},N/Ta/29	DFT(B3LYP)/$LANL2DZ_{Ta}$ 6-31G(d,p)	E M	[102]
127	N,C^{NHC},N/Fe/33	DFT(B3LYP)/def2-TZVP def2-SV(P)	E	[111]
130, 131	N,C^{NHC},N/Fe/34	DFT & BS-DFT(UB3LYP)/def2-TZVP	E	[116]
136, 141	N,C^{NHC},N/Ru/34–36	DFT(M06-L)/TZVP/TZVPFit, QZVP	M	[117,118]
149, 150	N,C^{NHC},N/Pt/38	DFT(B3LYP)/LANL2DZ	E	[139]
178, 179	N,C^{NHC},N/Rh, Ir/48	DFT(B3PW91)	E	[149]
186, 187	N,C^{NHC},N/Ni/50	DFT(B3LYP)/6–31 + G(d,p)	M	[54]
202, 203	N,C^{NHC},N/Ni/54	DFT(RPBE0)/def2-TZVP	M	[159]
253, 257	N,C^{NHC},N/Ge/66	DFT(MN15-L)/def2-TZVPP$D_{Ge,1}$def2-SVPD	M	[175]
329, 331	P,C^{NHC},P/Mo/80	DFT(B3LYP)/$LANL2DZ_{Mo}$6-311G	E	[193]
354, 356, 358	P,C^{NHC},P/Mo/83	DFT(B3LYP-D3)/SDD_{Mo} 6-31G(d)	E M	[202]
384–387	P,C^{NHC},P/Fe/88	DFT(PBE0-D3BJ)/SDD	E M	[213,215]
409, 410	P,C^{NHC},P/Fe/90	DFT(OPBE)/def2TZVPP 6–311 + G(d,p)	M	[219]
429	P,C^{NHC},P/Ru/92	DFT(M06-L)/def2-SVP NBO:M06L/def2TZVP/W06	E M	[222]
445, 448	P,C^{NHC},P/Ir/96	DFT(M06-L)/SDD_{Ir}6-311 + G(d,p)	E M	[226]
511, 512	P,C^{NHC},P/Ni/105	DFT(BP86)/TZP	M	[247]
516, 517	P,C^{NHC},P/Pd, Pt/111	DFT(B3LYP)/LANL2DZ	E	[251]
523–526	P,C^{NHC},P/Pd, Pt/112	DFT(B3LYP)/LANL2DZ	M	[252]
528–531	P,C^{NHC},P/Ni/113	DFT(B3LYP)/LANL2DZ	E M	[252]
588 592 594	O,C^{NHC},O/Ti/121	DFT(PBE-D3(BJ))/	M	[268]
605–607	O,C^{NHC},O/Ti/123	DFT(B97D)/SDD	M	[52]
715	O,C^{NHC},O/Fe/139	DFT(BP86, B3LYP and TPSSh)/ZORA-def2-SVP ZORA-def2-$TZVP_{Fe}$ CASSCF, NEVPT2/ZORA-def2-TZVPP	E	[291]
723, 728, 730	O,C^{NHC},O/Co/141	DFT(BP86-D3)/def2-TZVP	E	[293]
741 (simplified)	O,C^{NHC},O/Ir/143	DFT(BVP86)/SDD LANL2DZ	E	[299]

[a] Studies have been grouped as regarding the electronic structure and relevant properties (E) or the computed mechanism of a reaction (M).

infra) and/or experimental data. Although DFT methods generally calculate the ground state geometry accurately, they may fail to do so for excited states.

Consequently, the popular *B3LYP functional* [330,331] provides good results on geometry and can correctly predict absorption spectra; furthermore, if dispersion correction is necessary, it can be properly added, *via* semiempirical corrections, like Grimme's -D3 [332]. Lately, the Minnesota family of functionals, M06 and M06-L [333] have become very popular as alternative choices for metal complexes and pincers in particular. Despite the fact that they lack any dispersion built-in, the M06-L performs well as a local functional in transition metal chemistry and with noncovalent interactions at a relatively low computational cost. Lastly, the family of long-range corrected hybrid functionals wB97, wB97X, wB97X-D, wB97X-2 include a full Hartree-Fock exchange at long-range interelectron distance, resulting in a reduction of the self-interaction errors; they are suitable for general applications, such as thermochemistry, thermal kinetics, noncovalent systems, and calculation of spectra *via* time-dependent DFT [334]; PBE0 [335] is another choice that predicts metrical parameters for complexes.

With respect to the *basis sets*, an augmented double zeta quality basis set is appropriate for large complexes of about 100–150 atoms. For instance, the 6–31 + G(d,p) family of basis sets [336] combined with a basis set including pseudopotential such as LANL2DZ for the metals [337], or the Def2-SVP [338] for all atoms is a good choice. For smaller

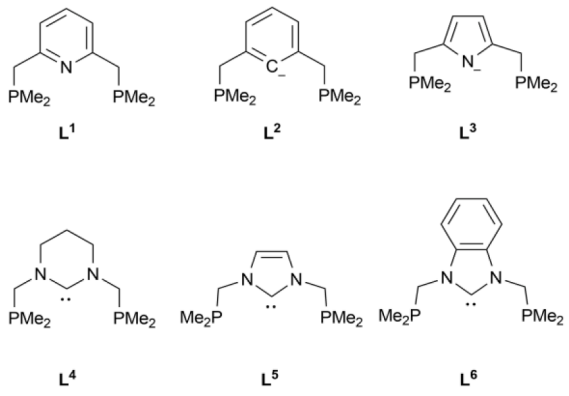

Chart 9. Six simplified pincer architectures that have been used for the preliminary DFT calculations, described above.

complexes an augmented triplet quality basis set is an excellent choice, for instance the def2-TZVP [338] or aug-cc-pVTZ(-PP) [339,340].

Finally, when the calculated states of the complexes feature diradical or open singlet states, DFT is combined with the *broken-symmetry (BS) method*. BS-DFT works quite well for the prediction of the geometry of complexes involving multiple transition metals. However, it describes a weighted average over multiplet states resulting in a non-efficient calculation of the correlation energy of very multireference systems. Accordingly, BS is widely used in the field of molecular magnetism for the calculation of exchange coupling constants [341,342] and can reproduce the experimental trends and yield insights into the operating exchange mechanisms, especially in metal-metal and metal-ligand transfer terms [343]. In contrast, for complexes presenting a very dense spectrum, BS-DFT will not be efficient and may predict wrongly the exchange couplings [332,344,345]. In this case, the geometries are to be calculated *via* an appropriate combination of functional and basis set (*vide supra*), and the electronic structures *via* a multireference *ab initio* methodology. A very good choice of the latter is the complete active space self-consistent field method (CASSCF) [346], followed by the second-order perturbation treatment (CASPT2), or by a second-order perturbation treatment of the dynamic electron correlation (NEVPT2 [347]). Finally, the *ab initio* ligand field theory (AILFT) [348] method allows to calculate all ligand field parameters and it is used widely in the areas of magnetism and *d-d* absorption spectroscopy, allowing the interpretation and prediction of exciting spectroscopic and magnetic properties [349].

The *population analysis* can provide useful information on bonding. Mulliken population analysis is extensively used, mainly because it is the default analysis in many computational packages, however, it is well-known that Mulliken charges may show basis set dependency or underestimate ionic character [350,351]. Alternatively, the natural population analysis (NPA) method can be used, which is generally basis set independent, but, on the contrary, may overestimate the ionic character of the atoms [352,353]. However, it is believed that population analyses are indicative and help to make comparisons and find trends for similar structures within the same methodology. For instance, the use of natural charges obtained *via* DFT explains the electronic structure of **429** and proposes a zwitterionic non-carbenoid ligand structure as the most plausible description of **429** [222].

Solvent effects can be added *via* dielectric constant (implicit model) [354], as molecules (explicit model), or *via* both dielectric constant and as molecules (hybrid model). In the latter case, the first solvation sphere is studied explicitly and the rest of the solvent implicitly. Generally, the implicit treatment does not significantly affect the geometry or the spectra while the inclusion of one or more solvent molecules in the right position, or the inclusion of the first sphere of solvation at the same computational level or *via* a multi-scaling methodology may affect the outcome [355]. In general, preliminary calculations should be carried out to reveal if the electrostatic interactions with a noncoordinating solvent or solid-state environment affect the spectral properties of the complexes [356] and then a decision should be made regarding how the solvent will be added, *i.e.* implicitly, explicitly or *via* a hybrid model.

In view of this methodological summary, we highlight a few selected cases, where computational approaches have provided a detailed insight of electronic structures and reactivity. A complete compilation of computational studies in the literature covered in the review is given in Table 6.

The plot of the energies of frontiers molecular orbitals (Fig. 2) provided useful information on the parameters controlling the σ-donor/π-acceptor/π-donor characteristics of the NHC bridgehead donors and other NHC co-ligands (if present). A guided choice of the NHC types to manipulate the HOMO-LUMO gap and, consequently, the donor properties of the bridgehead are important to consider in ligand design [32,33].

Analysis of the nature of the computed orbitals in addition to the calculation of the differences in atomic charges (Δq, obtained by NPA (*vide supra*) and the Mayer bond orders) provided a detailed mapping of the σ- and π-interactions of two related pincer ligands (PCP and PNP) on a Mo center with catalytic activity towards N_2 reduction (in **354** and **358**, respectively), explained the catalytic longevity of **354** and rationalized the stronger activation of coordinated N_2 in **354** [38,202].

DFT studies (spin-unrestricted using B3LYP/def2-TZVP, THF solvent model) provided detailed insight (complex geometries, nature and energies of MOs, nature of the metal – ligand bonding from charge donation and Mayer bond orders and overall strength of ligand binding) in a series of structurally related Fe^{II}-pincer complexes with NHC bridgehead or NHC side-arm moieties; a direct correlation was found between increasing the strength of Fe – L bonding and the pincer-donating abilities [61].

DFT calculations (B3LYP/BS1 level on simplified models) were used to elucidate the mechanism of the metala-aziridine formation in the complexes **114**–**116**; from the two models studied, *i.e.* either a σ-bond metathesis pathway or a two-step C–H abstraction/alkylidene-mediated C–H activation pathway, the gathered evidence pointed to the likelihood of the latter. In addition, the energetic stabilization of the metala-aziridine species in **114**–**117** (Scheme 29) was studied by NBO analysis of the metal-ligand (NHC and alkyls) bonding in the complexes, concluding that it is due to the facilitation of preferred (shorter) Ta–NHC and Ta–methyl bonding interactions [102].

Computational studies (DFT, B3LYP, 6–31 + G**) have been carried out to rationalize the lack of N^{imine},C^{NHC},Ni^{mine} formation from the reaction of the precursor **185** with [Ni(1,5-COD)$_2$]; in this case analysis involving the energetics of plausible intermediates concluded that the observed reactivity can be traced back to ligand rigidity and steric restrictions [54].

A comparative study of the electronic properties of $PC^{NHC}P$ and $PN^{pyridine}P$ ligands on Ir that formed efficient catalysts for the hydrogenation of CO_2 to formates in the presence of triethanolamine was extended to computational methods (M06L level using SDD basis sets for transition metals and 6–311 + G** basis sets for all light elements and NBO analysis), in order to get insight into the nature of the pincer-Ir bonding and rationalize the higher activity and longevity of the $PC^{NHC}P$ complex **442**. The improved reactivity of the $PC^{NHC}P$ complex was attributed to the stabilization of the cationic key transition state due to the higher electron-donating nature of the ligand; in the Ir^{I} ground state, strong π back-donation as well as σ donation exists that made the catalyst robust [226].

7. Catalytic applications

Although we have indicated in the text specific examples of catalytic applications, an overview of the major catalytic applications of the complexes covered in this review are presented in a tabular manner for convenience and conciseness. Valuable comparisons between systems originating from different groups are almost impossible to make in view of the various experimental conditions used. The reader interested in a specific catalytic reaction will find below which metals and complexes have been reported to display catalytic activity, as well as the section in this review where these complexes are discussed and the original references which should be consulted.****

Hydrogenation of C–C bonds (H_2)

Metal	Complex	Section	Reference
Ru	8	3.1.1	[66–68]
Rh	178	3.6.6	[149]
Ir	179	3.6.6	[149]
Mn	360C	3.10.2	[204]

**** A very recent review of the catalytic applications of RE-NHC complexes is cited at the end of the document in the Note added in proofs.

Hydrogenation of C–O bonds (H_2, silanes)

Metal	Complex	Section	Reference
Ru	**138**	3.6.5	[118]
Cu	**245A, 245B**	3.6.8	[172]
Mn	**265–266**	3.7.1	[176]
Ir	**442,445–446,449**	3.10.4	[226]

Transfer hydrogenation – Hydrogen borrowing reactions (not H_2 as hydrogen source)

Metal	Complex	Section	Reference
Mn	**361B, 361C**	3.10.2	[205]
Ru	**70**	3.3.1	[89]
Ru	**152**	3.6.5	[140]
Ru	**154**	3.6.5	[141]
Ru	**150**	3.6.5	[126]
Ru	**374**	3.10.3	[211]
Rh	**178**	3.6.6	[149]
Ir	**179**	3.6.6	[149]
Ru	**830**	5.1.1	[140]

C–H activation

Metal	Complex	Section	Reference
Pd	**309**	3.8.2	[188]

H/D exchange

Metal	Complex	Section	Reference
Fe	**384**	3.10.3	[214]

C–C coupling (Heck)

Metal	Complex	Section	Reference
Pd	**306**	3.8.2	[187]
Pd	**490**	3.10.5	[248]
Pd	**749**	3.13.8	[187]
Pd	**315**	3.8.2	[189]

C–C coupling (Suzuki-Miyaura)

Metal	Complex	Section	Reference
Ni	**189**	3.6.7	[151]
Ni	**228–229**	3.6.7	[162]
Ni	**219–225**	3.6.7	[161]
Pd	**230**	3.6.7	[151]
Pd	**236**	3.6.7	[163]
Pd	**243**	2.6.7	[165]
Pd	**315**	3.8.2	[189]
Pd	**817**	4.2.3	[320]

C–C coupling (Kumada-Corriu)

Metal	Complex	Section	Reference
Co	**166**	3.6.6	[144]
Ni	**189**	3.6.7	[151]
Ni	**228–229**	3.6.7	[162]
Ni	**197–198**	3.6.7	[158]
Ni	**192–193**	3.6.7	[157]

Allylation of aldehydes

Metal	Complex	Section	Reference
Pd	**82**	3.4.2	[97]
Pd	**804**	4.1	[97]

Arene C–H trifluoromethylation

Metal	Complex	Section	Reference
Co	**732**	3.13.7	[298]

Dimerization of terminal alkyne

Metal	Complex	Section	Reference
Fe	**56**	3.2.1	[23,83,85]
Fe	**384**	3.10.3	[214]

Addition of styrene derivatives

Metal	Complex	Section	Reference
Ir	**36**	3.1.2	[76]

Addition of amines to unsaturated C – C bond

Metal	Complex	Section	Reference
Rh	**170–171**	3.6.6	[147]
Ir	**173**	3.6.6	[147]
Pd	**499, 501**	3.10.5	[249]
Zr	**631–632**	3.13.2	[271]

Imidization

Metal	Complex	Section	Reference
Ru	**370–371**	3.10.3	[209]

Amidation

Metal	Complex	Section	Reference
Ru	**719–721**	3.13.6	[292]

Chan-Lam coupling

Metal	Complex	Section	Reference
Cu	**246, 248–249**	3.6.8	[173,174]

Buchwald-Hartwig amination

Metal	Complex	Section	Reference
Pd	**525–526**	3.10.5	[252]

Hydrocarboxylation

Metal	Complex	Section	Reference
Rh	**170–171**	3.6.6	[147]
Ir	**173**	3.6.6	[147]

Hydrosilylation of terminal alkynes

Metal	Complex	Section	Reference
Rh	**170**	3.6.6	[147]
Rh	**452–454**	3.10.4	[228]
Pd	**832**	5.1.2	[328]
Pd	**833**	5.1.2	[328]

Hydrosilylation of carbonyl compounds and nitroaromatics

Ni	**489D 489E**	3.10.5	[49]

Hydroboration of Alkynes

Metal	Complex	Section	Reference
Fe	**384**	3.10.3	[214]

Isomerization of terminal alkenes

Metal	Complex	Section	Reference
Fe	**387**	3.10.3	[215]

Olefin isomerization

Metal	Complex	Section	Reference
Ir	**36**	3.1.2	[76]

Oxidation of alcohols and benzaldehydes

Metal	Complex	Section	Reference
Ru	**146**	3.6.5	[119]
Ru	**291**	3.8.1	[184]

Oxidation of water

Metal	Complex	Section	Reference
Ru	**282**	3.8.1	[181]
Ru	**284–286**	3.8.1	[182]
Ru	**287–288**	3.8.1	[183]

Reduction

Metal	Complex	Section	Reference
Ni (H^+ to H_2)	**326, 327**	3.9.1	[191]
Mo (N_2 to NH_3)	**348, 350**	3.10.1	[201]
Mo (N_2 to NH_3)	**354, 356**	3.10.1	[38]
Mo (Nitroarenes)	**700, 701**	3.13.4	[290]

Oligomerization of alkenes

Metal	Complex	Section	Reference
Cr (ethylene)	**124–125**	3.6.3	[105]
Ni (ethylene)	**213–214**	3.6.7	[105]
Zr (1-hexene)	**642**	3.13.2	[273]

Polymerization of alkenes (A) and lactide (Lac), Copolymerization

Metal	Complex	Section	Reference
Fe (Lac)	**129**	3.6.5	[115]
Ni (A, norbornene)	**295–297**	3.8.2	[185]
Pd (A, norbornene)	**301–304**	3.8.2	[186]
Nd (Lac)	**545, 551**	3.13.1	[255]
Nd (hexyl isocyanate)	**549**	3.13.1	[256]
Sm (Lac)	**546**	3.13.1	[255]
La (Lac)	**547**	3.13.1	[255]
Y (Lac)	**548**	2.13.1	[255]
Y (hexyl isocyanate)	**550**	3.13.1	[256]
Ti (ethylene)	**563–565, 569–571**	3.13.2	[262–264]
Ti (Lac)	**578–580**	3.13.2	[265]
Ti (cyclohexene oxide CO_2)	**583, 587, 589**	3.13.2	[55,268,357]
Ti (Lac)	**587**	3.13.2	[266]
Ti (cyclohexene oxide CO_2)	**596–604**	3.13.2	[55]
Ti (1-hexene)	**665–666**	3.13.2	[276]
Al (Lac, trimethylene carbonate)	**761**	3.13.9	[306]
Hf (Lac)	**622–624**	3.13.1	[265]
Zr (Lac)	**636**	3.13.1	[358]
Zr (cyclohexene oxide CO_2)	**636–637**	3.13.2	[275]
Zr (ethylene)	**627, 633**	3.13.2	[272]
Zr (Lac)	**615–621**	3.13.2	[265]

8. Conclusions

Pincer ligands with a bridgehead NHC donor are attracting increasing attention and could complement related species comprising NHCs at the side-arms and/or exclusively 'classical' donors. Striking features setting the different architectures apart may reside on diverse structural and electronic properties, reactivity and applications. In particular, in the regime of the 3*d* metals, where the high density of states [359] is common, fine tuning of electronic structures may favor the population of different electronic/spin states leading to diverse physical properties and reactivities. It is evident from the plethora of the complexes included in this review that the pincer ligands with bridgehead NHC donor are already well represented and have attained a good scope with metals from across the Periodic Table. Developments and in depth understanding on an *ad hoc* basis and for specific cases have benefitted from the employment of modern computational methodologies; however, transferable, empirical and theoretical guiding principles that can be widely applied and used for comparisons and contrasts within the pincer ligand paradigm have not been pursued. These are desirable and can support a'dial-a-pincer' strategy aiming at optimal ligand choices for specific jobs and rationalizations/predictions of ligand effects for desired applications. It is reasonable that a computational approach to qualitatively track down the nature, diversification and availability of the frontier orbitals of pincer ligands, in particular those with NHC donors, may constitute a starting point for this analysis. It should provide the first elements for systematically grouping and delineating of pincers ligands. For the conclusions of this review, the application of the strategy was initiated by performing calculations (at B3LYP/def2-TZVPP level of theory [330,360,361] on the six simplified pincer architectures ($\mathbf{L^1}$–$\mathbf{L^6}$ in Chart 9), based on structures obtained (i) from crystallographic data of a range of metal complexes after eliminating the metal center[a] or (ii) by energetically optimizing ligand geometries under C_s or C_{2v} symmetry, so as to retain the pincer structure (although at the lowest energy minima mutually *anti*-donor arrangement violating the pincer architecture is favored); all calculations were carried out using the Gaussian code [362]. The emphasis placed on the frontier orbitals led to some interesting common or differentiating features of the pincer ligand-metal bonding picture: intriguingly, it emerged that in pincer ligands with one NHC bridgehead, the HOMO was mainly localized over all three donors (*e.g.* on P and C atoms for P-C^{NHC}-P pincer) and in particular on the C^{NHC}. In contrast, from the $\mathbf{L^1}$-$\mathbf{L^3}$ only in $\mathbf{L^2}$ there is a HOMO of σ-symmetry on the bridgehead donor, while in $\mathbf{L^1}$ there is a near degeneracy of HOMO and HOMO-1, the latter having electron density localized on all three donors. Consequently, the introduction of the NHC not only increases the σ-donor strength of the bridgehead thanks to the nature of the NHC, but also enhances the participation of the side-arms (*i.e.* phosphanes in P-C^{NHC}-P) in the HOMO. Furthermore, the π symmetry LUMO of a lone NHC donor is also 'reproduced' on its integration to the pincer structure, thereby maintaining the classic and design-straightforward push-pull nature of the NHCs. For the $\mathbf{L^3}$, both HOMO and LUMO are not localized on the three donors but over the pyrrole bridgehead.

Apropos energetics, with the exception of $\mathbf{L^3}$, the same relative energy ordering is observed for the energies optimized following the methodologies (i) and (ii) outlined in the previous paragraph, although for $\mathbf{L^1}$, $\mathbf{L^2}$ and $\mathbf{L^4}$-$\mathbf{L^6}$ (i) leads to slightly higher HOMO and lower LUMO than (ii). However, for $\mathbf{L^3}$, since both HOMO and LUMO are localized over the pyrrole ring, the HOMO-LUMO energy difference remains the same in both approaches.

The initial qualitative comparisons that appeared from the previous discussion demonstrate that subtle effects are associated with the nature of the bridgehead donor, its electronic properties, and the creative management of the latter.

More detailed future understanding of these aspects may form the basis for novel coordination, organometallic chemistry and catalysis. Initial signs of these expectations, were apparent throughout the review, *e.g.,* concerning the reactivity of RE-NHC *vs.* pyridine bridgehead pincers (with a range of side-arm donors *e.g.* imines, phosphanes *etc.*), the reactivity of five membered imidazole type *vs.* RE-NHC as bridgehead donors, the effect of NHC bridgehead donors integrated in rigid polynuclear systems *etc*. We hope that by highlighting existing achievements and indicating under-represented categories of pincer ligands and complexes, this review will trigger new research in the area and that progressive developments still show a bright future in numerous areas.

[a] Crystallographic data for pincer complexes with the following database identifier in the CSD were used to 'demetalate' and produce the coordinates of the free pincer ligand: ACOTUK, ADUPAU, GULMUX, BEHBEZ, AHARUX, ADUNIY, AREZUU, BUKCES, GAXIA, XIYVUZ, XIYVIN, SOHREP, IKOGEX, XUCRIY, SAVNUC, UFAHAN, YUQCUK. CCDC (2017). CSD web interface intuitive, cross-platform, web-based access to CSD data. Cambridge Crystallographic Data Centre, 12 Union Road, Cambridge, UK.

Declaration of competing interest

The authors declare that they have no known competing financial interests or personal relationships that could have appeared to influence the work reported in this paper.

Data availability

No data was used for the research described in the article.

Acknowledgements

P. B and F. H. are grateful to the School of Chemistry and Chemical Engineering, Yangzhou University, Jiangsu, P. R. China for a post-doctoral grant to F.H. and to the China Postdoctoral Science Foundation (Grant No. 2019 M651975) for funding, and the CNRS and the MESRI (Paris) for support. A. A. D. acknowledges support by a Special Account for Research Grant (S.A.R.G.) for the "Re-initiation of Research" administered by the Rector of the National and Kapodistrian University. K.P.Z. acknowledges the Bodossaki Foundation for financial support (MSc scholarship 2023-2024).

Note added in proofs

The following publications are relevant to the pincer complexes discussed in this review.

$NC^{NHC}N$ Pincer Complexes

*Backbone of type **Ib***

Y. Hirota, S. Ando, T. Ishizuka, Bisamidate-functionalized NHC ligands: Electronic and steric influences of N-substituents on the bisamidate moieties, Tetrahedron 108 (2022) 132668, https://doi.org/10.1016/j.tet.2022.132668

A. Sarkar, S. Das, P. Mondal, B. Maiti, S. S. Gupta, Synthesis, Characterization, and Reactivity of High-Valent Carbene Dicarboxamide-Based Nickel Pincer Complexes, Inorg. Chem. 62 (2023) 20439-20449, https://doi.org/10.1021/acs.inorgchem.3c03465.

*Backbone of type **IIb***

C.E. Strasser, V.J. Catalano, Luminescent Copper(I) Halide Adducts of $[Au(im(CH_2py)_2)_2]PF_6$ Exhibiting Short Au(I)···Cu(I) Separations and Unusual Semibridging NHC Ligands, Inorg. Chem. 50 (2011) 11228-11234, https://doi.org/10.1021/ic201795b

H. Mourão, C.S.B. Gomes, S. Realista, B. Royo, Visible light-induced catalytic hydrosilylation of ketones mediated by manganese NHC complexes, Appl. Organomet. Chem. 36 (2022) e6846, https://doi.org/10.1002/aoc.6846

A. Piyasaengthong, L.J. Williams, D.S. Yufit, J.W. Walton, Novel ruthenium complexes bearing bipyridine-based and N-heterocyclic carbene-supported pyridine (NCN) ligands: the influence of ligands on catalytic transfer hydrogenation of ketones, Dalton Trans. 51 (2022) 340-351, https://doi.org/10.1039/D1DT03240B

R.R. Behera, R. Saha, A.A. Kumar, S. Sethi, N.Ch. Jana, B. Bagh, Hydrosilylation of Terminal Alkynes Catalyzed by an Air-Stable Manganese–NHC Complex, J. Org. Chem. 88 (2023) 8133-8149, https://doi.org/10.1021/acs.joc.3c00127

I.V. Lapshin, A.V. Cherkasov, A.A. Trifonov, Heteroleptic Bis(amido) Ca(II) and Yb(II) NHC Pincer Complexes: Synthesis, Characterization, and Catalytic Activity in Intermolecular Hydrofunctionalization of C═C Bonds, Organometallics 42 (2023) 2531-2540, https://doi.org/10.1021/acs.organomet.2c00596

*Backbone of type **IIIb***

J. Moussa, K. Haddouche, L.-M. Chamoreau, H. Amouri, J.A.G. Williams, New NˆCˆN-coordinated Pd(II) and Pt(II) complexes of a tridentate N-heterocyclic carbene ligand featuring a 6-membered central ring: synthesis, structures and luminescence, Dalton Trans. 45 (2016) 12644-12648, https://doi.org/10.1039/C6DT02415G

V. Friese, S. Nag, J. Wang, M.-P. Santoni, A. Rodrigue-Witchel, G.S. Hanan, F. Schaper, Red Phosphorescence in Ru(II) Complexes of a Tridentate N-Heterocyclic Carbene Ligand Incorporating Tetrahydropyrimidine, Eur. J. Inorg. Chem. (2011) 39-44, https://doi.org/10.1002/ejic.201000823

$PC^{NHC}P$ Pincer Complexes

*Backbone of type **VIb***

D.P. Zobernig, M. Luxner, B. Stöger, L. F. Veiros, K. Kirchner, Hydrogenation of Terminal Alkenes Catalyzed by Air-Stable Mn(I) Complexes Bearing an N-Heterocyclic Carbene-Based PCP Pincer Ligand, Chem. Eur. J. 30 (2023) e202302455, https://doi.org/10.1002/chem.202302455

Y. Ashida, T. Mizushima, K. Arashiba, A. Egi, H. Tanaka, K. Yoshizawa, Y. Nishibayashi, Catalytic production of ammonia from dinitrogen employing molybdenum complexes bearing N-heterocyclic carbene-based PCP-type pincer ligands, Nature Synthesis, 2 (2023) 635-644, https://doi.org/10.1038/s44160-023-00292-9

Y. Ashida, A. Egi, K. Arashiba, H. Tanaka, T. Mitsumoto, S. Kuriyama, K. Yoshizawa, Y. Nishibayashi, Catalytic Reduction of Dinitrogen into Ammonia and Hydrazine by Using Chromium Complexes Bearing PCP-Type Pincer Ligands, Chem. Eur. J. 28 (2022) e2022005, https://doi.org/10.1002/chem.202200557

*Backbone of type **VIc***

A. Luque-Gómez, P. Garcia-Orduña, F.J. Lahoz, M. Iglesias, Synthesis and catalytic activity of well-defined Co(I) complexes based on NHC-phosphane pincer ligands, Dalton Trans. 52 (2023) 12779-12788, https://doi.org/10.1039/d3dt00463e.

H.M. Lee, J.Y. Zeng, C.-H. Hu, M.-T. Lee, A New Tridentate Pincer Phosphine/*N*-Heterocyclic Carbene Ligand: Palladium Complexes, Their Structures, and Catalytic Activities, Inorg. Chem. 43 (2004) 6822-6829, https://doi.org/10.1021/ic049492x

*Backbone of type **VIIb***

S. Garhwal, J. Panda, N. Fridman, A. Karton, G. de Ruiter, Formation of distinct iron hydrides *via* mechanistic divergence in directed C–H bond activation of aryl ketones, esters and amides, Chem. Comm. 59 (2022) 426-429, https://doi.org/10.1039/D2CC04394G

R. Thenarukandiyil, R. Kamte, S. Garhwal, P. Effnert, N. Fridman, G. de Ruiter, α-Methylation of Ketones and Indoles Catalyzed by a Manganese(I) $PC_{NHC}P$ Pincer Complex with Methanol as a C_1 Source, Organometallics 42 (2022) 62-71, https://doi.org/10.1021/acs.organomet.2c00520

*Backbone of type **VIIIb***

L.J. Watson, A.F. Hill, Stable cyclopropenylvinyl ligands via insertion into a transient cyclopropenyl metal bond, Dalton Trans. 53 (2024) 3629-3637, https://doi.org/10.1039/D3DT03997H.

$OC^{NHC}O$ Pincer Complexes

*Backbone of type **XIIa***

C.S. Kuehner, A.G. Hill, C.F. Harris, C.A. Owens, J. Bacsa, J.D. Soper, Catalytic C–H Trifluoromethylation of Arenes and Heteroarenes via Visible Light Photoexcitation of a Co(III)–CF_3 Complex, ACS Catalysis 13 (2023) 13607-13617, https://doi.org/10.1021/acscatal.3c03832.

*Backbone of type **XIIb***

F.R. Neururer, K. Huter, M. Seidl, S. Hohloch, Reactivity and Structure of a Bis-phenolate Niobium NHC Complex, ACS Org. Inorg. Au, 3 (2022) 59-71, https://doi.org/10.1021/acsorginorgau.2c00028.

Catalytic Applications

T. Zhou, G. Utecht-Jarzyńska, M. Szostak, Ring-expanded N-heterocyclic carbene complexes: Applications in transition metal catalysis, Coord. Chem. Rev. 512 (2024) 215867. https:// doi.org/10.1016/j.ccr.2024.215867.

References

[1] C.J. Moulton, B.L. Shaw, Transition metal–carbon bonds. Part XLII, Complexes of nickel, palladium, platinum, rhodium and iridium with the tridentate ligand 2,6-bis[(di-t-butylphosphino)methyl]phenyl, J. Chem. Soc., Dalton Trans. (1976) 1020–1024, https://doi.org/10.1039/DT9760001020.

[2] G. van Koten, Tuning the reactivity of metals held in a rigid environment, Pure & Appl. Chem. 61 (1989) 1681–1694, https://doi.org/10.1351/pac198961101681.

[3] R. Arevalo, P.J. Chirik, Enabling two-electron pathways with iron and cobalt: from ligand design to catalytic applications, J. Am. Chem. Soc. 141 (2019) 9106–9123, https://doi.org/10.1021/jacs.9b03337.

[4] J.I. van der Vlugt, Redox-active pincer ligands, in: G. van Koten, K. Kirchner, M.-E. Moret (Eds.), Metal-Ligand Co-Operativity: Catalysis and the Pincer-Metal Platform, Springer International Publishing, Cham, 2021, pp. 135–179, https://doi.org/10.1007/3418_2020_68.

[5] J.C. Ott, D. Bürgy, H. Guan, L.H. Gade, 3d metal complexes in T-shaped geometry as a gateway to metalloradical reactivity, Acc. Chem. Res. 55 (2022) 857–868, https://doi.org/10.1021/acs.accounts.1c00737.

[6] J.R. Khusnutdinova, D. Milstein, Metal-ligand cooperation, Angew. Chem. Int. Ed. 54 (2015) 12236–12273, https://doi.org/10.1002/anie.201503873.

[7] A. Kumar, D. Milstein, Recent advances in the applications of metal-ligand cooperation via dearomatization and aromatization of pincer complexes, in: G. van Koten, K. Kirchner, M.-E. Moret (Eds.), Metal-Ligand Co-Operativity: Catalysis and the Pincer-Metal Platform, Springer International Publishing, Cham, 2021, pp. 1–23, https://doi.org/10.1007/3418_2020_67.

[8] A.J. Arduengo III, R.L. Harlow, M. Kline, A stable crystalline carbene, J. Am. Chem. Soc. 113 (1991) 361–363, https://doi.org/10.1021/ja00001a054.

[9] D. Bourissou, O. Guerret, F.P. Gabbaï, G. Bertrand, Stable carbenes, Chem. Rev. 100 (2000) 39–92, https://doi.org/10.1021/cr940472u.

[10] M.N. Hopkinson, C. Richter, M. Schedler, F. Glorius, An overview of N-heterocyclic carbenes, Nature 510 (2014) 485–496, https://doi.org/10.1038/nature13384.

[11] R. Jazzar, M. Soleilhavoup, G. Bertrand, Cyclic (alkyl)- and (aryl)-(amino)carbene coinage metal complexes and their applications, Chem. Rev. 120 (2020) 4141–4168, https://doi.org/10.1021/acs.chemrev.0c00043.

[12] P. Bellotti, M. Koy, M.N. Hopkinson, F. Glorius, Recent advances in the chemistry and applications of N-heterocyclic carbenes, Nat. Rev. Chem. 5 (2021) 711–725, https://doi.org/10.1038/s41570-021-00321-1.

[13] J.C.C. Chen, I.J.B. Lin, The first dicarbene double helical mercury complex, J. Chem. Soc., Dalton Trans. (2000) 839–840, https://doi.org/10.1039/B000971G.

[14] E. Peris, J.A. Loch, J. Mata, R.H. Crabtree, A Pd complex of a tridentate pincer CNC bis-carbene ligand as a robust homogenous Heck catalyst, Chem. Commun. (2001) 201–202, https://doi.org/10.1039/B008038L.

[15] A.A.D. Tulloch, A.A. Danopoulos, G.J. Tizzard, S.J. Coles, M.B. Hursthouse, R. S. Hay-Motherwell, W.B. Motherwell, Chiral 2,6-lutidinyl-biscarbene complexes of palladium, Chem. Commun. (2001) 1270–1271, https://doi.org/10.1039/B103330C.

[16] A.A. Danopoulos, S. Winston, W.B. Motherwell, Stable N-functionalised 'pincer' bis carbene ligands and their ruthenium complexes; synthesis and catalytic studies, Chem. Commun. (2002) 1376–1377, https://doi.org/10.1039/B202814J.

[17] D. Pugh, A.A. Danopoulos, Metal complexes with 'pincer'-type ligands incorporating N-heterocyclic carbene functionalities, Coord. Chem. Rev. 251 (2007) 610–641. https://www.sciencedirect.com/science/article/pii/S0010854506002323.

[18] V. Arora, H. Narjinari, P.G. Nandi, A. Kumar, Recent advances in pincer-nickel catalyzed reactions, Dalton Trans. 50 (2021) 3394–3428, https://doi.org/10.1039/D0DT03593A.

[19] Y. Wang, B. Zhang, S. Guo, Transition metal complexes supported by N-heterocyclic carbene-based pincer platforms: synthesis, reactivity and applications, Eur. J. Inorg. Chem. (2021) 188–204, https://doi.org/10.1002/ejic.202000911.

[20] D. Zhang, G. Zi, N-heterocyclic carbene (NHC) complexes of group 4 transition metals, Chem. Soc. Rev. 44 (2015) 1898–1921, https://doi.org/10.1039/C4CS00441H.

[21] V. Charra, P. de Frémont, P. Braunstein, Multidentate N-heterocyclic carbene complexes of the 3d metals: synthesis, structure, reactivity and catalysis, Coord. Chem. Rev. 341 (2017) 53–176. https://www.sciencedirect.com/science/article/pii/S0010854517300243.

[22] A.A. Danopoulos, T. Simler, P. Braunstein, N-heterocyclic carbene complexes of copper, nickel, and cobalt, Chem. Rev. 119 (2019) 3730–3961, https://doi.org/10.1021/acs.chemrev.8b00505.

[23] Q. Liang, D. Song, Iron N-heterocyclic carbene complexes in homogeneous catalysis, Chem. Soc. Rev. 49 (2020) 1209–1232, https://doi.org/10.1039/C9CS00508K.

[24] R. Taakili, Y. Canac, NHC Core pincer ligands exhibiting two anionic coordinating extremities, Molecules 25 (2020) 2231. https://www.mdpi.com/1420-3049/25/9/2231.

[25] B.C. Lee, C.-F. Liu, L.Q.H. Lin, K.Z. Yap, N. Song, C.H.M. Ko, P.H. Chan, M.J. Koh, N-heterocyclic carbenes as privileged ligands for nickel-catalysed alkene functionalisation, Chem. Soc. Rev. 52 (2023) 2946–2991, https://doi.org/10.1039/D2CS00972B.

[26] E. Peris, R.H. Crabtree, Key factors in pincer ligand design, Chem. Soc. Rev. 47 (2018) 1959–1968, https://doi.org/10.1039/C7CS00693D.

[27] P. Dierkes, P.W.N.M. van Leeuwen, The bite angle makes the difference: a practical ligand parameter for diphosphine ligands, J. Chem. Soc., Dalton Trans. (1999) 1519–1530, https://doi.org/10.1039/A807799A.

[28] P. Braunstein, F. Naud, Hemilability of hybrid ligands and the coordination chemistry of oxazoline-based systems, Angew. Chem. Int. Ed. 40 (2001) 680–699, https://doi.org/10.1002/1521-3773(20010216)40:4<680::AID-ANIE6800>3.0.CO;2-0.

[29] R. Peloso, E. Carmona, Non-heteroatom-substituted alkylidene complexes of groups 10 and 11, Coord. Chem. Rev. 355 (2018) 116–132. https://www.sciencedirect.com/science/article/pii/S0010854517303120.

[30] R.A. Manzano, R.D. Young, Cataloguing a renaissance in late transition metal $PC_{carbene}P$ pincer complexes, Coord. Chem. Rev. 449 (2021) 214215. https://www.sciencedirect.com/science/article/pii/S0010854521004896.

[31] L.J. Donnelly, J.-B. Lin, B.S. Gelfand, C.Y. Chang, W.E. Piers, Ruthenium polyhydrides supported by rigid PCP pincer ligands: dynamic behaviour and reactions with CO_2, Dalton Trans. 53 (2024) 1862–1869, https://doi.org/10.1039/D3DT04014C.

[32] D.M. Andrada, N. Holzmann, T. Hamadi, G. Frenking, Direct estimate of the internal π-donation to the carbene centre within N-heterocyclic carbenes and related molecules, Beilstein J. Org. Chem. 11 (2015) 2727–2736, https://doi.org/10.3762/bjoc.11.294.

[33] D. Munz, Pushing electrons—Which carbene ligand for which application? Organometallics 37 (2018) 275–289, https://doi.org/10.1021/acs.organomet.7b00720.

[34] S.-K. Liu, W.-C. Shih, W.-C. Chen, T.-G. Ong, Carbodicarbenes and their captodative behavior in catalysis, ChemCatChem 10 (2018) 1483–1498, https://doi.org/10.1002/cctc.201701577.

[35] L. Maser, J. Herritsch, R. Langer, Carbodiphosphorane-based nickel pincer complexes and their (de)protonated analogues: dimerisation, ligand tautomers and proton affinities, Dalton Trans. 47 (2018) 10544–10552, https://doi.org/10.1039/C7DT04930G.

[36] J.S. Marcum, T.N. Cervarich, R.S. Manan, C.C. Roberts, S.J. Meek, (CDC)–Rhodium-catalyzed hydroallylation of vinylarenes and 1,3-dienes with AllylTrifluoroborates, ACS Catal. 9 (2019) 5881–5889, https://doi.org/10.1021/acscatal.9b01579.

[37] M. Klein, J. Sundermeyer, Modular design strategy toward second-generation tridentate carbodiphosphorane N, C, N ligands with a central four-electron carbon donor motif and their complexes, Organometallics 40 (2021) 2090–2099, https://doi.org/10.1021/acs.organomet.1c00231.

[38] A. Eizawa, K. Arashiba, H. Tanaka, S. Kuriyama, Y. Matsuo, K. Nakajima, K. Yoshizawa, Y. Nishibayashi, Remarkable catalytic activity of dinitrogen-bridged dimolybdenum complexes bearing NHC-based PCP-pincer ligands toward nitrogen fixation, Nat. Commun. 8 (2017) 14874, https://doi.org/10.1038/ncomms14874.

[39] J.S. Marcum, C.C. Roberts, R.S. Manan, T.N. Cervarich, S.J. Meek, Chiral pincer carbodicarbene ligands for enantioselective rhodium-catalyzed hydroarylation of terminal and internal 1,3-dienes with indoles, J. Am. Chem. Soc. 139 (2017) 15580–15583, https://doi.org/10.1021/jacs.7b08575.

[40] L. Zhao, C. Chai, W. Petz, G. Frenking, Carbones and carbon atom as ligands in transition metal complexes, Molecules 25 (2020) 4943. https://www.mdpi.com/1420-3049/25/21/4943.

[41] J. Terheijden, G. van Koten, I.C. Vinke, A.l. Spek, 1,2-methyl shift between platinum and the coordinated aryl group in the reaction of methyl iodide with 2,6-bis[(dimethylamino)methyl]phenyl-N, N', C complexes of platinum(II). X-ray crystal structure of the arenonium-platinum compound [Pt(o-tolyl)($MeC_6H_3(CH_2NMe_2)$2-o, o')]I, J. Am. Chem. Soc. 107 (1985) 2891–2898, https://doi.org/10.1021/ja00296a010.

[42] A. Vigalok, B. Rybtchinski, L.J.W. Shimon, Y. Ben-David, D. Milstein, Metal-stabilized methylene arenium and σ-arenium compounds: synthesis, structure, reactivity, charge distribution, and interconversion, Organometallics 18 (1999) 895–905, https://doi.org/10.1021/om980960i.

[43] J. Zhang, K.A. Barakat, T.R. Cundari, T.B. Gunnoe, P.D. Boyle, J.L. Petersen, C. S. Day, Synthesis of the five-coordinate ruthenium(II) complexes [(PCP)Ru(CO)(L)][BAr'$_4$] {PCP = 2,6-(CH$_2$PtBu$_2$)$_2$C$_6$H$_3$, BAr'$_4$ = 3,5-(CF$_3$)$_2$C$_6$H$_3$, L = η^1-ClCH$_2$Cl, η^1-N$_2$, or μ-Cl−Ru(PCP)(CO)}: reactions with phenyldiazomethane and phenylacetylene, Inorg. Chem. 44 (2005) 8379–8390, https://doi.org/10.1021/ic051074k.

[44] D. Himmelbauer, M. Mastalir, B. Stöger, L.F. Veiros, K. Kirchner, Synthesis and reactivity of group six metal PCP pincer complexes: reversible CO addition across the metal-aryl bond, Organometallics 37 (2018) 3631–3638, https://doi.org/10.1021/acs.organomet.8b00447.

[45] A. Vigalok, O. Uzan, L.J.W. Shimon, Y. Ben-David, J.M.L. Martin, D. Milstein, Formation of η^2 C−H agostic rhodium arene complexes and their relevance to electrophilic bond activation, J. Am. Chem. Soc. 120 (1998) 12539–12544, https://doi.org/10.1021/ja982534u.

[46] K.J. Jonasson, A.V. Polukeev, R. Marcos, M.S.G. Ahlquist, O.F. Wendt, Reversible α-hydrogen and α-alkyl elimination in PC(sp^3)P pincer complexes of iridium, Angew. Chem. Int. Ed. 54 (2015) 9372–9375, https://doi.org/10.1002/anie.201503593.

[47] D.G. Gusev, F.M. Dolgushin, M.Y. Antipin, Hydride, borohydride, and dinitrogen pincer complexes of ruthenium, Organometallics 19 (2000) 3429–3434, https://doi.org/10.1021/om0003842.

[48] L. Luconi, U.B. Demirci, M. Peruzzini, G. Giambastiani, A. Rossin, Ammonia borane and hydrazine bis(borane) dehydrogenation mediated by an unsymmetrical (PNN) ruthenium pincer hydride: metal–ligand cooperation for hydrogen production, Sustainable Energy Fuels 3 (2019) 2583–2596, https://doi.org/10.1039/C9SE00241C.

[49] T. Steinke, B.K. Shaw, H. Jong, B.O. Patrick, M.D. Fryzuk, J.C. Green, Noninnocent behavior of ancillary ligands: apparent trans coupling of a saturated N-heterocyclic carbene unit with an ethyl ligand mediated by nickel, J. Am. Chem. Soc. 131 (2009) 10461–10466, https://doi.org/10.1021/ja901346g.

[50] C. Romain, K. Miqueu, J.-M. Sotiropoulos, S. Bellemin-Laponnaz, S. Dagorne, Non-innocent behavior of a tridentate NHC chelating ligand coordinated onto a zirconium(IV) center, Angew. Chem. Int. Ed. 49 (2010) 2198–2201, https://doi.org/10.1002/anie.200906702.

[51] E. Despagnet-Ayoub, L.M. Henling, J.A. Labinger, J.E. Bercaw, Group 4 transition-metal complexes of an aniline–carbene–phenol ligand, Organometallics 32 (2013) 2934–2938, https://doi.org/10.1021/om4001567.

[52] C. Romain, D. Specklin, K. Miqueu, J.-M. Sotiropoulos, C. Fliedel, S. Bellemin-Laponnaz, S. Dagorne, Unusual benzyl migration reactivity in NHC-Bearing Group 4 metal chelates: synthesis, characterization, and mechanistic investigations, Organometallics 34 (2015) 4854–4863, https://doi.org/10.1021/om501143t.

[53] E. Despagnet-Ayoub, M.K. Takase, J.A. Labinger, J.E. Bercaw, Reversible 1,2-alkyl migration to carbene and ammonia activation in an N-heterocyclic carbene-zirconium complex, J. Am. Chem. Soc. 137 (2015) 10500–10503, https://doi.org/10.1021/jacs.5b06695.

[54] X. Ren, C. Gourlaouen, M. Wesolek, P. Braunstein, Tritopic NHC precursors: unusual nickel reactivity and ethylene insertion into a C(sp^3)–H bond, Angew. Chem. Int. Ed. 56 (2017) 12557–12560, https://doi.org/10.1002/anie.201706581.

[55] C.C. Quadri, R. Lalrempuia, J. Hessevik, K.W. Törnroos, E. Le Roux, Structural characterization of tridentate N-heterocyclic carbene titanium(IV) benzyloxide, silyloxide, acetate, and azide complexes and assessment of their efficacies for catalyzing the copolymerization of cyclohexene oxide with CO$_2$, Organometallics 36 (2017) 4477–4489, https://doi.org/10.1021/acs.organomet.7b00705.

[56] F. He, C. Gourlaouen, H. Pang, P. Braunstein, Influence of the flexibility of nickel PCP-pincer complexes on C−H and P−C bond activation and ethylene reactivity: a combined experimental and theoretical investigation, Chem. Eur. J. 28 (2022) e202104234, https://doi.org/10.1002/chem.202104234.

[57] A.A. Danopoulos, N. Tsoureas, J.C. Green, M.B. Hursthouse, Migratory insertion in N-heterocyclic carbene complexes of palladium; an experimental and DFT study, Chem. Commun. (2003) 756–757, https://doi.org/10.1039/B212453J.

[58] D. Pugh, A. Boyle, A.A. Danopoulos, 'Pincer' pyridine dicarbene complexes of nickel and their derivatives. Unusual ring opening of a coordinated imidazol-2-ylidene, Dalton Trans. (2008) 1087–1094, https://doi.org/10.1039/B715769J.

[59] R.M. Brown, J. Borau Garcia, J. Valjus, C.J. Roberts, H.M. Tuononen, M. Parvez, R. Roesler, Ammonia activation by a nickel NCN-pincer complex featuring a non-innocent N-heterocyclic carbene: ammine and amido complexes in equilibrium, Angew. Chem. Int. Ed. 54 (2015) 6274–6277, https://doi.org/10.1002/anie.201500453.

[60] D.V. Gutsulyak, W.E. Piers, J. Borau-Garcia, M. Parvez, Activation of water, ammonia, and other small molecules by PC$_{carbene}$P nickel pincer complexes, J. Am. Chem. Soc. 135 (2013) 11776–11779, https://doi.org/10.1021/ja406742n.

[61] T.M. Baker, T.L. Mako, A. Vasilopoulos, B. Li, J.A. Byers, M.L. Neidig, Magnetic circular dichroism and density functional theory studies of iron(II)-pincer complexes: insight into electronic structure and bonding effects of pincer N-heterocyclic carbene moieties, Organometallics 35 (2016) 3692–3700, https://doi.org/10.1021/acs.organomet.6b00651.

[62] H.-J. Liu, M.S. Ziegler, T.D. Tilley, Ring-opening and double-metallation reactions of the N-heterocyclic carbene ligand in Cp*(IXy)Ru (IXy = 1,3-bis(2,6-dimethylphenyl)imidazol-2-ylidene) complexes. Access to an anionic Fischer-type carbene complex of ruthenium, Polyhedron 84 (2014) 203–208. https://www.sciencedirect.com/science/article/pii/S0277538714005750.

[63] H.-J. Liu, M.S. Ziegler, T.D. Tilley, Synthesis, structures, and reactivity studies of cyclometalated N-heterocyclic carbene complexes of ruthenium, Dalton Trans. 47 (2018) 12138–12146, https://doi.org/10.1039/C8DT01925H.

[64] S.H. Hong, A. Chlenov, M.W. Day, R.H. Grubbs, Double C-H activation of an N-heterocyclic carbene ligand in a ruthenium olefin metathesis catalyst, Angew. Chem. Int. Ed. 46 (2007) 5148–5151, https://doi.org/10.1002/anie.200701234.

[65] J. Mathew, N. Koga, C.H. Suresh, C-H bond activation through σ-bond metathesis and agostic interactions: deactivation pathway of a Grubbs second-generation catalyst, Organometallics 27 (2008) 4666–4670, https://doi.org/10.1021/om800508s.

[66] D. Paul, B. Beiring, M. Plois, N. Ortega, S. Kock, D. Schlüns, J. Neugebauer, R. Wolf, F. Glorius, A cyclometalated ruthenium-NHC precatalyst for the asymmetric hydrogenation of (hetero)arenes and its activation pathway, Organometallics 35 (2016) 3641–3646, https://doi.org/10.1021/acs.organomet.6b00702.

[67] S. Urban, B. Beiring, N. Ortega, D. Paul, F. Glorius, Asymmetric hydrogenation of thiophenes and benzothiophenes, J. Am. Chem. Soc. 134 (2012) 15241–15244, https://doi.org/10.1021/ja306622y.

[68] W. Li, M. Wollenburg, F. Glorius, Enantioselective synthesis of 2-oxazolidinones by ruthenium(II)-NHC-catalysed asymmetric hydrogenation of 2-oxazolones, Chem. Sci. 9 (2018) 6260–6263, https://doi.org/10.1039/C8SC01869C.

[69] B. Eguillor, M.A. Esteruelas, V. Lezaun, M. Olivan, E. Onate, J.-Y. Tsai, C. Xia, A capped octahedral MHC$_6$ compound of a platinum group metal, Chem. Eur. J. 22 (2016) 9106–9110, https://doi.org/10.1002/chem.201601729.

[70] F.E. Hahn, C. Holtgrewe, T. Pape, M. Martin, E. Sola, L.A. Oro, Iridium complexes with N-allyl-substituted Benzimidazol-2-ylidene ligands and their application in catalytic transfer hydrogenation, Organometallics 24 (2005) 2203–2209, https://doi.org/10.1021/om0500873.

[71] F.E. Hahn, B. Heidrich, T. Pape, A. Hepp, M. Martin, E. Sola, L.A. Oro, Mononuclear and dinuclear bromo bridged iridium(I) complexes with N-allyl substituted imidazolin-2-ylidene ligands, Inorg. Chim. Acta 359 (2006) 4840–4846. https://www.sciencedirect.com/science/article/pii/S0020169306004269.

[72] A. Zanardi, E. Peris, J.A. Mata, Alkenyl-functionalized NHC iridium-based catalysts for hydrosilylation, New J. Chem. 32 (2008) 120–126, https://doi.org/10.1039/B707280E.

[73] P. Gao, D. Foster, G. Sipos, B.W. Skelton, A.N. Sobolev, R. Dorta, Chiral NHC-iridium complexes and their performance in enantioselective intramolecular hydroamination and ring-opening amination reactions, Organometallics 39 (2020) 556–573, https://doi.org/10.1021/acs.organomet.9b00770.

[74] J. Navarro, O. Torres, M. Martin, E. Sola, Iridium complexes of the doubly cyclometalated NHC ligand IMes'', J. Am. Chem. Soc. 133 (2011) 9738–9740, https://doi.org/10.1021/ja204522e.

[75] C.Y. Tang, N. Phillips, M.J. Kelly, S. Aldridge, Hydrogen shuttling: synthesis and reactivity of a 14-electron iridium complex featuring a bis(alkyl) tethered N-heterocyclic carbene ligand, Chem. Commun. 48 (2012) 11999–12001, https://doi.org/10.1039/C2CC35947B.

[76] Z.-B. Yan, K.-L. Dai, B.-M. Yang, Z.-H. Li, Y.-Q. Tu, F.-M. Zhang, X.-M. Zhang, M. Peng, Q.-L. Chen, Z.-R. Jing, Development of unique dianionic Ir(III) CCC pincer complexes with a favourable spirocyclic NHC framework, Sci. China Chem. 63 (2020) 1761–1766, https://doi.org/10.1007/s11426-020-9875-6.

[77] M. Viciano, E. Mas-Marza, M. Poyatos, M. Sanau, R.H. Crabtree, E. Peris, An N-heterocyclic carbene/iridium hydride complex from the oxidative addition of a ferrocenyl-bisimidazolium salt: implications for synthesis, Angew. Chem. Int. Ed. 44 (2005) 444–447, https://doi.org/10.1002/anie.200461918.

[78] K. Nakanishi, J.O.C. Jimenez-Halla, S. Yamazoe, M. Nakamoto, R. Shang, Y. Yamamoto, Synthesis and Isolation of an Anionic Bis(dipyrido-annulated) N-Heterocyclic Carbene CCC-Pincer Iridium(III) Complex by Facile C-H Bond Activation, Inorg. Chem. 60 (2021) 9970-9976. https://doi.org/10.1021/acs.inorgchem.1c01236.

[79] M. Poyatos, J.A. Mata, E. Peris, Complexes with poly(N-heterocyclic carbene) ligands: structural features and catalytic applications, Chem. Rev. 109 (2009) 3677–3707, https://doi.org/10.1021/cr800501s.

[80] N. Darmawan, C.H. Yang, M. Mauro, M. Raynal, S. Heun, J. Pan, H. Buchholz, P. Braunstein, L. De Cola, Efficient near-UV emitters based on cationic bis-pincer iridium(III) carbene complexes, Inorg. Chem. 52 (2013) 10756–10765, https://doi.org/10.1021/ic302695q.

[81] N. Stylianides, A.A. Danopoulos, D.H. Pugh, F. Hancock, A. Zanotti-Gerosa, Cyclometalated and alkoxyphenyl-substituted palladium imidazolin-2-ylidene complexes. synthetic, structural, and catalytic studies, Organometallics 26 (2007) 5627–5635, https://doi.org/10.1021/om700603d.

[82] R. Taakili, C. Lepetit, C. Duhayon, D.A. Valyaev, N. Lugan, Y. Canac, Palladium (II) pincer complexes of a C, C, C-NHC, diphosphonium bis(ylide) ligand, Dalton Trans. 48 (2019) 1709–1721, https://doi.org/10.1039/C8DT04316G.

[83] Q. Liang, K.M. Osten, D. Song, Iron-catalyzed *gem*-specific dimerization of terminal alkynes, Angew. Chem. Int. Ed. 56 (2017) 6317–6320, https://doi.org/10.1002/anie.201700904.

[84] Q. Liang, D. Song, Reactivity of Fe and Ru complexes of picolyl-substituted N-heterocyclic carbene ligand: diverse coordination modes and small molecule binding, Inorg. Chem. 56 (2017) 11956–11970, https://doi.org/10.1021/acs.inorgchem.7b01918.

[85] Q. Liang, K. Sheng, A. Salmon, V.Y. Zhou, D. Song, Active iron(II) catalysts toward gem-specific dimerization of terminal alkynes, ACS Catal. 9 (2019) 810–818, https://doi.org/10.1021/acscatal.8b03552.

[86] Y. Jiang, C. Gendy, R. Roesler, Nickel, ruthenium, and rhodium NCN-pincer complexes featuring a six-membered N-heterocyclic carbene central moiety and pyridyl pendant arms, Organometallics 37 (2018) 1123–1132, https://doi.org/10.1021/acs.organomet.8b00022.

[87] J.E. Wheatley, C.A. Ohlin, A.B. Chaplin, Solvent promoted reversible cyclometalation in a tethered NHC iridium complex, Chem. Commun. 50 (2014) 685–687, https://doi.org/10.1039/C3CC48015A.

[88] M.R. Chapman, C.M. Pask, A. Ariafard, C.E. Willans, σ-Alkenyl endo-palladacycle formation via regiospecific functionalisation of an unreactive NHC-tethered C (sp^2)-H bond, Chem. Commun. 51 (2015) 5513–5515, https://doi.org/10.1039/C4CC10163D.

[89] M.E. Humphries, W.H. Pecak, S.A. Hohenboken, S.R. Alvarado, D.C. Swenson, G. J. Domski, ruthenium(II) supported by phosphine-functionalized N-heterocyclic carbene ligands as catalysts for the transfer hydrogenation of ketones, Inorg. Chem. Commun. 37 (2013) 138–143. https://www.sciencedirect.com/science/article/pii/S1387700313003973.

[90] B.K. Shaw, B.O. Patrick, M.D. Fryzuk, Thermal rearrangement via P-C bond cleavage of a tridentate diphosphine–N-heterocyclic carbene ligand system coordinated to rhodium, Organometallics 31 (2012) 783–786, https://doi.org/10.1021/om201233e.

[91] H.-L. Qin, J. Leng, W. Zhang, E.A.B. Kantchev, DFT modelling of a diphosphane-N-heterocyclic carbene-Rh(I) pincer complex rearrangement: a computational evaluation of the electronic effects in C-P bond activation, Dalton Trans. 47 (2018) 2662–2669, https://doi.org/10.1039/C7DT04759B.

[92] M. Ameskal, R. Taakili, E.S. Gulyaeva, C. Duhayon, J. Willot, N. Lugan, C. Lepetit, D.A. Valyaev, Y. Canac, Phosphine-NHC-phosphonium ylide pincer ligand: complexation with Pd(II) and unconventional P-coordination of the ylide moiety, Inorg. Chem. 62 (2023) 20129–20141, https://doi.org/10.1021/acs.inorgchem.3c03025.

[93] R. Srivastava, R. Moneuse, J. Petit, P.A. Pavard, V. Dardun, M. Rivat, P. Schiltz, M. Solari, E. Jeanneau, L. Veyre, C. Thieuleux, E.A. Quadrelli, C. Camp, Early/Late heterobimetallic tantalum/rhodium species assembled through a novel bifunctional NHC-OH ligand, Chem. Eur. J. 24 (2018) 4361–4370, https://doi.org/10.1002/chem.201705507.

[94] Z.H. Wei, W.B. Zhang, G.M. Luo, F. Xu, Y.X. Mei, H. Cai, Mono- and bis-N-heterocyclic carbene complexes of tantalum and niobium with high oxidation states, New J. Chem. 40 (2016) 6270–6275, https://doi.org/10.1039/C6NJ00223D.

[95] T.R. Helgert, X. Zhang, H.K. Box, J.A. Denny, H.U. Valle, A.G. Oliver, G. Akurathi, C.E. Webster, T.K. Hollis, Extreme π-loading as a design element for accessing imido ligand reactivity. A CCC-NHC pincer tantalum bis(imido) complex: synthesis, characterization, and catalytic oxidative amination of alkenes, Organometallics 35 (2016) 3452–3460, https://doi.org/10.1021/acs.organomet.6b00216.

[96] M. Bortoluzzi, E. Ferretti, F. Marchetti, G. Pampaloni, S. Zacchini, Coordination complexes of niobium and tantalum pentahalides with a bulky NHC ligand, Dalton Trans. 45 (2016) 6939–6948, https://doi.org/10.1039/C6DT00533K.

[97] R. Taakili, C. Barthes, A. Goëffon, C. Lepetit, C. Duhayon, D.A. Valyaev, Y. Canac, NHC Core phosphonium ylide-based palladium(II) pincer complexes: the second ylide extremity makes the difference, Inorg. Chem. 59 (2020) 7082–7096, https://doi.org/10.1021/acs.inorgchem.0c00561.

[98] M. Teci, E. Brenner, D. Matt, C. Gourlaouen, L. Toupet, Directional properties of fluorenylidene moieties in unsymmetrically substituted N-heterocyclic carbenes. Unexpected CH activation of a methylfluorenyl group with palladium. Use in palladium catalysed Suzuki-Miyaura cross coupling of aryl chlorides, Dalton Trans. 43 (2014) 12251–12262, https://doi.org/10.1039/C4DT01102C.

[99] L.P. Spencer, M.D. Fryzuk, Synthesis and reactivity of zirconium and hafnium complexes incorporating chelating diamido-N-heterocyclic-carbene ligands, J. Organomet. Chem. 690 (2005) 5788–5803, https://doi.org/10.1016/j.organchem.2005.07.121.

[100] L.D. Durfee, I.P. Rothwell, Chemistry of η^2-acyl, η^2-iminoacyl, and related functional groups, Chem. Rev. 88 (1988) 1059–1079, https://doi.org/10.1021/cr00089a005.

[101] J.M. Manriquez, P.J. Fagan, T.J. Marks, C.S. Day, V.W. Day, Bis(pentamethylcyclopentadienyl)actinide alkyls: facile activation of carbon monoxide, carbon-carbon double bond formation, and the production of unusual oxygen-bonded migratory insertion products, J. Am. Chem. Soc. 100 (1978) 7112–7114, https://doi.org/10.1021/ja00490a077.

[102] L.P. Spencer, C. Beddie, M.B. Hall, M.D. Fryzuk, Synthesis, Reactivity, and DFT Studies of Tantalum Complexes Incorporating Diamido-N-heterocyclic Carbene Ligands. Facile endocyclic C-H bond activation, J. Am. Chem. Soc. 128 (2006) 12531–12543, https://doi.org/10.1021/ja063282x.

[104] Y. Uetake, T. Niwa, M. Nakada, Synthesis and characterization of a new C2-symmetrical chiral tridentate N-heterocyclic carbene ligand coordinated Cr(III) complex, Tetrahedron Asymmetry 26 (2015) 158–162. https://www.sciencedirect.com/science/article/pii/S0957416615000051.

[105] X. Ren, M. Wesolek, P. Braunstein, Cu(I), Ag(I), Ni(II), Cr(III) and Ir(I) complexes with tritopic $N^{imine}C^{NHC}N^{amine}$ pincer ligands and catalytic ethylene oligomerization, Dalton Trans. 48 (2019) 12895–12909, https://doi.org/10.1039/C9DT02400J.

[106] J.A. Thagfi, G.G. Lavoie, Preparation and reactivity study of chromium(III), iron (II), and cobalt(II) complexes of 1,3-bis(imino)benzimidazol-2-ylidene and 1,3-bis (imino)pyrimidin-2-ylidene, Organometallics 31 (2012) 7351–7358, https://doi.org/10.1021/om300873k.

[107] D.S. McGuinness, V.C. Gibson, D.F. Wass, J.W. Steed, Bis(carbene)pyridine complexes of CR(III): exceptionally active catalysts for the oligomerization of ethylene, J. Am. Chem. Soc. 125 (2003) 12716–12717, https://doi.org/10.1021/ja037217o.

[108] J. Al Thagfi, G.G. Lavoie, Synthesis, characterization, and ethylene polymerization studies of chromium, iron, and cobalt complexes containing 1,3-bis(imino)-N-heterocyclic carbene ligands, Organometallics 31 (2012) 2463–2469, https://doi.org/10.1021/om3001058.

[109] D. Pugh, J.A. Wright, S. Freeman, A.A. Danopoulos, 'Pincer' dicarbene complexes of some early transition metals and uranium, Dalton Trans. (2006) 775–782, https://doi.org/10.1039/B512133G.

[110] H.Z. Kaplan, B. Li, J.A. Byers, Synthesis and characterization of a bis(imino)-N-heterocyclic carbene analogue to bis(imino)pyridine iron complexes, Organometallics 31 (2012) 7343–7350, https://doi.org/10.1021/om300885d.

[111] J.L. Drake, H.Z. Kaplan, M.J. Wilding, B. Li, J.A. Byers, Spin transitions in bis(amidinato)-N-heterocyclic carbene iron(II) and iron(III) complexes, Dalton Trans. 44 (2015) 16703–16707, https://doi.org/10.1039/C5DT02440D.

[112] Y. Ohki, T. Hatanaka, K. Tatsumi, C-H bond activation of heteroarenes mediated by a half-sandwich iron complex of N-heterocyclic carbene, J. Am. Chem. Soc. 130 (2008) 17174–17186, https://doi.org/10.1021/ja8063028.

[113] B. Liu, Q. Xia, W. Chen, Direct synthesis of iron, cobalt, nickel, and copper complexes of N-heterocyclic carbenes by using commercially available metal powders, Angew. Chem. Int. Ed. 48 (2009) 5513–5516, https://doi.org/10.1002/anie.200901850.

[114] D.R. Gong, X.Y. Jia, B.L. Wang, F. Wang, C.Y. Zhang, X.Q. Zhang, L.S. Jiang, W. M. Dong, Highly trans-1,4 selective polymerization of 1,3-butadiene initiated by iron(III) bis(imino)pyridyl complexes, Inorg. Chim. Acta 373 (2011) 47–53, https://doi.org/10.1016/j.ica.2011.03.047.

[115] C.M. Manna, H.Z. Kaplan, B. Li, J.A. Byers, High molecular weight poly(lactic acid) produced by an efficient iron catalyst bearing a bis(amidinato)-N-heterocyclic carbene ligand, Polyhedron 84 (2014) 160–167. https://www.sciencedirect.com/science/article/pii/S0277538714004707.

[116] H.Z. Kaplan, T.L. Mako, M.J.T. Wilding, B. Li, J.A. Byers, Electron-donating capabilities and evidence for redox activity in low oxidation state iron complexes bearing bis(amidine)pyrimidylidene ligands, J. Coord. Chem. 69 (2016) 2047–2058, https://doi.org/10.1080/00958972.2016.1176158.

[117] D.E. Prokopchuk, B.T. Tsui, A.J. Lough, R.H. Morris, Intramolecular C-H/O-H bond cleavage with water and alcohol using a phosphine-free ruthenium carbene NCN pincer complex, Chem. Eur. J. 20 (2014) 16960–16968, https://doi.org/10.1002/chem.201404819.

[118] M.M.H. Sung, D.E. Prokopchuk, R.H. Morris, Phosphine-free ruthenium NCN-ligand complexes and their use in catalytic CO_2 hydrogenation, Dalton Trans. 48 (2019) 16569–16577, https://doi.org/10.1039/C9DT03143J.

[119] Y. Shimoyama, T. Ishizuka, H. Kotani, Y. Shiota, K. Yoshizawa, K. Mieda, T. Ogura, T. Okajima, S. Nozawa, T. Kojima, A ruthenium(III)-oxyl complex bearing strong radical character, Angew. Chem. Int. Ed. 55 (2016) 14041–14045, https://doi.org/10.1002/anie.201607861.

[120] S. Ohzu, T. Ishizuka, H. Kotani, T. Kojima, Reactivity of a Ru(III)-hydroxo complex in substrate oxidation in water, Chem. Commun. 50 (2014) 15018–15021, https://doi.org/10.1039/C4CC07488B.

[121] H.-W. Tseng, R. Zong, J.T. Muckerman, R. Thummel, Mononuclear Ru(II) complexes that catalyze water oxidation, Inorg. Chem. 47 (2008) 11763–11773, https://doi.org/10.1021/ic8014817.

[122] Y. Pushkar, D. Moonshiram, V. Purohit, L. Yan, I. Alperovich, Spectroscopic analysis of catalytic water oxidation by $[Ru^{II}(bpy)(tpy)H_2O]^{2+}$ suggests that Ru^{V}=O is not a rate-limiting intermediate, J. Am. Chem. Soc. 136 (2014) 11938–11945, https://doi.org/10.1021/ja506586b.

[123] Y. Hirai, T. Kojima, Y. Mizutani, Y. Shiota, K. Yoshizawa, S. Fukuzumi, Ruthenium-catalyzed selective and efficient oxygenation of hydrocarbons with water as an oxygen source, Angew. Chem. Int. Ed. 47 (2008) 5772–5776, https://doi.org/10.1002/anie.200801170.

[124] S. Ohzu, T. Ishizuka, Y. Hirai, H. Jiang, M. Sakaguchi, T. Ogura, S. Fukuzumi, T. Kojima, Mechanistic insight into catalytic oxidations of organic compounds by ruthenium(IV)-oxo complexes with pyridylamine ligands, Chem. Sci. 3 (2012) 3421–3431, https://doi.org/10.1039/C2SC21195E.

[125] H. Yamada, T. Koike, J.K. Hurst, Water exchange rates in the diruthenium μ-oxo ion cis, cis-$[(bpy)_2Ru(OH_2)]_2O^{4+}$, J. Am. Chem. Soc. 123 (2001) 12775–12780, https://doi.org/10.1021/ja010594l.

[126] C. Chen, C. Lu, Q. Zheng, S. Ni, M. Zhang, W. Chen, Synthesis and structures of ruthenium-NHC complexes and their catalysis in hydrogen transfer reaction, Beilstein J. Org. Chem. 11 (2015) 1786–1795, https://doi.org/10.3762/bjoc.11.194.

[127] G. Su, X.-K. Huo, G.-X. Jin, Half-sandwich Ru(II), Ir(III) and Rh(III) complexes with bridging or chelating N-heterocyclic bis-carbene ligand: synthesis and characterization, J. Organomet. Chem. 696 (2011) 533–538. https://www.sciencedirect.com/science/article/pii/S0022328X10005231.

[128] B. Saha, G. Sengupta, A. Sarbajna, I. Dutta, J.K. Bera, Amide synthesis from alcohols and amines catalyzed by a Ru(II)–N-heterocyclic carbene (NHC)–carbonyl complex, J. Organomet. Chem. 771 (2014) 124–130. https://www.sciencedirect.com/science/article/pii/S0022328X14000023.

[129] D. Yang, Y. Tang, H. Song, B. Wang, o-Aryloxide-N-heterocyclic carbenes: efficient synthesis of the proligands and their *p*-cymene ruthenium complexes, Organometallics 34 (2015) 2012–2017, https://doi.org/10.1021/acs.organomet.5b00256.

[130] M. Dakkach, X. Fontrodona, T. Parella, A. Atlamsani, I. Romero, M. Rodriguez, Polypyrrole-functionalized ruthenium carbene catalysts as efficient heterogeneous systems for olefin epoxidation, Dalton Trans. 43 (2014) 9916–9923, https://doi.org/10.1039/C4DT00698D.

[131] A.T. Normand, K.J. Cavell, Donor-functionalised N-heterocyclic carbene complexes of group 9 and 10 metals in catalysis: trends and directions, Eur. J. Inorg. Chem. 2008 (2008) 2781–2800, https://doi.org/10.1002/ejic.200800323.

[132] S. Horn, C. Gandolfi, M. Albrecht, Transfer hydrogenation of ketones and activated olefins using chelating NHC ruthenium complexes, Eur. J. Inorg. Chem. 2011 (2011) 2863–2868, https://doi.org/10.1002/ejic.201100143.

[133] L.H. Chung, K.S. Cho, J. England, S.C. Chan, K. Wieghardt, C.Y. Wong, Ruthenium (II) and osmium(II) complexes bearing bipyridine and the N-heterocyclic carbene-based CˆNˆC pincer ligand: an experimental and density functional theory study, Inorg. Chem. 52 (2013) 9885–9896, https://doi.org/10.1021/ic4010196.

[134] C. Chen, Y. Zhang, S.H. Hong, N-heterocyclic carbene based ruthenium-catalyzed direct amide synthesis from alcohols and secondary amines: involvement of esters, J. Org. Chem. 76 (2011) 10005–10010, https://doi.org/10.1021/jo201756z.

[135] F.E. Fernández, M.C. Puerta, P. Valerga, Half-Sandwich ruthenium(II) picolyl-NHC complexes: synthesis, characterization, and catalytic activity in transfer hydrogenation reactions, Organometallics 30 (2011) 5793–5802, https://doi.org/10.1021/om200665f.

[136] W.W.N. O, A.J. Lough, R.H. Morris, Factors favoring efficient bifunctional catalysis. study of a ruthenium(II) hydrogenation catalyst containing an N-heterocyclic carbene with a primary amine donor, Organometallics 31 (2012) 2137–2151, https://doi.org/10.1021/om300108p.

[137] J. DePasquale, M. Kumar, M. Zeller, E.T. Papish, Variations on an NHC theme: which features enhance catalytic transfer hydrogenation with ruthenium complexes? Organometallics 32 (2013) 966–979, https://doi.org/10.1021/om300547f.

[138] S. Semwal, D. Ghorai, J. Choudhury, Wingtip-dictated cyclometalation of N-heterocyclic carbene ligand framework and its implication toward tunable catalytic activity, Organometallics 33 (2014) 7118–7124, https://doi.org/10.1021/om500876k.

[139] S. Das Adhikary, T. Samanta, G. Roymahapatra, F. Loiseau, D. Jouvenot, S. Giri, P. K. Chattaraj, J. Dinda, Synthesis, structure and electrochemical behaviour of Ru (II)- and Pt(II)-carbene complexes of the NCN-pincer 1,3-bis(2-pyridylmethyl)-1H-benzimidazolium chloride, New J. Chem. 34 (2010) 1974–1980, https://doi.org/10.1039/B9NJ00698B.

[140] M. Hollering, M. Albrecht, F.E. Kühn, Bonding and catalytic application of ruthenium N-heterocyclic carbene complexes featuring triazole, triazolylidene, and imidazolylidene ligands, Organometallics 35 (2016) 2980–2986, https://doi.org/10.1021/acs.organomet.6b00504.

[141] A.G. Nair, R.T. McBurney, D.B. Walker, M.J. Page, M.R. Gatus, M. Bhadbhade, B. A. Messerle, Ruthenium(II) complexes of hemilabile pincer ligands: synthesis and catalysing the transfer hydrogenation of ketones, Dalton Trans. 45 (2016) 14335–14342, https://doi.org/10.1039/C6DT02459A.

[142] T. Toda, S. Kuwata, Central N-heterocyclic carbene moieties in protic pincer-type bis(pyrazole) ligands: perturbation on steric and electronic properties of ruthenium center, J. Organomet. Chem. 917 (2020) 121270. https://www.sciencedirect.com/science/article/pii/S0022328X20301728.

[143] V. Friese, S. Nag, J. Wang, M.P. Santoni, A. Rodrigue-Witchel, G.S. Hanan, F. Schaper, Red phosphorescence in Ru^{II} complexes of a tridentate N-heterocyclic carbene ligand incorporating tetrahydropyrimidine, Eur. J. Inorg. Chem. 2011 (2011) 39–44, https://doi.org/10.1002/ejic.201000823.

[144] Z. Xi, B. Liu, C. Lu, W. Chen, Cobalt(III) complexes bearing bidentate, tridentate, and tetradentate N-heterocyclic carbenes: synthesis, X-ray structures and catalytic activities, Dalton Trans. (2009) 7008–7014, https://doi.org/10.1039/B906242D.

[145] P. Braunstein, D.G. Kelly, A. Tiripicchio, F. Ugozzoli, Complexes of functional phosphines. 22. Cobalt(II) complexes with β-keto phosphines and corresponding cobalt(III) enolates. Crystal and molecular structures of the fac and mer isomers of $[Co\{Ph_2PCH\cdots C(\cdots O)Ph\}_3]$, Inorg. Chem., 32 (1993) 4845-4852. https://doi.org/10.1021/ic00074a032.

[146] B. Liu, X. Liu, C. Chen, C. Chen, W. Chen, Carbene transfer reactivities of nickel (II)–N-heterocyclic carbene complexes and their applications in the synthesis of metal–NHC complexes, Organometallics 31 (2012) 282–288, https://doi.org/10.1021/om200881s.

[147] G. Mancano, M.J. Page, M. Bhadbhade, B.A. Messerle, Hemilabile and bimetallic coordination in Rh and Ir complexes of NCN pincer ligands, Inorg. Chem. 53 (2014) 10159–10170, https://doi.org/10.1021/ic501158x.

[148] N. Schneider, V. César, S. Bellemin-Laponnaz, L.H. Gade, Modular assembly of a chiral bis(oxazolinyl)carbene: a new meridionally coordinating tridentate spectator ligand, Organometallics 24 (2005) 4886–4888, https://doi.org/10.1021/om0506769.

[149] P.D. Newman, K.J. Cavell, A.J. Hallett, B.M. Kariuki, Rhodium and iridium complexes of an asymmetric bicyclic NHC bearing secondary pyridyl donors, Dalton Trans. 40 (2011) 8807–8813, https://doi.org/10.1039/C1DT10582E.

[150] B.M. Kariuki, J.A. Platts, P.D. Newman, It's all about Me: methyl-induced control of coordination stereochemistry by a flexible tridentate N, C, N' ligand, Dalton Trans. 43 (2014) 2971–2978, https://doi.org/10.1039/C3DT52841C.

[151] C. Chen, H. Qiu, W. Chen, Trinuclear copper(I) complex of 1,3-bis(2-pyridinylmethyl)imidazolylidene as a carbene-transfer reagent for the preparation of catalytically active nickel(II) and palladium(II) complexes, J. Organomet. Chem. 696 (2012) 4166–4172. https://www.sciencedirect.com/science/article/pii/S0022328X11005973.

[152] T. Zell, M. Feierabend, B. Halfter, U. Radius, Stoichiometric and catalytic C-cl activation of aryl chlorides using an NHC-stabilized nickel(0) complex, J. Organomet. Chem. 696 (2011) 1380–1387. https://www.sciencedirect.com/science/article/pii/S0022328X11000246.

[153] F. Li, J.J. Hu, L.L. Koh, T.S.A. Hor, Substituent-dependent structures and catalysis of benzimidazole-tethered N-heterocyclic carbene complexes of Ag(I), Ni(II) and Pd(II), Dalton Trans. 39 (2010) 5231–5241, https://doi.org/10.1039/C000722F.

[154] F. Jean-Baptiste dit Dominique, H. Gornitzka, C. Hemmert,, Chiral variation of a hybrid bis(carbene-amido) ligand system, Organometallics 29 (2010) 2868–2873, https://doi.org/10.1021/om100048d.

[155] M.K. Samantaray, M.M. Shaikh, P. Ghosh, Rare $[(NHC)_2Ni\text{-}OH]$-type terminal nickel hydroxo and $[(NHC)_2Ni]$-type complexes of N/O-functionalized N-heterocyclic carbenes as precatalysts for highly Desirable Base-free Michael reactions in air at ambient temperature, Organometallics 28 (2009) 2267–2275, https://doi.org/10.1021/om801186f.

[156] C. Zhang, Z.-X. Wang, N-heterocyclic carbene-based nickel complexes: synthesis and catalysis in cross-couplings of aryl chlorides with ArMX (M = Mg or Zn), Organometallics 28 (2009) 6507–6514, https://doi.org/10.1021/om9006399.

[157] S. Ando, N. Nakano, H. Matsunaga, T. Ishizuka, Synthesis and catalytic activities of ni complexes bearing a novel N-C–N pincer ligand containing NHC with a bicyclic motif, J. Organomet. Chem. 913 (2020) 121200. https://www.sciencedirect.com/science/article/pii/S0022328X20301017.

[158] A.G. Nair, R.T. McBurney, M.R.D. Gatus, D.B. Walker, M. Bhadbhade, B. A. Messerle, Synthesis and catalytic activity of nickel(II) complexes containing NCN pincer ligands, J. Organomet. Chem. 845 (2017) 63–70. https://www.sciencedirect.com/science/article/pii/S0022328X17300955.

[159] P.D. Newman, K.J. Cavell, B.M. Kariuki, Metal complexes of chiral NHCs containing a fused six- and seven-membered central ring, Organometallics 29 (2010) 2724–2734, https://doi.org/10.1021/om1002107.

[160] X. Ren, M. Wesolek, P. Braunstein, Nickel(II) complexes with tritopic $N_{imine}C^{NHC}N_{amine}$ pincer ligands, Chem. Eur. J. 24 (2018) 14794–14801, https://doi.org/10.1002/chem.201802969.

[161] S. Gu, J. Du, J. Huang, Y. Guo, L. Yang, W. Xu, W. Chen, Unsymmetrical NCN-pincer mononuclear and dinuclear nickel(II) complexes of N-heterocyclic carbene (NHC): synthesis, structure and catalysis for Suzuki-miyaura cross-coupling, Dalton Trans. 46 (2017) 586–594, https://doi.org/10.1039/C6DT03944H.

[162] Y. Zhou, Z. Xi, W. Chen, D. Wang, Dinickel(II) complexes of Bis(N-heterocyclic carbene) ligands containing $[Ni_2(\mu\text{-}OH)]$ cores as highly efficient catalysts for the coupling of aryl chlorides, Organometallics 27 (2008) 5911–5920, https://doi.org/10.1021/om800711g.

[163] S. Gu, H. Xu, N. Zhang, W. Chen, Triazole-functionalized N-heterocyclic carbene complexes of palladium and platinum and efficient aqueous Suzuki-Miyaura coupling reaction, Chem. Asian J. 5 (2010) 1677–1686, https://doi.org/10.1002/asia.201000071.

[164] C. Chen, H. Qiu, W. Chen, Synthesis and characterization of nickel inverse 9-metallacrown-3, palladium-silver, and dinuclear platinum complexes containing pyrazole-functionalized NHC ligands, Inorg. Chem. 50 (2011) 8671–8678, https://doi.org/10.1021/ic2012233.

[165] C.-Y. Liao, K.-T. Chan, J.-Y. Zeng, C.-H. Hu, C.-Y. Tu, H.M. Lee, Nonchelate and chelate complexes of palladium(II) with N-heterocyclic carbene ligands of amido functionality, Organometallics 26 (2007) 1692–1702, https://doi.org/10.1021/om0610041.

[166] D.J. O'Hearn, R.D. Singer, Direct synthesis of a copper(II) N-heterocyclic carbene complex in air, Organometallics 36 (2017) 3175–3177, https://doi.org/10.1021/acs.organomet.7b00489.

[167] A.O. Larsen, W. Leu, C.N. Oberhuber, J.E. Campbell, A.H. Hoveyda, Bidentate NHC-based chiral ligands for efficient Cu-catalyzed enantioselective allylic alkylations: structure and activity of an air-stable chiral cu complex, J. Am. Chem. Soc. 126 (2004) 11130–11131, https://doi.org/10.1021/ja046245j.

[168] P.L. Arnold, M. Rodden, K.M. Davis, A.C. Scarisbrick, A.J. Blake, C. Wilson, Asymmetric lithium(I) and copper(II) alkoxy-N-heterocyclic carbene complexes; crystallographic characterisation and Lewis acid catalysis, Chem. Commun. 14 (2004) 1612–1613, https://doi.org/10.1039/B404614E.

[169] J.J. Van Veldhuizen, J.E. Campbell, R.E. Giudici, A.H. Hoveyda, A readily available chiral Ag-based N-heterocyclic carbene complex for use in efficient and highly enantioselective Ru-catalyzed olefin metathesis and Cu-catalyzed allylic alkylation reactions, J. Am. Chem. Soc. 127 (2005) 6877–6882, https://doi.org/10.1021/ja050179j.

[170] E.L. Kolychev, V.V. Shuntikov, V.N. Khrustalev, A.A. Bush, M.S. Nechaev, Dual reactivity of N-heterocyclic carbenes towards copper(II) salts, Dalton Trans. 40 (2011) 3074–3076, https://doi.org/10.1039/C0DT01630F.

[171] M. Sharma, B. Adhikari, R.F. Awoyemi, A.M. Perkins, A.K. Duckworth, B. Donnadieu, D.O. Wipf, S.L. Stokes, J.P. Emerson, Copper(II) NHC catalysts for the formation of phenol from arylbozonic acid, Chemistry (2022) 560–575, https://doi.org/10.3390/chemistry4020040.

[172] M. Sharma, A.M. Perkins, R.F. Awoyemi, A.N. Schmittou, S. Raju, B.S. Pierce, B. Donnadieu, D.O. Wipf, S.L. Stokes, J.P. Emerson, Three water-soluble copper (II) N-heterocyclic carbene complexes: toward copper-catalyzed ketone reduction under sustainable conditions, Dalton Trans. (2024), https://doi.org/10.1039/D3DT03406B.

[173] B. Liu, B. Liu, Y. Zhou, W. Chen, Copper(II) hydroxide complexes of N-heterocyclic carbenes and catalytic oxidative amination of arylboronic acids, Organometallics 29 (2010) 1457–1464, https://doi.org/10.1021/om100009u.

[174] B. Liu, X. Ma, F. Wu, W. Chen, Simple synthesis of neutral and cationic Cu-NHC complexes, Dalton Trans. 44 (2015) 1836–1844, https://doi.org/10.1039/C4DT02986K.

[175] M.T. Nguyen, D. Gusev, A. Dmitrienko, B.M. Gabidullin, D. Spasyuk, M. Pilkington, G.I. Nikonov, Ge(0) compound stabilized by a diimino-carbene ligand: synthesis and ambiphilic reactivity, J. Am. Chem. Soc. 142 (2020) 5852–5861, https://doi.org/10.1021/jacs.0c01283.

[176] R. Buhaibeh, C. Duhayon, D.A. Valyaev, J.-B. Sortais, Y. Canac, Cationic PCP and PCN NHC Core pincer-type Mn(I) complexes: from synthesis to catalysis, Organometallics 40 (2021) 231–241, https://doi.org/10.1021/acs.organomet.0c00717.

[177] M. Bouché, M. Mordan, B.M. Kariuki, S.J. Coles, J. Christensen, P.D. Newman, Mono- and dimeric complexes of an asymmetric heterotopic P, C^{NHC}, pyr ligand, Dalton Trans. 45 (2016) 13347–13360, https://doi.org/10.1039/C6DT02476A.

[178] D.A. Valyaev, J. Willot, L.P. Mangin, D. Zargarian, N. Lugan, Manganese-mediated synthesis of an NHC core non-symmetric pincer ligand and evaluation of its coordination properties, Dalton Trans. 46 (2017) 10193–10196, https://doi.org/10.1039/C7DT02190A.

[179] Z. Xi, X. Zhang, W. Chen, S. Fu, D. Wang, Synthesis and structural characterization of nickel(II) complexes supported by pyridine-functionalized N-heterocyclic carbene ligands and their catalytic acitivities for Suzuki coupling, Organometallics 26 (2007) 6636–6642, https://doi.org/10.1021/om700796g.

[180] S. Haslinger, J.W. Kück, M.R. Anneser, M. Cokoja, A. Pöthig, F.E. Kühn, Formation of highly strained N-heterocycles via decomposition of iron N-heterocyclic carbene complexes: the value of labile Fe-C bonds, Chem. Eur. J. 21 (2015) 17860–17869, https://doi.org/10.1002/chem.201503282.

[181] W. Su, H.A. Younus, K. Zhou, Z.A.K. Khattak, S. Chaemcheun, C. Chen, F. Verpoort, Chemical and photochemical water oxidation catalyzed by novel ruthenium complexes comprising a negatively charged $NC^{NHC}O$ ligand, Catal. Sci. Technol. 7 (2017) 387–395, https://doi.org/10.1039/C6CY02333A.

[182] W. Su, H.A. Younus, S. Chaemchuen, C. Chen, F. Verpoort, Chemical and photochemical water oxidation by [RuCl($NC^{NHC}O$)(DMSO)(Py)]-type complexes, ChemCatChem 9 (2017) 2565–2573, https://doi.org/10.1002/cctc.201700049.

[183] F. Cai, W. Su, H.A. Younus, K. Zhou, C. Chen, S. Chaemchuen, F. Verpoort, Synthesis and characterization of [Ru($NC^{NHC}O$)(bpy)L]$^+$ complexes and their reactivity towards water oxidation, New J. Chem. 42 (2018) 2476–2482, https://doi.org/10.1039/C7NJ03198J.

[184] A.R. Naziruddin, C.S. Zhuang, W.J. Lin, W.S. Hwang, Donor functionalized ruthenium N-heterocyclic carbene complexes in alcohol oxidation reactions, Dalton Trans. 43 (2014) 5335–5342, https://doi.org/10.1039/C3DT53125B.

[185] D. Yang, J. Dong, B. Wang, Homo- and copolymerization of norbornene with tridentate nickel complexes bearing *o*-aryloxide-N-heterocyclic carbene ligands, Dalton Trans. 47 (2018) 180–189, https://doi.org/10.1039/C7DT03928J.

[186] D. Yang, Y. Tang, H. Song, B. Wang, Synthesis, structures, and norbornene polymerization behavior of palladium complexes bearing tridentate *o*-aryloxide-N-heterocyclic carbene ligands, Organometallics 35 (2016) 1392–1398, https://doi.org/10.1021/acs.organomet.5b01006.

[187] T. Yagyu, S. Oya, M. Maeda, K. Jitsukawa, Syntheses and characterization of palladium(II) complexes with tridentate N-heterocyclic carbene ligands containing aryloxy groups and their application to Heck reaction, Chem. Lett. 35 (2006) 154–155, https://doi.org/10.1246/cl.2006.154.

[188] J.H. Lee, K.S. Yoo, C.P. Park, J.M. Olsen, S. Sakaguchi, G.K. Surya Prakash, T. Mathew, K.W. Jung, An Air/Water-Stable Tridentate N-Heterocyclic Carbene Palladium(II) Complex: Catalytic C-H Activation of Hydrocarbons *via* Hydrogen/Deuterium Exchange Process in Deuterium Oxide, Adv. Synth. Catal., 351 (2009) 563-568. https://doi.org/10.1002/adsc.200800698.

[189] V. Leigh, W. Ghattas, H. Mueller-Bunz, M. Albrecht, Synthesis of pincer-type N-heterocyclic carbene palladium complexes with a hemilabile ligand and their application in cross-coupling catalysis, J. Organomet. Chem. 771 (2014) 33–39. https://www.sciencedirect.com/science/article/pii/S0022328X14002599.

[190] D. Cherukaraveedu, P.T. Cowling, G.P. Birch, M. Bradley, A. Lilienkampf, Solid-phase synthesis of biocompatible N-heterocyclic carbene-Pd catalysts using a sub-monomer approach, Org. Biomol. Chem. 17 (2019) 5533–5537, https://doi.org/10.1039/C9OB00716D.

[191] S. Luo, M.A. Siegler, E. Bouwman, Dinuclear nickel complexes of thiolate-functionalized carbene ligands and their electrochemical properties, Organometallics 37 (2018) 740–747, https://doi.org/10.1021/acs.organomet.7b00576.

[192] T.-H. Wang, W.-C. Chen, T.-G. Ong, Carbodicarbenes or bent allenes, J. Chin. Chem. Soc. 64 (2017) 124–132, https://doi.org/10.1002/jccs.201600241.

[193] C. Gradert, J. Krahmer, F.D. Sönnichsen, C. Näther, F. Tuczek, Small-molecule activation with Molybdenum(0) complexes supported by mixed imidazol-2-ylidene/phosphanyl hybrid ligands - electronic and structural consequences of substituting a phosphane by a carbene group, Eur. J. Inorg. Chem. 2013 (2013) 3943–3955, https://doi.org/10.1002/ejic.201300177.

[194] C. Gradert, J. Krahmer, F.D. Sönnichsen, C. Näther, F. Tuczek, Molybdenum(0)–carbonyl complexes supported by mixed benzimidazol-2-ylidene/phosphine ligands: influence of benzannulation on the donor properties of the NHC groups, J. Organomet. Chem. 770 (2014) 61–68. https://www.sciencedirect.com/science/article/pii/S0022328X14003878.

[195] C. Gradert, N. Stucke, J. Krahmer, C. Nather, F. Tuczek, Molybdenum complexes supported by mixed NHC/phosphine ligands: activation of N_2 and reaction with P$(OMe)_3$ to the first meta-phosphite complex, Chem. Eur. J. 21 (2015) 1130–1137, https://doi.org/10.1002/chem.201405737.

[196] E. Niecke, M. Engelmann, H. Zorn, B. Krebs, G. Henkel, Complex-stabilization of an aminooxophosphane (phosphinidene oxide), Angew. Chem. Int. Ed. 19 (1980) 710–712, https://doi.org/10.1002/anie.198007101.

[197] M. Alonso, M.E. García, M.A. Ruiz, H. Hamidov, J.C. Jeffery, Chemistry of the phosphinidene oxide ligand, J. Am. Chem. Soc. 126 (2004) 13610–13611, https://doi.org/10.1021/ja045487g.

[198] O. Krahe, F. Neese, R. Streubel, The quest for ring opening of oxaphosphirane complexes: a coupled-cluster and density functional study of CH_3PO isomers and their $Cr(CO)_5$ complexes, Chem. Eur. J. 15 (2009) 2594–2601, https://doi.org/10.1002/chem.200801494.

[199] M. Alonso, M.A. Alvarez, M.E. Garcia, M.A. Ruiz, H. Hamidov, J.C. Jeffery, Chemistry of the oxophosphinidene ligand. 2. Reactivity of the anionic complexes $[MCp\{P(O)R^*\}(CO)_2]^-$ (M = Mo, W; R* = 2,4,6–$C_6H_2tBu_3$) toward electrophiles based on elements different from carbon, Inorg. Chem. 49 (2010) 11595–11605, https://doi.org/10.1021/ic101839k.

[200] A. Grundmann, M.B. Sárosi, P. Lönnecke, R. Frank, E. Hey-Hawkins, Terminal alkylphosphanylidene Organo-tantalum(V) complexes, Eur. J. Inorg. Chem. 2013 (2013) 3137–3140, https://doi.org/10.1002/ejic.201300500.

[201] A. Eizawa, K. Arashiba, A. Egi, H. Tanaka, K. Nakajima, K. Yoshizawa, Y. Nishibayashi, Catalytic reactivity of molybdenum-trihalide complexes bearing PCP-type pincer ligands, Chem. Asian J. 14 (2019) 2091–2096, https://doi.org/10.1002/asia.201900496.

[202] A. Egi, H. Tanaka, A. Konomi, Y. Nishibayashi, K. Yoshizawa, Nitrogen fixation catalyzed by dinitrogen-bridged dimolybdenum complexes bearing PCP- and PNP-type pincer ligands: a shortcut pathway deduced from free energy profiles, Eur. J. Inorg. Chem. 2020 (2020) 1490–1498, https://doi.org/10.1002/ejic.201901160.

[203] L. Maser, P. Korziniowski, R. Langer, Flexible coordination of carbodiphosphorane-based pincer ligands in chromium(0) carbonyl complexes, Can. J. Chem. 99 (2021) 253–258, https://doi.org/10.1139/cjc-2020-0351.

[204] D.P. Zobernig, M. Luxner, B. Stöger, L.F. Veiros, K. Kirchner, Hydrogenation of terminal alkenes catalyzed by air-stable Mn(I) complexes bearing an N-heterocyclic carbene-based PCP pincer ligand, Chem. Eur. J. 30 (2024) e202302455, https://doi.org/10.1002/chem.202302455.

[205] R. Thenarukandiyil, R. Kamte, S. Garhwal, P. Effnert, N. Fridman, G. de Ruiter, α-Methylation of ketones and indoles catalyzed by a Manganese(I) $PC^{NHC}P$ pincer complex with methanol as a C_1 source, Organometallics 42 (2023) 62–71, https://doi.org/10.1021/acs.organomet.2c00520.

[206] O. Kaufhold, A. Stasch, T. Pape, A. Hepp, P.G. Edwards, P.D. Newman, F.E. Hahn, Metal template controlled formation of [11]ane-P_2C^{NHC} macrocycles, J. Am. Chem. Soc. 131 (2009) 306–317, https://doi.org/10.1021/ja807333f.

[207] O. Kaufhold, A. Stasch, P.G. Edwards, F.E. Hahn, Template controlled synthesis of a coordinated [11]ane-P_2C^{NHC} macrocycle, Chem. Commun. (2007) 1822–1824, https://doi.org/10.1039/B617033A.

[208] V. Blase, T. Pape, F.E. Hahn, Template synthesis of a macrocycle with a mixed NHC/phosphine donor set, J. Organomet. Chem. 696 (2011) 3337–3342. https://www.sciencedirect.com/science/article/pii/S0022328X11004554.

[209] A. Eizawa, S. Nishimura, K. Arashiba, K. Nakajima, Y. Nishibayashi, Synthesis of ruthenium complexes bearing PCP-type pincer ligands and their application to direct synthesis of imines from amines and benzyl alcohol, Organometallics 37 (2018) 3086–3092, https://doi.org/10.1021/acs.organomet.8b00465.

[210] B. Gnanaprakasam, J. Zhang, D. Milstein, Direct synthesis of imines from alcohols and amines with liberation of H_2, Angew. Chem. Int. Ed. 49 (2010) 1468–1471. https://onlinelibrary.wiley.com/doi/abs/10.1002/anie.200907018.

[211] P.L. Chiu, H.M. Lee, Chemistry of the $PC^{NHC}P$ ligand: silver and ruthenium complexes, facial/meridional coordination, and catalytic transfer hydrogenation, Organometallics 24 (2005) 1692–1702, https://doi.org/10.1021/om049070v.

[212] S. Gischig, A. Togni, Synthesis and coordination chemistry of a new chiral tridentate PCP N-heterocyclic carbene ligand based on a ferrocene backbone, Organometallics 23 (2004) 2479–2487, https://doi.org/10.1021/om049893k.

[213] S. Garhwal, A. Kaushansky, N. Fridman, L.J.W. Shimon, G. Ruiter, Facile H/D exchange at (hetero)aromatic hydrocarbons catalyzed by a stable trans-dihydride N-heterocyclic carbene (NHC) iron complex, J. Am. Chem. Soc. 142 (2020) 17131–17139, https://doi.org/10.1021/jacs.0c07689.

[214] S. Garhwal, N. Fridman, G. de Ruiter, Z-selective alkyne functionalization catalyzed by a trans-dihydride N-heterocyclic carbene (NHC) iron complex, Inorg. Chem. 59 (2020) 13817–13821, https://doi.org/10.1021/acs.inorgchem.0c02057.

[215] S. Garhwal, A. Kaushansky, N. Fridman, G. de Ruiter, Part per million levels of an anionic iron hydride complex catalyzes selective alkene isomerization via two-state reactivity, Chem Catal. 1 (2021) 631–647. https://www.sciencedirect.com/science/article/pii/S2667109321000336.

[216] V. Tegethoff, T. Lübbering, C. Schulte to Brinke, B. Schirmer, J. Neugebauer, F.E. Hahn,, Synthesis of ruthenium(II) complexes bearing macrocyclic [11]ane-P_2C^{NHC} ligands by a template-controlled domino reaction, Organometallics 40 (2021) 606–617, https://doi.org/10.1021/acs.organomet.0c00812.

[217] A. Flores-Figueroa, T. Pape, J.J. Weigand, F.E. Hahn, Template-controlled formation of an [11]ane-P_2C^{NHC} macrocyclic ligand at an iron(II) template, Eur. J. Inorg. Chem. 2010 (2010) 2907–2910, https://doi.org/10.1002/ejic.201000467.

[218] A. Flores-Figueroa, O. Kaufhold, A. Hepp, R. Fröhlich, F.E. Hahn, Synthesis of a ruthenium(II) complex containing an [11]ane-P_2C^{NHC} (NHC = Imidazolidin-2-ylidene) macrocycle, Organometallics 28 (2009) 6362–6369, https://doi.org/10.1021/om900703q.

[219] J. Petit, A. Cavaillé, N. Saffon-Merceron, M. Fustier-Boutignon, N. Mézailles, Double α, α-CH bond insertion into sp^3 CH_2 moiety: synthesis of a Fe carbene bis-hydride dinitrogen complex, Dalton Trans. 50 (2021) 9554–9559, https://doi.org/10.1039/D1DT00610J.

[220] A.F. Hill, C.M.A. McQueen, Dihydroperimidine-derived PNP pincer complexes as intermediates en route to N-heterocyclic carbene pincer complexes, Organometallics 33 (2014) 1909–1912, https://doi.org/10.1021/om5000985.

[221] C.M. McQueen, A.F. Hill, C. Ma, J.S. Ward, Ruthenium and osmium complexes of dihydroperimidine-based N-heterocyclic carbene pincer ligands, Dalton Trans. 44 (2015) 20376–20385, https://doi.org/10.1039/C5DT03728J.

[222] S. Tang, N. von Wolff, Y. Diskin-Posner, G. Leitus, Y. Ben-David, D. Milstein, Pyridine-based PCP-ruthenium complexes: unusual structures and metal-ligand cooperation, J. Am. Chem. Soc. 141 (2019) 7554–7561, https://doi.org/10.1021/jacs.9b02669.
[223] S. Zhang, J.P. Krogman, Synthesis and characterization of bis(phosphine) carbodicarbene complexes of iron, cobalt, and nickel, Organometallics 40 (2021) 1926–1933, https://doi.org/10.1021/acs.organomet.1c00241.
[224] D.A. Valyaev, O.A. Filippov, N. Lugan, G. Lavigne, N.A. Ustynyuk, Umpolung of methylenephosphonium ions in their manganese half-sandwich complexes and application to the synthesis of chiral phosphorus-containing ligand scaffolds, Angew. Chem. Int. Ed. 54 (2015) 6315–6319, https://doi.org/10.1002/anie.201501256.
[225] A. Plikhta, A. Pothig, E. Herdtweck, B. Rieger, Toward new organometallic architectures: synthesis of carbene-centered rhodium and palladium bisphosphine complexes. stability and reactivity of [PC(BIm)PRh(L)][PF_6] pincers, Inorg. Chem. 54 (2015) 9517–9528, https://doi.org/10.1021/acs.inorgchem.5b01428.
[226] S. Takaoka, A. Eizawa, S. Kusumoto, K. Nakajima, Y. Nishibayashi, K. Nozaki, Hydrogenation of carbon dioxide with organic base by $PC^{II}P$-Ir catalysts, Organometallics 37 (2018) 3001–3009, https://doi.org/10.1021/acs.organomet.8b00377.
[227] K. Matoba, A. Eizawa, S. Nishimura, K. Arashiba, K. Nakajima, Y. Nishibayashi, Practical synthesis of a PCP-type pincer ligand and its metal complexes-, Synthesis 50 (2017) 1015–1019. http://www.thieme-connect.com/products/ejournals/abstract/10.1055/s-0036-1589153.
[228] J.Y. Zeng, M.-H. Hsieh, H.M. Lee, Rhodium complexes of $PC^{NHC}P$: oxidative addition of dichloromethane and catalytic hydrosilylation of alkynes affording (E)-alkenylsilanes, J. Organomet. Chem. 690 (2005) 5662–5671. https://www.sciencedirect.com/science/article/pii/S0022328X05005449.
[229] E.W. Ainscough, A.M. Brodie, A.K. Burrell, A. Derwahl, S.K. Taylor, A rhodium(I) complex containing a mixed donor 'P_2N' tridentate ligand, Inorg. Chim. Acta 357 (2004) 2379–2384. https://www.sciencedirect.com/science/article/pii/S0020169303004833.
[230] R. Dorta, L.J.W. Shimon, H. Rozenberg, D. Milstein, Facile oxidative addition of C-Cl bonds to new neutral and cationic rhodium(I)-bipyridine complexes, Eur. J. Inorg. Chem. (2002) 1827–1834, https://doi.org/10.1002/1099-0682(200207)2002:7<1827::AID-EJIC1827>3.0.CO;2-Q.
[231] K.J. Bradd, B.T. Heaton, C. Jacob, J.T. Sampanthar, A. Steiner, Oxidative addition of chlorinated solvents (e.g. CH_2Cl_2 and $CHCl_3$) with rhodium(I) complexes; crystal structure of mer-[$Rh(py)_3(CH_2Cl)Cl_2$], J. Chem. Soc., Dalton Trans. (1999) 1109–1112, https://doi.org/10.1039/A809652J.
[232] K. Kashiwabara, A. Morikawa, T. Suzuki, K. Isobe, K. Tatsumi, Oxidative additions of dichloromethane and cyclo-octasulfur to rhodium(I) complexes containing (2-aminoethyl)-dimethylphosphine or -diphenylphosphine, J. Chem. Soc., Dalton Trans. (1997) 1075–1081, https://doi.org/10.1039/A606730A.
[233] L. Maser, C. Schneider, L. Vondung, L. Alig, R. Langer, Quantifying the donor strength of ligand-stabilized main group fragments, J. Am. Chem. Soc. 141 (2019) 7596–7604, https://doi.org/10.1021/jacs.9b02598.
[234] M.V. Jiménez, J.J. Pérez-Torrente, M.I. Bartolomé, V. Gierz, F.J. Lahoz, L.A. Oro, Rhodium(I) complexes with hemilabile N-heterocyclic carbenes: efficient alkyne hydrosilylation catalysts, Organometallics 27 (2008) 224–234, https://doi.org/10.1021/om700728a.
[235] M.P. Mitoraj, H. Zhu, A. Michalak, T. Ziegler, On the origin of the *trans*-influence in square planar d^8-complexes: a theoretical study, Int. J. Quant. Chem. 109 (2009) 3379–3386, https://doi.org/10.1002/qua.21910.
[236] S.-I. Fuku-en, J. Yamamoto, S. Kojima, Y. Yamamoto, Synthesis and application of new dipyrido-annulated N-heterocyclic carbene with phosphorus substituents, Chem. Lett. 43 (2014) 468–470, https://doi.org/10.1246/cl.131074.
[237] A.F. Hill, C.M.A. McQueen, Dihydroperimidine-derived N-heterocyclic pincer carbene complexes via double C-H activation, Organometallics 31 (2012) 8051–8054, https://doi.org/10.1021/om300897w.
[238] A.F. Hill, C. Ma, C.M.A. McQueen, J.S. Ward, Iridium complexes of perimidine-based N-heterocyclic carbene pincer ligands via aminal C-H activation, Dalton Trans. 47 (2018) 1577–1587, https://doi.org/10.1039/C7DT04572G.
[239] L.J. Watson, A.F. Hill, C-H activation in bimetallic rhodium complexes to afford N-heterocyclic carbene pincer complexes, Dalton Trans. 52 (2023) 2164–2174, https://doi.org/10.1039/D2DT03984B.
[240] S. Langbein, H. Wadepohl, L.H. Gade, Ditopic N-heterocyclic pincer carbene complexes containing a perylene backbone, Organometallics 35 (2016) 809–815, https://doi.org/10.1021/acs.organomet.6b00049.
[241] P.D. Newman, K.J. Cavell, B.M. Kariuki, Variable coordination of a chiral diphosphine containing an amidinium/NHC group within its backbone: μ-P, P', κ^2-P, P' and κ^3-P, C, P' coordination modes, Dalton Trans. 41 (2012) 12395–12407, https://doi.org/10.1039/C2DT31475D.
[242] C.C. Roberts, D.M. Matías, M.J. Goldfogel, S.J. Meek, Lewis acid activation of carbodicarbene catalysts for Rh-catalyzed hydroarylation of dienes, J. Am. Chem. Soc. 137 (2015) 6488–6491, https://doi.org/10.1021/jacs.5b03510.
[243] M.J. Goldfogel, C.C. Roberts, R.S. Manan, S.J. Meek, Diastereoselective synthesis of gamma-substituted 2-butenolides via (CDC)-Rh-catalyzed intermolecular hydroalkylation of dienes with silyloxyfurans, Org. Lett. 19 (2017) 90–93, https://doi.org/10.1021/acs.orglett.6b03369.
[244] M.J. Goldfogel, C.C. Roberts, S.J. Meek, Intermolecular hydroamination of 1,3-dienes catalyzed by bis(phosphine)carbodicarbene-rhodium complexes, J. Am. Chem. Soc. 136 (2014) 6227–6230, https://doi.org/10.1021/ja502275w.
[245] W. Xu, L. Maser, L. Alig, R. Langer, Rhodium carbonyl complexes featuring carbodiphosphorane-based pincer ligands, Polyhedron 196 (2021) 115018. https://www.sciencedirect.com/science/article/pii/S0277538720306756.
[246] T. Steinke, B.K. Shaw, H. Jong, B.O. Patrick, M.D. Fryzuk, Synthesis and coordination chemistry of a tridentate *o*-phenylene-bridged diphosphine-NHC system, Organometallics 28 (2009) 2830–2836, https://doi.org/10.1021/om9000764.
[247] A. Kumar, R. Gupta, G. Mani, PCP pincer carbene nickel(II) chloride, hydride, and thiolate complexes: hydrosilylation of aldehyde, ketone, and nitroarene by the thiolate complex, Organometallics 42 (2023) 732–744, https://doi.org/10.1021/acs.organomet.3c00106.
[248] F.E. Hahn, M.C. Jahnke, T. Pape, Synthesis of palladium and platinum complexes with phosphine-functionalized benzimidazolin-2-ylidene ligands, Organometallics 25 (2006) 5927–5936, https://doi.org/10.1021/om060741u.
[249] S. Gischig, A. Togni, Pd(II) complexes of tridentate PCP N-heterocyclic carbene ligands: structural aspects and application in asymmetric hydroamination of cyano olefins, Eur. J. Inorg. Chem. 2005 (2005) 4745–4754, https://doi.org/10.1002/ejic.200500612.
[250] E.M. Schuster, M. Botoshansky, M. Gandelman, 1,2,3-triazolylidene based complexes via post-modification of pincer click ligands, Dalton Trans. 40 (2011) 8764–8767, https://doi.org/10.1039/C1DT10264H.
[251] B. Pan, S. Pierre, M.W. Bezpalko, J.W. Napoline, B.M. Foxman, C.M. Thomas, Isolation of N-heterocyclic alkyl intermediates en route to transition metal N-heterocyclic carbene complexes: insight into a C-H activation mechanism, Organometallics 32 (2013) 704–710, https://doi.org/10.1021/om301230f.
[252] V. Subramaniyan, B. Dutta, A. Govindaraj, G. Mani, Facile synthesis of Pd(II) and Ni(II) pincer carbene complexes by the double C-H bond activation of a new hexahydropyrimidine-based bis(phosphine): catalysis of C-N couplings, Dalton Trans. 48 (2019) 7203–7210, https://doi.org/10.1039/C8DT03413C.
[253] C. Reitsamer, S. Stallinger, W. Schuh, H. Kopacka, K. Wurst, D. Obendorf, P. Peringer, Novel access to carbodiphosphoranes in the coordination sphere of group 10 metals: template synthesis and protonation of PCP pincer carbodiphosphorane complexes of $C(dppm)_2$, Dalton Trans. 41 (2012) 3503–3514, https://doi.org/10.1039/C2DT11949H.
[254] C. Reitsamer, I. Hackl, W. Schuh, H. Kopacka, K. Wurst, P. Peringer, Gold(I) and gold(III) complexes of the $[CH(dppm)_2]^+$ and $C(dppm)_2$ PCP pincer ligand systems, J. Organomet. Chem. 830 (2017) 150–154. https://www.sciencedirect.com/science/article/pii/S0022328X1630585X.
[255] M. Zhang, X. Ni, Z. Shen, Synthesis of bimetallic bis(phenolate) N-heterocyclic carbene lanthanide complexes and their applications in the ring-opening polymerization of l-lactide, Organometallics 33 (2014) 6861–6867, https://doi.org/10.1021/om500930m.
[256] M. Zhang, J. Zhang, X. Ni, Z. Shen, Bis(phenolate) N-heterocyclic carbene rare earth metal complexes: synthesis, characterization and applications in the polymerization of n-hexyl isocyanate, RSC Adv. 5 (2015) 83295–83303, https://doi.org/10.1039/C5RA16447H.
[257] J. Long, D.M. Lyubov, G.A. Gurina, Y.V. Nelyubina, F. Salles, Y. Guari, J. Larionova, A.A. Trifonov, Using N-heterocyclic carbenes as weak equatorial ligands to design single-molecule magnets: zero-field slow relaxation in two octahedral dysprosium(III) complexes, Inorg. Chem. 61 (2022) 1264–1269, https://doi.org/10.1021/acs.inorgchem.1c03429.
[258] G.A. Gurina, A.V. Markin, A.V. Cherkasov, I.A. Godovikov, A.M. Ob'edkov, A. A. Trifonov, Sc^{3+} chloro and alkyl complexes coordinated by pincer NHC-tethered bis(phenolate) ligands, Eur. J. Inorg. Chem. (2023) e202300392, https://doi.org/10.1002/ejic.202300392.
[259] H. Yao, Y. Zhang, H. Sun, Q. Shen, Anionic lanthanide complexes bearing a bis (phenoxy)-functionalized N-heterocyclic carbene ligand: syntheses and molecular structures, Eur. J. Inorg. Chem. 2009 (2009) 1920–1925, https://doi.org/10.1002/ejic.200801109.
[260] K. Lv, D. Cui, Tridentate CCC-pincer bis(carbene)-ligated rare-earth metal dibromides, Synthesis and Characterization, Organometallics 27 (2008) 5438–5440, https://doi.org/10.1021/om800801k.
[261] J. Zhang, H. Yao, Y. Zhang, H. Sun, Q. Shen, Lanthanide carbene halides through protonolysis of Ln-N bonds by imidazolium salts: synthesis and structure of salicylaldiminato-functionalized N-heterocyclic carbene lanthanide bromides, Organometallics 27 (2008) 2672–2675, https://doi.org/10.1021/om8001922.
[262] H. Aihara, T. Matsuo, H. Kawaguchi, Titanium N-heterocyclic carbene complexes incorporating an imidazolium-linked bis(phenol), Chem. Commun. (2003) 2204–2205, https://doi.org/10.1039/B305745C.
[263] D. Zhang, N. Liu, Titanium complexes bearing bisaryloxy-N-heterocyclic carbenes: synthesis, reactivity, and ethylene polymerization study, Organometallics 28 (2009) 499–505, https://doi.org/10.1021/om800717h.
[264] D. Zhang, Dinuclear titanium(IV) complexes bearing phenoxide-tethered N-heterocyclic carbene ligands with cisoid conformation through control of hydrolysis, Eur. J. Inorg. Chem. 2007 (2007) 4839–4845, https://doi.org/10.1002/ejic.200700464.
[265] N. Zhao, G. Hou, X. Deng, G. Zi, M.D. Walter, Group 4 metal complexes with new chiral pincer NHC-ligands: synthesis, structure and catalytic activity, Dalton Trans. 43 (2014) 8261–8272, https://doi.org/10.1039/C4DT00510D.
[266] C. Romain, L. Brelot, S. Bellemin-Laponnaz, S. Dagorne, Synthesis and structural characterization of a novel family of titanium complexes bearing a tridentate bis-phenolate-N-heterocyclic carbene dianionic ligand and their use in the controlled ROP of *rac*-lactide, Organometallics 29 (2010) 1191–1198, https://doi.org/10.1021/om901084n.
[267] C. Romain, S. Choua, J.P. Collin, M. Heinrich, C. Bailly, L. Karmazin-Brelot, S. Bellemin-Laponnaz, S. Dagorne, Redox and luminescent properties of robust and air-stable N-heterocyclic carbene group 4 metal complexes, Inorg. Chem. 53 (2014) 7371–7376, https://doi.org/10.1021/ic500718y.

[268] J. Hessevik, R. Lalrempuia, H. Nsiri, K.W. Tornroos, V.R. Jensen, E. Le Roux, Sterically (un)encumbered mer-tridentate N-heterocyclic carbene complexes of titanium(IV) for the copolymerization of cyclohexene oxide with CO_2, Dalton Trans. 45 (2016) 14734–14744, https://doi.org/10.1039/C6DT01706A.
[269] M. Baltrun, F.A. Watt, R. Schoch, C. Wölper, A.G. Neuba, S. Hohloch, A new bis-phenolate mesoionic carbene ligand for early transition metal chemistry, Dalton Trans. 48 (2019) 14611–14625, https://doi.org/10.1039/C9DT03099A.
[270] D. Zhang, H. Aihara, T. Watanabe, T. Matsuo, H. Kawaguchi, Zirconium complexes of the tridentate bis(aryloxide)-N-heterocyclic-carbene ligand: chloride and alkyl functionalized derivatives, J. Organomet. Chem. 692 (2007) 234–242. https://www.sciencedirect.com/science/article/pii/S0022328X06006644.
[271] S. Barroso, S.R.M.M. de Aguiar, R.F. Munhá, A.M. Martins, New zirconium complexes supported by N-heterocyclic carbene (NHC) ligands: synthesis and assessment of hydroamination catalytic properties, J. Organomet. Chem. 760 (2014) 60–66. https://www.sciencedirect.com/science/article/pii/S0022328X13008887.
[272] D. Zhang, G. GengShi, J. Wang, Q. Yue, W. Zheng, L. Weng, Macrocyclic hexanuclear zirconium(IV) complex bearing a bisaryloxyl N-heterocyclic-carbene ligand: synthesis, structure, and catalytic properties, Inorg. Chem. Commun. 13 (2010) 433–435. https://www.sciencedirect.com/science/article/pii/S1387700310000225.
[273] S. Dagorne, S. Bellemin-Laponnaz, C. Romain, Neutral and cationic N-heterocyclic carbene zirconium and hafnium benzyl complexes: highly regioselective oligomerization of 1-hexene with a preference for trimer formation, Organometallics 32 (2013) 2736–2743, https://doi.org/10.1021/om400182d.
[274] R. Lalrempuia, J. Underhaug, K.W. Tornroos, E. Le Roux, Anionic hafnium species: an active catalytic intermediate for the coupling of epoxides with CO_2? Chem. Commun. 55 (2019) 7227–7230, https://doi.org/10.1039/C9CC02695A.
[275] R. Lalrempuia, F. Breivik, K.W. Törnroos, E. Le Roux, Coordination behavior of bis-phenolate saturated and unsaturated N-heterocyclic carbene ligands to zirconium: reactivity and activity in the copolymerization of cyclohexene oxide with CO_2, Dalton Trans. 46 (2017) 8065–8076, https://doi.org/10.1039/C7DT01117B.
[276] E. Despagnet-Ayoub, L.M. Henling, J.A. Labinger, J.E. Bercaw, Addition of a phosphine ligand switches an N-heterocyclic carbene-zirconium catalyst from oligomerization to polymerization of 1-hexene, Dalton Trans. 42 (2013) 15544–15547, https://doi.org/10.1039/C3DT52342J.
[277] E. Despagnet-Ayoub, M.K. Takase, L.M. Henling, J.A. Labinger, J.E. Bercaw, Mechanistic insights on the controlled switch from oligomerization to polymerization of 1-hexene catalyzed by an NHC-zirconium complex, Organometallics 34 (2015) 4707–4716, https://doi.org/10.1021/acs.organomet.5b00472.
[278] S. Bellemin-Laponnaz, R. Welter, L. Brelot, S. Dagorne, Synthesis and structure of V(V) and Mn(III) NHC complexes supported by a tridentate bis-aryloxide-N-heterocyclic carbene ligand, J. Organomet. Chem. 694 (2009) 604–606. https://www.sciencedirect.com/science/article/pii/S0022328X08008607.
[279] J. Cheng, L. Wang, P. Wang, L. Deng, High-oxidation-state 3d metal (Ti-Cu) complexes with N-heterocyclic carbene ligation, Chem. Rev. 118 (2018) 9930–9987, https://doi.org/10.1021/acs.chemrev.8b00096.
[280] L. Suresh, J. Finnstad, K.W. Törnroos, E. Le Roux, Bis(phenolate)-functionalized N-heterocyclic carbene complexes of oxo- and imido-vanadium(V), Inorg. Chim. Acta 521 (2021) 120301. https://www.sciencedirect.com/science/article/pii/S0020169321000578.
[281] F.R. Neururer, S. Liu, D. Leitner, M. Baltrun, K.R. Fisher, H. Kopacka, K. Wurst, L. J. Daumann, D. Munz, S. Hohloch, Mesoionic carbenes in low- to high-valent vanadium chemistry, Inorg. Chem. 60 (2021) 15421–15434, https://doi.org/10.1021/acs.inorgchem.1c02087.
[282] C.D. Abernethy, G.M. Codd, M.D. Spicer, M.K. Taylor, A highly stable N-heterocyclic carbene complex of trichloro-oxo-vanadium(V) displaying novel Cl-$C_{carbene}$ bonding interaction, J. Am. Chem. Soc. 125 (2003) 1128–1129, https://doi.org/10.1021/ja0276321.
[283] M. Bortoluzzi, E. Ferretti, F. Marchetti, G. Pampaloni, S. Zacchini, A structurally-characterized $NbCl_5$-NHC adduct, Chem. Commun. 50 (2014) 4472–4474, https://doi.org/10.1039/C4CC01575D.
[284] M. Bortoluzzi, E. Ferretti, F. Marchetti, G. Pampaloni, C. Pinzino, S. Zacchini, Coordination compounds of niobium(IV) oxide dihalides including the synthesis and the crystallographic characterization of NHC complexes, Inorg. Chem. 55 (2016) 4173–4182, https://doi.org/10.1021/acs.inorgchem.5b02888.
[285] M. Bortoluzzi, E. Ferretti, F. Marchetti, G. Pampaloni, S. Zacchini, A crystallographic and DFT study on a NHC complex of niobium oxide trifluoride, J. Coord. Chem. 69 (2016) 2766–2774, https://doi.org/10.1080/00958972.2016.1214950.
[286] J.A. Ziegler, C. Prange, T.D. Lohrey, R.G. Bergman, J. Arnold, Hydroboration reactivity of niobium bis(N-heterocyclic carbene)borate complexes, Inorg. Chem. 57 (2018) 5213–5224, https://doi.org/10.1021/acs.inorgchem.8b00247.
[287] I. Elser, J. Groos, P.M. Hauser, M. Koy, M. van der Ende, D. Wang, W. Frey, K. Wurst, J. Meisner, F. Ziegler, J. Kästner, M.R. Buchmeiser, Molybdenum and tungsten alkylidyne complexes containing mono-, bi-, and tridentate N-heterocyclic carbenes, Organometallics 38 (2019) 4133–4146, https://doi.org/10.1021/acs.organomet.9b00481.
[288] P.M. Hauser, M. Van der Ende, J. Groos, W. Frey, D. Wang, M.R. Buchmeiser, Cationic tungsten alkylidyne N-heterocyclic carbene complexes: synthesis and reactivity in alkyne metathesis, Eur. J. Inorg. Chem. 2020 (2020) 3070–3082, https://doi.org/10.1002/ejic.202000503.
[289] M. Baltrun, F.A. Watt, R. Schoch, S. Hohloch, Dioxo-, oxo-imido-, and bis-imido-molybdenum(VI) complexes with a bis-phenolate-NHC ligand, Organometallics 38 (2019) 3719–3729, https://doi.org/10.1021/acs.organomet.9b00472.
[290] S. Liu, J.I. Amaro-Estrada, M. Baltrun, I. Douair, R. Schoch, L. Maron, S. Hohloch, Catalytic deoxygenation of nitroarenes mediated by high-valent molybdenum (VI)–NHC complexes, Organometallics 40 (2021) 107–118, https://doi.org/10.1021/acs.organomet.0c00352.
[291] L. Gravogl, F.W. Heinemann, D. Munz, K. Meyer, An iron pincer complex in four oxidation states, Inorg. Chem. 59 (2020) 5632–5645, https://doi.org/10.1021/acs.inorgchem.0c00355.
[292] M. Nirmala, P. Viswanathamurthi, Design and synthesis of ruthenium(II) OCO pincer type NHC complexes and their catalytic role towards the synthesis of amides, J. Chem. Sci. 128 (2015) 9–21, https://doi.org/10.1007/s12039-015-0997-5.
[293] C.F. Harris, M.B. Bayless, N.P. van Leest, Q.J. Bruch, B.N. Livesay, J. Bacsa, K. I. Hardcastle, M.P. Shores, B. de Bruin, J.D. Soper, Redox-active bis(phenolate) N-heterocyclic carbene [OCO] pincer ligands support cobalt electron transfer series spanning four oxidation states, Inorg. Chem. 56 (2017) 12421–12435, https://doi.org/10.1021/acs.inorgchem.7b01906.
[294] L. Oehninger, R. Rubbiani, I. Ott, N-heterocyclic carbene metal complexes in medicinal chemistry, Dalton Trans. 42 (2013) 3269–3284, https://doi.org/10.1039/C2DT32617E.
[295] D.J. Harrison, A.L. Daniels, I. Korobkov, R.T. Baker, d^{10} nickel difluorocarbenes and their cycloaddition reactions with tetrafluoroethylene, Organometallics 34 (2015) 5683–5686, https://doi.org/10.1021/acs.organomet.5b00808.
[296] Y.S. Meng, Z. Mo, B.W. Wang, Y.Q. Zhang, L. Deng, S. Gao, Observation of the single-ion magnet behavior of d(8) ions on two-coordinate Co(I)-NHC complexes, Chem. Sci. 6 (2015) 7156–7162, https://doi.org/10.1039/C5SC02611C.
[297] A. Massard, P. Braunstein, A.A. Danopoulos, S. Choua, P. Rabu, Studies on three-coordinate $[Co\{N(SiMe_3)_2\}_2L]$ complexes, L = N-heterocyclic carbene, Organometallics 34 (2015) 2429–2438, https://doi.org/10.1021/om501178p.
[298] C.F. Harris, C.S. Kuehner, J. Bacsa, J.D. Soper, Photoinduced cobalt(III)-trifluoromethyl bond activation enables arene C-H trifluoromethylation, Angew. Chem. Int. Ed. 57 (2018) 1311–1315, https://doi.org/10.1002/anie.201711693.
[299] D.R. Weinberg, N. Hazari, J.A. Labinger, J.E. Bercaw, Iridium(I) and iridium(III) complexes supported by a diphenolate imidazolyl-carbene ligand, Organometallics 29 (2010) 89–100, https://doi.org/10.1021/om900803r.
[300] A.J. Arduengo, J.S. Dolphin, G. Gurău, W.J. Marshall, J.C. Nelson, V.A. Petrov, J. W. Runyon, Synthesis and complexes of fluoroalkoxy carbenes, Angew. Chem. Int. Ed. 52 (2013) 5110–5114, https://doi.org/10.1002/anie.201301503.
[301] C. Gandara, C. Philouze, O. Jarjayes, F. Thomas, Coordination chemistry of a redox non-innocent NHC bis(phenolate) pincer ligand with nickel(II), Inorg. Chim. Acta 482 (2018) 561–566. https://www.sciencedirect.com/science/article/pii/S0020169318307187.
[302] E. Borré, G. Dahm, A. Aliprandi, M. Mauro, S. Dagorne, S. Bellemin-Laponnaz, Tridentate complexes of group 10 bearing bis-aryloxide N-heterocyclic carbene ligands: synthesis, structural, spectroscopic, and computational characterization, Organometallics 33 (2014) 4374–4384, https://doi.org/10.1021/om5003446.
[303] L.G. Bonnet, R.E. Douthwaite, R. Hodgson, Synthesis of constrained-geometry chiral di-N-heterocyclic carbene ligands and their silver(I) and palladium(II) complexes, Organometallics 22 (2003) 4384–4386, https://doi.org/10.1021/om030527v.
[304] B.E. Ketz, A.P. Cole, R.M. Waymouth, Structure and reactivity of an allylpalladium N-heterocyclic carbene enolate complex, Organometallics 23 (2004) 2835–2837, https://doi.org/10.1021/om049838b.
[305] A.W. Waltman, R.H. Grubbs, A new class of chelating N-heterocyclic carbene ligands and their complexes with palladium, Organometallics 23 (2004) 3105–3107, https://doi.org/10.1021/om049727c.
[306] C. Romain, C. Fliedel, S. Bellemin-Laponnaz, S. Dagorne, NHC bis-phenolate aluminum chelates: synthesis, structure, and use in lactide and trimethylene carbonate polymerization, Organometallics 33 (2014) 5730–5739, https://doi.org/10.1021/om5004557.
[307] C. Fliedel, G. Schnee, T. Avilés, S. Dagorne, Group 13 metal (Al, Ga, In, Tl) complexes supported by heteroatom-bonded carbene ligands, Coord. Chem. Rev. 275 (2014) 63–86. https://www.sciencedirect.com/science/article/pii/S0010854514001155.
[308] Y. Lee, B. Li, A.H. Hoveyda, Stereogenic-at-metal Zn- and Al-based N-heterocyclic carbene (NHC) complexes as bifunctional catalysts in Cu-free enantioselective allylic alkylations, J. Am. Chem. Soc. 131 (2009) 11625–11633, https://doi.org/10.1021/ja904654j.
[309] S.G. Alexander, M.L. Cole, C.M. Forsyth, Tertiary amine and N-heterocyclic carbene coordinated haloalanes–synthesis, structure, and application, Chem. Eur. J. 15 (2009) 9201–9214, https://doi.org/10.1002/chem.200900365.
[310] A.L. Speelman, K.L. Skubi, B.Q. Mercado, P.L. Holland, Synthesis and reactivity of iron complexes with a biomimetic SCS pincer ligand, Inorg. Chem. 60 (2021) 1965–1974, https://doi.org/10.1021/acs.inorgchem.0c03427.
[311] S. Fuku-en, J. Yamamoto, M. Minoura, S. Kojima, Y. Yamamoto, Synthesis of new dipyrido-annulated N-heterocyclic carbenes with ortho substituents, Inorg. Chem. 52 (2013) 11700–11702, https://doi.org/10.1021/ic402301u.
[312] D. Sellmann, W. Prechtel, F. Knoch, M. Moll, Transition-metal complexes with sulfur ligands. 89. Unexpected formation of the highly stable binuclear nickel carbene complex $[Ni(S_2C)]_2$ from nickel(II) salts, diamine-dithiolate ligands, and C1 components [S2C2- = 1,3-imidazolidine-1,3-diylbis(2-benzenethiolate)2-], Organometallics 11 (1992) 2346–2348, https://doi.org/10.1021/om00043a012.
[313] D. Sellmann, W. Prechtel, F. Knoch, M. Moll, Transition-metal complexes with sulfur ligands. 94. Synthesis and reactivity of nickel, palladium, and platinum

complexes with the thiolate carbene ligand '$S_2C'^{2-}$. X-ray structure determinations of [Ni(PMe_3)('S_2C')], [Ni(PPh_3)('S_2C')], [Ni('SC')$_2$], [Pt(PMe_3)('S_2C')], and ('S_2CO')$_2$, Inorg. Chem., 32 (1993) 538–546. https://doi.org/10.1021/ic00057a009.
[314] D. Sellmann, C. Allmann, F. Heinemann, F. Knoch, J. Sutter, Übergangsmetallkomplexe mit Schwefelliganden CXXIV. Koordination von C- und S-Liganden an Metall—Carben—Thiolat-Fragmente [M('S_2C')] [M = Ni^{II}, Pd^{II}, Pt^{II}; '$S_2C'^{2-}$ = 1,3-Imidazolidinyl-N,N-bis(2-benzolthiolat)$^{2-}$]. [M(L)('S_2C')]-Komplexe mit L = CN−, CH_3−, $COCH_3$−, CNBu, CR_2, SH− und SR− (R = Et, Ph, *o*-$C_6H_4NH_2$), J. Organomet. Chem., 541 (1997) 291-305. https://www.sciencedirect.com/science/article/pii/S0022328X97000739.
[315] J. Iglesias-Sigüenza, A. Ros, E. Diez, A. Magriz, A. Vazquez, E. Alvarez, R. Fernandez, J.M. Lassaletta, C_2-symmetric S/C/S ligands based on N-heterocyclic carbenes: a new ligand architecture for asymmetric catalysis, Dalton Trans. (2009) 8485–8488, https://doi.org/10.1039/B910846G.
[316] C. Fliedel, A. Sabbatini, P. Braunstein, Synthesis of N, N'-bis(thioether)-functionalized imidazolium salts: their reactivity towards ag and pd complexes and first S, C(NHC), S free carbene, Dalton Trans. 39 (2010) 8820–8828, https://doi.org/10.1039/C0DT00351D.
[317] S. Haslinger, A.C. Lindhorst, J.W. Kück, M. Cokoja, A. Pöthig, F.E. Kühn, Isocyanide substitution reactions at the trans labile sites of an iron(II) N-heterocyclic carbene complex, RSC Adv. 5 (2015) 85486–85493, https://doi.org/10.1039/C5RA18270K.
[318] A.S. Phearman, R.M. Bullock, Synthesis and reactivity of Fe(II) complexes containing cis ammonia ligands, Inorg. Chem. 63 (2024) 2024–2033, https://doi.org/10.1021/acs.inorgchem.3c03757.
[319] I. Klawitter, S. Meyer, S. Demeshko, F. Meyer, Nickel(II) and iron(II) complexes with tetradentate NHC/Amide hybrid ligands, Z. Naturforsch. B 68 (2013) 458–466, https://doi.org/10.5560/znb.2013-3091.
[320] Y. Imanaka, N. Shiomoto, M. Tamaki, Y. Maeda, H. Nakajima, T. Nishioka, The arrangement of two N-heterocyclic carbene moieties in palladium pincer complexes affects their catalytic activity towards Suzuki-Miyaura cross-coupling reactions in water, Bull. Chem. Soc. Jpn. 90 (2017) 59–67, https://doi.org/10.1246/bcsj.20160300.
[321] J.M. Mueller, D. Stephen, C. Lund, M. Sgro, C. Ong, R. Cariou, Ruthenium-Based Complex Catalysts. WO2013024119A1 (2013).
[322] J. Müller, C. Ong, D. Wade, C. Lund, M. Sgro, R. Cariou, Ruthenium-Based Complex Catalysts EP2614887A1 (2013).
[323] C.L. Lund, M.J. Sgro, D.W. Stephan, Neutral and cationic tridentate bis(N-heterocyclic carbene) ether ruthenium alkylidene complexes in metathesis, Organometallics 31 (2012) 580–587, https://doi.org/10.1021/om200848d.
[324] D.T. Weiss, M.R. Anneser, S. Haslinger, A. Pöthig, M. Cokoja, J.-M. Basset, F. E. Kühn, NHC versus pyridine: how "teeth" change the redox behavior of iron(II) complexes, Organometallics 34 (2015) 5155–5166, https://doi.org/10.1021/acs.organomet.5b00732.
[325] M. Hollering, D.T. Weiss, M.J. Bitzer, C. Jandl, F.E. Kühn, Controlling coordination geometries: ru-carbene complexes with tetra-NHC ligands, Inorg. Chem. 55 (2016) 6010–6017, https://doi.org/10.1021/acs.inorgchem.6b00509.
[326] C. Tubaro, D. Bertinazzo, M. Monticelli, O. Saoncella, A. Volpe, M. Basato, D. Badocco, P. Pastore, C. Graiff, A. Venzo, Synthesis and reactivity of cationic Bis (N-heterocyclic dicarbene) ruthenium(II) complexes, Eur. J. Inorg. Chem. 2014 (2014) 1524–1532, https://doi.org/10.1002/ejic.201301583.
[327] Z. Lu, S.A. Cramer, D.M. Jenkins, Exploiting a dimeric silver transmetallating reagent to synthesize macrocyclic tetracarbene complexes, Chem. Sci. 3 (2012) 3081–3087, https://doi.org/10.1039/C2SC20628E.
[328] D. Rendón-Nava, D. Angeles-Beltrán, A.L. Rheingold, D. Mendoza-Espinosa, Palladium(II) complexes of a neutral CCC-Tris(N-heterocyclic carbene) pincer ligand: synthesis and catalytic applications, Organometallics 40 (2021) 2166–2177, https://doi.org/10.1021/acs.organomet.1c00324.
[329] H. Ryu, J. Park, H.K. Kim, J.Y. Park, S.-T. Kim, M.-H. Baik, Pitfalls in computational modeling of chemical reactions and how to avoid them, Organometallics 37 (2018) 3228–3239, https://doi.org/10.1021/acs.organomet.8b00456.
[330] C. Lee, W. Yang, R.G. Parr, Development of the Colle-Salvetti correlation-energy formula into a functional of the electron density, Phys. Rev. B 37 (1988) 785–789. https://link.aps.org/doi/10.1103/PhysRevB.37.785.
[331] A.D. Becke, Density-functional thermochemistry. III, The role of exact exchange, J. Chem. Phys. 98 (1993) 5648–5652, https://doi.org/10.1063/1.464913.
[332] M. Steinmetz, S. Grimme, Benchmark study of the performance of density functional theory for bond activations with (Ni, Pd)-based transition-metal catalysts, ChemistryOpen 2 (2013) 115–124, https://doi.org/10.1002/open.201300012.
[333] Y. Zhao, D.G. Truhlar, The M06 suite of density functionals for main group thermochemistry, thermochemical kinetics, noncovalent interactions, excited states, and transition elements: two new functionals and systematic testing of four M06-class functionals and 12 other functionals, Theor. Chem. Acc. 120 (2008) 215–241, https://doi.org/10.1007/s00214-007-0310-x.
[334] J.-D. Chai, M. Head-Gordon, Systematic optimization of long-range corrected hybrid density functionals, J. Chem. Phys. 128 (2008) 084106, https://doi.org/10.1063/1.2834918.
[335] C. Adamo, V. Barone, Toward reliable density functional methods without adjustable parameters: the PBE0 model, J. Chem. Phys. 110 (1999) 6158–6170, https://doi.org/10.1063/1.478522.
[336] V.A. Rassolov, M.A. Ratner, J.A. Pople, P.C. Redfern, L.A. Curtiss, 6–31G* basis set for third-row atoms, J. Comput. Chem. 22 (2001) 976–984, https://doi.org/10.1002/jcc.1058.
[337] P.J. Hay, W.R. Wadt, Ab initio effective core potentials for molecular calculations. potentials for K to au including the outermost core orbitals, J. Chem. Phys. 82 (1985) 299–310, https://doi.org/10.1063/1.448975.
[338] F. Weigend, R. Ahlrichs, Balanced basis sets of split valence, triple zeta valence and quadruple zeta valence quality for H to Rn: design and assessment of accuracy, PCCP 7 (2005) 3297–3305, https://doi.org/10.1039/B508541A.
[339] R.A. Kendall, T.H. Dunning Jr., R.J. Harrison, Electron affinities of the first-row atoms revisited. Systematic basis sets and wave functions, J. Chem. Phys. 96 (1992) 6796–6806, https://doi.org/10.1063/1.462569.
[340] K.A. Peterson, D. Figgen, M. Dolg, H. Stoll, Energy-consistent relativistic pseudopotentials and correlation consistent basis sets for the 4d elements Y-Pd, J. Chem. Phys. 126 (2007) 124101, https://doi.org/10.1063/1.2647019.
[341] L. Noodleman, D.A. Case, Density-functional theory of spin polarization and spin coupling in iron—Sulfur clusters, in: R. Cammack (Ed.), Adv, Academic Press, Inorg. Chem., 1992, pp. 423–470, https://www.sciencedirect.com/science/article/pii/S0898883808600707.
[342] N. Ferré, N. Guihéry, J.-P. Malrieu, Spin decontamination of broken-symmetry density functional theory calculations: deeper insight and new formulations, PCCP 17 (2015) 14375–14382, https://doi.org/10.1039/C4CP05531D.
[343] N. Onofrio, J.-M. Mouesca, Analysis of the singlet-triplet splitting computed by the density functional theory–broken-symmetry method: is it an exchange coupling constant? Inorg. Chem. 50 (2011) 5577–5586, https://doi.org/10.1021/ic200198f.
[344] I. Rudra, Q. Wu, T. Van Voorhis, Predicting exchange coupling constants in frustrated molecular magnets using density functional theory, Inorg. Chem. 46 (2007) 10539–10548, https://doi.org/10.1021/ic700871f.
[345] C. Mejuto-Zaera, D. Tzeli, D. Williams-Young, N.M. Tubman, M. Matoušek, J. Brabec, L. Veis, S.S. Xantheas, W.A. de Jong, The effect of geometry, spin, and orbital optimization in achieving accurate, correlated results for iron-sulfur cubanes, J. Chem. Theory Comput. 18 (2022) 687–702, https://doi.org/10.1021/acs.jctc.1c00830.
[346] P.-Å. Malmqvist, B.O. Roos, The CASSCF state interaction method, Chem. Phys. Lett. 155 (1989) 189–194. https://www.sciencedirect.com/science/article/pii/0009261489853473.
[347] C. Angeli, R. Cimiraglia, S. Evangelisti, T. Leininger, J.P. Malrieu, Introduction of n-electron valence states for multireference perturbation theory, J. Chem. Phys. 114 (2001) 10252–10264, https://doi.org/10.1063/1.1361246.
[348] M. Atanasov, D. Ganyushin, K. Sivalingam, F. Neese, A modern first-principles view on ligand field theory through the eyes of correlated multireference wavefunctions, in: D.M.P. Mingos, P. Day, J.P. Dahl (Eds.), Molecular Electronic Structures of Transition Metal Complexes II, Springer, Berlin Heidelberg, Berlin, Heidelberg, 2012, pp. 149–220, https://doi.org/10.1007/430_2011_57.
[349] S.K. Singh, J. Eng, M. Atanasov, F. Neese, Covalency and chemical bonding in transition metal complexes: an ab initio based ligand field perspective, Coord. Chem. Rev. 344 (2017) 2–25. https://www.sciencedirect.com/science/article/pii/S0010854517300528.
[350] F.M. Bickelhaupt, N.J.R. van Eikema Hommes, C. Fonseca Guerra, E.J. Baerends, The Carbon−Lithium Electron Pair Bond in $(CH_3Li)_n$ (n = 1, 2, 4), Organometallics, 15 (1996) 2923-2931. https://doi.org/10.1021/om950966x.
[351] E.J. Baerends, O.V. Gritsenko, A quantum chemical view of density functional theory, J. Phys. Chem. A 101 (1997) 5383–5403, https://doi.org/10.1021/jp9703768.
[352] C. Fonseca Guerra, J.-W. Handgraaf, E.J. Baerends, F.M. Bickelhaupt, Voronoi deformation density (VDD) charges: assessment of the Mulliken, Bader, Hirshfeld, Weinhold, and VDD methods for charge analysis, J. Comput. Chem. 25 (2004) 189–210, https://doi.org/10.1002/jcc.10351.
[353] F. Maseras, K. Morokuma, Application of the natural population analysis to transition-metal complexes. should the empty metal p orbitals be included in the valence space? Chem. Phys. Lett. 195 (1992) 500–504. https://www.sciencedirect.com/science/article/pii/000926149285551K.
[354] S. Miertuš, E. Scrocco, J. Tomasi, Electrostatic interaction of a solute with a continuum. a direct utilizaion of AB initio molecular potentials for the prevision of solvent effects, Chem. Phys. 55 (1981) 117–129. https://www.sciencedirect.com/science/article/pii/0301010481850902.
[355] C.E. Tzeliou, D. Tzeli, 3-input AND molecular logic gate with enhanced fluorescence output: the key atom for the accurate prediction of the spectra, J. Chem. Inf. Model. 62 (2022) 6436–6448, https://doi.org/10.1021/acs.jcim.2c00257.
[356] J. Föller, C. Ganter, A. Steffen, C.M. Marian, Computer-aided Design of Luminescent Linear N-heterocyclic carbene Copper(I) pyridine complexes, Inorg. Chem. 58 (2019) 5446–5456, https://doi.org/10.1021/acs.inorgchem.9b00334.
[357] C.C. Quadri, E. Le Roux, Copolymerization of cyclohexene oxide with CO_2 catalyzed by tridentate N-heterocyclic carbene titanium(IV) complexes, Dalton Trans. 43 (2014) 4242–4246, https://doi.org/10.1039/C3DT52804A.
[358] C. Romain, B. Heinrich, S.B. Laponnaz, S. Dagorne, A robust zirconium N-heterocyclic carbene complex for the living and highly stereoselective ring-opening polymerization of rac-lactide, Chem. Commun. 48 (2012) 2213–2215, https://doi.org/10.1039/C2CC16819G.
[359] J. Hachmann, B.A. Frazier, P.T. Wolczanski, G.-K.-L. Chan, A theoretical study of the 3d-M(smif)$_2$ complexes: structure, magnetism, and oxidation states, ChemPhysChem 12 (2011) 3236–3244, https://doi.org/10.1002/cphc.201100286.

[360] A.D. Becke, A new mixing of Hartree-Fock and local density-functional theories, J. Chem. Phys. 98 (1993) 1372–1377, https://doi.org/10.1063/1.464304.
[361] F. Weigend, Accurate Coulomb-fitting basis sets for H to Rn, Phys. Chem. Chem. Phys. 8 (2006) 1057–1065, https://doi.org/10.1039/B515623H.
[362] Gaussian 16, Revision C.01, M.J. Frisch, G.W. Trucks, H.B. Schlegel, G.E. Scuseria, M.A. Robb, J.R. Cheeseman, G. Scalmani, V. Barone, G.A. Petersson, H. Nakatsuji, X. Li, M. Caricato, A.V. Marenich, J. Bloino, B.G. Janesko, R. Gomperts, B. Mennucci, H.P. Hratchian, J.V. Ortiz, A.F. Izmaylov, J.L. Sonnenberg, Williams, F. Ding, F. Lipparini, F. Egidi, J. Goings, B. Peng, A. Petrone, T. Henderson, D. Ranasinghe, V.G. Zakrzewski, J. Gao, N. Rega, G. Zheng, W. Liang, M. Hada, M. Ehara, K. Toyota, R. Fukuda, J. Hasegawa, M. Ishida, T. Nakajima, Y. Honda, O. Kitao, H. Nakai, T. Vreven, K. Throssell, J.A. Montgomery Jr., J.E. Peralta, F. Ogliaro, M.J. Bearpark, J.J. Heyd, E.N. Brothers, K.N. Kudin, V.N. Staroverov, T.A. Keith, R. Kobayashi, J. Normand, K. Raghavachari, A.P. Rendell, J.C. Burant, S.S. Iyengar, J. Tomasi, M. Cossi, J.M. Millam, M. Klene, C. Adamo, R. Cammi, J.W. Ochterski, R.L. Martin, K. Morokuma, O. Farkas, J.B. Foresman, D.J. Fox, Gaussian, Inc. Wallingford, CT, 2016.